EXPERIMENTAL AND THEORETICAL STUDIES OF THE FILTRATION OF CERAMIC SUSPENSIONS

by

J. Holly D. Hampton

July 1991

Civil Engineering and Applied Mechanics

McGill University

Montreal, Canada

A THESIS SUBMITTED TO THE FACULTY OF GRADUATE STUDIES AND RESEARCH IN PARTIAL FULFILMENT OF THE REQUIREMENTS FOR THE DEGREE OF DOCTOR OF PHILOSOPHY

To my parents

and

my two brothers

Abstract

The filtration mechanics of the slip casting and filter pressing ceramic forming processes are analyzed so that better control can be achieved over these processes. The rheological behaviour of alumina suspensions with different solids loadings, particle size distributions and amounts of deflocculant as well as the effects that these suspensions have on the filtration process were studied.

During slip casting the formation of the filter cake occurs as a result of the capillary suction pressure of the pores in the plaster of Paris molds. Therefore, the mold microstructure, density, permeability, suction pressure and the effects that these mold properties have on the filtration process are analyzed as a function of the plaster/water ratio used to form the molds.

During filtration, as the cake thickness increases with casting time, fine particles can be carried along with the filtrate and deposited within the filter cake and/or filter medium thereby clogging and reducing the permeabilities of the porous media. This in turn affects the growth rate as well as the permeability, density and porosity of the cake. Evidence of cake and filter medium clogging was obtained by: (1) SEM analysis of cakes and filter media, (2) surface area measurements of cross-sections of cakes, and (3) measurements of cake thickness as a function of casting time.

A computer model consisting of a network of tubes with a random size distribution has been developed to simulate the filtration process. The model accounts for porous media clogging due to: (1) fine particles depositing on the pore walls and gradually reducing the pore radii and (2) pores trapping particles larger than the pore

openings. The network model shows that the permeability of the porous medium is dependent upon its pore size distribution rather than its average pore size. The model also illustrates that minor changes in the pore size distribution due to clogging can significantly affect its permeability and casting rate.

Résumé

La mécanique de filtration des procédés de formation de céramiques par coulage et par passage au filtre-presse a été analysée afine de parvenir à un meilleur contrôle de ces processus. On a donc étudié le comportement rhéologique de suspensions d'alumine avec différentes teneurs en solides, granulométries et quantités de défloculants, ainsi que les effets de ces suspensions sur la filtration.

Pendant la coulée en barbotine, la formation du gâteau de filtre-presse résulte de la tension capillaire des pores dans les moules en plâtre de Paris On a donc analysé la microstructure des moules, la densité, la perméabilité, la pression d'aspiration et les effets que ces proprieétés des moules ont sur le procédé de filtration en tenant compte du rapport plâtre/eau utilisé pour former les moules.

Pendant la filtration, l'épaisseur du gâteau augmente en fonction du temps; de fines particules peuvent donc être entraînées avec le filtrat et s'accumuler à l'intérieur du gâteau et(ou) du milieu filtrant, ce qui provoque un engorgement et réduit la perméabilité du milieu poreux. Ce dernier phénomème affecte à son tour le taux de croissance ainsi que la perméabilité, la densité et la porosité du gâteau. Nous avons démontré qu'il y a engorgement dans le gâteau et le milieu filtrant par (1) analyse au microscope électronique à balayage des gâteaux et milieux filtrants; (2) mesure de la superficie de coupes de gâteaux; (3) mesure de l'épaisseur du gâteau en fonction de la durée de coulée.

Un modèle informatique consistant en un réseau de tubes de dimensions réparties de manière aléatoire a été mis au point pour simuler le procédé de filtration. Ce

modèle tient compte de l'engorgement du milieu poreux dû: (1) à l'accumulation de fines particules dans les parois des pores et à la diminution graduelle du rayon de celles-ci; (2) à l'obturation des pores par des particules de taille supérieure aux pores. Ce modèle de réseau montre que la perméabilité du milieu poreux est fonction de la répartition des pores selon leur taille plutôt que de la taille moyenne des pores. Le modèle montre également que de petites variations dans la répartition de la taille des pores par suite de l'engorgement de celles-ci peut avoir un effet appréciable sur la perméabilité et le taux de coulée.

Acknowledgements

The author wishes to express her sincere thanks to her research supervisor, Professor S. B. Savage and co-supervisor, Professor R. A. L. Drew for their guidance, valuable advice, support and constant encouragement during the course of this study.

In addition the author wishes to express her gratitude to Nick Chepurniy and CRAY Canada Inc. for providing free computer time on the CRAY X-MP supercomputer. The author is indebted to Nick Chepurniy for his assistance in the use of the supercomputer.

The kind assistance of Dr. W. D. Cook concerning the computer work is gratefully acknowledged.

The construction of the filter pressing apparatus made by the lab technician, Claudio Navas is greatly appreciated.

The financial assistance provided by the Natural Sciences and Engineering Research Council of Canada (NSERC) and by the Fonds pour la Formation de Chercheurs et l'Aide à la Recherche (FCAR) of the Government of Quebec is gratefully acknowledged. The author was supported by an NSERC Postgraduate Scholarship.

Table of Contents

List of Figures

List of Tables

List of Symbols

Latin Symbols

A	cross-sectional area, (m^2)
A_a	internal cross-sectional area of standpipe, (m^2)
$A(\iota)$	area of tube ι, (m^2)
A_p	average tube area, (m^2)
A_{tot}	total area under comparison curve of $f(x)$, (m^2)
a_v^3	atomic volume of diffusing vacancy, (m^3)
a_o	constant in comparison function, $f(x)$
B	constant ($= L^2/t$), (m^2/sec)
B	constant of integration
b	number of cake layers
b_c	critical bond concentration
b_u	fraction of uncut bonds remaining
COV	coefficient of variation of x
C	constant ($= t/L^n$), (sec/m^n)
C_n	network constant, (N·sec/m^2)
C_f	constant ($= \mathcal{FR}$)
C_s	suspended particle concentration (i.e., average number of suspended particles per tube)
C_v	volume concentration (i.e., volume of suspended particles in a layer/total tube volume of layer)
c_o	constant in comparison function, $f(x)$
D	diffusion constant, (m^2/sec)
D	constant of integration
D^*	self-diffusing coefficient, (m^2/sec)
d	distance between sphere surfaces, (m)
d_c	center-to-center distance between two particles, (m)

d_o	distance of closest approach, (m)
d_p	particle diameter, (m)
d_t	tube diameter, (m)
E_H	enthalpy, (J)
E_S	entropy, (J/K)
F	Faraday constant, (C/mol)†
F_A	van der Waals attraction force, (N)
F_H	hydrodynamic force in direction perpendicular to the flow, (N)
F^*	critical value of F_H, (N)
F_p	force between two colloidal particles in the presence of a polymer
$\mathcal{F}$	friction factor
f	friction coefficient, (N·sec/m)
$f(x)$	comparison function
ΔG	change in Gibbs free energy, (J)
G_c	network constant, (m^2/sec)
H_A	Hamaker constant, (J)
H_t	head of water at time t_t, (m)
H_o	head of water at $t = 0$, (m)
h	Kozeny constant
I	total number of columns in network
I_c	current, (amp)
i	column number
J	total number of layers in network
J_s	surface charge, (C)
j	tube layer number
j'	particle flux to tube surface, (no./m^2·sec)
K	permeability, (m^2)
K_{ave}	permeability of system, (m^2)
K_c	cake permeability, (m^2)
K_m	mold permeability, (m^2)
K_o	permeability of network with all network tube radii = 1.0 μm, (m^2)

†C = Coulomb

K_{b-1}	permeability of network with (b - 1) layers, (m^2)
k	Boltzmann constant, (J/K)
L	cake thickness, (m)
L	tube length, (m)
L	distance between the electrodes, (m)
L_c	critical network length, (m)
L_m	depth of penetration of filtrate into the mold, (m)
L_{m_t}	L_m at time t_t, (m)
ΔL	network length of a unit layer, (m)
$\Delta L/L_o$	linear shrinkage (i.e., sintering rate), (m/m)
l_b	bond length, (m)
l_p	distance along tube, (m)
M_R	molar gas constant, (J/mol·K)
m	hydraulic radius of pore (= (pore volume)/(internal pore surface area)), (m)
N_b	number of blocked tubes in a layer
N_{dep}	number of particles deposited in pore i
N	number of tubes per network row
N_{tot}	total number of tubes in a layer
n	constant (= $\ln(t/C)/\ln L$)
n_i	concentration of ions of type i, (mol/m^3)
P	applied or mold suction pressure, (Pa)
P_l	hydraulic pressure, (Pa)
ΔP	pressure drop, (Pa)
ΔP_c	pressure drop across cake, (Pa)
ΔP_m	pressure drop across mold, (Pa)
ΔP_o	pressure drop with all network tube radii = 1.0 μm, (Pa)
p	probability
dP_l/dx	pressure gradient, (Pa/m)
$p(x)$	probability density function of x
$p_g(x)$	Gaussian probability density function of x
$p_l(x)$	log-normal probability density function of x
$p_r(x)$	Rayleigh probability density function of x

Q	volumetric flow rate, (m^3/sec)
Q_{ave}	average volumetric flow rate, (m^3/sec)
Q_{inf}	total volumetric network inflow rate, (m^3/sec)
$Q(i)$	volumetric flow rate in tube i, (m^3/sec)
Q_o	volumetric flow rate with all network tube radii = 1.0 μm, (m^3/sec)
$Q(b)_{so}$	sum of positive volumetric flow rates of unclogged small pores in layer b, (m^3/sec)
$Q(b)_{tot}$	sum of positive volumetric flow rates of all tubes in layer b, (m^3/sec)
q	apparent flow rate per unit area (i.e., filtration velocity), (m/sec)
q_i	initial filtration velocity, (m/sec)
R	tube radius, (m)
R_o	tube radius = 1.0 μm
R_1, R_2	radii of the surface curvature of the particles and the contact area between the two touching particles, respectively, (m)
$\mathcal{R}$	Reynolds number
$\mathcal{R}_m$	modified Reynolds number
r	particle radius, (m)
r	radius from tube center, (m)
r_s	radius of suspended particles, (m)
S_o	specific surface (i.e., surface area per unit volume of solid), (1/m)
T	temperature, (K)
t	time, (sec)
t_i	time at measurement number i, (sec)
U	uniform deviate between 0 and 1
u	velocity, (m/sec)
$u(i)$	velocity in tube i, (m/sec)
u_c	critical velocity, (m/sec)
u_o	maximum velocity, (m/sec)
u_r	mean fluid velocity, (m/sec)
V	network tube volume, (m^3)
V_{att}	attraction energy, (J)
$V(b)_{sc}$	volume of small pores in layer b that are clogged, (m^3)
$V(b)_{sus}$	volume of suspended particles in layer b, (m^3)

V_{cl}	tube volume of a layer after clogging, (m^3)
V_m	atomic volume of the mobile species, (m^3)
V_o	network tube volume with all network tube radii = 1.0 μm, (m^3)
V_{op}	original tube volume of a layer (i.e., no clogging), (m^3)
V_R	electrostatic repulsion energy, (J)
W	volume of filtrate per unit area, (m^3/m^2)
x	distance, (m)
x_o	constant in comparison function, $f(x)$
y	variable = $R - r$, (m)
$[Z]$	network resistance matrix, ($N \cdot sec/m^5$)
z_i	charge number of ions of type i
subscript *cc*	counterclockwise direction
subscript *cl*	clockwise direction

Greek Symbols

α^{-1}	characteristic tube radius. (m)
γ	specific weight, (N/m^3)
γ_s	surface energy per unit area, (J/m^2)
$\dot{\gamma}$	shear rate, (1/sec)
ϵ_{cav}	volume fraction of solids in cake
ϵ_m	volume fraction of filtrate in the wetted part of the mold
ϵ_{sl}	volume fraction of solids in slip
ϵ	relative permittivity
ϵ_o	permittivity of vacuum, ($C^2 \cdot N^{-1} \cdot m^{-2}$)
$1/\eta$	thickness of electrical double layer, (m)
θ	wetting angle
λ	fraction of suspended particles depositing per second, (1/sec)
λ'	fraction of suspended particles depositing per pore
λ_m	mean of ln (*variate*)
μ	viscosity, ($N \cdot sec/m^2$)
μ_m	mean of the variate

ν	porosity
ρ	suspended particle concentration (i.e., number of particles/tube volume), (no./m^3)
ρ_o	suspended particle concentration away from tube wall, (no./m^3)
ρ_f	density of filtrate, (kg/m^3)
σ	standard deviation of variate
σ_w	surface tension of water, (N/m)
τ	shear stress, (Pa)
$\phi(b)$	average number of suspended particles per tube in layer b
ξ	standard deviation of ln (*variate*)
χ	intramolecular expansion factor
ψ	dimensionless quantity $= (u_o/DR)^{1/3}y/x^{1/3}$
ω_c	volume of solids per unit area of cake, (m^3/m^2)
ζ	zeta potential, (J/C)

Chapter 1

INTRODUCTION

Advanced, structural ceramics exhibit valuable properties such as high strength (often at high temperature), and resistance to abrasion and corrosion. The fabrication of ceramic products of high reliability involves four basic stages: (1) raw materials, (2) forming well-compacted shapes (green bodies), (3) densification and (4) final machining. At present ceramic shape-forming is the most poorly understood in a scientific context This is the most unforgiving stage of the overall process, because microstructural defects present in the green body cannot be easily eliminated, and therefore carry through to the subsequent two stages, resulting in a defective ceramic article.[1, 2]

The present thesis studies the filtration mechanics of slip casting and filter pressing of alumina (Al_2O_3) powder. Slip casting is a shape forming method now being used in the advanced ceramic industry to produce high strength products with complex shapes. The ceramic green body is formed by pouring a slip composed of micron sized powder and liquid into a plaster of Paris (gypsum) mold. The mold behaves like a sponge and withdraws the liquid (filtrate) from the slip to form a consolidated compact (also referred to as a cake) on the surface of the mold. The cake thickness and the depth of penetration of the filtrate into the mold both increase with casting time. Once the desired cake thickness is achieved and the excess slip is poured off, the cake is removed, dried and then sintered to obtain the final ceramic

product. The selection and processing of the powder as well as the slip and mold preparation all greatly affect the overall process. At present, slip casting is still somewhat of an art, therefore, to reliably reproduce advanced ceramic products a clearer understanding of the filtration mechanics must be achieved. Filter pressing is a shape forming process similar to slip casting except that an external air pressure or a vacuum is applied to the slip and a permeable membrane is used as the filter medium.

During the filtration process, the filtrate may transport fine particles through the filter cake. The fine particles may be completely leached out or may be redeposited and cause clogging in the cake.

The objectives of this research work are:

1. To study the rheology of alumina (Al_2O_3) slips with different particle size distributions.

2. To study the effect that slip rheology and mold preparation have on the cake green densities and rate of cake growth.

3. To obtain qualitative and quantitative evidence that the filter medium can become clogged due to particles depositing in its pores and that the cake can become clogged due to fine particles migrating through the cake and accumulating near the cake-filter medium interface.

4. To develop a random tube model to simulate the filtration process taking into account clogging.

This thesis is divided into eight chapters and the presentation is as follows. Chapter 2 provides a literature review of the ceramic fabrication process and filtration theory applied to filter pressing and slip casting. Chapter 3 presents an experimen-

tal study of the rheological behaviour of alumina slips with different solids loadings, particle-size distributions and amounts of deflocculant. Filtration experiments and their results are discussed in Chapter 4. Chapter 5 provides quantitative and qualitative evidence of cake and filter medium clogging. A description and results of the random tube computer model to simulate filtration are presented in Chapter 6. In Chapter 7 the tube model is developed further to simulate the cake build-up process taking into account the clogging effects. Chapter 8 is a summary of the thesis and some sample computer programs that were developed to simulate the filtration process are listed in the appendices.

Chapter 2

LITERATURE REVIEW

2.1 THE CERAMIC FABRICATION PROCESS

The ceramic fabrication process can be seen as consisting of three stages. The fabrication process begins with finely ground powder. The ceramic powder is then consolidated into a green body (or green compact). The green body is then formed into a dense product by sintering.

2.1.1 ALUMINA

The raw materials and their preparation are critical factors which affect the forming and firing processes of ceramic components. One must be concerned with both the particle size and the particle size distribution of the raw materials. Naturally occurring minerals can be refined or new compositions synthesized so that they are of highly controlled composition and structure.

Alumina (Al_2O_3) is the ceramic powder that was used for all of the experimental work presented in this thesis. Alumina is the most universally used and the cheapest of the high-temperature single-component ceramics. Melting at 2050^oC, it remains refractory up to 1900^oC and is not attacked by molten metals and slags. It has good mechanical strength and abrasion resistance and has excellent electrical properties (high electrical resistivity and high dielectric strength).[3]

Most alumina powder is produced from the mineral bauxite by the Bayer process. Bauxite is primarily colloidal aluminum hydroxide ($Al(OH)_3$) intimately mixed with iron hydroxide (FeOH) and other impurities. This process involves leaching with a sodium hydroxide (NaOH) solution to produce sodium aluminate ($NaAlO_2$) followed by controlled precipitation of aluminum hydroxide through careful seeding which has a purity of 99.5 to 99.8%. The resulting fine-particle-size aluminum hydroxide can then be thermally converted to alpha alumina powder.[4]

$$2Al(OH)_3 \xrightarrow{900°C} Al_2O_3 + 3H_2O \tag{2.1}$$

Several comminution (particle size reduction) methods such as: ball milling, attrition milling, vibratory milling, shatterbox milling and fluid energy milling can be applied to produce fine-grained alumina powders.

2.1.2 SHAPE FORMING METHODS

The ceramic industry employs many forming methods such as: pressing, injection and extrusion molding, tape forming, slip casting and filter pressing. Pressing, slip casting and filter pressing will be presented in the following sections.

2.1.2.1 Compaction by Pressing

Most polycrystalline ceramic products (non-clay based) are formed by dry uniaxial pressing, where less than 2% moisture is present and a pressure between 20-150 MPa is applied. Other pressing processes include: (1) dry isostatic pressing (less than 2% moisture) where a pressure between 30-700 MPa is applied; and (2) semidry pressing which is often used with 5 to 20% moisture where a pressure between 7-100 MPa is applied.

Uniaxial pressing involves the compaction of powder into a die by applying pressure uniaxially. With this method production rates as high as 5,000 pieces/minute with dimensional tolerances to +/- 1% can be achieved. The disadvantage of this process arises from lack of uniformity in green-density caused by friction at the die walls.

With isostatic pressing, the powder is contained in a flexible mold and pressure is applied through a fluid. The absence of die-wall friction leads to a uniform density throughout the sample. Furthermore, long tubes and rods can be readily produced because the pressure can be applied across the long axis. The primary disadvantages of isostatic pressing are a limited production rate and difficulty in achieving close tolerances.

Complicated shapes cannot be made conveniently with isostatic and uniaxial pressing.[5, 6, 7, 8]

2.1.2.2 Slip Casting and Filter Pressing

Slip casting of clay wares is generally conceded to have originated somewhere between the years 1700 and 1740.[9] Alumina was the first non-clay material to which slip-casting was applied. It was documented in a patent by Count Schwerin, published in 1910.[3] Slip casting of advanced ceramics offers the possibility of producing complex shapes with precise tolerances. Furthermore, slip cast pieces often have a higher and more uniform density than pressed ones.

Slip casting refers to the filling of a plaster of Paris mold, a negative of the desired shape, with a slip consisting of a suspension of fine (micrometer size) ceramic powder in liquid. The porous nature of the mold provides a capillary (suction) pressure in the range of 100-200 kPa[10, 11, 12, 13] and this capillary action causes liquid (filtrate) to be withdrawn from the slip. As the liquid penetrates the mold, a cast

(also referred to as a cake) is simultaneously formed on the plaster surface. The depth of liquid penetration into the mold and cake thickness both increase with time. Figure 2.1 illustrates schematically the slip casting process. Sometimes to increase the casting rate, an air pressure is applied to the slip (pressure casting). The selection and processing of the powder as well as the slip and mold preparation must be carefully controlled to reliably reproduce advanced ceramic products.

The slip casting process may be divided into two classes: (1) drain casting, in which the slip is poured into the mold, left a short time, and then drained out, leaving a thin shell against the inside of the mold (see Figure 2.2); and (2) solid casting, in which the mold is filled with a slip and left until it casts into a solid piece (see Figure 2.3).

About 30 years ago there was a controversy about whether casting of clay slips could be attributed to both the physical capillary action of the mold and a chemical interaction between the mold and slip that leads to local flocculation of the latter by migrating calcium ions from the mold to the developing cast.[14, 15, 16] The chemical process, however was shown not to play a major role in the development of the cast.[11, 15, 17] Currently it is accepted that slip casting is a dewatering process.

Filter pressing is a shape forming process similar to slip casting except that an external air pressure or vacuum is applied to the slip and a permeable membrane is used as the filter medium.[11] Filter pressing is commonly used by chemical engineers to remove unwanted solids from liquids (or vice versa). The green compact formed by the chemical engineer is frequently discarded as waste. Despite the different uses that the chemical engineer and ceramist have for the compact they share common goals with slip casting and filter pressing. The ceramist's goals are to maximize green density and casting rate and similarly the chemical engineer wishes to minimize water

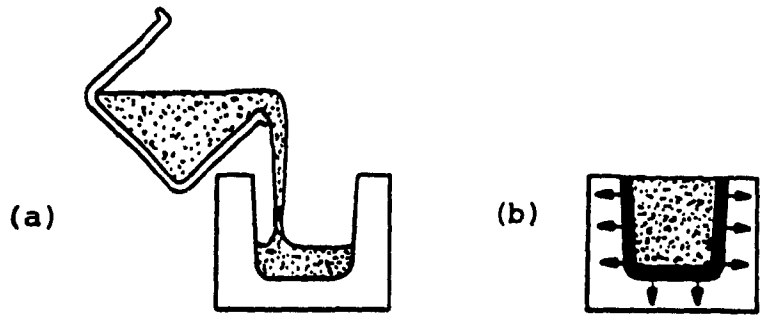

Figure 2.1: Slip casting: (a) fill mold with slip; (b) mold extracts liquid, forms compact along mold walls (After Ref. 4).

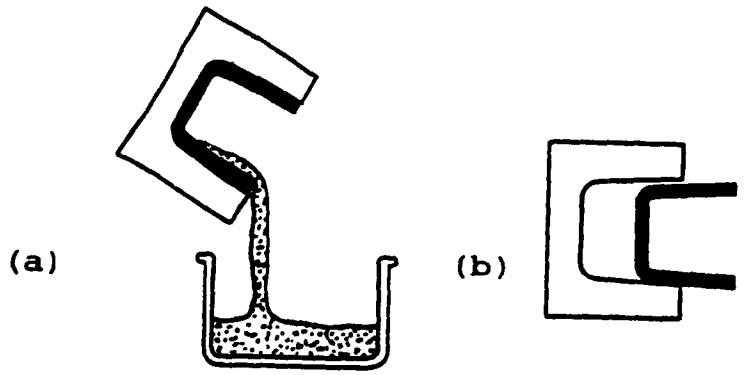

Figure 2.2: Drain casting: (a) excess slip is drained; (b) and casting is removed after partial drying (after Ref. 4).

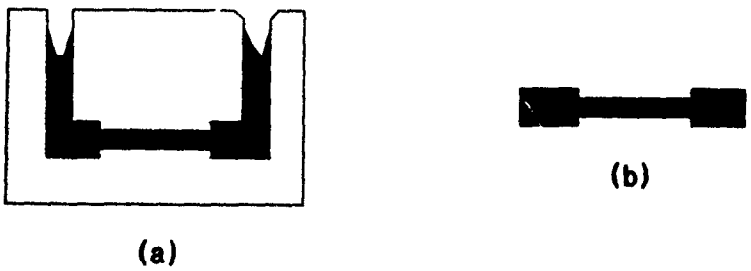

Figure 2.3: Solid casting: (a) casts into a solid piece; (b) and casting is removed after partial drying.

content in the cake and maximize the filtration rate. Because of the similarity in the processes the ceramists have recently become interested in filter pressing and can borrow theory and techniques from the chemical engineering filtration literature.[18]

2.1.3 DENSIFICATION

Green compacts are converted into a dense polycrystalline solid by a process known as sintering. Sintering is essentially a removal of the pores between the starting particles which results in: (1) shrinkage of the compact, (2) growth of the primary grains and (3) strong bonding between adjacent particles. The primary driving force for densification of a compacted powder at high temperature is the reduction in surface free energy. Differential surface curvature causes material to be transported to the contact region between touching particles and is described by the Gibbs-Kelvin equation:

$$\Delta G = \gamma_s V_m \left(\frac{1}{R_2} - \frac{1}{R_1}\right) \tag{2.2}$$

where ΔG is the change in free energy on going across the curved interface, γ_s is the surface energy per unit area, V_m is the atomic volume of the mobile species and R_1 and R_2 are the radii of the surface curvatures of the particles and the contact area between the two touching particles, respectively (see Figure 2.4). The radius R_2 is negative and small and R_1 is positive and large, therefore the free energy of the system will decrease (ΔG is negative) when mass is transferred to the region where the two particles contact one another.[2] This mass transport will lead to shrinkage and densification. As sintering proceeds a grain boundary forms for particles that are crystals.

Once initially touching particles sinter, adjacent sintered grains will have different radii of curvature that will drive interparticle mass transport and will result

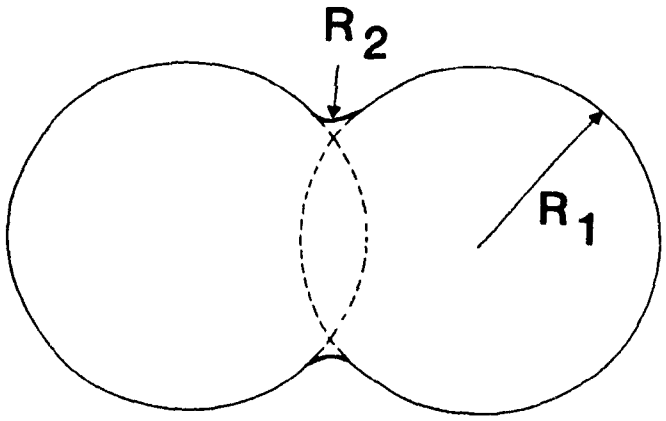

Figure 2.4: Schematic illustration of material transport.

in grain coarsening (grain growth). That is, smaller grains will disappear as larger grains grow. Therefore in a great majority of cases, two basic macroscopic aspects of densification may be distinguished. In the initial stage, adhesion of initially loose grains increases and a decrease in the volume fraction of pores takes place due to rearrangement of grains in the powder. The grains become more closely packed. At the next stage, pores are completely eliminated by the approach of grain centers and increase of the area of contact between the grains, due to mass transport from the intergrain contacts towards the pores.

Diffusion can consist of movement of vacancies along a surface or grain boundary or through the volume of the material. Surface diffusion may contribute to an increase in area of the grain contacts and, in this way, to greater cohesion of the assembly of grains. Surface diffusion can change the pore shape only and not the volume fraction of the pores (i.e., no shrinkage). Volume diffusion whether along the grain boundaries, or through the bulk volume of the grains, does result in shrinkage (see Figure 2.5).[19, 20, 21]

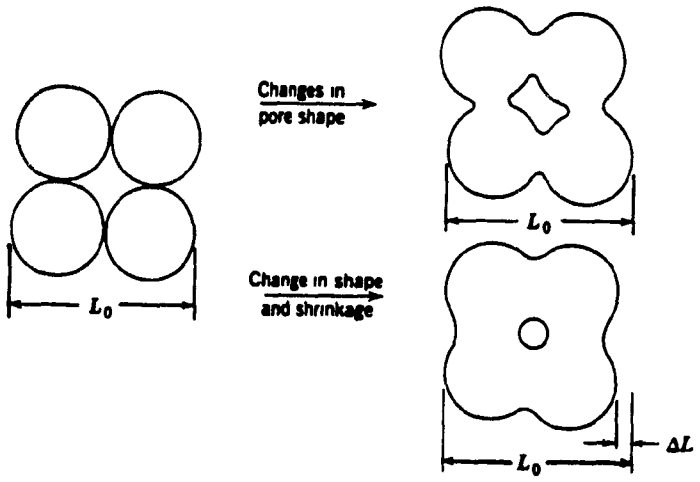

Figure 2.5: Surface and volume diffusion during sintering (after Ref. 19).

2.1.3.1 Effects of Particle Size and Green Microstructure

When sintering, the particle size and size distribution are important variables for achieving the optimum properties in the final powder compact. Typically, the finer the powder and the greater its surface area, the lower are the temperature and shorter time required for densification. This can be shown by the mathematical model developed by Kingery which determines the sintering rate.[19]

$$\frac{\Delta L}{L_o} = \left(\frac{20\gamma_s a_v^3 D^*}{\sqrt{2}kT}\right)^{2/5} r^{-6/5} t^{2/5} \tag{2.3}$$

where $\Delta L/L_o$ is the linear shrinkage (i.e. sintering rate), a_v^3 the atomic volume of the diffusing vacancy, D^* the self-diffusing coefficient, k the Boltzmann constant, T the temperature, r the particle radius (assuming equal-size spherical starting particles) and t is time.

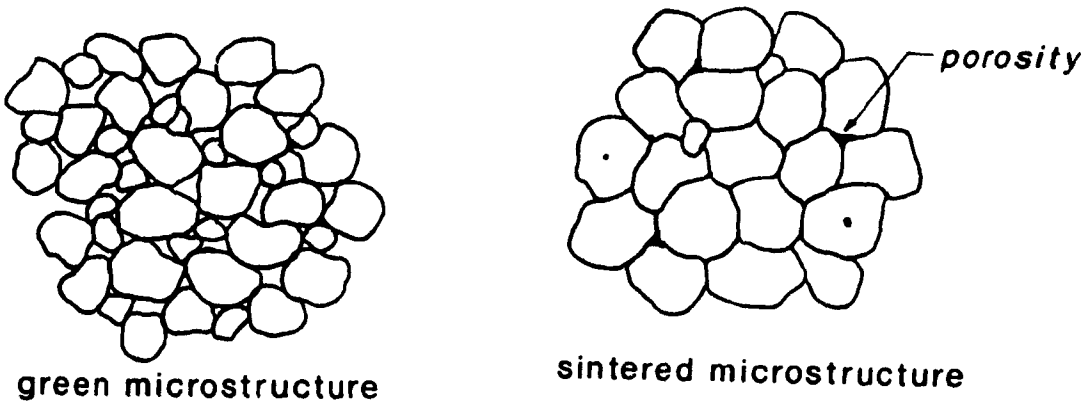

Figure 2.6: Schematic representation of a uniform green microstructure and the resulting uniform sintered microstructure.

For various Bayer alumina powders, a tenfold reduction in particle size reduces the sintering temperature by approximately 200 ^{0}C (with all else held constant)[22] and 0.01 μm powders will sinter 10^{6} - 10^{8} times faster than micron size powders.[23] A long time at a high temperature results in increased grain growth and lower strength. To optimize strength, a powder that can be densified quickly with minimal grain growth is desired.

In most cases the objective of the consolidation step is to achieve maximum particle packing and uniformity, so that minimum shrinkage and minimum residual porosity will result from sintering. Figure 2.6 schematically illustrates that a uniform green microstructure can result in a dense sintered ceramic with the grain size slightly larger than the particle size.

A controlled optimum particle size distribution is required to achieve maximum, reproducible strength. The strength is controlled by flaws in the material. A single particle which is significantly larger than the other particles in the distribution can

become the critical flaw that limits the strength of the final component. Similarly, a large void resulting from a nonhomogeneous particle size distribution or from particles too close to the same size may not be eliminated during sintering and may become the strength-limiting flaw.

Submicrometer-sized particles are sintered to reduce the sintering temperature and to obtain a fine-grain microstructure. A major problem of submicrometer-sized particulate technology is that in this size range particles spontaneously agglomerate due to van der Waals attractive forces. As a result, when these agglomerated units are used as the building blocks of a green compact, wide variations in pore-size distribution are inevitably introduced into the compact. Hard agglomerates retard sintering. Large voids result, caused by poor packing around aggregates (bridging of aggregates). Such voids, much larger than the surrounding grains, cannot be removed during sintering; as there is no driving force for elimination of such oversize porosity. Inhomogeneous sintering results due to a non-uniform packing density. Figure 2.7 schematically illustrates the effects that a non-uniform green microstructure has on the sintered microstructure. The small particles tend to dissolve into the larger ones, and allows the grain boundaries to pull away from the pores. Around isolated aggregates, the inhomogeneous shrinkage creates local microstresses which can lead to crack formation.[24, 25]

2.2 COLLOIDAL SUSPENSIONS

The formation of ceramic components with submicron size particles requires control over particle-particle interactions. In dry shape forming processes the particle-particle interactions are difficult to control because submicron size powders in the dry

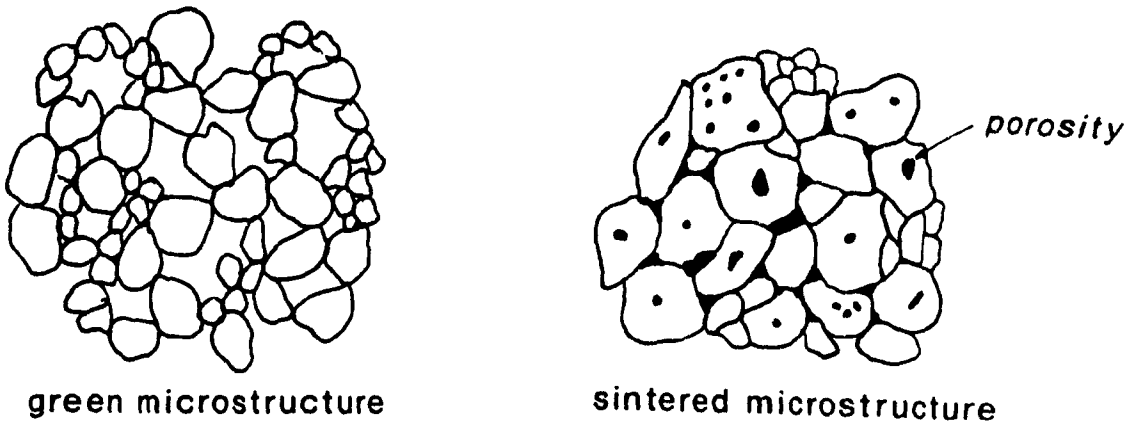

Figure 2.7: Schematic representation of a sintered microstructure with dense and porous regions resulting from a non-uniform green microstructure.

state spontaneously agglomerate due to van der Waals attractive forces which can result in heterogeneous microstructures.

Filtration of colloidal suspensions allow control over particle-particle interactions. The stability of a suspension with respect to flocculation depends on the relative magnitude of the attractive and repulsive forces of the particles involved. The state of dispersion of colloial suspensions influence particle packing during filtration and the resulting microstructure development during sintering.

In a poorly deflocculated suspension individual particles can form agglomerates that are referred to as "first-generation" agglomerates and aggregates of these first-generation agglomerates form "second-generation" agglomerates and so on. This concept of hierarchical agglomeration is schematically illustrated in Figure 2.8. Ascending levels of agglomerate hierarchy respectively associate with ascending sizes of interagglomerate pores. Schilling and Aksay[26] have shown that multi-generation agglomerates formed in the suspension can retain their shape in the filter cakes and the

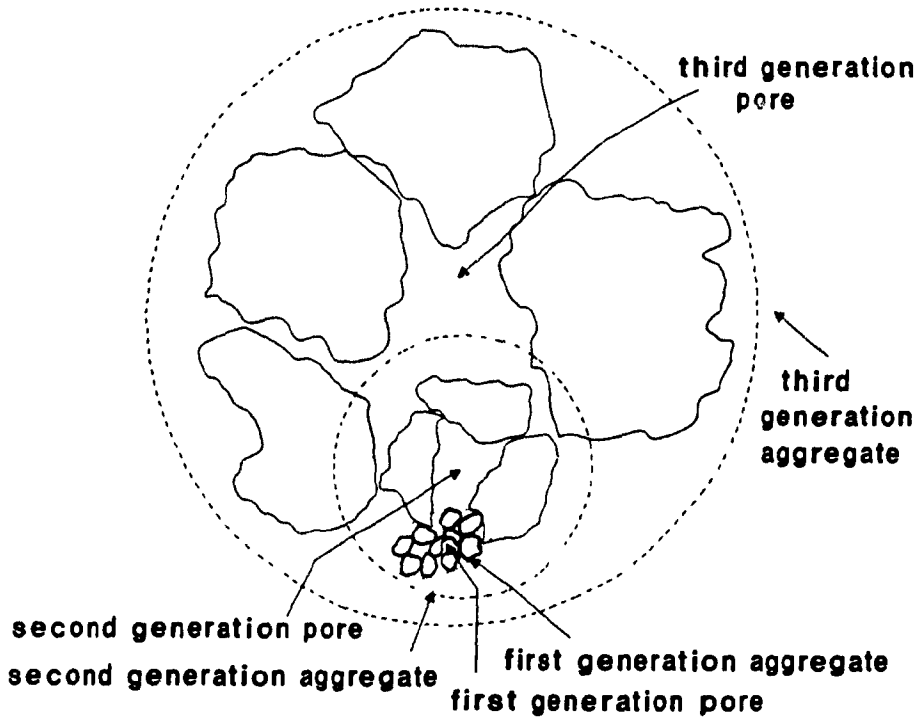

Figure 2.8: Schematic illustration of hierarchical agglomeration.

resulting sintered microstructures uniquely evolve according to the particle packing of the green microstructure. Well dispersed suspensions produce green microstructures mainly with first-generation pores that subsequently evolve during sintering into a dense ceramic with grains slightly larger than the particle size. In contrast, flocculated suspensions produce fewer first-generation pores and more second-generation pores resulting in a less densely packed and more open framework.

Often deflocculants are used to disperse a ceramic suspension. Deflocculants can be in the form of an electrolyte, polymer (long-chain molecules) or polyelectrolyte (ionic polymer). Therefore, a suspension can be dispersed through particle-particle repulsive forces resulting from electrostatic interaction, the interaction of polymers or a combination of both.[27, 28]

2.2.1 VAN DER WAALS FORCES

London showed that an attraction exists between all molecules (van der Waals attraction). The van der Waals force may be visualized by the following. In a neutral molecule the electrons generate a rapidly fluctuating dipole moment. The frequency of the fluctuation is of the order of 10^{15} or 10^{16} per second. Interaction of these fluctuating dipoles between molecules leads to attraction.[29]

The van der Waals attraction energy between two spheres of the same nature, with radius r and center-to-center distance d_c, is given by:[27]

$$V_{att} = \frac{-H_A}{6}\left(\frac{2r^2}{d_c^2 - 4r^2} + \frac{2r^2}{d_c^2} + \ln\left(\frac{d_c^2 - 4r^2}{d_c^2}\right)\right) \tag{2.4}$$

where H_A is the Hamaker constant, which depends on the properties of the particles and dispersion medium. Its value generally varies between about 10^{-20} J and 10^{-19} J. For the shortest distance d between the sphere surfaces not greater than 10 nm to 20 nm and when $d \ll r$, van der Waals attraction energy can be approximated by:[30]

$$V_{att} = \frac{-H_A r}{12d}. \tag{2.5}$$

2.2.2 ELECTROSTATIC FORCES

In most cases, when an electrolyte is added to a suspension, the colloidal particles will possess an electrostatic charge due too a tightly adhering layer (Stern layer) adjacent to the particle surface which contains adsorbed ions. Oxide surfaces in an aqueous medium are generally charged positively under acidic and negatively under basic conditions.[28] However, a colloidal solution as a whole must be electrically neutral because the charge of the particles is neutralized by an equal amount

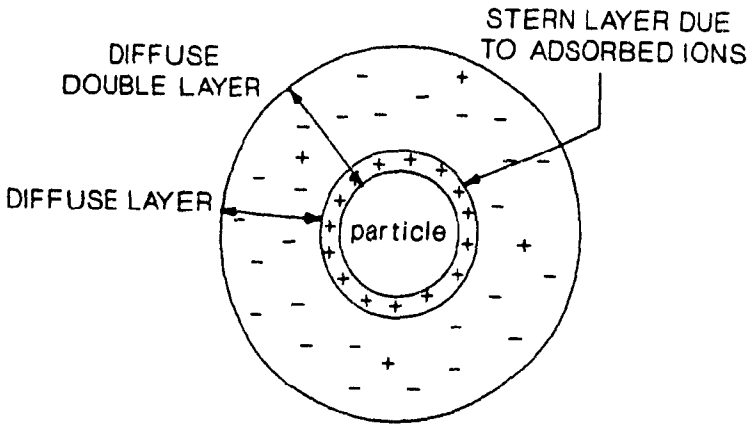

Figure 2.9: Electrically charged particle surrounded by a diffuse double layer.

of counter-charges (or counter-ions) in the system. The excess of counter-ions will be centered around the charged particle, forming a so-called diffuse double layer or electrical double layer around it (see Figure 2.9).[31]

When two of these such particles approach each other, their double layers start to overlap, giving rise to a repulsive force which increases with the inverse of the distance between the particles. As illustrated in Figure 2.10, the electrostatic repulsion falls off as an exponential function of the distance between the particles. The distance at which the repulsive forces become significant increases with the thickness of the electrical double layer, $1/\eta$:[32, 33]

$$1/\eta = \left(\frac{\epsilon\epsilon_o M_R T}{F^2 \sum n_i z_i^2}\right)^{1/2} \tag{2.6}$$

where ϵ_o is the permittivity of the vacuum, ϵ is the relative permittivity* (= dielectric

*for water $\epsilon = 80$

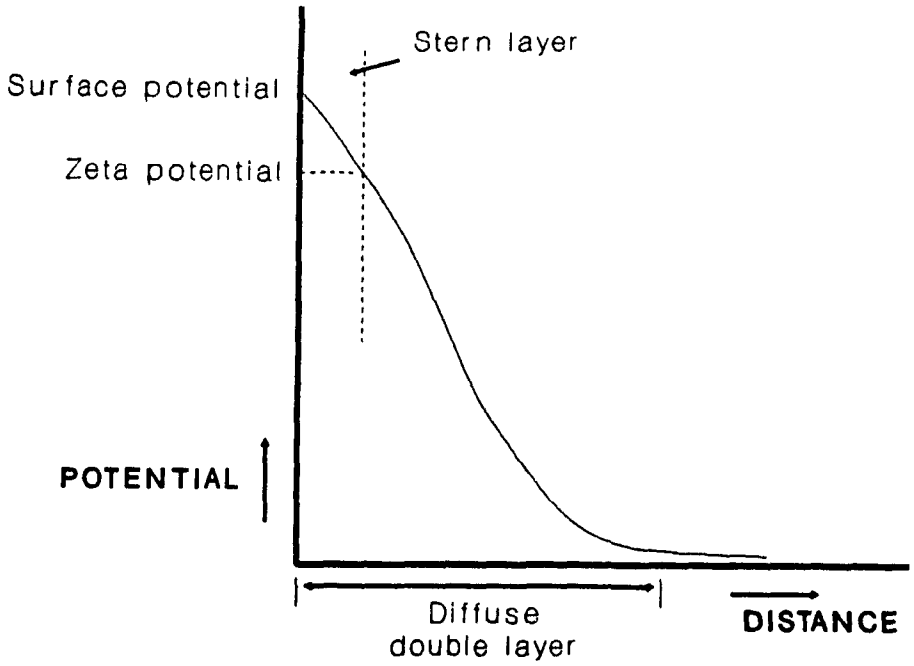

Figure 2.10: Schematic representation of the diffuse double layer model.

constant) of the dispersion medium, M_R is the gas constant, T is the absolute temperature, F is the Faraday constant, n_i and z_i are the concentration and the charge number of the ions of type i in the dispersion medium. For symmetrical electrolytes (only one electrolyte with ions of charge number $+z$ and $-z$),

$$1/\eta \approx 3 \times 10^{-10} z_i^{-1} n_i^{-1/2}\ (m) \qquad at\ T = 298\ K \tag{2.7}$$

where n_i is in units of moles/liter. For small zeta potentials, ζ and small values of $exp(-\eta d)$ an approximation for the electrostatic repulsion is:[27]

$$V_R = 2\pi\epsilon\epsilon_o r\zeta^2 \exp(-\eta d). \tag{2.8}$$

The zeta-potential is the potential at the plane of shear. It is assumed that liquid

within the plane of shear is bound to the surface. The plane of shear and Stern plane are nearly identical.[1, 34]

The higher the zeta potential of the particles, the larger are the repulsive forces between two approaching particles. A simplified relationship exists between ζ, the surface charge, J_s, and the diffuse double layer thickness for spherical particles:[30, 35]

$$\zeta = \frac{J_s}{4\pi\epsilon\epsilon_o}\left(\frac{1}{r} - \frac{1}{r + 1/\eta}\right). \tag{2.9}$$

As the electrolyte concentration in a suspension is increased the surface charge density will increase (thereby increasing ζ) if the potential determining ions are of the same charge sign as the particles. However, this causes the diffuse double layer thickness to decrease (thereby decreasing ζ). Therefore, there is an optimum amount of an electrolyte that can be added to a suspension to produce maximum deflocculation.

2.2.3 FORCES DUE TO POLYMERS

Adding polymers to a colloidal suspension affects the stability of the suspension. Adsorption of polymers onto the particles either stabilize or destabilize the dispersion. When two polymer-coated particles approach one another repulsion (steric hindrance) can occur due to two effects: (1) If the length of the dangling chains or loops is larger than the distance between the surfaces, their segment density distribution and segment configuration will change (volume restriction effect). This will lead to a decrease in entropy (i.e., decrease in disorder). (2) Furthermore, because the concentration of the polymer will be higher in the gap than in the solution, there exists an osmotic pressure difference between the gap and the bulk resulting in an increase in enthalpy. In general the quantitative influence of the osmotic effect is the more important of the two. The change in the Gibbs free energy, ΔG, of the system

is given by:

$$\Delta G = \Delta E_H - T\Delta E_S \tag{2.10}$$

where E_H is the enthalpy, T the absolute temperature, and E_S the entropy. The force between two colloidal particles in the presence of a polymer can be found from:

$$F_p = \frac{-d\Delta G}{dx}. \tag{2.11}$$

Repulsion increases with the chain length, with the quality of the solvency of the dispersion medium for the chains and with the number of chains per unit area.

Polymers can lead to attraction rather than repulsion if the particles are only partly covered with a polymer, and the adsorbed polymer forms a macromolecular bridge by adsorbing on two particles simultaneously (bridging flocculation). Attraction can also occur if the particles are suspended in a poor solvent where the intramolecular expansion factor, χ is less than 1. The intramolecular expansion factor is a measure of the solvency of the dispersion medium for the stabilizing polymers. At $\chi = 1$ the repulsive potential is 0. A decrease in solvency of the dispersion medium leads to contraction and increased entanglement of the polymer coil

Polymers may have no affinity to the surface of a colloidal particle and remain free in the solution. Repulsion will occur between two approaching particles because the free polymers must be squeezed out of the gap between the particles (depletion stabilization). However, at small separations the gap contains no polymer and therefore an osmotic-pressure difference exists between the gap and solution. This results in an attraction between the particles due to the liquid wanting to leave the gap (depletion flocculation).[36]

2.3 THEORY OF SLIP CASTING AND FILTER PRESSING

The theory of slip casting and filter pressing is governed by the laws of flow through porous media.[37, 38] During filtration, the solid particles originally suspended in the filtrate are deposited at the surface of the filter medium while the filtrate passes through it. A pressure gradient across the filter cake and medium is required to drive the filtrate through the two porous media. In filter pressing the pressure gradient can be due to an externally applied pressure. In slip casting the pressure gradient results from the porous structure of the mold. The frictional force due to the filtrate balances the driving force due to the pressure gradient. The frictional forces, therefore control the flow rate and rate of cake deposition. An understanding of the interplay of the hydraulic pressure, flow resistance and flow rate are essential to the theory of slip casting and filter pressing.

Some of the earlier studies dealing with the mechanics of colloidal consolidation incorrectly treated the case as a diffusional process.[39, 40] In 1957, Adcock and McDowall[11] were the first to analyze the slip casting process as a filtration problem. However, their model only considered the flow of the filtrate through an incompressible cake and neglected the flow resistance of the mold. Dal and Deen[12] later improved the slip casting model by taking into account the resistance to flow that occurs due to both the cake and mold. Their model was later verified by Aksay and Schilling.[13]

Tiller and co-workers have also studied and analyzed the internal flow mechanism in cakes formed by slip casting[41] and filter pressing.[42–50] Tiller has further extended the slip casting model to account for cake compressibility.

It is customary to divide the mathematical analysis of filter operations into two parts; (a) the mechanism of flow within the cake and (b) the external conditions

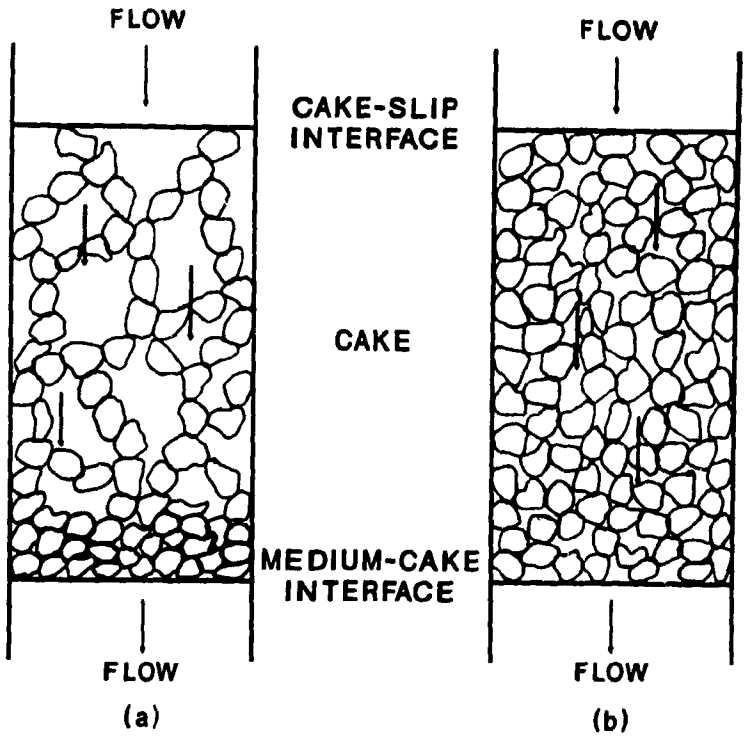

Figure 2.11: Schematic diagram of (a) a compressible and (b) an incompressible cake structure.

imposed upon the filter cake by the filtering system.[44] In analyzing the internal flow (i.e., within the cake itself) it must be recognized that the distribution of hydraulic pressure, P_l and cake porosity are functions of distance through the cake, x whereas the volume of filtrate per unit area, W and cake thickness, L are functions of time, t.

It is well established that flocculated slips always result in a cake that is more loosely packed at the cake-slip interface than at the filter medium-cake interface. The compressible cake is characterized by variation in porosity with distance through the cake. However, deflocculated slips result in a more uniform density throughout the thickness of the cake.[28]

Figure 2.11 illustrates schematically a flocculated (compressible) and a deflocculated (incompressible) cake structure. Flow is from the slip through the cake and

through the filter medium. For a compressible cake (Figure 2.11(a)), maximum porosity occurs at the cake-slip interface ($x = L$). The drag force imparted to the particles results in a compaction process that causes the porosity to decrease; thus, the porosity is a minimum at the filter medium-cake interface. For an incompressible cake (Figure 2.11(b)), the porosity is constant throughout the cake.

2.3.1 PRESSURE DISTRIBUTION

The applied pressure, P or more specifically for slip casting, the capillary suction pressure of the mold, causes the filtrate to flow into the mold leaving behind layers of deposit (cake) through which subsequent liquid must flow. The hydraulic pressure, P_l drops throughout the cake and mold due to the liquid flowing frictionally past the particles of both the cake and mold. The positive pressure developed at the cake-slip interface due to the head of the slip is negligible compared to the suction pressure. Therefore, the drop in hydraulic pressure from the cake-slip interface to the liquid-vapor interface in the mold (or filter medium) is equal to the suction pressure of the mold (or applied pressure). This pressure drop is the sum of the drops across the cake, ΔP_c and mold, ΔP_m:

$$P = \Delta P_c + \Delta P_m \tag{2.12}$$

Figure 2.12 shows a schematic diagram of the pressure distribution.

2.3.2 VARIATIONS IN CAKE DENSITY

The particle size, shape, size distribution, solids content of the slip as well as the degree of stability (in terms of flocculation) all affect the cake density. Cakes of equivalent masses may have different volumes. Therefore, a material balance based upon volume is required for the slip, cake and filtrate.

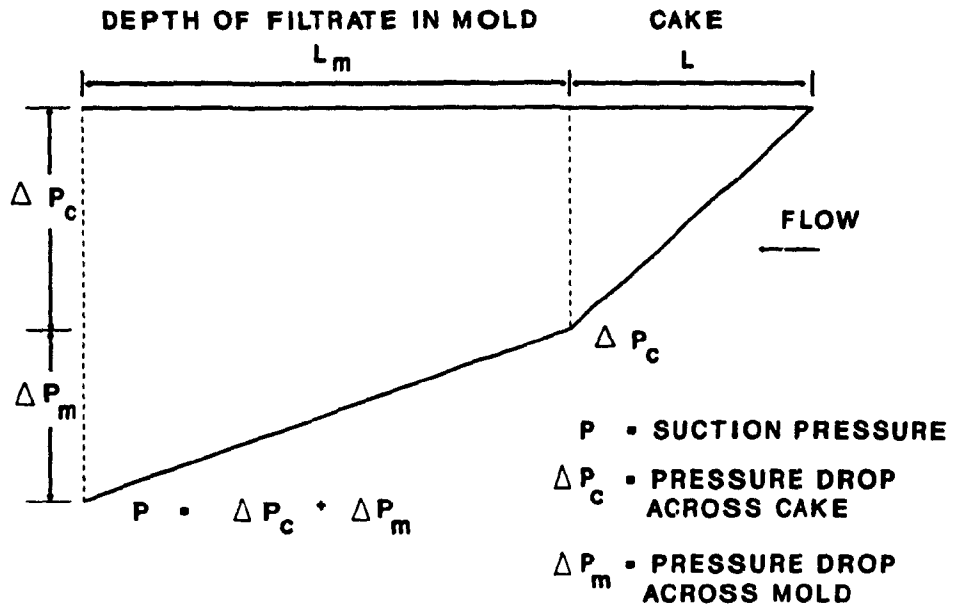

Figure 2.12: Schematic diagram of the pressure distribution across the cake and mold for an incompressible cake.

The volume of slip must equal the volume of cake plus the volume of filtrate. A volumetric balance on a unit cross-sectional area gives:

$$\frac{\omega_c}{\epsilon_{sl}} = \frac{\omega_c}{\epsilon_{cav}} + W \tag{2.13}$$

and

$$\omega_c = \epsilon_{cav} L \tag{2.14}$$

where ω_c is the volume of solids per unit area in the cake, L is the cake thickness, ϵ_{sl} and ϵ_{cav} are the volume fractions of solids in the slip and cake, respectively and W is the volume of filtrate per unit area. Substituting equation (2.14) into (2.13) and rearranging yields:

$$W = L(\epsilon_{cav}/\epsilon_{sl} - 1) \tag{2.15}$$

For slip casting where the filtrate is permeating a distance L_m into a mold:

$$W = \epsilon_m L_m \tag{2.16}$$

where ϵ_m can be considered to be constant and is the volume fraction of water in the wetted part of the mold. The cake thickness can be related to L_m by combining equations (2.15) and (2.16):

$$\frac{L_m}{L} = \frac{\epsilon_{cav}/\epsilon_{sl} - 1}{\epsilon_m} \tag{2.17}$$

These volume balance relationships are combined with flow equations in the following section to obtain an expression for the growth rate of the cake thickness.

2.3.3 FLOW THROUGH POROUS MEDIA

Flow through porous media is described by Darcy's law:

$$\frac{dP_l}{dx} = \mu q/K \tag{2.18}$$

where μ is the viscosity of the filtrate, q is the apparent flow rate per unit area and dP_l/dx is the pressure gradient. The proportionality factor K is called the permeability and only depends on the structure of the porous medium. The flow rate, q is the same in both the mold and cake. By integrating the above equation over the cake thickness the pressure drop across the cake, ΔP_c is determined:

$$\int_{-P_c}^{0} dP_l = \Delta P_c = \int_0^L \mu q/K dx = \mu q L/K_c \tag{2.19}$$

where K_c is the permeability of the cake. Similarly, by integrating equation (2.18) over the depth of penetration of the filtrate into the mold, L_m the following expression

is obtained for ΔP_m:

$$\int_{-P}^{-P_c} dP_l = P - \Delta P_c = \int_{-L_m}^{0} \mu q/K dx = \mu q L_m/K_m \tag{2.20}$$

where K_m is the permeability. By dividing equation (2.19) by (2.20) and solving for ΔP_c yields:

$$\Delta P_c = \frac{P}{(L_m K_c)/(LK_m) + 1} \tag{2.21}$$

Substituting equation (2.17) into (2.21) yields:

$$\Delta P_c = \frac{P}{\frac{\epsilon_{cav}/\epsilon_{sl}-1}{\epsilon_m}(\frac{K_c}{K_m}) + 1} \tag{2.22}$$

For compressible cakes, Tiller has considered K_c and ϵ_{cav} to be unique functions of ΔP_c. Equation (2.22) shows that ΔP_c is independent of time and is therefore a constant. As soon as liquid penetrates the mold and a cake begins to form, the equilibrium ΔP_c is reached and remains constant throughout the process. Consequently, ϵ_{cav} and K_c also remain constant.

In filter pressing, the medium (filter paper) has a constant resistance (L_m/K_m) since L_m is constant but the cake resistance (L/K_c) increases with time. As the cake builds up, ΔP_c increases with time.

2.3.4 GROWTH RATE OF CAKE THICKNESS

Using Darcy's law a relationship for the variation of cake thickness with time can be found. From equations (2.15), (2.19) and (2.22) it is found that:

$$q = \frac{dW}{dt} = \frac{dL}{dt}(\epsilon_{cav}/\epsilon_{sl} - 1) = \frac{P}{\mu L((\frac{\epsilon_{cav}/\epsilon_{sl}-1}{\epsilon_m})(\frac{1}{K_m}) + \frac{1}{K_c})}. \tag{2.23}$$

Integrating the above equation shows that the cake thickness is proportional to the square root of the casting time:

$$\begin{aligned} L^2 &= \frac{2Pt/\mu}{(\epsilon_{cav}/\epsilon_{sl}-1)(\frac{1}{K_c}+\frac{(\epsilon_{cav}/\epsilon_{sl}-1)}{\epsilon_m K_m})} \\ &= Bt \end{aligned} \tag{2.24}$$

where B is a constant.

2.4 MIGRATION OF FINE PARTICLES

The filtration process is not as straightforward as the above theory indicates. As described by Heertjes[66], two important conditions that can lead to results different from those predicted by theory is: (1) The filter medium resistance is not just that of the medium but results from cake and filter medium interactions at the start of filtration. (2) Fine particles can migrate in the cake.

The beginning of cake filtration is usually different from the rest of the process and depends on interactions between the particles of the slip and filter medium. In general, the filter medium is inhomogeneous. The pores of plaster of Paris molds or filter paper are not uniform in size and are unevenly distributed over the surface. Therefore, over the surface of the filter medium, the local flow-rate of the filtrate will show large differences leading to inhomogeneity of the cake.

During filtration the permeability of the filter medium need not be constant. Some particles, depending on the ratio of pore diameter to particle diameter can either enter a pore or cover the pore opening. Clogging of the filter medium pores will cause a decrease in filter medium permeability. The filter medium permeability will also

decrease if particles that are very small with respect to the pore diameter adsorb onto the pore walls and reduce the pore radii. A derivation of the so-called blocking laws for filter media are presented by Hermia.[67] Rushton and Hassan[68] have studied filter medium clogging and bridging as a function of the medium pore structure, filtration velocity and slip concentration. They found that medium clogging is reduced with increase in slip concentration and filtration velocity.

Another effect which perturbs the simple theory is that of the migration of fine particles. The filtration theory assumes that when a suspension is passed through a filter medium the solid particles are deposited layer upon layer to form the cake. However, fine particles present in the slip can migrate through the cake. These particles may be completely leached out or may re-deposit in the cake and/or filter medium. The re-deposited fines can clog the free flow paths of the cake and/or filter medium and thus influence the cake and filter medium permeabilities.

Tiller and co-workers[44, 45] have shown that during the filtration of liquefied coal: (1) The permeability of the filter medium can decrease throughout the entire filtration process. (2) Variation in local cake permeability can occur due to deposition of small particles migrating through the pores.

Notebaert et al.[69] as well as Karr and Keinath[70] have studied clogging in filtration experiments. They observed deviations from straight line plots of total resistance versus volume of filtrate These deviations were a result of cake and filter medium clogging.

At present clogging during filtration is not fully understood. To account for migration and deposition of fine particles Tiller and Chow[42] have only suggested some empirical equations to describe the cake and filter resistances and no analyses of clogging during slip casting has yet been developed.

Chapter 3

RHEOLOGY OF ALUMINA SLIPS WITH DIFFERENT PARTICLE SIZE DISTRIBUTIONS

It is widely recognized that the characteristics of the slip plays a major role in determining the characteristics of the green microstructure formed during filtration.[15, 62-65] Uniformity of the green microstructure is essential for producing a compact with a high uniform density. Sintering of ideally packed green microstructures results in significantly reduced sintering temperatures, very little grain growth, reduced defect size and most importantly, a reliable final product. Control over the rheology (i.e., dispersion) of the slip is required to obtain a uniform microstructure. As discussed in the literature review, deflocculants in the form of an electrolyte, polymer or polyelectrolyte can be used to disperse colloidal suspensions. Particle-particle repulsion helps assure both the breakup of the soft agglomerates held together by van der Waals forces and the formation of a well-dispersed suspension. A knowledge of the rheological behaviour of suspensions is essential to gain quality control over the stability of the suspensions.

An experimental study of the rheological behaviour of alumina slips with different solids loadings, particle-size distributions, and amounts of deflocculant will be presented in this Chapter. Filtration experiments will demonstrate that the rheology of a slip greatly affects the green density and growth rate of the cake.

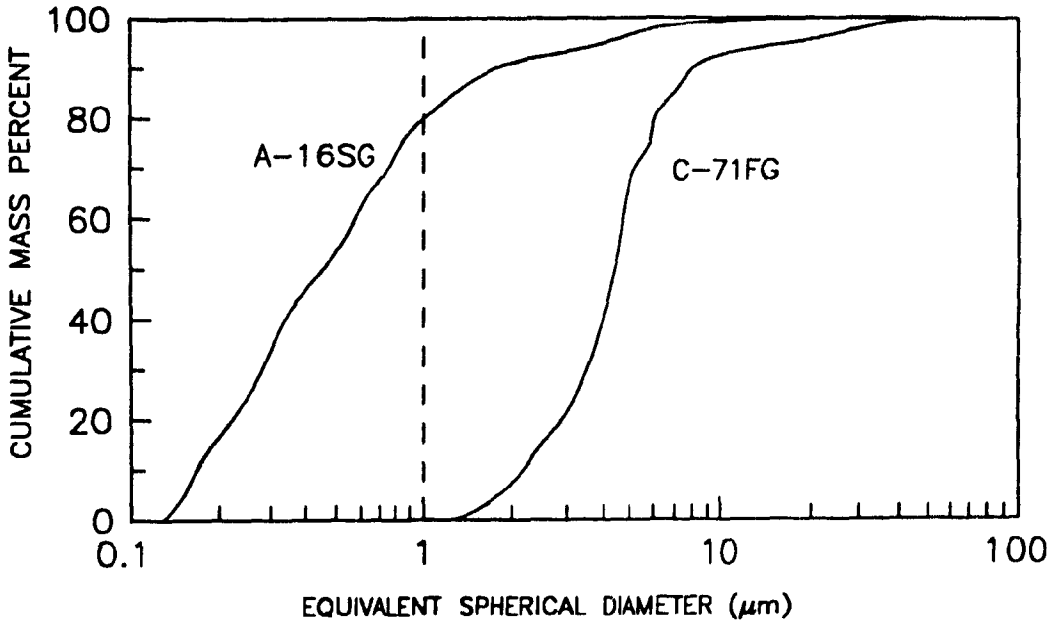

Figure 3.1: Particle size distribution curves for the fine and coarse alumina powders.

3.1 POWDER CHARACTERISTICS

A coarse (C-71FG), fine (A-16SG) and a mixture of these two grades of alumina powders were used for the rheological study and filtration experiments. The particle size distribution of each powder as measured by X-ray sedimentation (i.e., sedigraph) is shown in Figure 3.1 The coarse and fine powders had median particle sizes of 4.2 μm and 0.4 μm, respectively. Table 3.1 is a summary of the characteristics of the alumina powders.

Two types of deflocculants were used: (1) sodium polymethacrylate in an aqueous solution (Darvan 7), and (2) hydrochloric acid (HCl). Viscosity measurements were carried out to analyze the state of deflocculation of the alumina slips A model

Table 3.1: Properties of aluminas

Powder Grade	C-71FG	A-16SG
Al_2O_3, %	99.5+	99.5+
Na_2O_3, %	0.3	0.08
Median Particle size*	4.2	0.4
Surface Area, m^2/g	1	9
Thermal Reactivity	nonreactive	reactive
Purity	intermediate	high
Supplier	Alcan	Alcoa

*Measured by X-ray sedimentation

Source: Adapted from references 51, 52, and 53.

115 Rheomat viscometer, fitted with a cup and bob was used for the viscosity measurements.

3.2 DEFLOCCULATION AND VISCOSITY

Viscosity μ is defined as the ratio of the applied shear stress, τ to the shear rate, $\dot{\gamma}$:

$$\mu = \frac{\tau}{\dot{\gamma}} \tag{3.1}$$

Figure 3.2 shows different types of rheological behaviour. For a Newtonian fluid such as water, the viscosity is a material constant; there is a linear relation between τ and $\dot{\gamma}$ and its viscosity is low. If a small amount of particles is added and if they stay well dispersed in the water then a low Newtonian viscosity is still measured.

When the concentration of the suspension is increased, there are two possibilities:

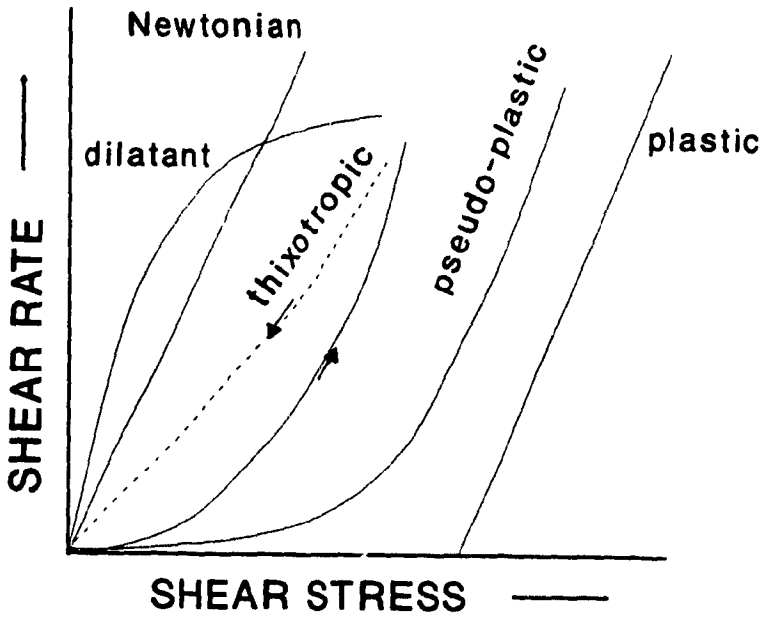

Figure 3.2: Different types of rheological behaviour.

(1) The system is an unstable, flocculated suspension, which means that the particles are aggregated. A shearing force has to overcome the structural forces. If this happens at a critical value of the shearing stress (i.e., the yield stress beyond which flow occurs more readily) a Bingham type of flow, or plastic behaviour occurs. If the structural forces are less well defined, a more continuous curve is measured and this type of flow is referred to as pseudo-plastic (or shear thinning)

(2) The system is deflocculated and for low rates of shear the fluid shows Newtonian behaviour, as no structural network is built up. However, with increasing shear rate the viscosity increases. This flow behaviour is referred to as dilatancy (or shear thickening). Dilatancy occurs when the concentration of a stable suspension is increased. A high shearing force presses the particles together in an irregular pattern and, as a result, the resistance to flow increases quickly with shearing stress.

Thixotropy can occur both in stable and in unstable suspensions. During flow there is continuous disruption and re-linking of interparticle bonds. The re-linking has a certain relaxation time and at high shear rates no re-linking occurs, resulting in a decrease in viscosity. Therefore, the "up" and "down" shear rate versus shear stress curves differ because of time effects. In many ceramic suspensions there is a combination of the different types of rheological behaviour described above.[54]

Deflocculation depends on the forces of attraction and repulsion between the particles. The suspension viscosity changes with the amount of deflocculant added. The lower the viscosity of a suspension for a given solids loading the better deflocculated it is because decreased flocculation increases the amount of liquid available in the slip for shear. Anderson and Murray[55] have shown that a low viscosity of a suspension is associated with a high zeta potential (i.e., well deflocculated) of the particles and vice versa.

3.2.1 ALUMINA SUSPENSIONS

To explain the rheological behaviour of alumina slips an understanding of the chemistry of alumina-water systems is essential. Particles present in the suspensions can be divided into two classes: those particles having colloidal dimensions that affect the rheological behaviour of the suspension upon addition of a deflocculant, and those particles larger than colloidal size that are inert and act as a filler in the suspension. A colloid is considered to be approximately 1 μm or less but this upper limit is somewhat arbitrary.

Each particle of alumina of colloidal size holds an attached water layer, and possesses a net charge at the outer edge of this layer due to the presence of preferentially adsorbed ions on the surface of the particle and counterions in the medium surrounding the particle.

In an acidic slip the preferentially adsorbed ions are hydrogen ions (H^+).[56, 57] In a basic slip, the hydroxyl ions (OH^-) are preferentially adsorbed or, for carboxylated (COO^-) based polymers it is the carboxylate ions that are preferentially adsorbed.[58, 59]

3.2.1.1 Hydrochloric Acid

The surface crystal structure of alumina is shown in Figure 3.3. When hydrochloric acid (HCl) is added to the alumina suspensions, HCl dissociates in the presence of water to produce hydrogen cations (H^+) and chloride anions (Cl^-). As the acid is added to the suspension, the hydrogen cations are adsorbed onto the surface of the alumina particles and the chloride anions act as the countercharges forming the diffuse layer surrounding the positively charged alumina particles (see Figure 3.3). This system gives rise to repulsive forces between particles and, under proper conditions, deflocculation results.

3.2.1.2 Darvan 7

Darvan 7 is a sodium polymethacrylate in an aqueous solution (i.e., polyelectrolyte) and has a pH of approximately 10. The chemical structure of sodium polymethacrylate [60] is shown in Figure 3.4. Because this ionic polymer has ionizable side groups (COONa) it will deflocculate the alumina suspensions both by electrostatic effects and polymeric adsorption.

Upon the addition of Darvan 7 to the slip hydroxyl (OH^-) as well as the polymers will tend to be adsorbed onto the alumina. The carboxylate (COO^-) anions and sodium (Na^+) cations will dissociate producing charged polymer side groups and will give the particles a negative surface charge. Since the suspension as a whole must be electrically neutral, the excess of positive ions (Na^+) over negative ions (COO^-) that

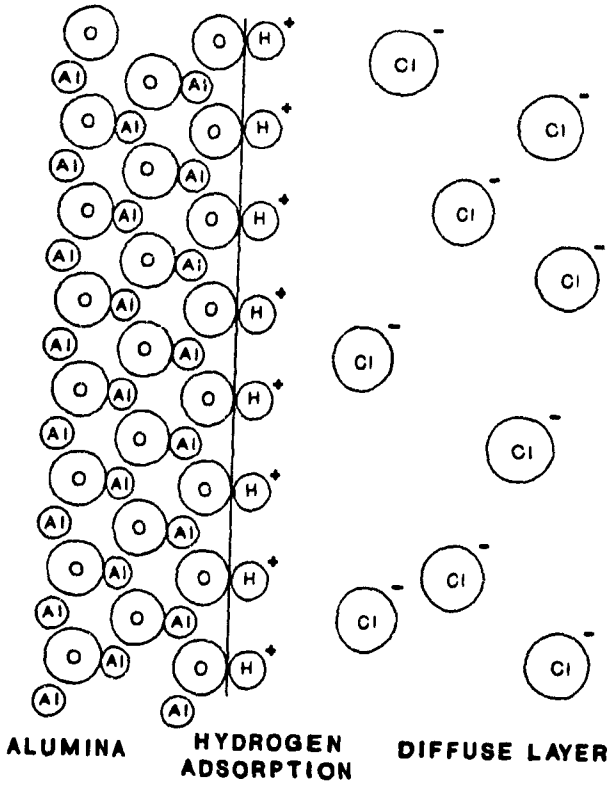

Figure 3.3: Adsorption behaviour of alumina in the presence of HCl.

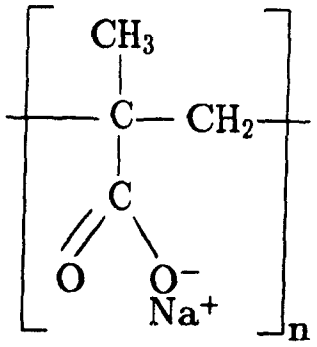

Figure 3.4: Chemical structure of sodium polymethacrylate.

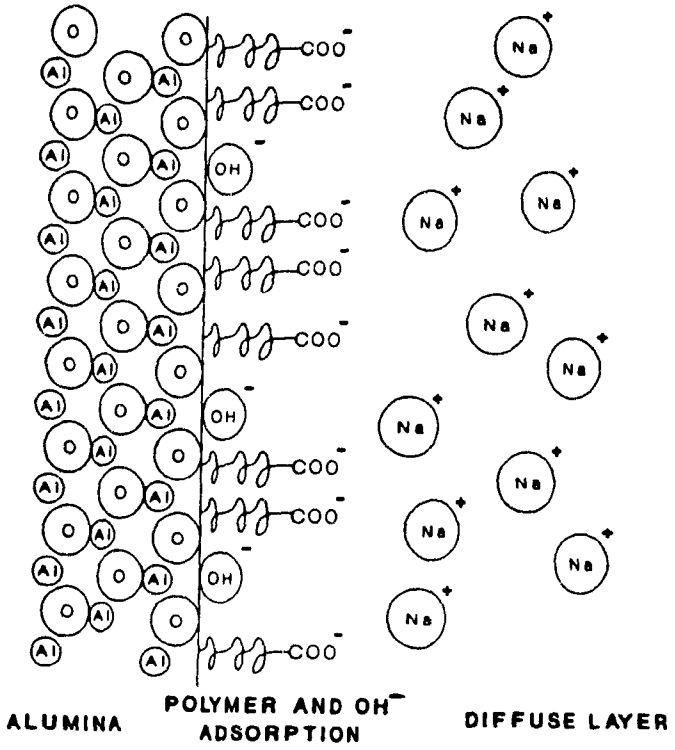

Figure 3.5: Schematic illustration of alumina suspension deflocculated using Darvan 7.

exist in the solution will surround the particles to form a diffuse layer of positively charged ions (see Figure 3.5). Thus, under appropriate conditions this system will produce repulsive forces between the particles.

3.3 SLIP RHEOLOGY

Figures 3.6, 3.7, 3.8 are graphs of viscosity versus volume concentration of Darvan 7 for A-16SG (fine powder) slips with different volume solids loadings, ϵ_{sl}. Volume concentration is defined as the volume of deflocculant per unit volume of slip

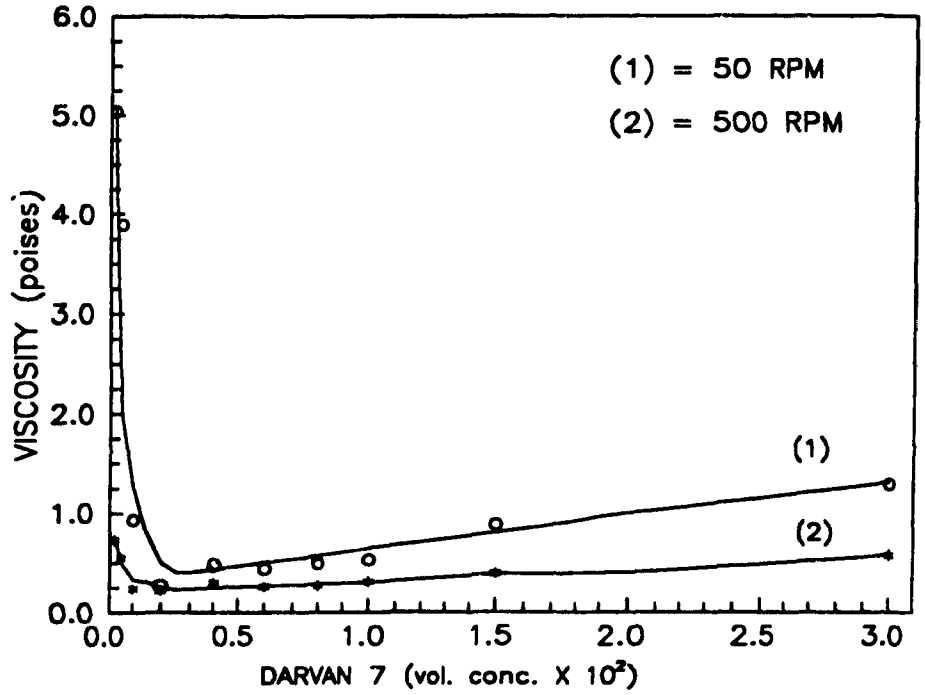

Figure 3.6: Viscosity versus deflocculant concentration for A-16SG slips; $\epsilon_{sl} = 0.39$.

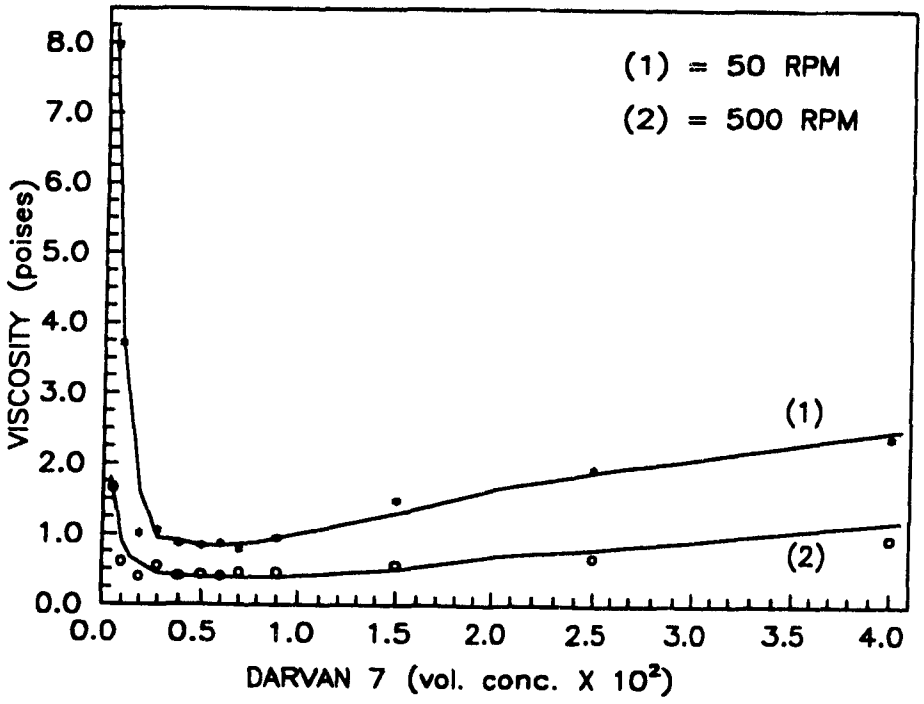

Figure 3.7: Viscosity versus deflocculant concentration for A-16SG slips; $\epsilon_{sl} = 0.43$.

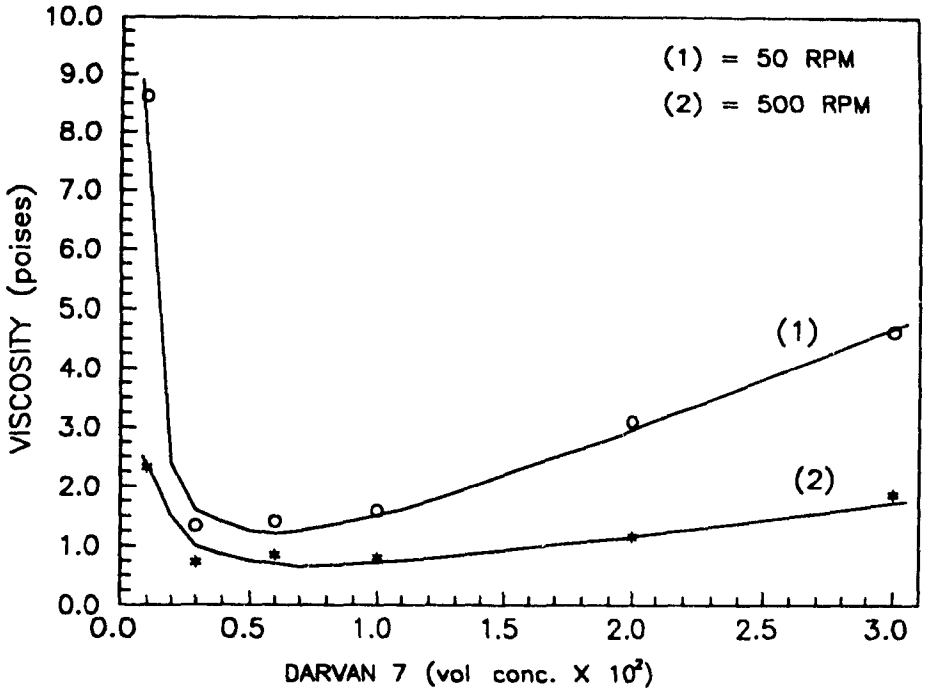

Figure 3.8: Viscosity versus deflocculant concentration for A-16SG slips; $\epsilon_{sl} = 0.47$.

and solids loading is defined as the volume of solids per unit volume of slip. The graphs show that slip viscosity initially decreases with increasing concentrations of Darvan 7 and, after a minimum in viscosity is reached (i.e., maximum deflocculation), a levelling off followed by a gradual increase in viscosity occurs. The viscosity versus deflocculant concentration curves for the C-71FG (coarse) powder and a 50/50 mixture of the coarse and fine powder had similar shapes to the A-16SG curves.

An increase in the amount of Darvan 7 added to the slip can result in two opposing electrostatic effects: (1) an increase in the zeta potential (i.e., decreases viscosity) because of an increase in the surface charge density and (2) a decrease in the zeta potential (i.e., increases viscosity) because the diffuse layer is compressed. It is also known that for adsorbing non-ionic polymers there is a compromise between attractive and repulsive forces. The repulsive forces arise from changes in entropy of the system when two surfaces coated with the polymer approach one another, begin to

interpenetrate and compress during the collision process. The attractive forces result from polymer bridging (segment-segment interaction). As a result of the opposing attractive and repulsive forces due to electrostatic and polymeric effects there is an optimum amount of Darvan 7 that must be added to the alumina slips to maximize deflocculation (i.e., minimize viscosity). This is illustrated in Figures 3.6-3.8.

The addition of Darvan 7 has much less effect on slip viscosity at a high shear rate (curve (2) in Figures 3.6-3.8). The differences in the viscosities for the two curves can be attributed to the shear-thinning (i.e., μ decreasing with increase in $\dot{\gamma}$) behaviour of the slips. Shear thinning can be a characteristic of a flocculated slip since, under low shear rate conditions, liquid is immobilized in the interparticulate void space of the flocs and floc networks. As the shear rate is increased, the flocs and floc networks break down and the entrapped liquid is released.[61] This shear thinning behaviour is illustrated in Figure 3.9. It is a graph of viscosity versus shear rate for A-16SG slips that contained an amount of Darvan 7 that maximized deflocculation (curve (1)) and poorly deflocculated the slip (curve (2)). Curve (2) is shear thinning to a much greater extent than compared to curve (1).

The viscosity is also dependent upon the solids loading, ϵ_{sl} of the slip as shown in Figure 3.10. The A-16SG slips in Figure 3.10 are at maximum deflocculation. With an increase in ϵ_{sl} the effective separation of the particles is reduced and increased interference between the particles causes an increase in the viscosity. The graph also shows that the slips are all shear thinning and this behaviour is more pronounced with increase in solids loading. Despite the large repulsive forces, the formation of flocs and floc networks is unavoidable under conditions of high solids loadings and low shear rates.

A-16SG slips were also deflocculated with hydrochloric acid (HCl). Figure 3.11

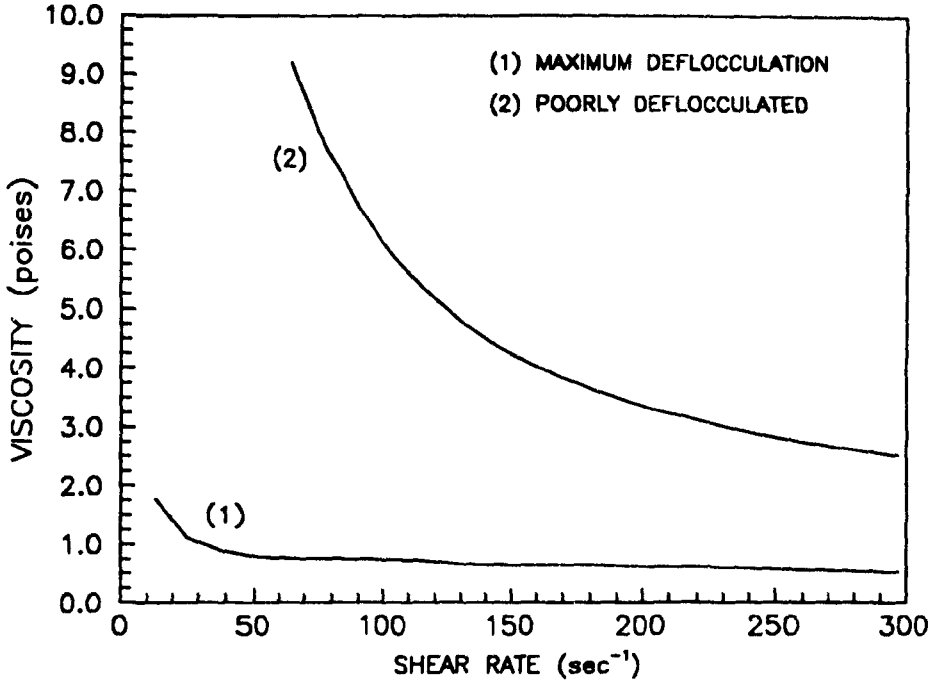

Figure 3.9: Viscosity versus shear rate for A-16SG slips; $\epsilon_{sl} = 0.43$.

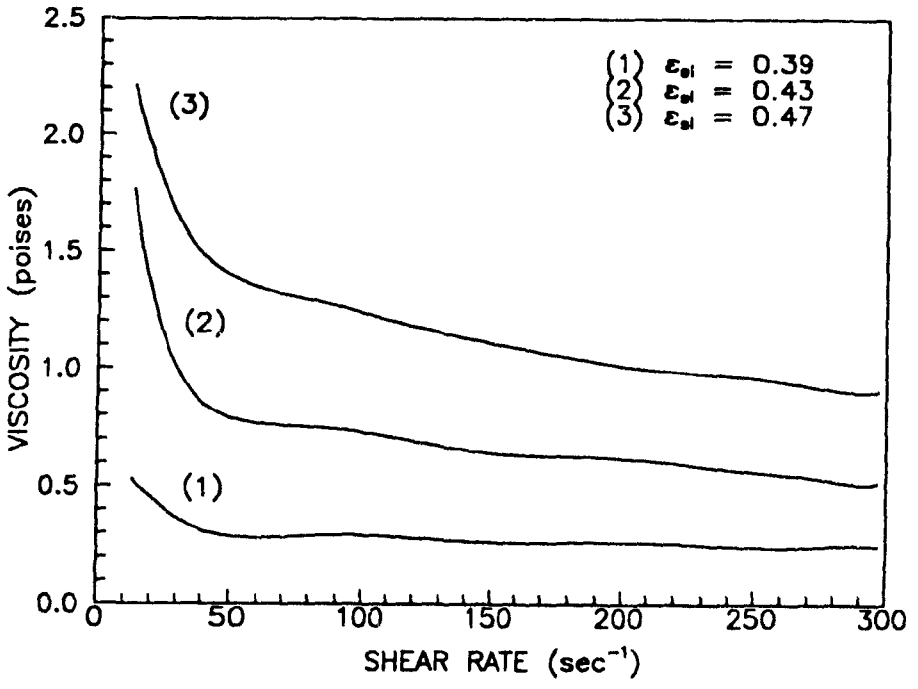

Figure 3.10: Viscosity versus shear rate for A-16SG slips with different solids loadings of slips at maximum deflocculation.

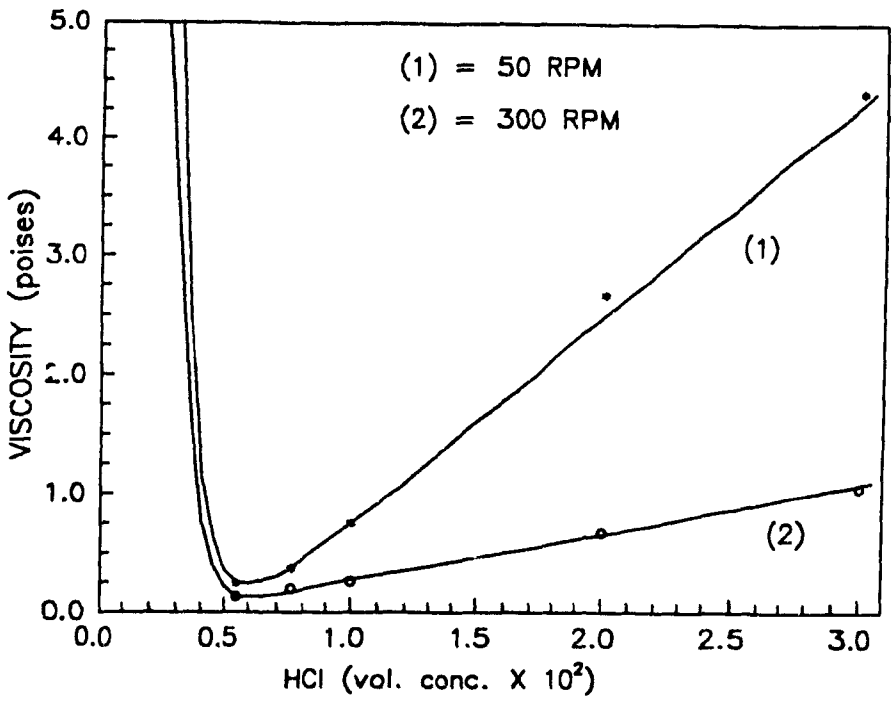

Figure 3.11: Viscosity versus deflocculant concentration for A-16SG slips; $\epsilon_{sl} = 0.39$.

is a graph of viscosity versus HCl volume concentration. As was also found for Darvan 7; viscosity decreased with increase HCl concentration and after a minimum viscosity was reached the viscosity gradually increased with increase in HCl concentration. The minimum viscosities obtained for the Darvan 7 and HCl slips are approximately equal.

The A-16SG powder has a larger proportion of colloidal-size particles than the C-71FG powder (Figure 3.1); therefore, each powder and the mixture of powders exhibit different rheological properties. Figure 3.12 shows viscosity versus shear rate curves for the three grades of alumina powder. The slips were at maximum deflocculation.

The slip that consisted of coarse (C-71FG) powder (curve (1)) was shear thickening. Shear thickening can be attributed to the solids forming a close-packed system.

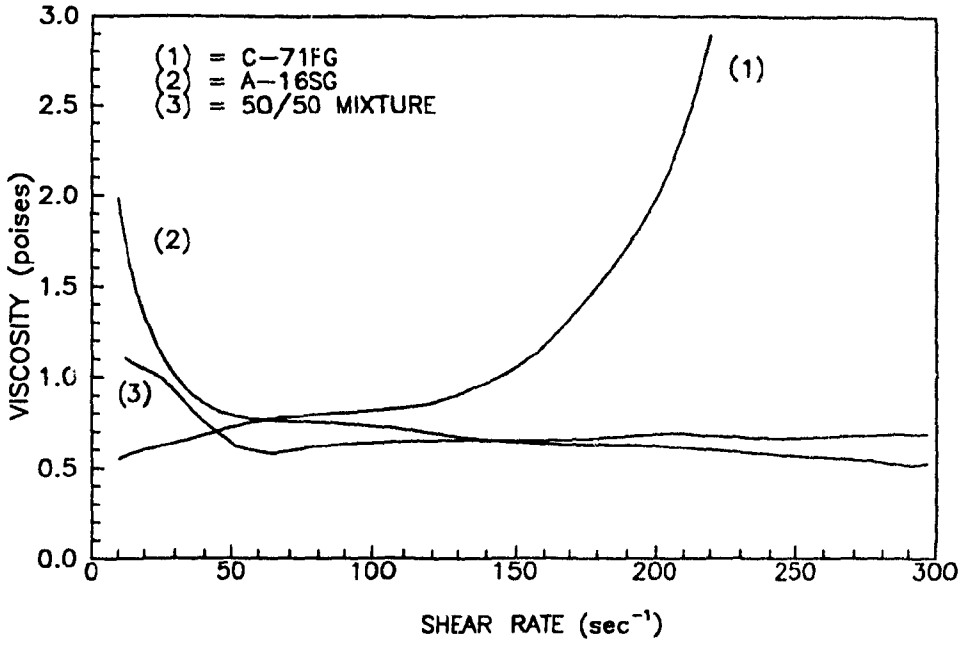

Figure 3.12: Viscosity versus shear rate curves for slips containing different size ranges of alumina; $\epsilon_{sl} = 0.43$.

Therefore, when the slip is subjected to a shear stress, the solids packing is disturbed and the packing density decreases. The liquid must flow through the narrow passages and fill the voids. At low shear rates, this occurs easily; however, at high shear rates, the flow becomes disordered, leading to an increase in viscosity.[56, 61] The particles must be deflocculated and be able to move freely over one another to assume these closed packed positions. The slip was well deflocculated due to the small fraction of colloidal particles in the C-71FG powder. Shear thickening was found to be more pronounced with increase in solids loading as a result of the smaller particle-particle separation distances.

Slips that contained a 50/50 mixture of coarse and fine alumina were initially shear thinning with an increase in the shear rate, reached a minimum viscosity, and then began to slightly shear thicken (curve (3)). This would appear to be a combi-

nation of curves (1) and (2), as might be expected.

In the following chapter it will be shown how the rheological properties of these slips affect the green microstructure and casting behaviour during filtration.

Chapter 4

EXPERIMENTAL INVESTIGATION OF PARAMETERS THAT AFFECT THE FILTRATION PROCESS

4.1 SLIP CASTING AND FILTER PRESSING EXPERIMENTS

To analyze the slip casting process one-dimensionally, beds of plaster of Paris about 70 mm deep were cast in 25 mm diameter glass tubes (see Figure 4.1). The tubes with the beds of plaster were dried at 80 ^{0}C to constant weights before use. During filtration, due to the difference in solids concentrations between the slip and cake, the slip-cake interface could be seen with the aid of a bright light. To analyze the rate of cake growth, the slip was poured into the tube and measurements of the cake thickness, L, as a function of time, t, were made. After the process had been allowed to continue for 1 hour, the excess slip was poured off the cake. The cake and the glass tube were dried and then the cake was removed from the tube so that its green density could be measured.

The experimental filter pressing assembly consists of a 40 mm (inner) diameter clear Plexiglass tube fitted with a perforated Plexiglass bottom plate. Filter paper rests on top of a metal grid that rests on top of the perforated Plexiglass plate. The top of the tube is capped by a horizontal plate that has an air inlet and a slip inlet. The slip inlet is sealed by a plug after the slip has been poured into the filter press

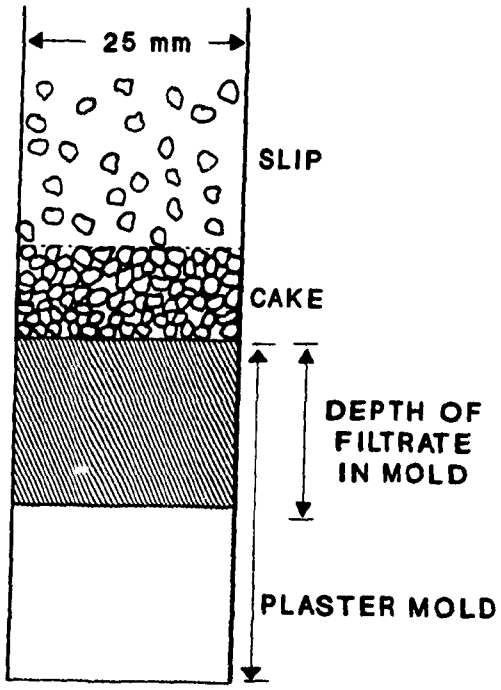

Figure 4.1: Slip casting apparatus.

(see Figure 4.2). The filter pressing operation is carried out by applying a steady air pressure to the top free surface of the slip. The filtrate drains out of the slip through the perforated bottom plate and the cake deposits on the filter medium. The lower section of the apparatus can be easily separated from the upper section to facilitate removal of the cake. Again, as with the slip casting experiments, the boundary between the cake and slip could be seen with the aid of a bright light and therefore the cake growth rate could be studied.

In this chapter, results of slip casting experiments will be presented and in the following chapter most of the results pertain to filter pressing experiments.

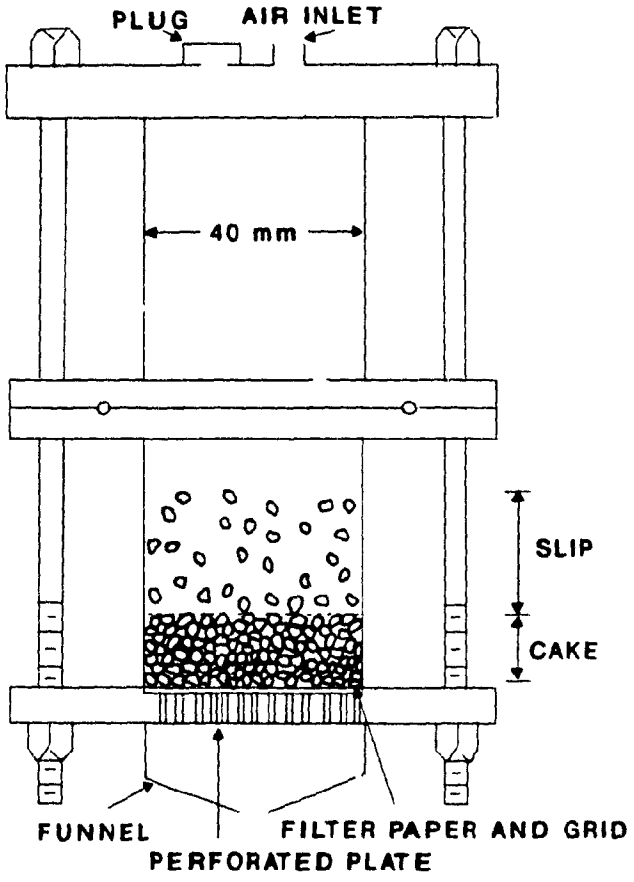

Figure 4.2: Filter pressing apparatus.

4.2 PLASTER OF PARIS MOLDS

Plaster of Paris is prepared commercially by calcining naturally occurring gypsum (calcium sulphate di-hydrate; $CaSO_4 \cdot 2H_2O$) at approximately 160 ^{0}C until about three-quarters of the water of crystallization has been driven off, leaving calcium sulphate hemi-hydrate ($CaSO_4 \cdot 0.5H_2O$) as the product:[71, 72]

$$CaSO_4 \cdot 2H_2O \rightleftharpoons CaSO_4 \cdot 0.5H_2O + 1.5H_2O. \tag{4.1}$$

Molds are formed by mixing water with the hemi-hydrate. At room temperature the solution is super-saturated with the calcium sulphate di-hydrate and so the di-hydrate crystallizes out and sets into a porous solid. The microstructure of the mold plays a vital role in the slip casting process because it is the mold pore structure that provides the capillary suction pressure and therefore affects the growth rate of the cake.

Capillary pressure is equal to:

$$P = \sigma_w \cos\theta / m \tag{4.2}$$

where σ_w is the surface tension of water, $\cos\theta$ defines the degree of wetting of the capillary walls and m is the hydraulic radius of the pores. The hydraulic radius, m is defined as the quotient of the volume and the internal surface area of the pores. Therefore, for complete wetting ($\cos\theta = 1$) of a circular tube of diameter, d_t:

$$P = 4\sigma_w / d_t. \tag{4.3}$$

In general, the finer the pore structure the greater the capillary pressure.

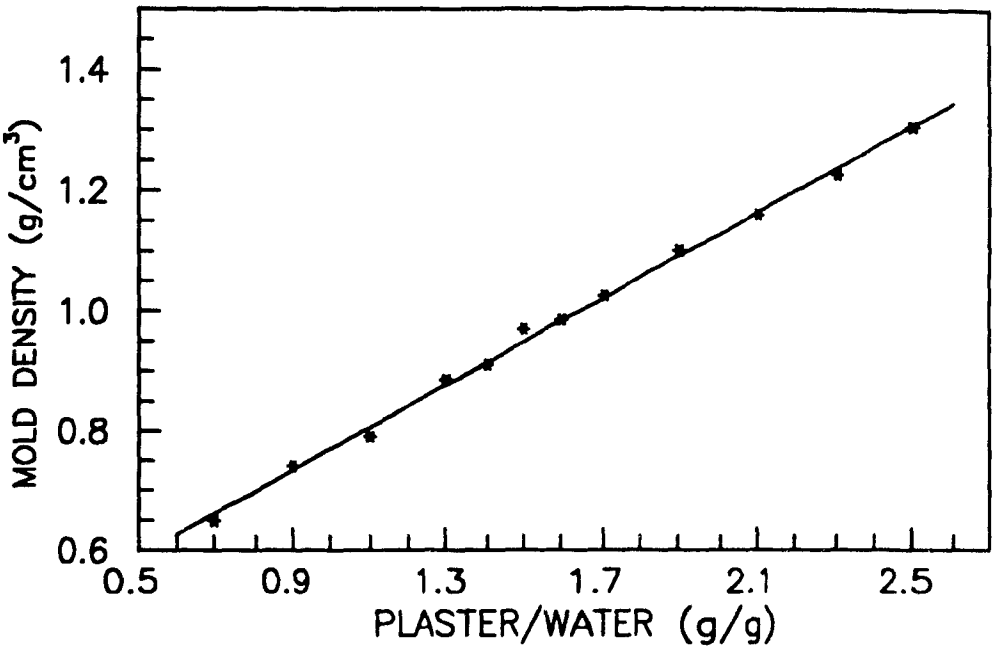

Figure 4.3: Mold density versus plaster/water ratio used to form the mold.

4.2.1 PLASTER/WATER RATIO

The microstructure of the mold is affected by the amount of water mixed with the plaster of Paris powder (i.e., plaster/water ratio) and also by the stirring rate and stirring time.[73] Figure 4.3 shows that the mold density increases significantly with the plaster/water ratio.

The microstructures of molds with different densities were examined to observe qualitatively what effect the change in mold density had on the pore structure. Figure 4.4 shows SEM micrographs of molds with three different densities. The gypsum crystals of the mold with the low plaster/water ratio of 0.9 (Figure 4.4(A)) have the largest aspect ratios and these lath shaped crystals are randomly stacked in bundles. However, the crystals of the mold with the high plaster/water ratio of 2.1 (Figure 4.4(C)) have much smaller aspect ratios and have a more disorderly crystal

packing arrangement.

Experiments were carried out to examine how the plaster/water ratio (i.e., mold density) affects the suction pressure and hence the filtration process.

According to Darcy's law, the suction pressure, P can be determined if the permeability, K_m of the mold and the flow rate, q of water through the mold are known:

$$P = \mu q \frac{L_m}{K_m}. \tag{4.4}$$

The flow rate can be expressed as:

$$q = \epsilon_m \frac{dL_m}{dt} \tag{4.5}$$

where ϵ_m, as defined earlier in section (2.3.2), is the fraction of water in the wetted p rt of the mold. Hence, the suction pressure can be expressed by the ratio of the square of L_m and time, t:

$$P = \frac{L_m^2}{t} \cdot \frac{\mu \epsilon_m}{2K_m}. \tag{4.6}$$

To obtain values for L_m^2/t and ϵ_m, water was poured into the glass tube and mold assembly. Measurements were then taken of the depth of penetration of the water, L_{m_i} and drop in head of water in the tube, $(H_o - H_i)$ as a function of time, t_i (see Figure 4.5). The volume fraction of water in the wetted section of the mold, ϵ_m is given by the following ratio:

$$\epsilon_m = \frac{(H_o - H_i)}{L_{m_i}}. \tag{4.7}$$

The permeabilities of the saturated molds were measured by using a method similar to the "falling head" permeability test used for fine-grained soil permeability

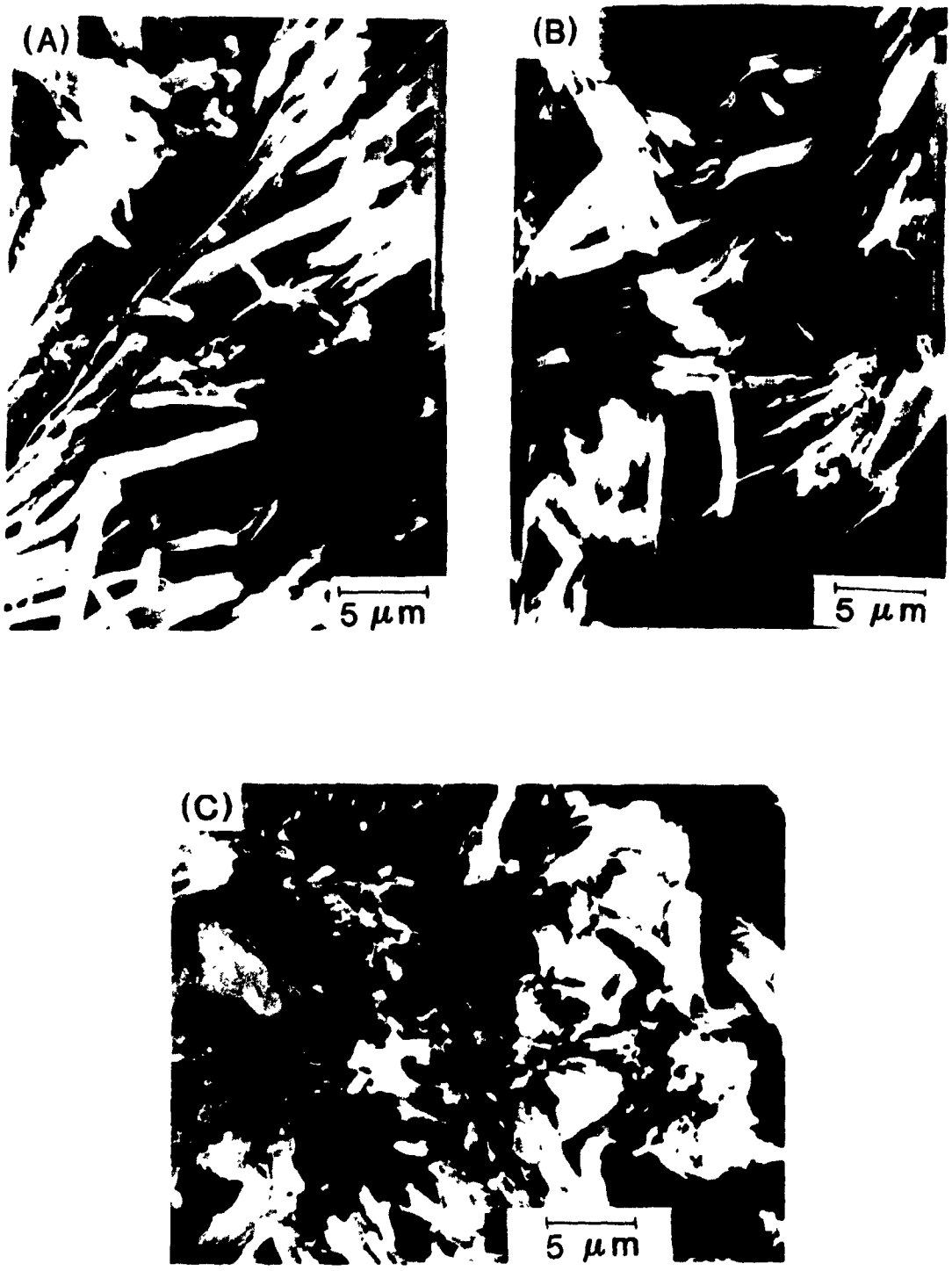

Figure 4.4: SEM micrographs of cross-sections of molds formed by using plaster/water (g/g) ratios of (A) 0.9, (B) 1.5, and (C) 2.1.

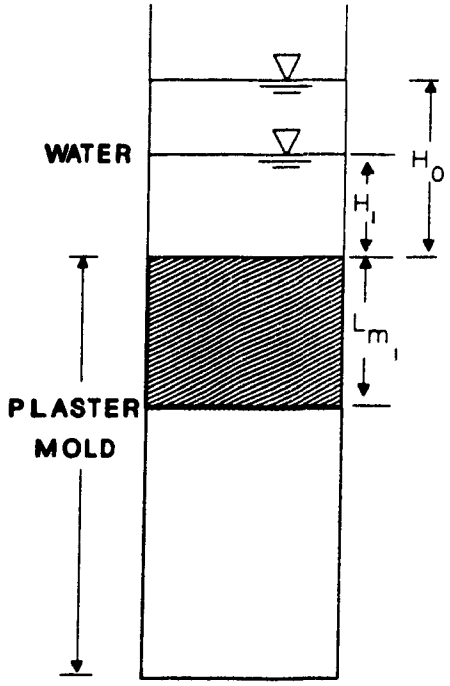

Figure 4.5: Depth of penetration of water into the mold, L_{m_1} and drop in head of water in tube at time, t_1.

measurements.[74] The experimental set-up is shown in Figure 4.6. The molds were tested in the glass tubes that they were originally formed in. The length of the mold is L_m and has a cross-sectional area A. A cork with a standpipe of internal area A_a is connected to the top of the tube. The tube rests on a coarse wire grid and sits in a dish filled with water. The water drains into the dish and spills over its sides. The dish serves as constant level reservoir. The standpipe is filled with water and a measurement is made of the time t_1 for the water level (relative to the water level in the dish) to fall from H_o to H_1. At any intermediate time t the water level in the standpipe is given by H and its rate of change by $-dH/dt$. At time t the difference in total head between the top and bottom of the mold is H. Therefore, applying Darcy's law:

$$-A_a\frac{dH}{dt} = \frac{AK_m\gamma H}{\mu L_m} \tag{4.8}$$

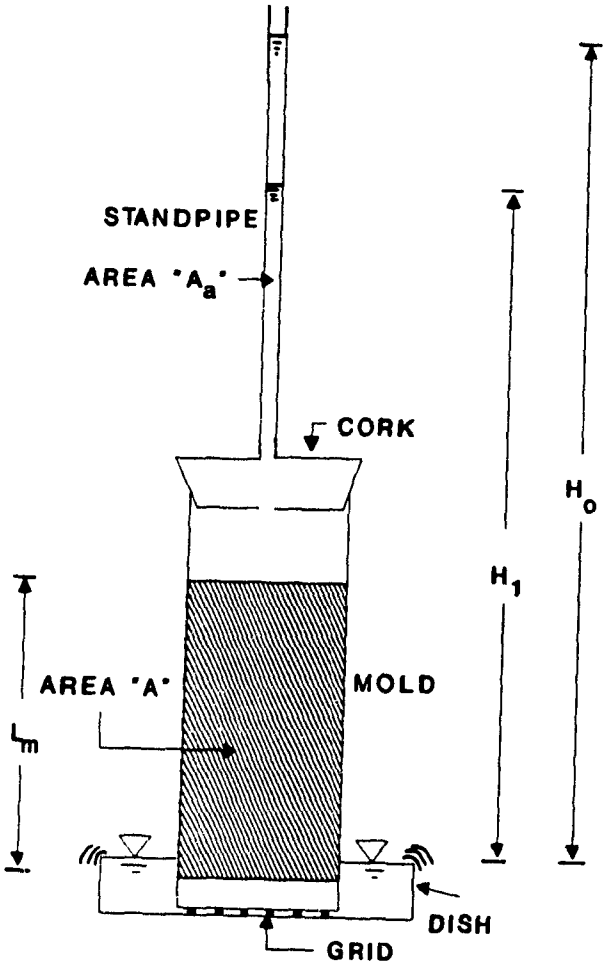

Figure 4.6: Schematic diagram of experimental set-up for plaster of Paris mold permeability measurements.

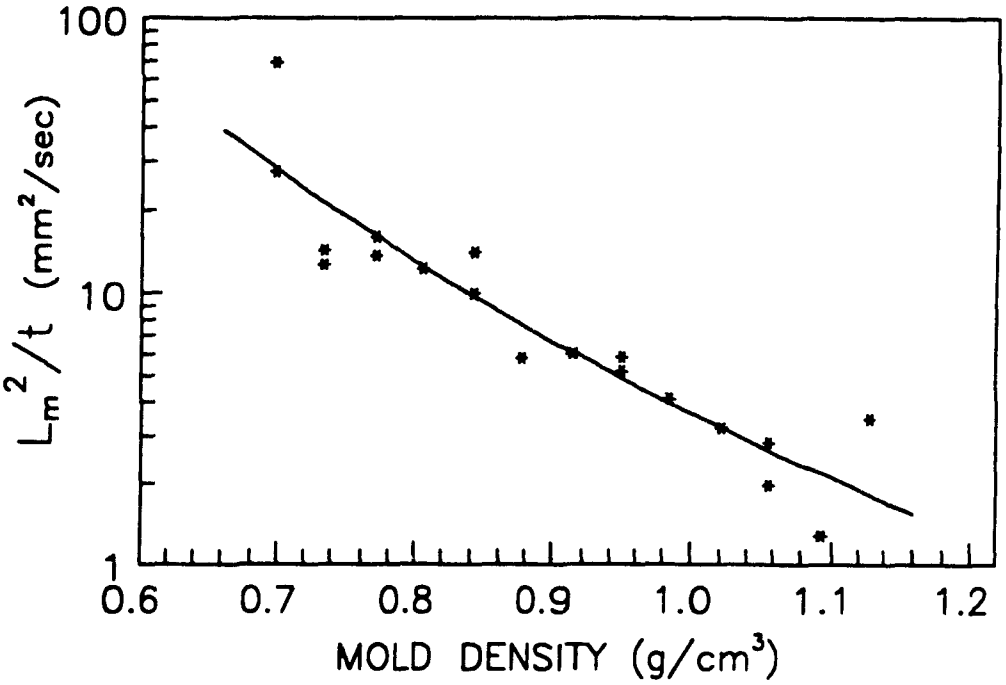

Figure 4.7: Mold adsorption rate of water as a function of mold density.

and applying the limits of integration yields,

$$-A_a \int_{H_o}^{H_1} \frac{dH}{H} = \frac{AK_m\gamma}{\mu L_m} \int_0^{t_1} dt. \tag{4.9}$$

By integrating equation 4.9 it is found that:

$$K_m = \frac{A_a \mu L_m}{A\gamma t_1} \ln \frac{H_0}{H_1} \tag{4.10}$$

Figures 4.7-4.10 show graphs of L_m^2/t, ϵ_m, K_m and P as a function of mold density, respectively. With increase in mold density, L_m^2/t, ϵ_m and K_m all decrease. Figure 4.8 shows that the values of ϵ_m are lower than the mold porosities* implying that all the pores are not completely filled with water. The mold porosities are

*density of gypsum = 2.32 g/cm^3

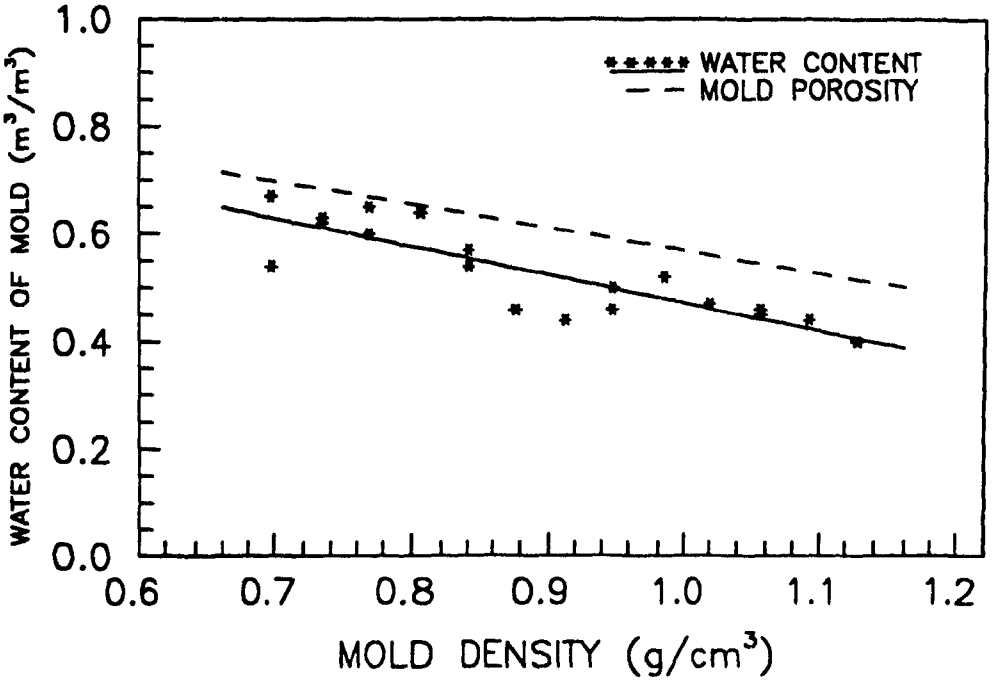

Figure 4.8: Fraction of water in the wetted part of the mold, ϵ_m as a function of mold density. The dashed line shows the porosity of the mold.

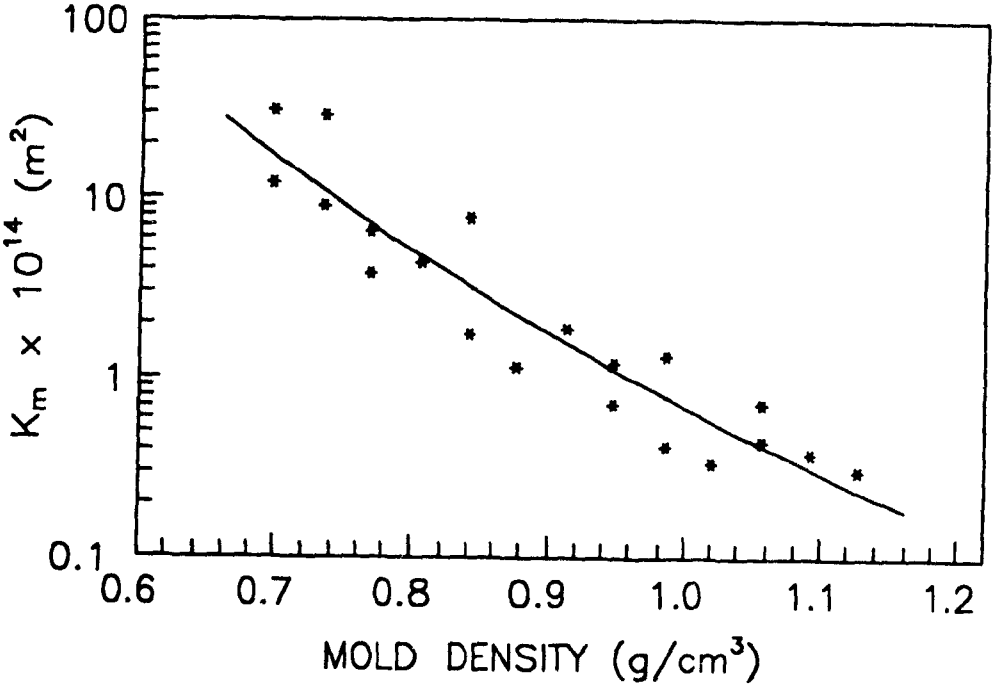

Figure 4.9: Permeability of mold, K_m as a function of mold density.

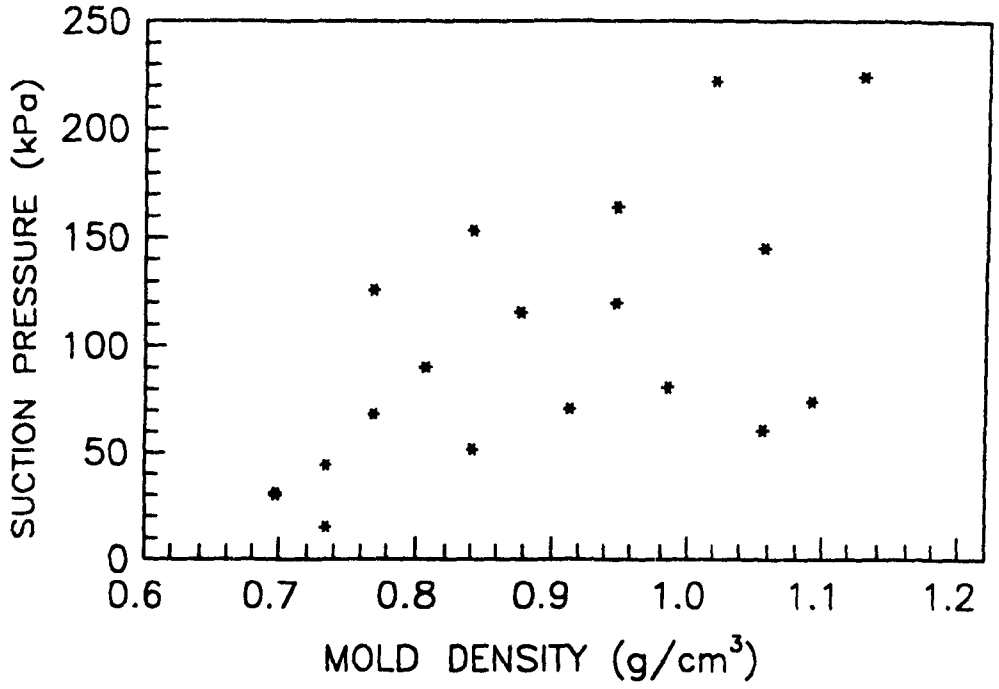

Figure 4.10: The suction pressure, P of the mold as a function of mold density.

represented in Figure 4.8 by the dashed line. The experimental data for the suction pressure results are in the range of 100 kPa (see Figure 4.10). The results imply a slight increase in pressure with increase in mold density but these results are not totally conclusive due to the large scatter in the data.

During slip casting part of the suction pressure is required to overcome the resistance to flow in the pores of the mold. Equation(2.21) of section (2.3.3) showed that the pressure drop across the cake, ΔP_c, or in other words the pressure available for cake formation is equal to the following expression:

$$\Delta P_c = \frac{P}{(L_m K_c)/(L K_m) + 1} \tag{4.11}$$

This expression shows that the larger the permeability of the mold the greater proportion of the suction pressure is available for cake formation.

Fine pores exert a high suction pressure but also a high resistance to flow thereby reducing the fraction of the suction pressure available for cake formation. Hence the rate of cake buildup, (L^2/t) does not necessarily increase with suction pressure. The ratio, $(L_m K_c)/(L K_m)$ is critical to determining the extent to which the suction pressure contributes to cake formation.

A-16SG slips were cast using molds formed with different plaster/water ratios to examine the effects the different mold microstructures have on the filtration process. The experimentally measured permeabilities of the A-16SG cakes are of the order of 1×10^{-16} m^2 and ratios of L_m/L are typically about 2. The K_m versus mold density graph (see Figure 4.9) shows that K_m ranges from about 200×10^{-15} m^2 to 3×10^{-15} m^2 for mold densities ranging from about 0.7 to 1.1 g/cm^3. The low mold densities have significantly higher permeabilities than the cake permeabilities and therefore the suction pressure exerted by the mold is almost completely utilized for cake formation (see Table 4.1). However, with increase in mold density the mold resistance becomes

Table 4.1: $\Delta P_c/P^*$ for different values of K_m

$K_m \times 10^{15}$ (m^2)	200	100	10	5	1	0.5	0.1
$\Delta P_c/P^*$	0.999	0.998	0.980	0.962	0.833	0.714	0.333

*$L_m/L = 2$ and $K_c = 1 \times 10^{-16}$ m^2

more significant and more of the suction pressure of the mold is used to overcome flow resistance in the mold.

Figure 4.11 is a graph of constant B $(= L^2/t)$ and cake density versus mold density for A-16SG slips. As the plaster/water ratio increases (i.e., increase in mold density), cake density remains constant and constant B showed only a very slight, if any, trend of an increase. There was some variability in these results as was also found for the suction pressure results. Figure 4.10 showed that the increase in suc-

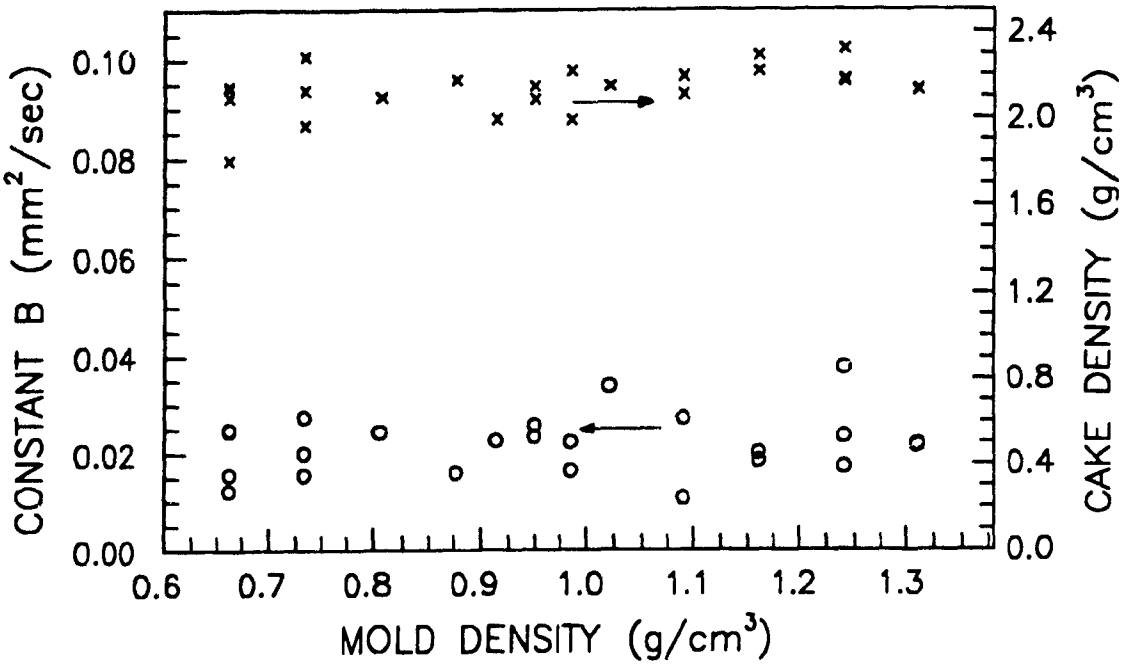

Figure 4.11: Effect of mold density on the cake green density and constant $B(= L^2/t)$ for A-16SG slips; $\epsilon_{sl} = 0.39$.

tion pressure with mold density was minor but still more significant than what was found for constant B. A possible explanation for this is that as the suction pressure increases with mold density, the fraction of pressure utilized to overcome flow resistance in the mold becomes more important at the higher mold densities thereby negating the increase in pressure available for cake formation.

4.3 INFLUENCE OF PARTICLE SIZE DISTRIBUTION ON CAKE DENSITIES

The porosity for randomly packed unagglomerated mono-sized particles is approximately 40% regardless of the particle diameter.[5] However, mixing fine particles with coarser particles allows the fines to fill the voids between the coarse particles.

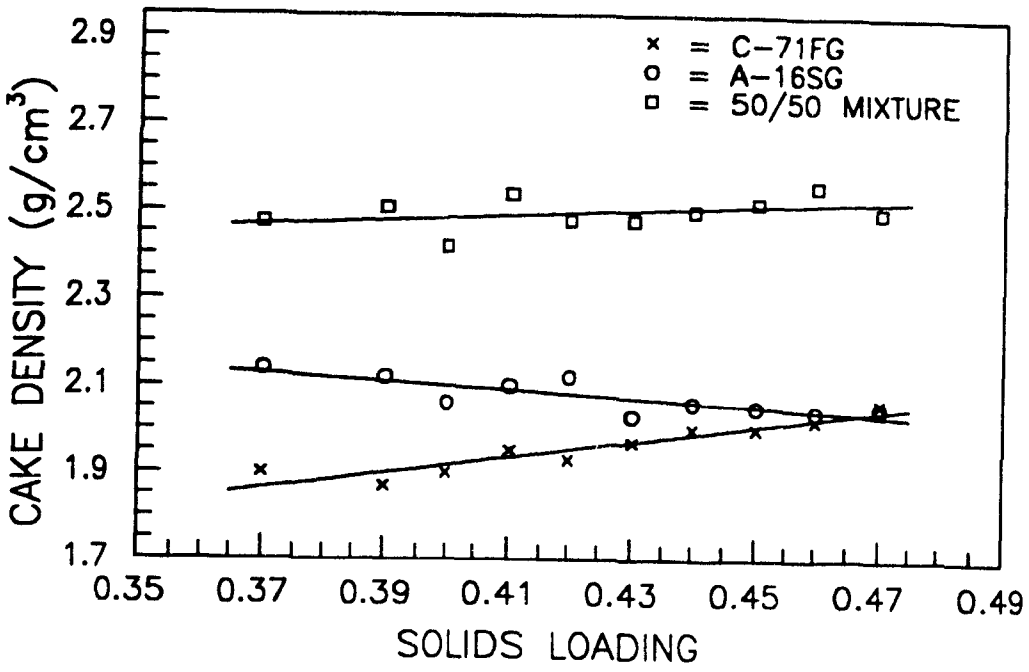

Figure 4.12: Cake green density versus slip volume solids loading (mold formed using a plaster/water (g/g) ratio of 1.5).

The wider and more continuous the particle size distribution, the lower the voids volume of the system.

Figure 4.12 is a graph of cake density versus slip volume solids fraction, ϵ_{sl} for the coarse (C-71FG), fine (A-16SG), and 50/50 mixture of the coarse and fine alumina powders being analyzed. All the slips contained an amount of Darvan 7 that produced a minimum in viscosity. As expected, this graph shows that the compacts containing a 50/50 mixture of the alumina powders give the highest green densities for all slip solids loadings.

The degree of flocculation in the slips also affects the cake green densities. Hauth[57] has analyzed the variation in alumina cake green densities (produced by slip casting) with the change in degree of flocculation in the slips. With all else held constant, it appears that the greater the flocculation in a slip, the higher is the porosity and, therefore, the higher the cake permeability and lower the green density.

As discussed in Chapter 3, the A-16SG slips, at minimum viscosity, were found to be shear thinning, which could suggest that some degree of flocculation exists. The shear-thinning behaviour increased with an increase in solids loading. This explains why the densities of the A-16SG cakes decrease with an increase in ϵ_{sl}.

The densities of the C-71FG cakes increase with an increase in solids loading. In Chapter 3, slips containing an amount of Darvan 7 that produced a minimum in viscosity showed shear-thickening behaviour, and this behaviour became more pronounced as the solids loading was increased. Shear-thickening behaviour is a characteristic of a slip that forms a close-packed solids arrangement. Therefore, the cake green density increases with an increase in shear-thickening behaviour.

Equation (2.24) of section (2.3.4) implies, in general, that constant B should increase with ϵ_{sl} or K_c or decrease with cake density with all else held constant. Plots of constant B versus slip solids loading are presented in Figure 4.13. The rates of cake buildup for A-16SG slips increase, due to flocculation, with solids loading; this is the critical parameter causing the cake density to decrease.

The rate of cake buildup of C-71FG slips increases slightly with solids loading, even though the cake densities are also increasing. It is important to note that an increase in cake density does not always assure a decrease in K_c. Permeability is very sensitive to the pore size distribution. In Chapter 6, a computer model will show that two cakes with the same porosity and mean pore size can have very different permeabilities The model found that the wider the pore size distribution the lower the cake permeability. Therefore, the very slight increase in constant B for the C-71FG slips can possibly be attributed to two factors: (1) the increase in ϵ_{sl} is more critical in affecting constant B than is the cake density and (2) even though the cake density is increasing with ϵ_{sl}, cake permeability may not be decreasing. The denser

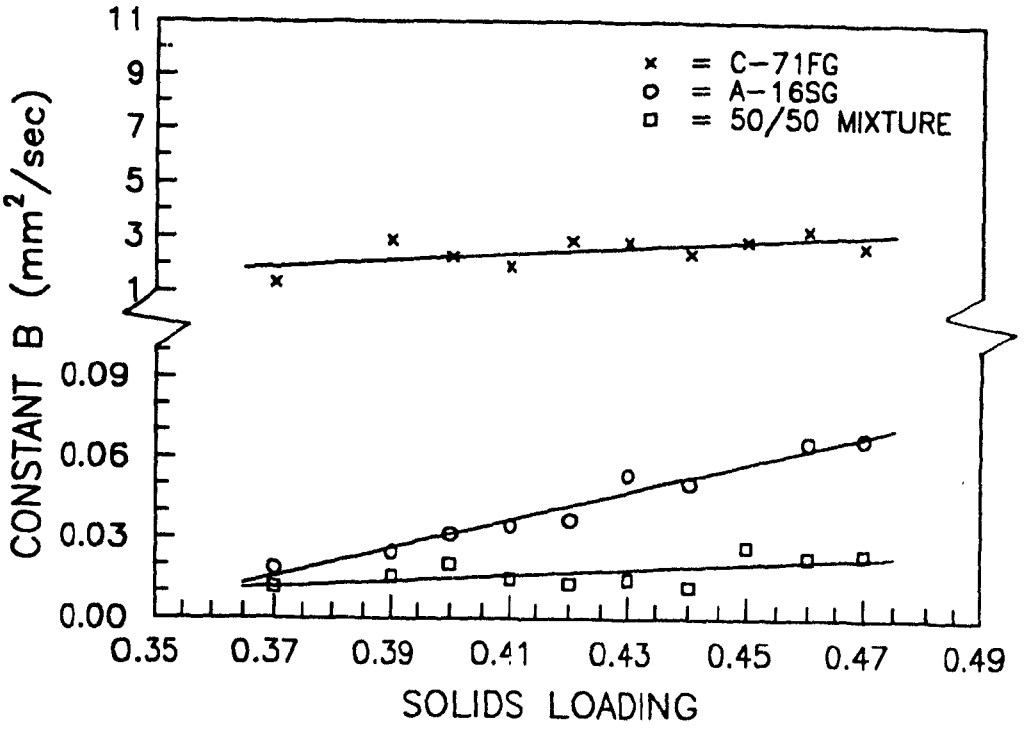

Figure 4.13: Constant $B(= L^2/t)$ versus slip volume solids loading (mold formed using a plaster/water (g/g) ratio of 1.5).

packing arrangement may also be more uniform, negating any decrease in K_c. The cake density and constant B values are relatively constant for the 50/50 alumina mixture due to a combination of effects: (1) the C-71FG powder forming a tighter packing arrangement and (2) the A-16SG powder forming more flocs with increase in solids loading.

Chapter 5

EXPERIMENTAL OBSERVATIONS OF MIGRATION OF FINE PARTICLES

Experimental work that has been carried out shows qualitatively and quantitatively that a cake and/or filter medium can become clogged due to fine particles migrating through the cake and accumulating near the cake-filter medium interface. This in turn will affect the growth rate of cake thickness as well as the permeability, density and porosity of the cake.

5.1 SEM CAKE MICROSTRUCTURES

Slip cast and filter pressed alumina cakes were examined using a scanning electron microscope (SEM) to illustrate cake clogging.

Three grades of alumina powder were used for most of the filtration experiments: (1) a coarse powder (C-71FG), (2) a fine powder (A-16SG) and (3) a wide particle size distribution powder (A-17). The A-17 powder is commonly used for slip casting. The C-71FG, A-16SG and A-17 powders have median particle sizes of 4.2 μm, 0.4 μm, and 3.0 - 3.5 μm, respectively. The slips had a volume solids loading, $\epsilon_{sl} = 0.39$ and were deflocculated with Darvan 7.

SEM micrographs of alumina microstructures illustrate that a higher concentration of fine particles can accumulate at the bottom section of a cake. Figure 5.1 shows

micrographs of longitudinal cross-sections of a green cake consisting of 90 % coarse and 10 % fine alumina. The slip was filter pressed at 345 kPa (50 psi). Micrograph (A) shows an area near the top surface of the cake and is relatively free of fine particles. Micrograph (B) is of the same magnification and shows a cross-section at the bottom of the cake near the interface with the filter paper. The fine particles that have percolated to the bottom of the cake are quite evident. Figure 5.2 is a micrograph of a top view of the powder that has remained on the filter paper after the cake was separated from the filter paper. The micrograph shows that a large amount of fines have accumulated at the cake bottom. Figure 5.3 is a micrograph of the powder that passed through the filter paper along with the filtrate. The micrograph shows that most of the powder that passed through the filter paper is fine. During the filtration process, a cloudy filtrate was observed indicating that powder was passing through the filter paper along with the filtrate.

The micrographs in Figure 5.4 show longitudinal cross-sections of a green slip cast A-17 cake. These micrographs again show that a higher concentration of fines has accumulated at the bottom of the cake. Presintered and sintered filter pressed A-17 cakes were also examined. These cakes were sectioned and polished prior to SEM examination (see Figures 5.5 and 5.6). The micrographs show that a thin layer (about 10 μm) with a higher concentration of fine particles has accumulated at the cake bottom. Above this layer the cake microstructure is quite uniform.

To further illustrate the percolation of fine particles during filtration slips consisting of 20% unground yttria (Y_2O_3) and 79% C-71 unground alumina and 1% C-71FG alumina were slip cast. Composite slips were cast so that by using SEM back scattering imagery and carbon coating the samples the yttria and alumina could be distinguished on the micrograph. Yttria was also chosen to be combined with alumina

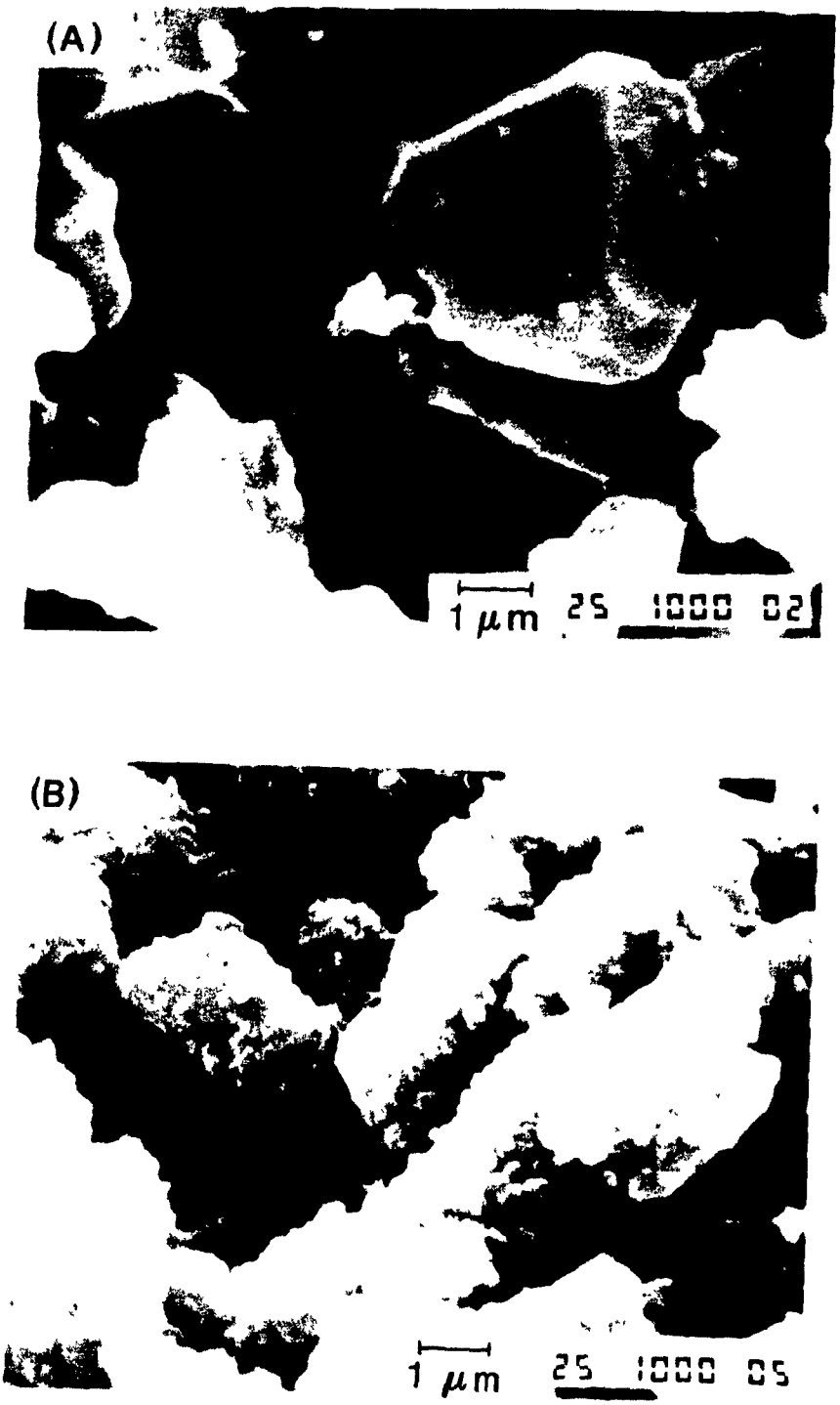

Figure 5.1: Longitudinal cross-sections of a cake (A) near the top surface and (B) near the bottom surface (90% C-71FG and 10% A-16SG, filter paper pore size = 2.5 μm).

Figure 5.2: Top view of powder remaining on filter paper (90% C-71FG and 10% A-16SG, filter paper pore size = 2.5 μm, and P = 345 kPa)

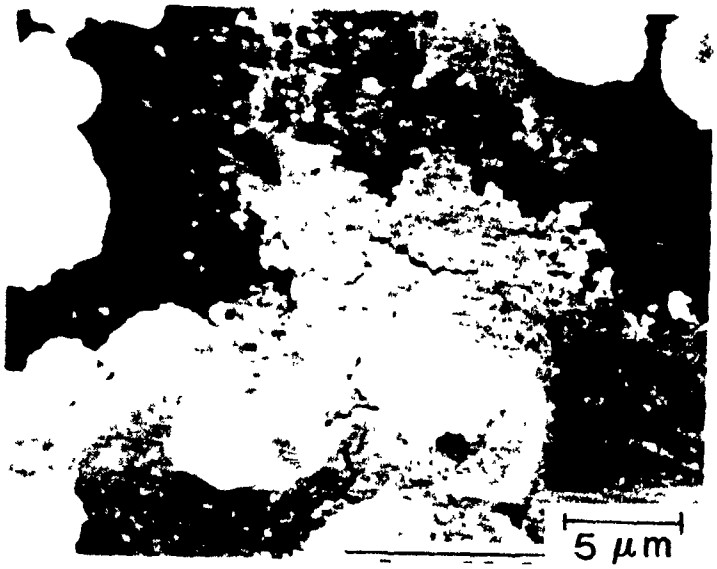

Figure 5.3: Powder that passed through filter paper (90% C-71FG and 10% A-16SG; filter paper pore size = 2.5 μm, and P = 345 kPa).

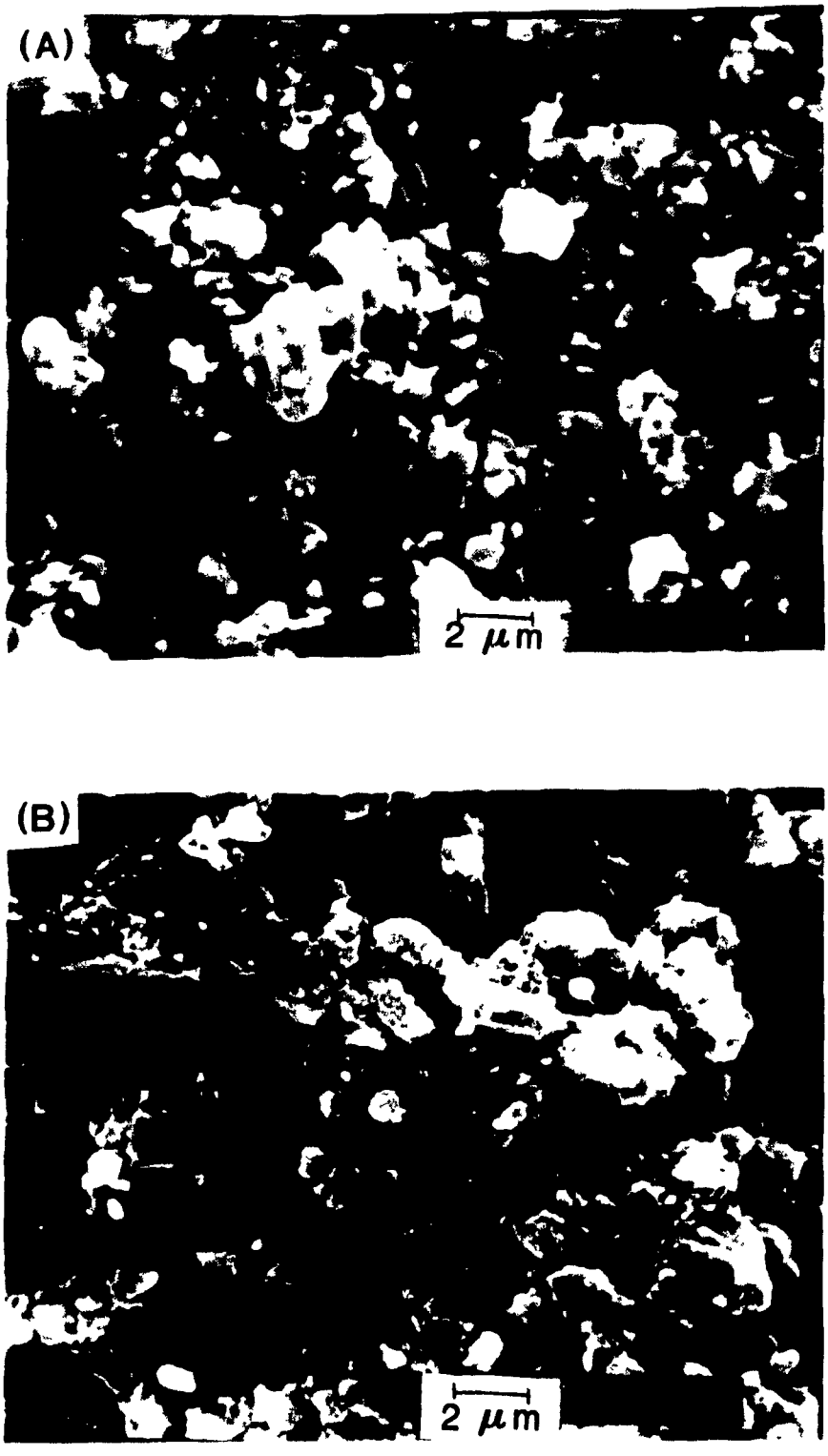

Figure 5.4: Longitudinal cross-sections of a slip cast A-17 cake (A) near the top surface and (B) near the bottom surface.

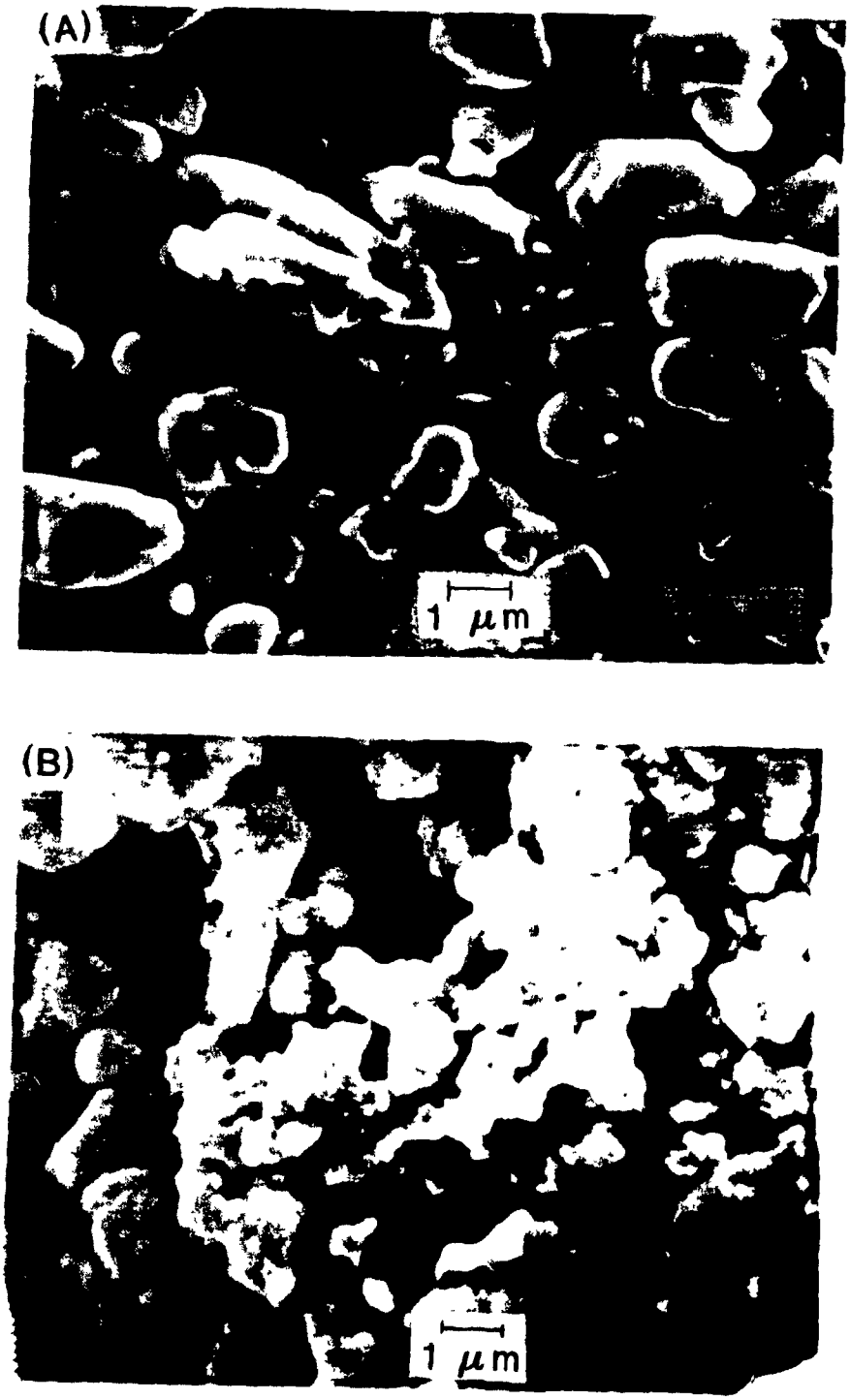

Figure 5.5: Longituinal cross-sections (A) near the middle and (B) near the bottom surface of an A-17 cake. The cake was presintered at 1500 °C for one hour (filter paper pore size = 0.1 μm, and P = 345 kPa).

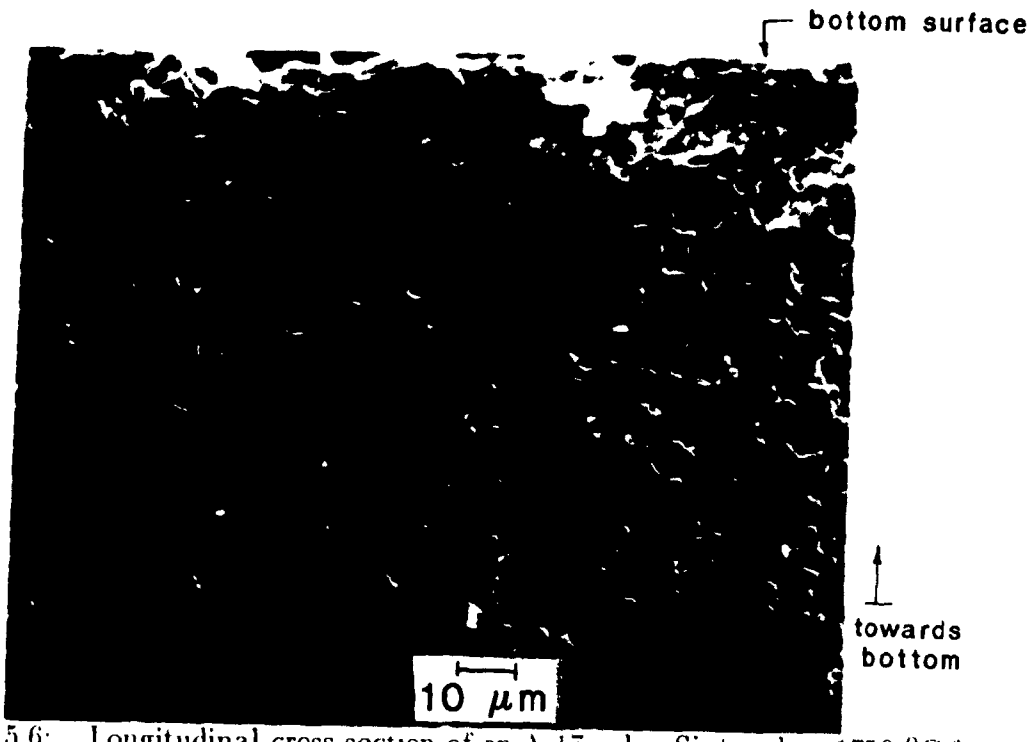

Figure 5.6: Longitudinal cross-section of an A-17 cake. Sintered at 1750 ^{o}C for one hour (filter paper pore size = 0.1 μm, and P = 345 kPa).

because of their similar deflocculation behaviour and relatively similar densities. Yttria and alumina have densities of 5.01 g/cm^3 and 3.98 g/cm^3, respectively. A small amount of C-71FG powder was added to the slip to help hold the cast together. Figure 5.7 shows micrographs of longitudinal sections near the middle (micrograph (A)) and bottom (micrograph (B)) of the cake. The atomic numbers of aluminum and yttrium are 13 and 39, respectively. Yttria shows up as the light colored powdered and alumina as the dark powder on the micrograph as a result of yttrium having a higher atomic number than aluminum. The particle size of the yttria powder is approximately 2 μm and has agglomerates of the order of 10 μm whereas the size of the agglomerates for the unground C-71 powder are of the order of 100 μm. The micrographs clearly show that there is a much higher concentration of the yttria powder and C-71FG powder in micrograph (B). Again, these results illustrate that some of

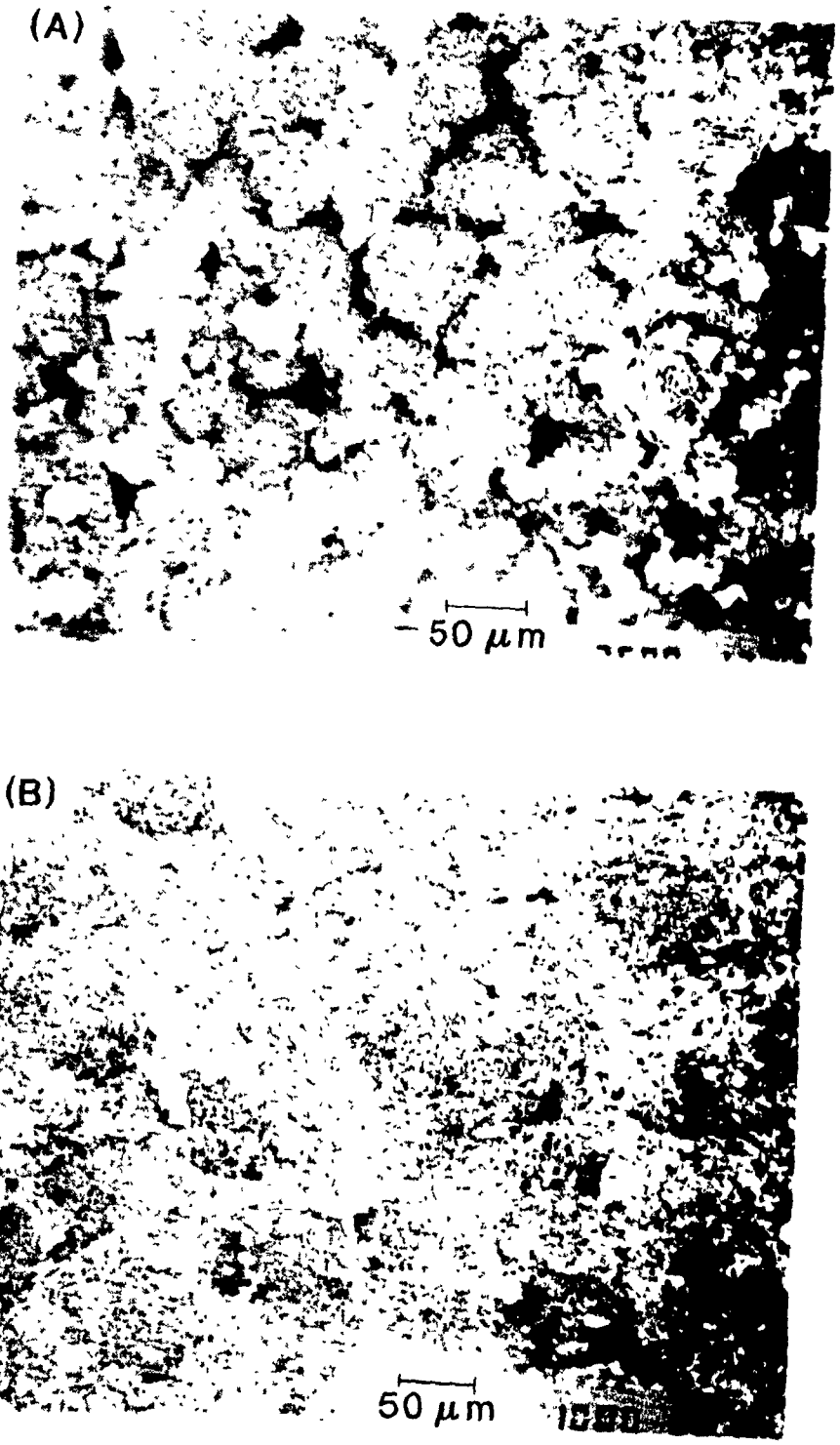

Figure 5.7: Longitudinal cross-sections of a slip cast alumina-yttria cake near (A) the middle and (B) bottom of the cake. The light coloured powder is yttria.

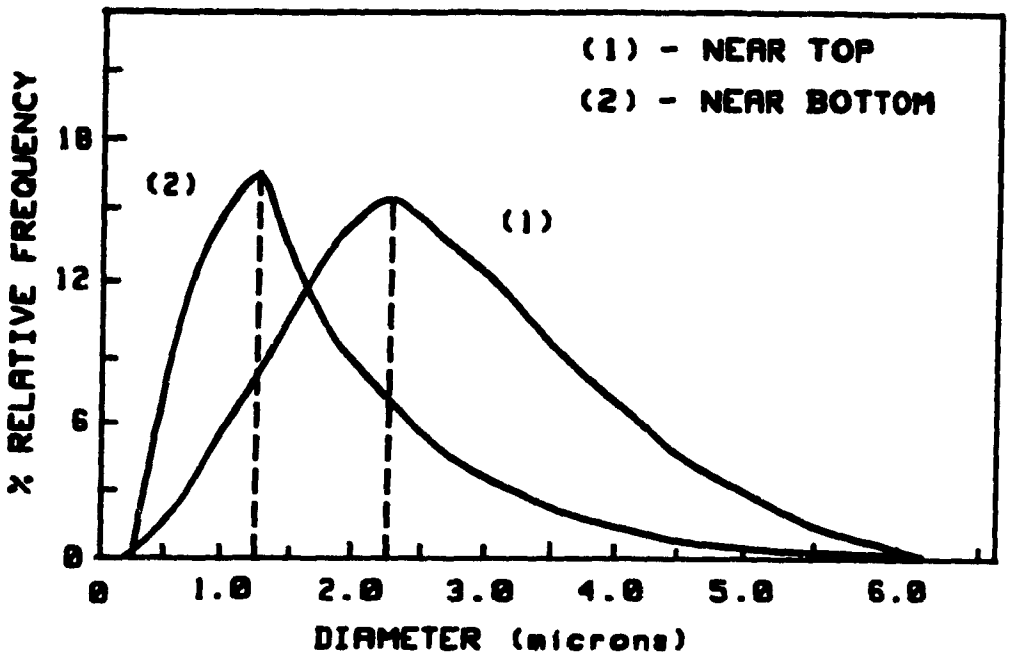

Figure 5.8: Particle size distribution curves for a longitudinal cross-section of a C-71FG cake.

the finer powder (i.e., yttria and C-71FG) can percolate through the cake and deposit near the cake-filter medium interface.

5.2 QUANTITATIVE ANALYSIS

5.2.1 SEM IMAGE ANALYSIS

A cake consisting of C-71FG powder was slip cast so that quantitative data could be obtained for the concentration differences of fines in the top and bottom sections of the cake. Curves (1) and (2) in Figure 5.8 were obtained by using image analysis on SEM micrographs. The curves illustrate that there is a shift from a coarser to a finer particle size distribution from the top to the bottom of the cake. This analysis also confirms that fine particles can be transported by the filtrate to

the bottom of the cake leading to non-uniformity in the cake density.

5.2.2 SURFACE AREA MEASUREMENTS

The concentration gradients of fines from the top to the bottom of filter pressed cakes were analyzed by taken "single point BET" surface area measurements of cake sections.

The ratio of the filter medium pore size to diameter of fines will determine whether or not the fines will pass through the filter medium. Therefore, the type of medium used will affect the migration of fines during filtration.

Slips consisting of 20% A-16SG (fine) and 80% C-71FG (coarse) alumina powder were cast using different filter pressures and filter papers with different mean pore sizes. The slips had a volume solids fraction, $\epsilon_{sl} = 0.39$ Each cake was then divided transversely into sections from the bottom to the top of the cake. The surface areas of the sections were then measured. Figure 5.9 is a graph of surface area versus cake depth. A cake depth equal to zero refers to the cake-filter paper interface (i.e., cake bottom). The filter paper had a mean pore size equal to 0.1 μm. The slips were cast using a filter pressure of 140 kPa (20 psi), 275 kPa (40 psi), and 550 kPa (80 psi). All three cases show a trend of having a higher surface area near the cake bottom than in the rest of the cake where the surface area is rather constant. The higher surface area at the cake bottom indicates that some of the fine particles have migrated through the cake to its bottom.

Figure 5.10 is also a graph of surface area versus cake depth. However, for these experiments, a coarser filter paper was used. It had a mean pore size of 2.5 μm. The graph shows that the cake has a higher surface area near its bottom for the slips pressed at 35 kPa (5 psi), 140 kPa (20 psi), and 275 kPa (40 psi). The surface areas of the particles near the cake bottoms in this figure are not as high as for the surface

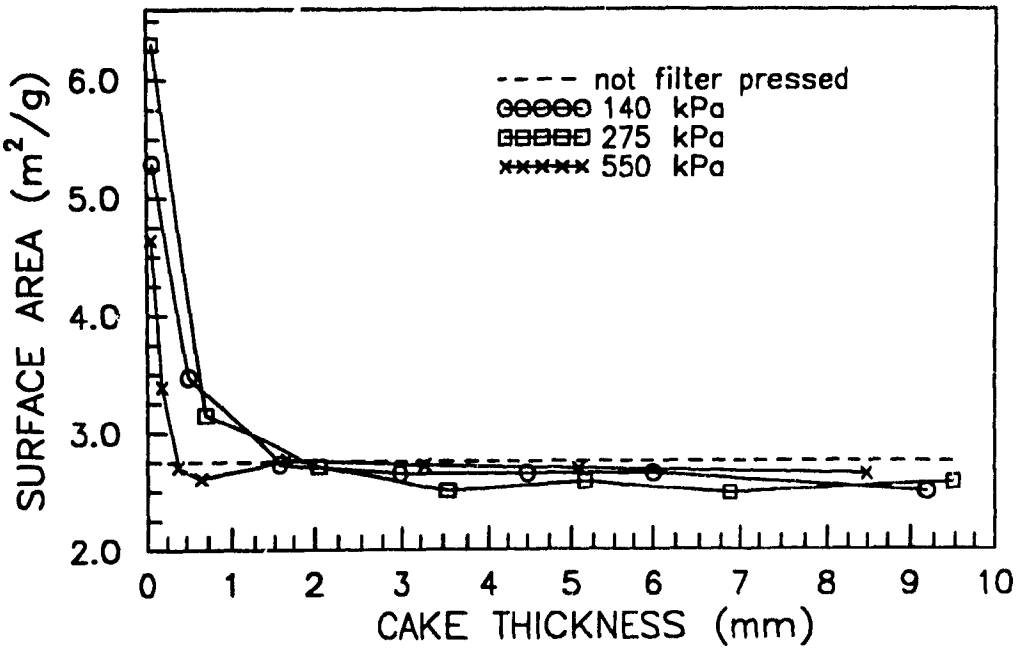

Figure 5.9: Surface area versus distance above cake bottom 20/80 mixture of A-16SG/C-71FG powder. Filter paper pore size = 0.1 μm. The dashed line shows the surface area for powder before being filter pressed.

areas near the cake bottoms in Figure 5.9. In Figure 5.10 the surface areas of the cake pressed at 550 kPa (80 psi) are relatively constant across the depth of the cake. As a result of using coarser filter paper some of the fine particles were driven right through the filter paper and others only penetrated and clogged the filter paper. During the filtration process it was observed that the filtrate was cloudy indicating that powder was passing through the filter medium along with the filtrate.

Surface area measurements were taken for the A-16SG and C- 71FG powder. A 20/80 mixture of the A-16SG/C-71FG powder has a surface area of 2.75 m^2/g. This value is shown by the dashed line in Figures 5.9 and 5.10. Both these figures show that the surface area measurements are higher than 2.75 m^2/g near the cake bottom and are lower than 2.75 m^2/g further out in the cake. In Figure 5.10 there is only a small increase in surface area near the cake bottom. However, the surface

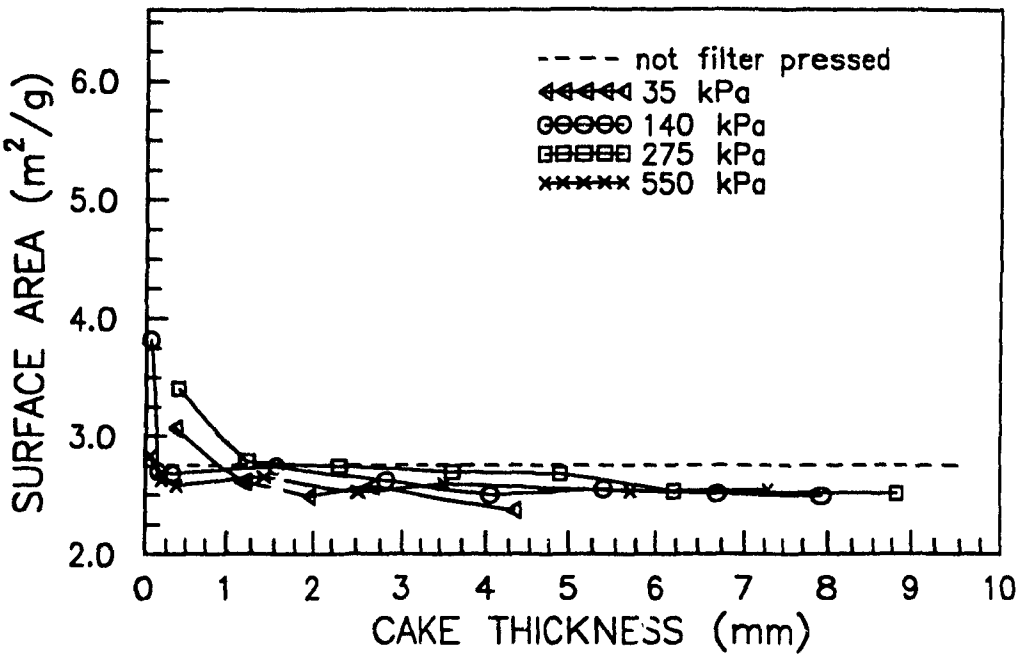

Figure 5.10: Surface area versus distance above cake bottom. 20/80 mixture of A-16SG/C-71FG powder. Filter paper pore size = 2.5 μm. The dashed line shows the surface area for powder before being filter pressed.

areas are less than 2.75 m^2/g further away from the cake bottom, which implies that some of the fine particles have migrated through the cake and into and/or through the filter medium. Surface area measurements were also found to be higher near the cake bottom for A-17 cakes as shown in Figure 5.11.

To illustrate the migration of fine particles through filter paper, a slip consisting of a 50/50 mixture of the C-71FG (coarse) and A-16SG (fine) powder was filter pressed at 550 kPa (80 psi) (see Figure 5.12). This mixture of powder, prior to being filter pressed has a surface area of 5.32 m^2/g and is shown by a dashed line on the graph. The filter paper had a mean pore size of 0.22 μm. The pore size of the paper is large enough to allow the fine particles to pass through the paper but small enough to prevent the larger particles from passing through the paper. The graph shows that there was a small increase in surface area near the bottom of the cake. With 50% of

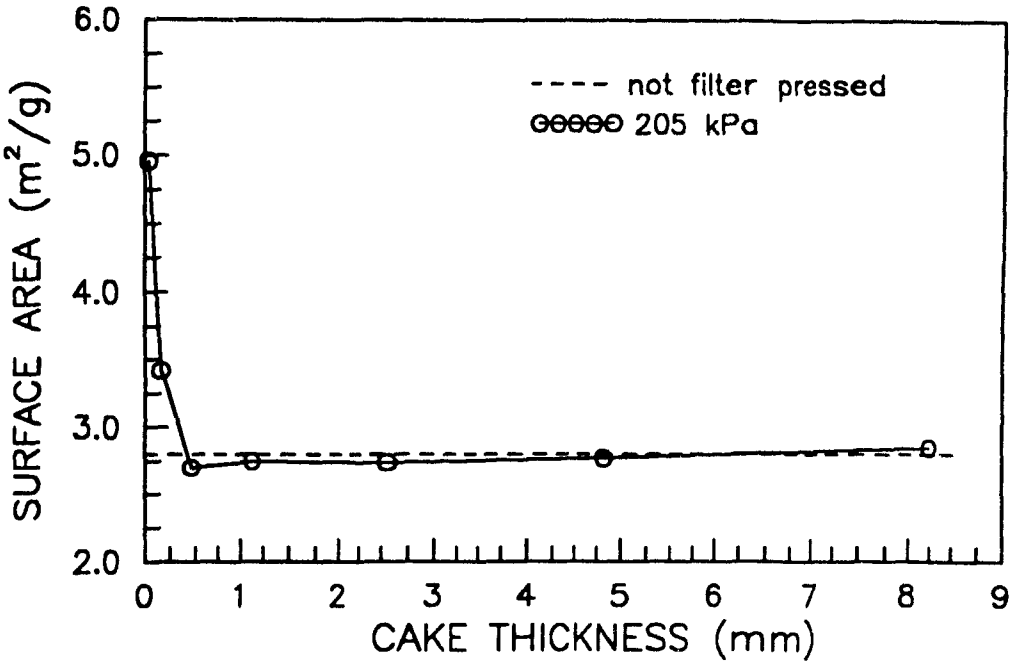

Figure 5.11: Surface area for an A-17 cake versus distance above cake bottom. Filter paper pore size = 2.5 μm. The dashed line shows the surface area for A-17 alumina powder before being filter pressed

the powder being fine, enough filtered through the medium ($\approx$ 0.05 g, 0.125% of the original weight of the solids) to enable a surface area measurement to be taken. This powder had a surface area of 10.67 m^2/g or an equivalent particle diameter size equal to 0.14 μm implying that some of the fine particles did percolate through the cake and filter paper. The particle size distribution of the slip as well as the pore size of the filter medium affects the filtration process.

5.3 FILTRATION EQUATIONS

In Chapter 2 (section 2.3) it was shown that:

$$P = \Delta P_m + \Delta P_c = \mu(L_m/K_m + L/K_c)\frac{dW}{dt} \tag{5.1}$$

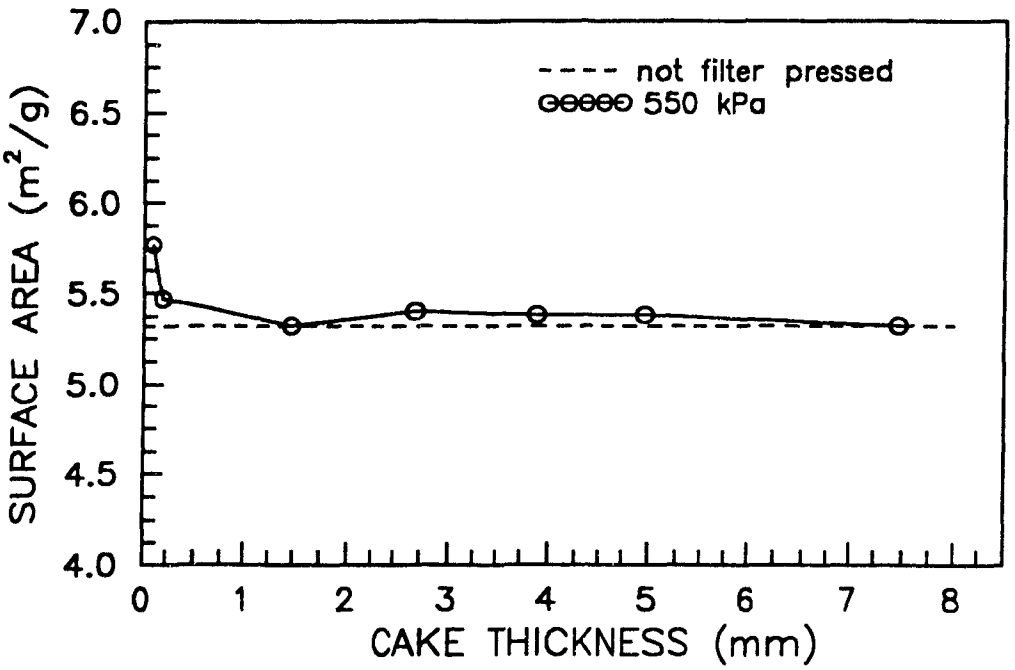

Figure 5.12: Surface area versus distance above cake bottom. 50/50 mixture of C-71FG and A-16SG powder. Filter paper pore size = 0.22 μm. The dashed line shows the surface area for powder before being filtered pressed.

and

$$W = L(\epsilon_{cav}/\epsilon_{sl} - 1) \tag{5.2}$$

In this analysis it will be considered that the resistance to filtration of the filter medium, L_m/K_m is part of the cake. The 2.5 μm and 0.1 μm pore size filter papers that were used for the filter pressing experiments have permeabilities equal to 1.5×10^{-14} m^2 and 4.5×10^{-16} m^2, respectively. The permeabilities of both filter papers are greater than the cake permeabilities and it takes no more than a couple of seconds before the cake becomes thicker than the filter paper. Therefore, the resistance to filtration of a filter medium that is not clogged is negligible compared to the resistance to filtration of the filter cake. If the filter medium is clogged it is in fact due to the nature of the slip. It is therefore logical to add this extra resistance to the overall

resistance of the cake. Hence, equation (5.1) reduces to:

$$\frac{dW}{dt} = (\epsilon_{cav}/\epsilon_{sl} - 1)\frac{dL}{dt} = \frac{PK_{ave}}{\mu L} \tag{5.3}$$

where K_{ave} is the permeability of the system. Assuming that K_{ave} and ϵ_{cav} are constant and integrating equation (5.3) yields:

$$L^2 = \frac{2PK_{ave}}{\mu(\epsilon_{cav}/\epsilon_{sl} - 1)} \cdot t = Bt \tag{5.4}$$

where B is a constant. The cake thickness squared, L^2 is proportional to time, t. This equation is only valid for an incompressible cake that has a constant permeability or in other words when no cake clogging occurs. In the analysis to follow of clogging during filtration the cakes are assumed to be incompressible since the cakes were cast from well deflocculated slips.

5.3.1 CAKE THICKNESS VERSUS TIME

If no cake or filter medium clogging occurs, then a plot of $\ln t$ versus $\ln L$ data should produce a line with a slope equal to two. Slopes different from this can infer that cake and/or filter medium clogging has occurred due to deposition of fine, migrating particles.

Figure 5.13 is a graph of $\ln t$ versus $\ln L$. The slips consisted of 20% A-16SG (fine) and 80% C-71FG (coarse) powder and had a volume solids loading, $\epsilon_{sl} = 0.39$. The filter paper used had a mean pore size of 2.5μm and the slips were filter pressed at different pressures. The slopes obtained for these four plots varied from 1.83 to 2.26. Figure 5.14 is a graph of $\ln t$ versus $\ln L$. For this set of experiments the filter paper had a mean pore size of 0.1μm. The slopes in this figure are all greater than

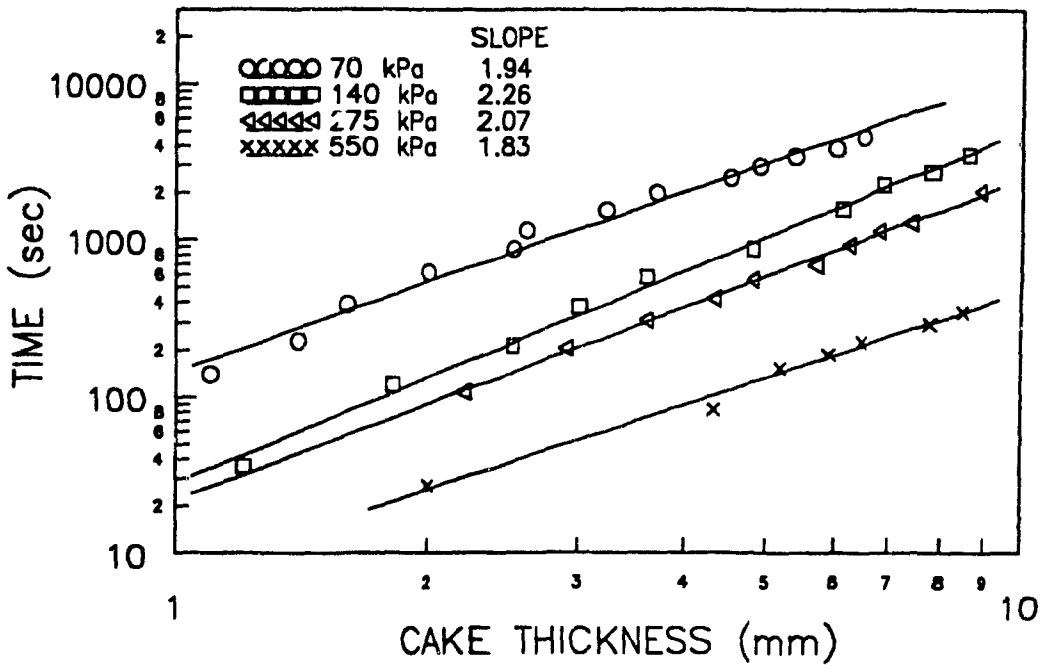

Figure 5.13: Time, t versus cake thickness, L for cakes consisting of 20% A-16SG and 80% C-71FG powder. Filter paper pore size = 2.5 μm. Slopes of lines for $\ln t$ versus $\ln L$ data are indicated on the graph.

two. The pores of the filter paper are finer than the fine particles and therefore the fines should not be able to penetrate the filter paper.

The physical meaning of the difference in slope, n of the graphs of $\ln t$ versus $\ln L$ needs to be addressed. A slope inferior to two could imply that the filter medium and/or cake is clogged very early during pressing while a slope greater than two could imply progressive clogging. To explain this concept further the permeabilities of the cake and filter medium will be considered for the following three cases (see Figure 5.15):

(1) No Clogging

(2) Progressive Clogging

(3) Rapid Initial Clogging

The medium and cake permeability will remain constant throughout the filtra-

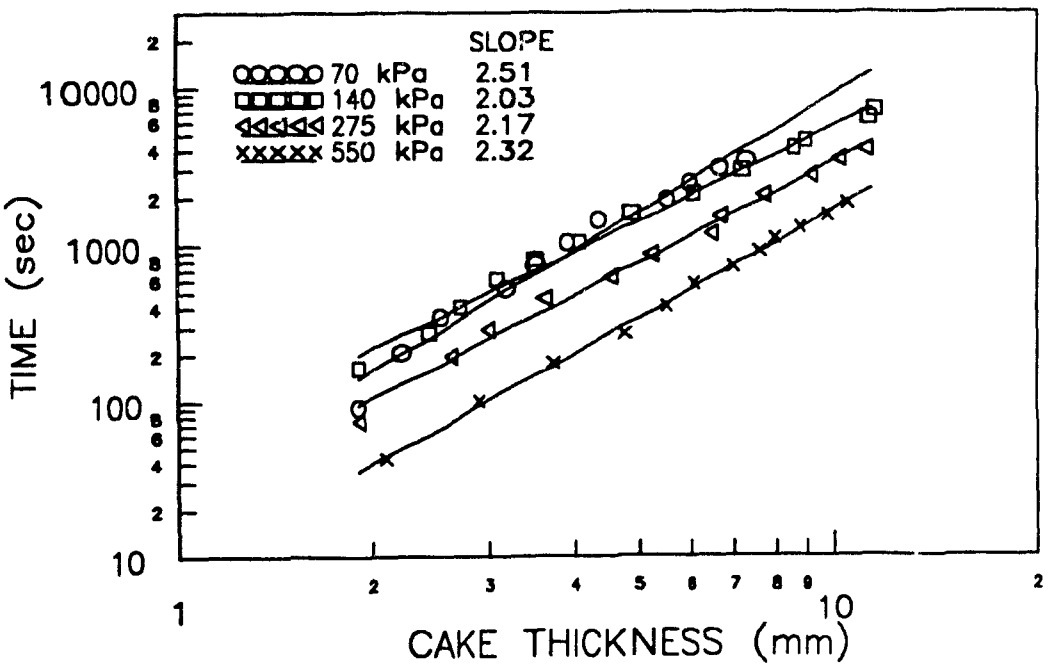

Figure 5.14: Time, t versus cake thickness, L for cakes consisting of 20% A-16SG and 80% C-71FG powder. Filter paper pore size = 0.1 μm Slopes of lines fitted for the $\ln t$ versus $\ln L$ data are indicated on the graph.

tion process if no clogging in the cake or filter medium occurs. The average permeability of the system will almost be equal to the cake permeability because the filter medium permeability is much greater than K_c (see Figure 5.15(a)).

If the fine particles are larger than the pores of the medium, the coarser particles will form some larger pores and the fine migrating particles can progressively clog the pores near the bottom of the cake. The pores near the cake bottom will get smaller and smaller thereby tending to decrease the permeability with increase in time. Progressive clogging will result in a slope greater than two for a plot of $\ln t$ versus $\ln L$ (see Figure 5.15(B)).

If particles are equal to the diameter of the pores of the filter medium these pores can become rapidly clogged in the initial phase of filtration resulting in a sharp decrease in permeability of the medium. As the cake gets thicker less and less clogging

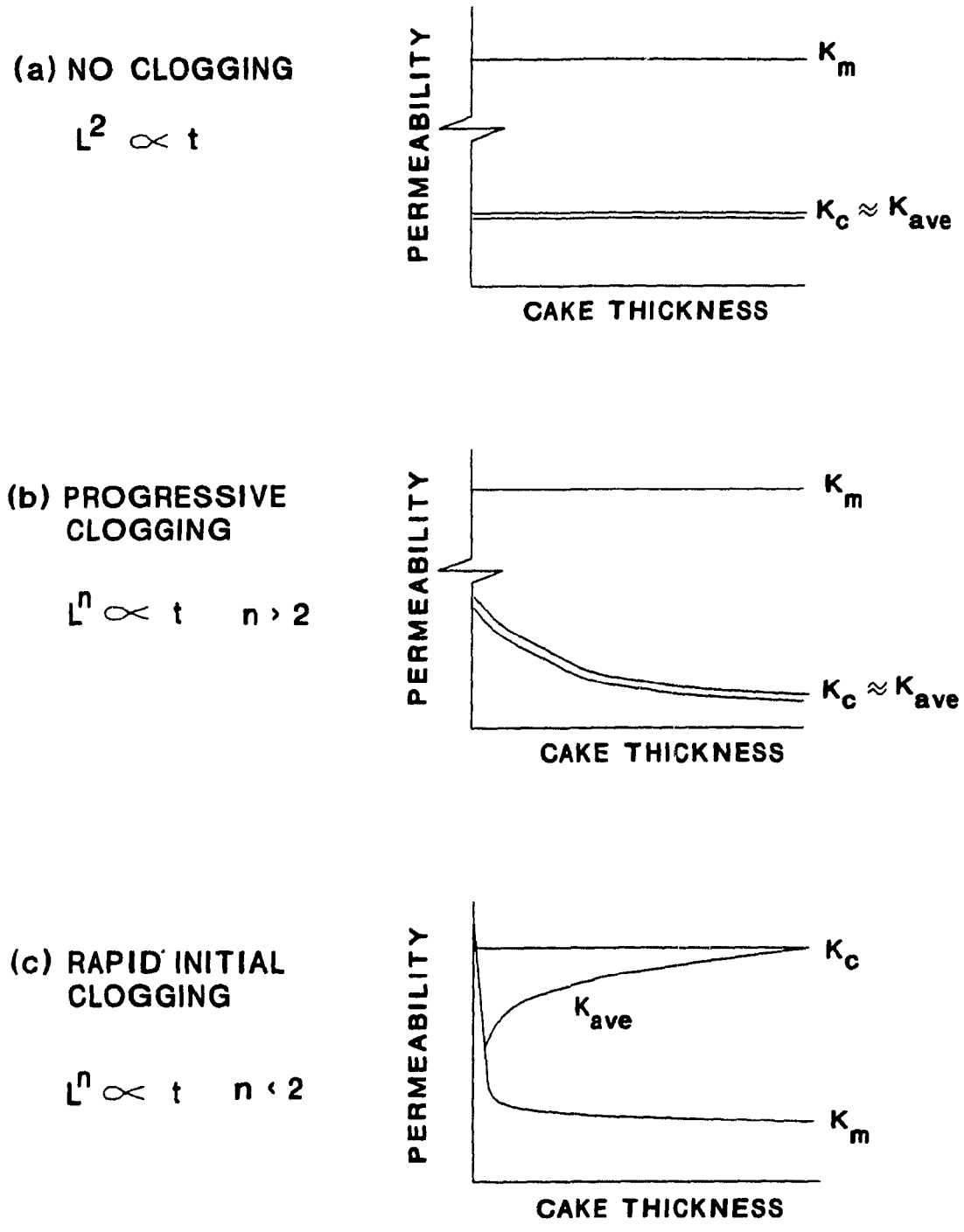

Figure 5.15: Schematic illustration of filter medium and cake permeability as a function of increasing cake thickness.

will occur in the filter medium and therefore the medium permeability will become constant (see Figure 5.15(c)). A slope less than two can also occur if the bottom layers of a cake becomes rapidly clogged in the early stages. As the filtration velocities decrease with time less particle migration and clogging can occur.

It is very possible for cake and filter medium clogging to occur at the same time. Therefore, a slope greater than, equal to, or less than two can result depending upon which clogging mechanism is most significant.

5.3.2 PERMEABILITY

From the graphs of $\ln t$ versus $\ln L$ it was shown that:

$$t = CL^n \tag{5.5}$$

where C and n are constants. Differentiating the above equation and substituting it into equation (5.3) yields:

$$K_{ave} = \frac{\mu}{PCn}(\epsilon_{cav}/\epsilon_{sl} - 1)L^{(2-n)} \tag{5.6}$$

Experimental constants were found for C and n for the data presented in Figures 5.13 and 5.14 by using regressional analysis. The slips had a solids loading, $\epsilon_{sl} = 0.39$. The solids loadings of the cakes, ϵ_{cav} (≈ 0.58) were determined by measuring the cake densities. Figures 5.16 and 5.17 are graphs of cake permeability as a function of L for the experimental data presented in Figures 5.13 and 5.14, respectively. The filter paper used for the experiments in Figure 5.16 had a mean pore size of 2.5 μm. Two of the permeability curves are decreasing and two are increasing with L. Figure 5.16 implies that both cake and medium clogging can occur. In Figure 5.17,

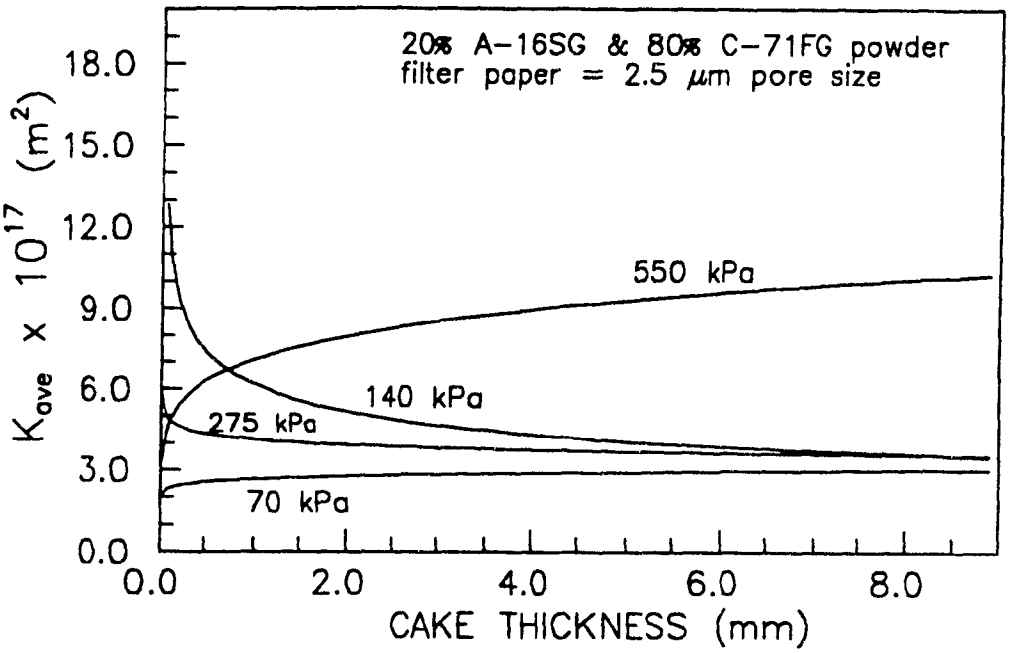

Figure 5.16: Permeability, K_{ave} versus cake thickness, L. Filter paper pore size = 2.5 μm.

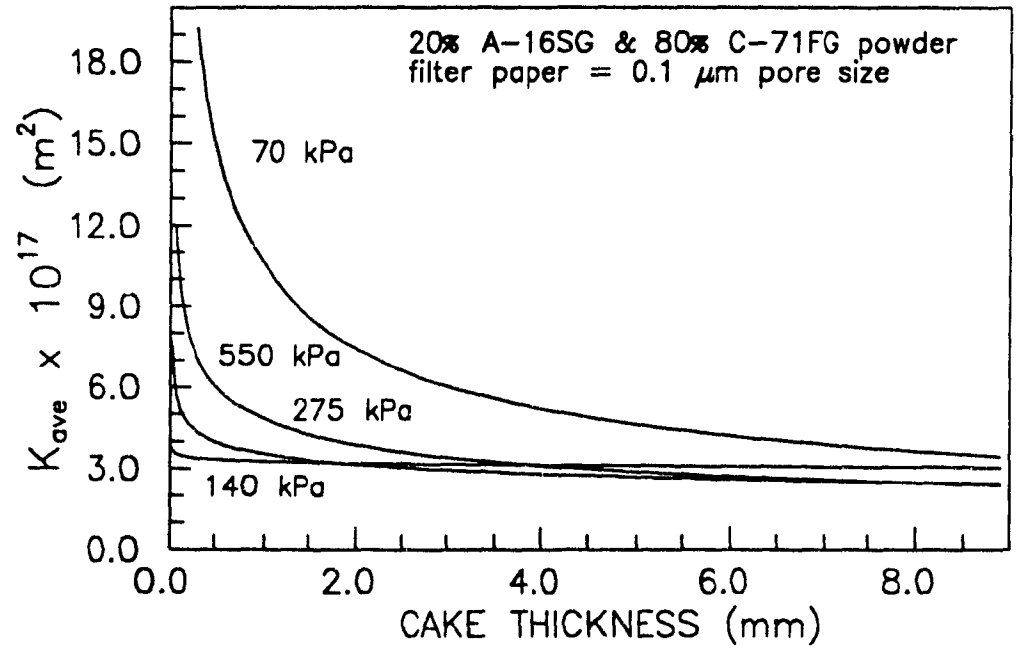

Figure 5.17: Permeability, K_{ave} versus cake thickness, L. Filter paper pore size = 0.1 μm.

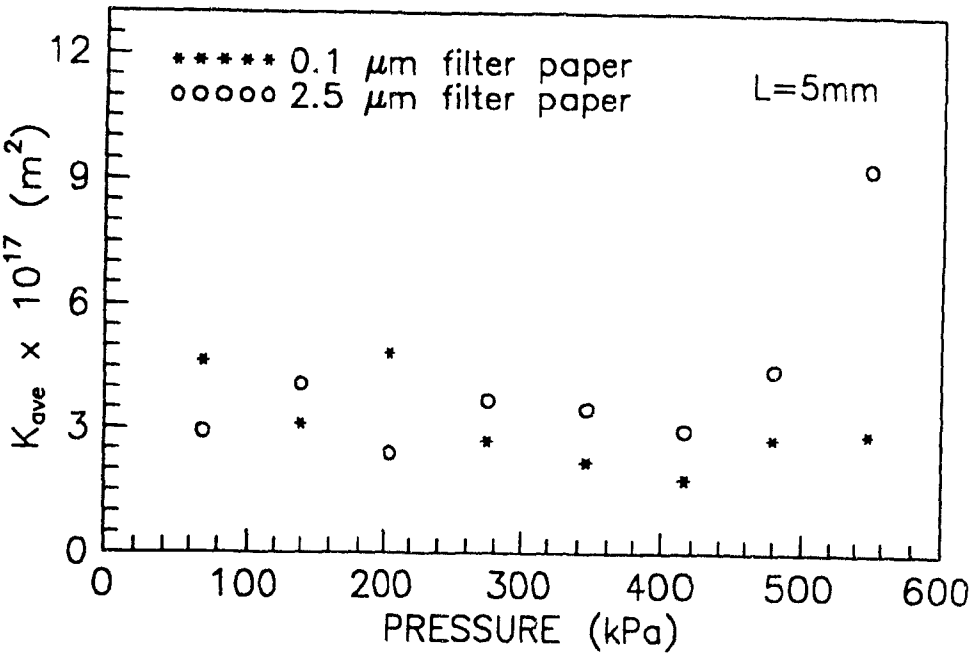

Figure 5.18: Permeability K_{ave} versus filter pressing pressure, P for cakes consisting of 20% A-16SG and 80% C-71FG.

where the filter paper had a mean pore size of 0.1 μm, the curves imply that the cakes were progressively being clogged.

Tables 5.1 and 5.2 list values of n, C and equations for K_{ave} for different filter pressing pressures and Figure 5.18 is a graph of K_{ave} versus filter pressing pressure (at $L = 5$ mm). In Tables 5.1 and 5.2, filter paper pore sizes of 2.5 μm and 0.1 μm were used, respectively. The tables and Figure 5.18 imply that K_{ave} is independent of filtration pressures between 70 kPa to 550 kPa Both tables suggest that cake clogging has occurred but it appears that more medium clogging resulted with the larger pore sized filter paper. These results imply that the permeabilities are independent of the filter pressing pressure, and that there can be some variability in permeability results from run to run. Figures 5.19 and 5.20 show the variability in permeability, for filter pressing experiments repeated under the same conditions.

Table 5.1: Values of n, C and K_{ave} as a function of L.

FILTER PAPER PORE SIZE = 2.5 μm			
PRESSURE (kPa)	n	C (sec/m^n)	K^*_{ave} (m^2)
70	1.94	9.08×10^7	$4.03 \times 10^{-17} L^{+0.06}$
140	2.26	6.76×10^7	$1.03 \times 10^{-17} L^{-0.26}$
205	2.04	6.00×10^7	$1.94 \times 10^{-17} L^{-0.04}$
275	2.07	3.36×10^7	$2.55 \times 10^{-17} L^{-0\,07}$
345	1.99	1.94×10^7	$3.69 \times 10^{-17} L^{+0\,01}$
415	2.09	3.07×10^7	$1\,85 \times 10^{-17} L^{-0\,09}$
480	1.95	$8\,93 \times 10^6$	$5\,83 \times 10^{-17} L^{+0\,05}$
550	1.83	2.12×10^6	$2.29 \times 10^{-16} L^{+0\,17}$

*L is in units of m

Table 5.2: Values of n, C and K_{ave} as a function of L.

FILTER PAPER PORE SIZE = 0.1 μm			
PRESSURE (kPa)	n	C (sec/m^n)	K^*_{ave} (m^2)
70	2.51	9.08×10^8	$3.12 \times 10^{-18} L^{-0\,51}$
140	2.03	6.59×10^7	$2.66 \times 10^{-17} L^{-0\,03}$
205	2.29	9.95×10^7	$1.04 \times 10^{-17} L^{-0\,29}$
275	2.17	7.50×10^7	$1.10 \times 10^{-17} L^{-0\,17}$
345	2.40	2.24×10^8	$2.65 \times 10^{-18} L^{-0\,40}$
415	2.22	9.55×10^7	$5.59 \times 10^{-18} L^{-0\,22}$
480	2.32	8.55×10^7	$5.12 \times 10^{-18} L^{-0\,32}$
550	2.32	7.20×10^7	$5\,32 \times 10^{-18} L^{-0\,32}$

*L is in units of m

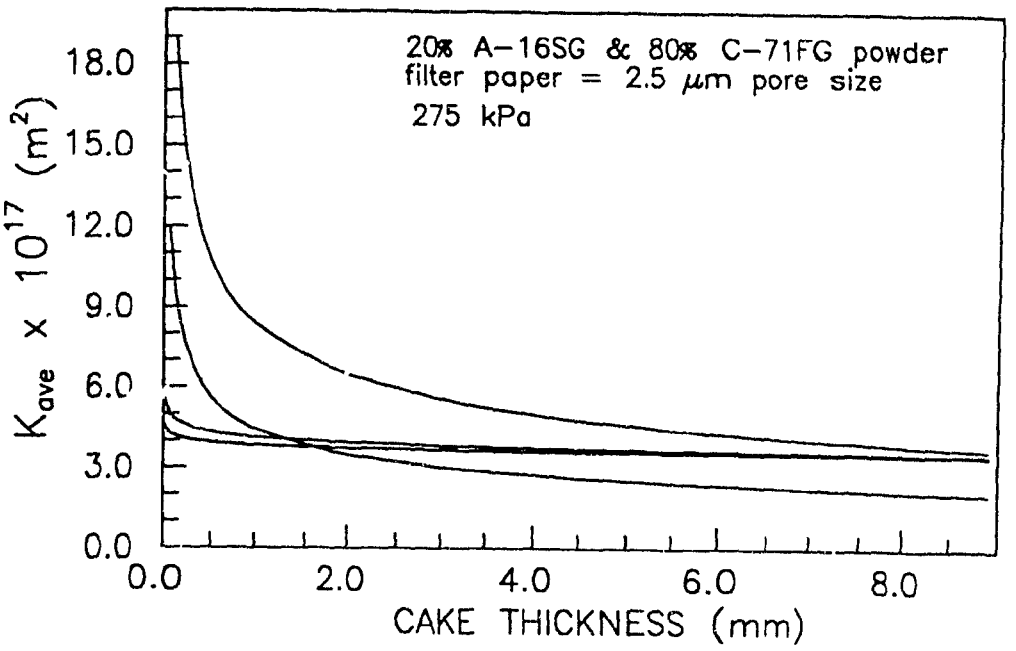

Figure 5.19: Curves of permeability, K_{ave} versus cake thickness, L for experiments repeated under the same conditions. Filter paper pore size = 2.5 μm.

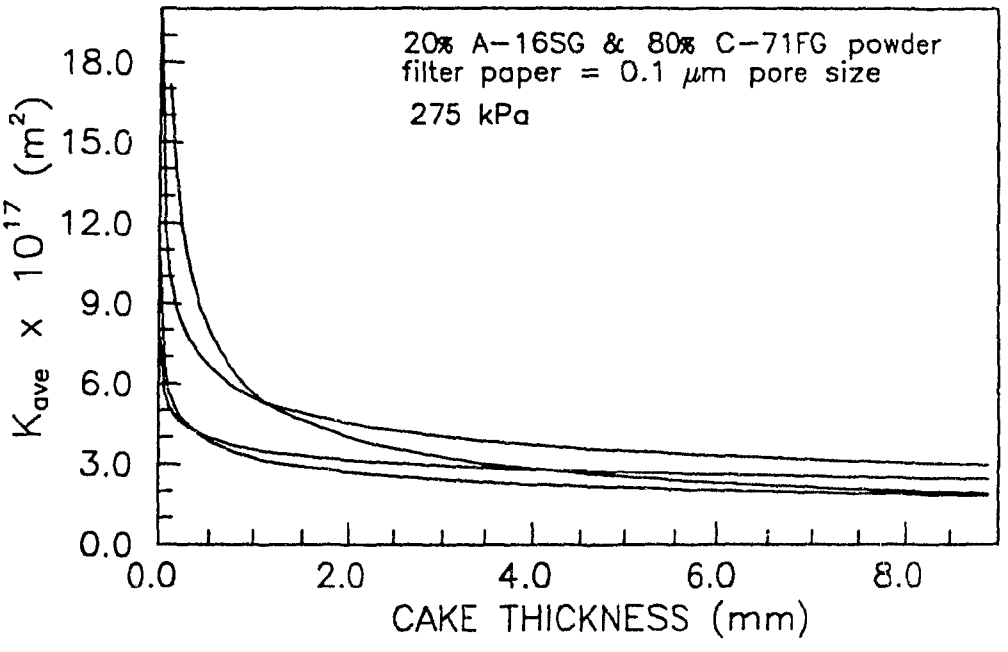

Figure 5.20: Curves of permeability, K_{ave} versus cake thickness, L for experiments repeated under the same conditions. Filter paper pore size = 0.1 μm.

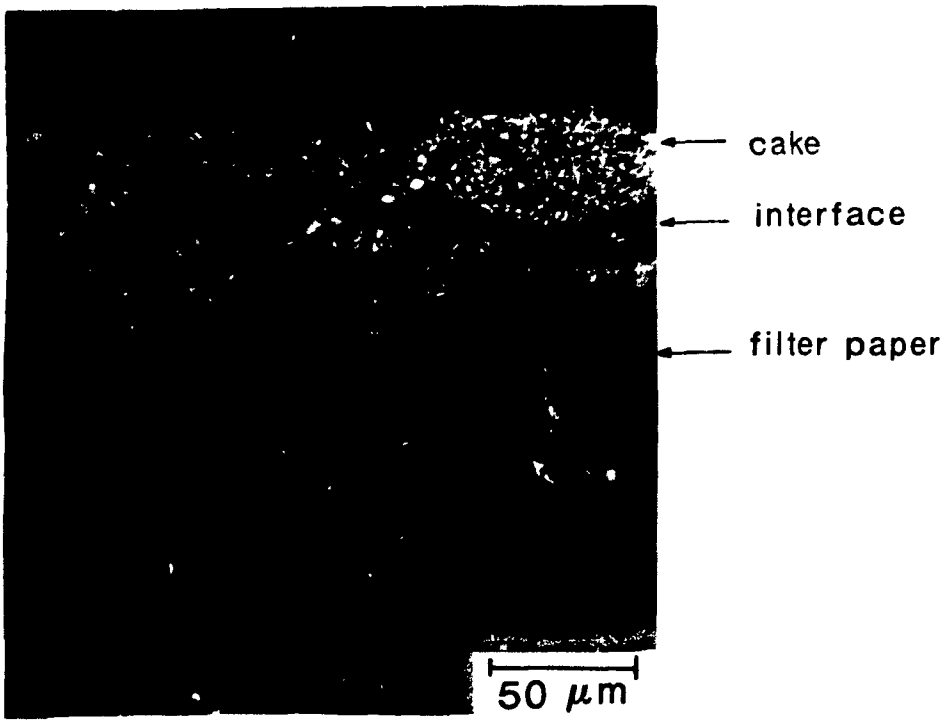

Figure 5.21: Longitudinal section of 2.5 μm pore size filter paper. Used to filter press an A-17 slip. Arrow indicates paper/cake interface (P = 345 kPa).

5.4 FILTER MEDIUM CLOGGING

It will be shown in this SEM study that the 2.5 μm filter paper can become clogged due to particles penetrating and filling the pores. After the cake was filter pressed, the filter paper was separated from the cake. The filter paper was then vacuum resin impregnated and a longitudinal section was polished and prepared for further SEM examination. The micrographs showed that the particles were penetrating the filter paper. The depth of penetration however was only approximately 10 μm - 20 μm (see Figure 5.21). In section 5.1 the microstructures of the cakes were found to have a layer about 10 μm thick at the cake bottom with a high concentration of fines. Clogging appears to occur very close to the cake-filter medium interface. It is this thin clogged layer that is essentially determining the filtration rate. The permeability curves were shown to tend to level off early in the filtration process (after

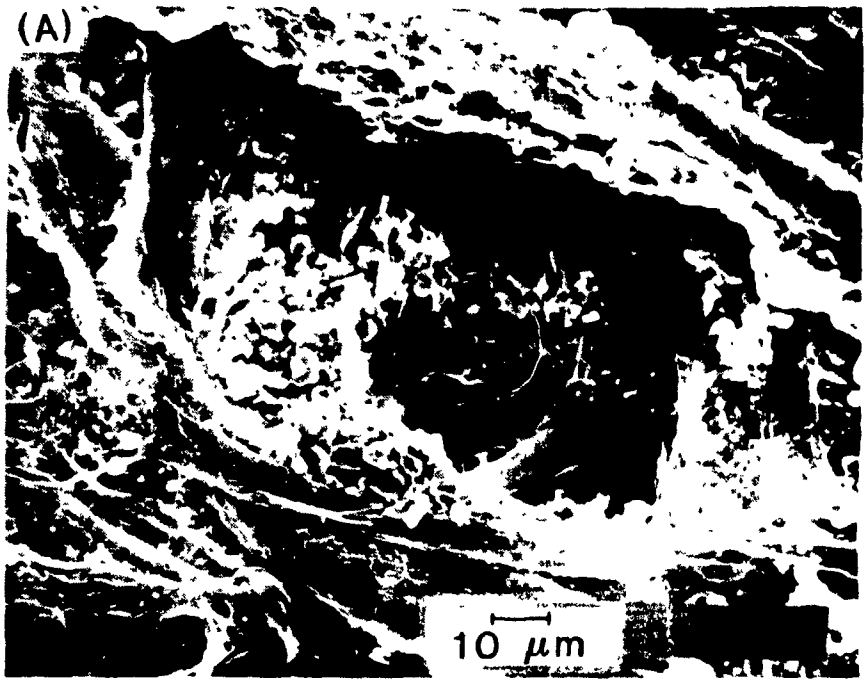

Figure 5.22: Top views of three layers of 2.5 μm pore sized filter paper after being used to filter press (at 345 kPa) a slip with a 20/80 mixture of A-16SG and C-71FG powder. (A) First layer (i.e., layer in contact with cake)

approximately 1 mm). The process is very sensitive to the degree of clogging that occurs in the cake-medium interface region.

5.4.1 FILTER PRESSING WITH MULTI-LAYERED FILTER PAPERS

Three layers of 2.5 μm pore paper was used during filter pressing to study whether particles pass through the filter paper and collect on the lower filter paper layers leading to clogging of the system. These experiments are an easy way to analyze the clogging that could occur in a plaster of Paris mold during slip casting. Figure 5.22 shows top views of micrographs for the three layers of paper. The second and third layers of the filter medium showed that small amounts of powder did accumulate on the paper. The permeability results (see Figure 5.23) are similar to the results where only 1 layer of paper was used (refer to Figures 5.16 and 5.19). Therefore, most of

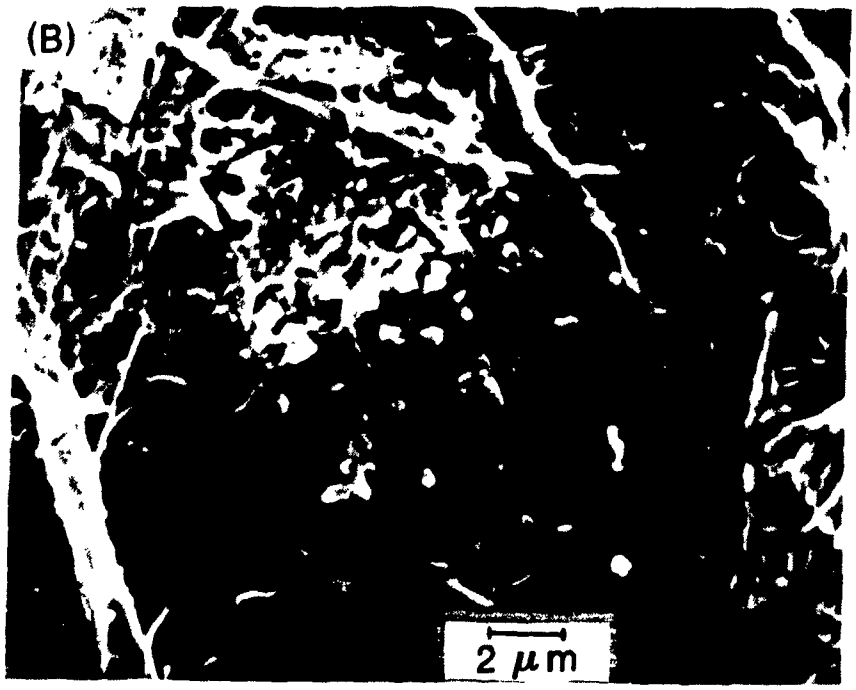

Figure 5.22: (B) Second layer (i.e., middle layer).

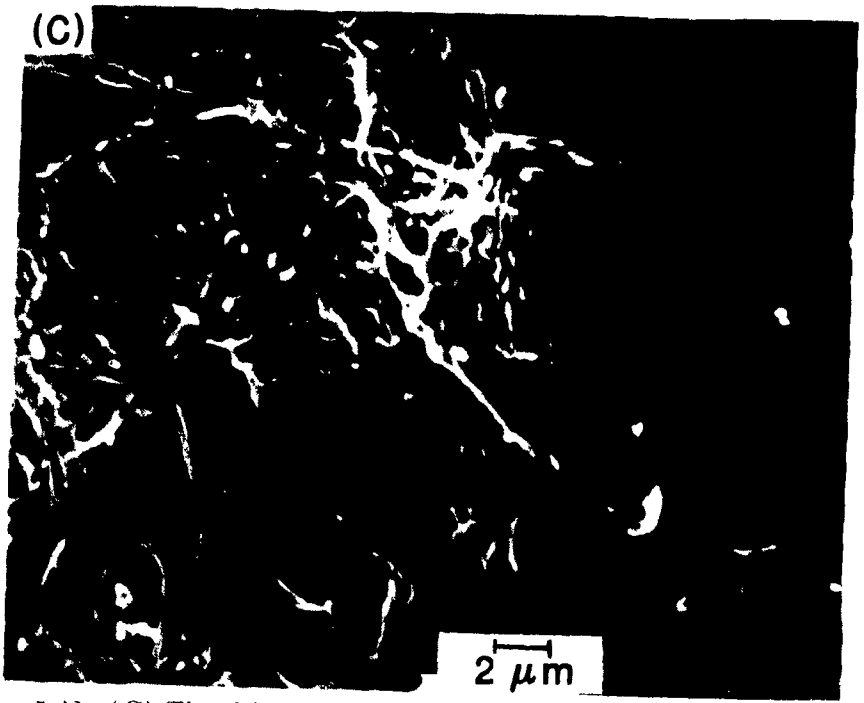

Figure 5.22: (C) Third layer (i.e., layer furthest away from cake bottom).

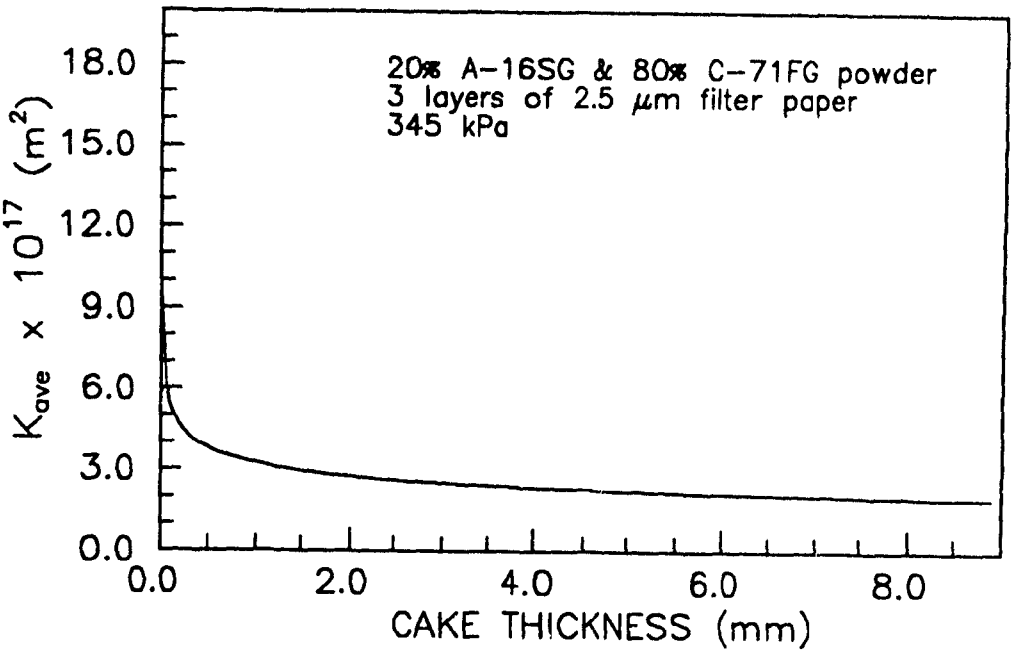

Figure 5.23: Permeability, K_{ave} versus cake thickness, L. Three layers of 2.5 μm pore sized filter paper was used to filter press (at 345 kPa) a slip with a 20/80 mixture of A-16SG and C-71FG powder

the filter medium clogging occurs in a very thin layer (approximately 10 μm - 20 μm) at the cake-filter medium interface.

When two layers of filter paper were used; the top layer being the 2.5 μm pore paper and 0.1 μm pore paper being the bottom layer, it was found that some of the fine particles percolated through the upper layer and deposited on the 0.1 μm pore paper. The micrographs in Figure 5.24 show top views of:

(1) The side of the 2.5 μm pore paper that was in contact with the cake (micrograph (A)).

(2) The side of the 2.5 μm pore paper that was in contact with the bottom filter paper layer (i.e., bottom side) (micrograph (B)).

(3) The side of the 0.1 μm pore paper that was in contact with the top filter paper layer (micrographs (C) and (D)).

Significantly more particles deposited on the second filter paper layer (0.1 μm pore paper) than did in the previous experiment where the same pore sized filter paper (2.5 μm) was used for all the layers. When the same pore sized filter paper is used for all the layers the particles that percolate through the top filter paper layer also tend to be transported right through the other layers. This is due to the much lower concentration of particles being filtered in the lower filter paper layers compared to the particle concentration of the slip. Initially, during filtration many particles are arriving at the same time at the cake-filter medium interface resulting in blocking and bridging of the pores of the filter medium. With the very dilute suspension being filtered in the lower filter paper layers each particle moves separately from the others and will easily follow the streamlines of flow directed towards the pores in the filter. The result will be that a particle, depending on the ratio of pore diameter to particle diameter, will either enter and pass through the pore or will cover the pore opening. Therefore, more particles were deposited on the second layer of the 0.1 μm pore paper as compared to the 2.5 μm pore paper. The permeability results (see Figure 5.25) for this experiment show that progressive clogging has occurred.

Experiments were also performed using a coarser filter paper (Whatman 1) that has an 11 μm particle size retention for the top layer, a 2.5 μm pore paper for the middle layer and a 0.1 μm pore paper for the bottom layer. Micrographs of top views of the filter papers are shown in Figure 5.26. Powder penetrated the top layer paper and some powder migrated through the top layer and deposited on the 2.5 μm pore paper. Furthermore, some of the powder has also migrated through the middle layer and deposited on the 0.1 μm pore paper. With the coarser filter paper used in this experiment significantly more particle migration through the filter medium occurred compared to the experiments where a 2.5 μm pore sized filter paper was used for

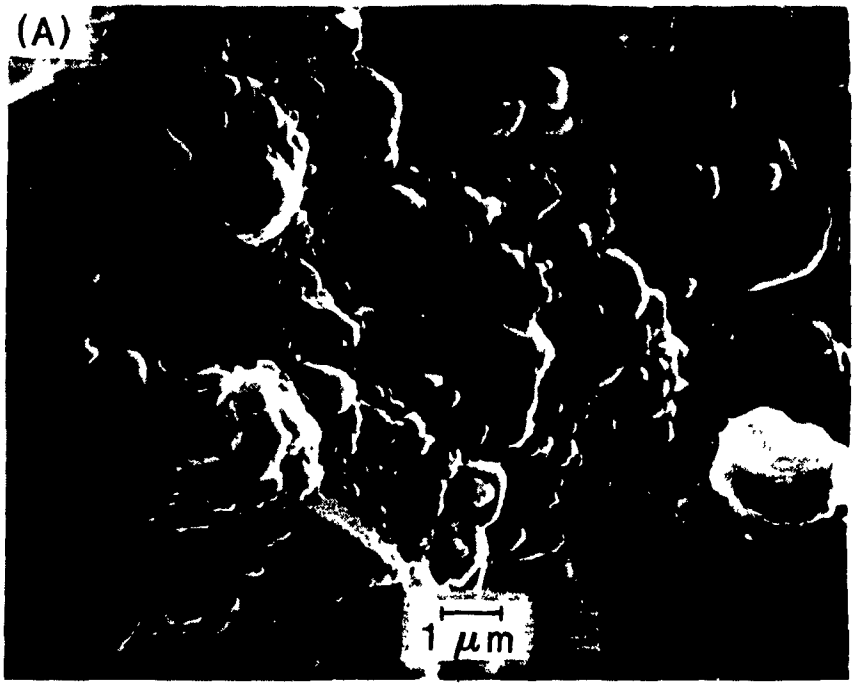

Figure 5.24: Top views of two layers of filter paper after being used to filter press (at 345 kPa) an A-17 slip. (A) First layer - 2.5 μm pore paper that was in contact with the cake.

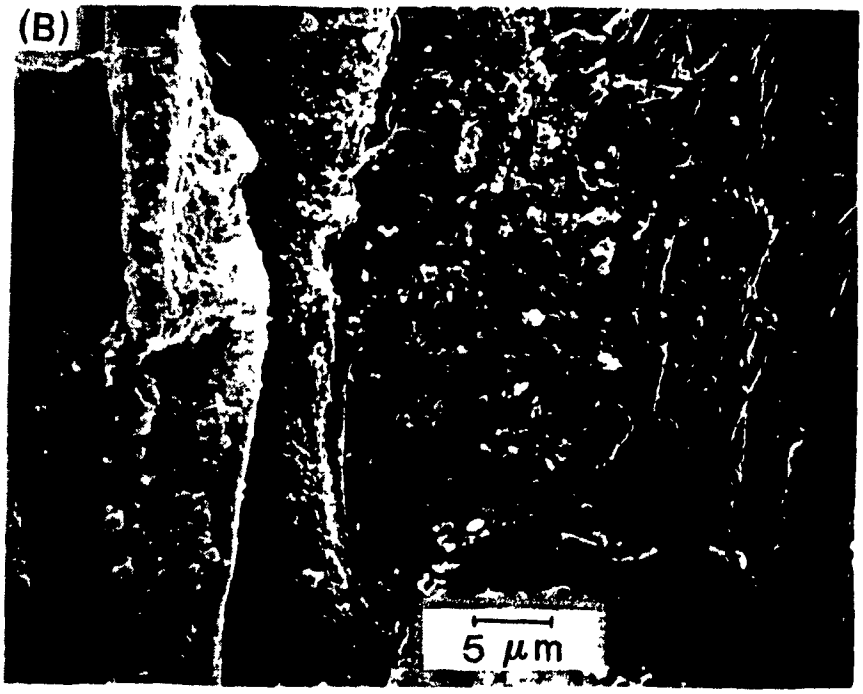

Figure 5.24: (B) View of bottom side of the first layer (i.e., side that was in contact with bottom filter paper layer.

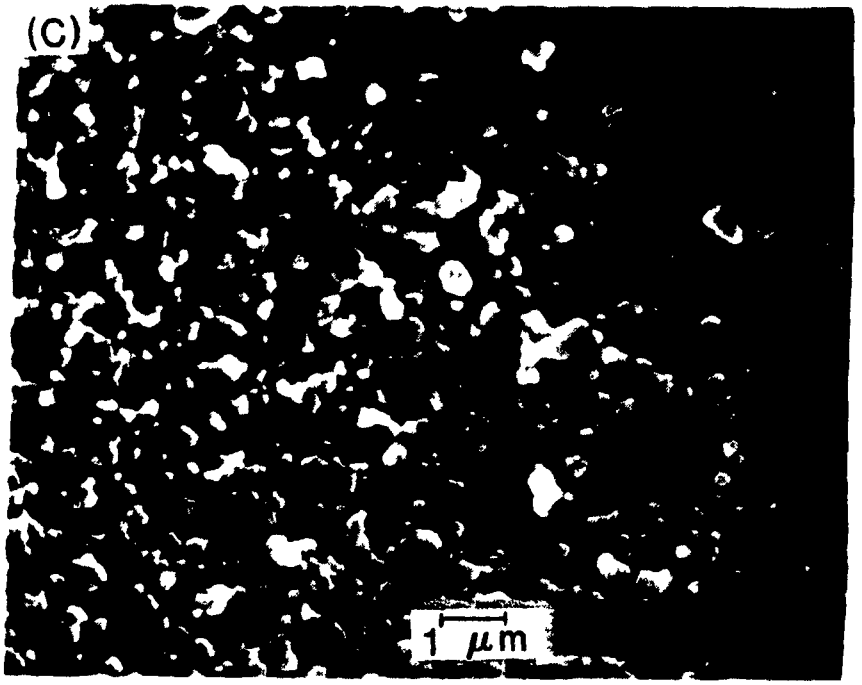

Figure 5.24. (C) Second layer - 0.1 μm pore size filter paper.

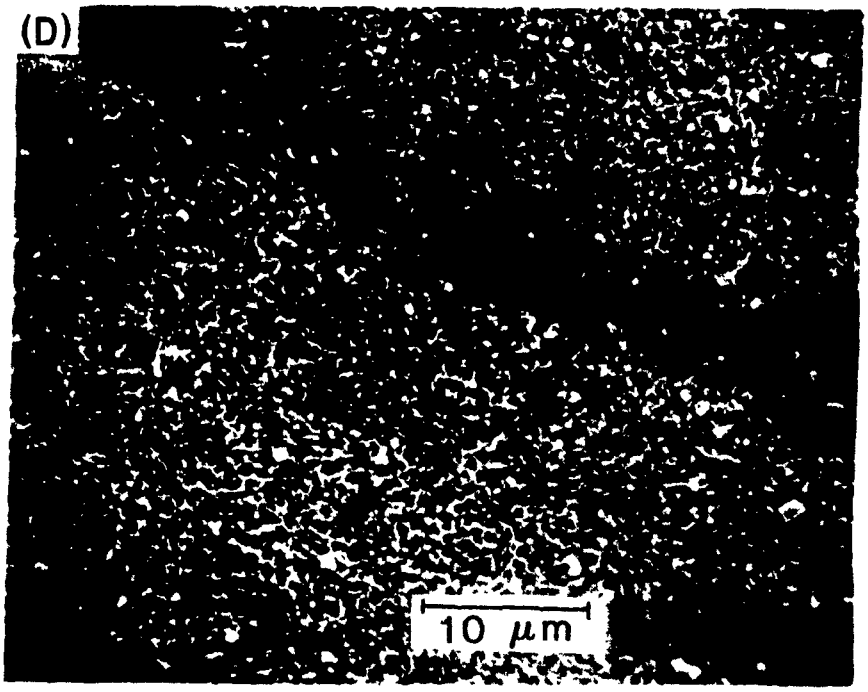

Figure 5.24: (D) Second layer but at a lower magnification than for micrograph (C).

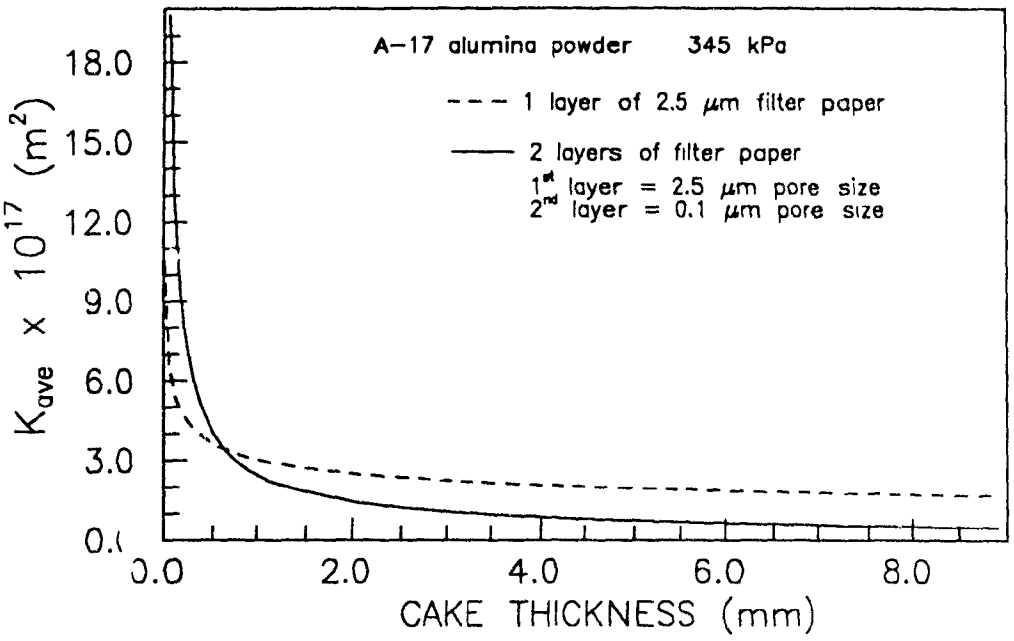

Figure 5.25: K_{ave} versus L. Two layers of 2.5 μm and 0.1 μm filter paper used (A-17 slip, $P = 345$ kPa). Dashed curve - one layer of 2.5 μm filter paper.

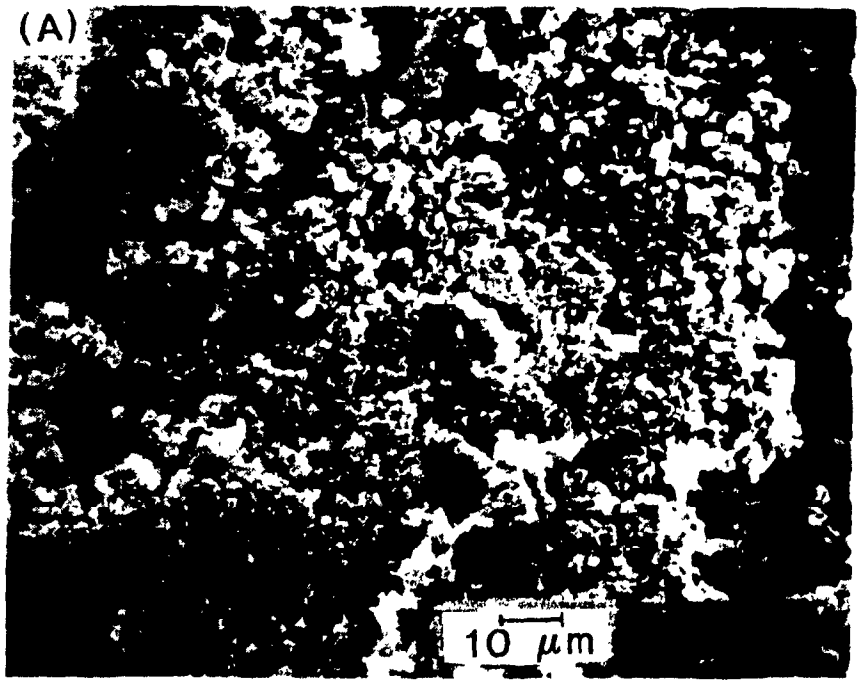

Figure 5.26: Top views of three layers of filter paper after being used to filter press (at 345 kPa) an A-17 slip. (A) First layer - 11 μm particle size retention that was in contact with the cake.

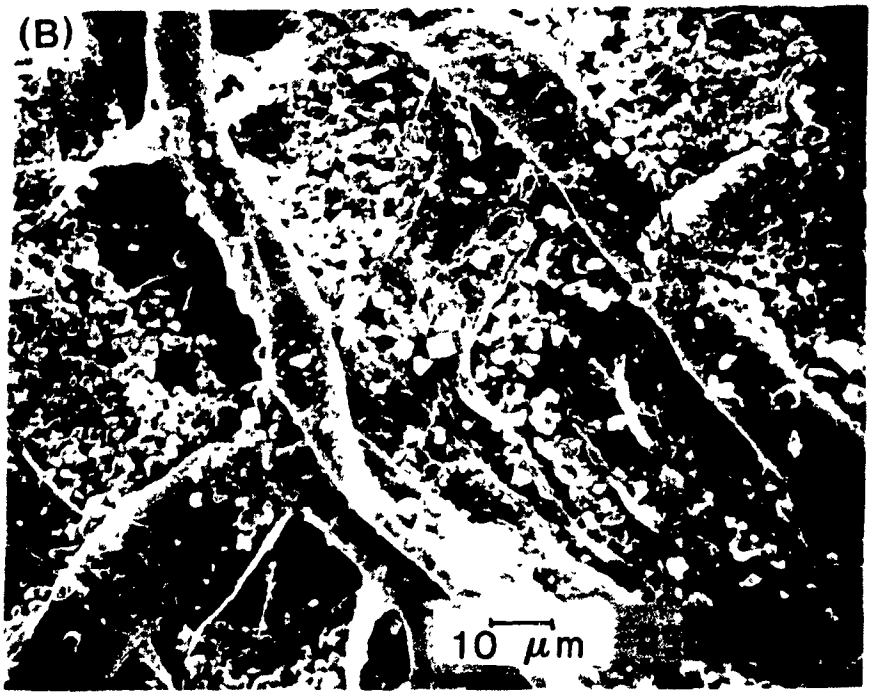

Figure 5.26. (B) Second layer - 2.5 μm pore size filter paper.

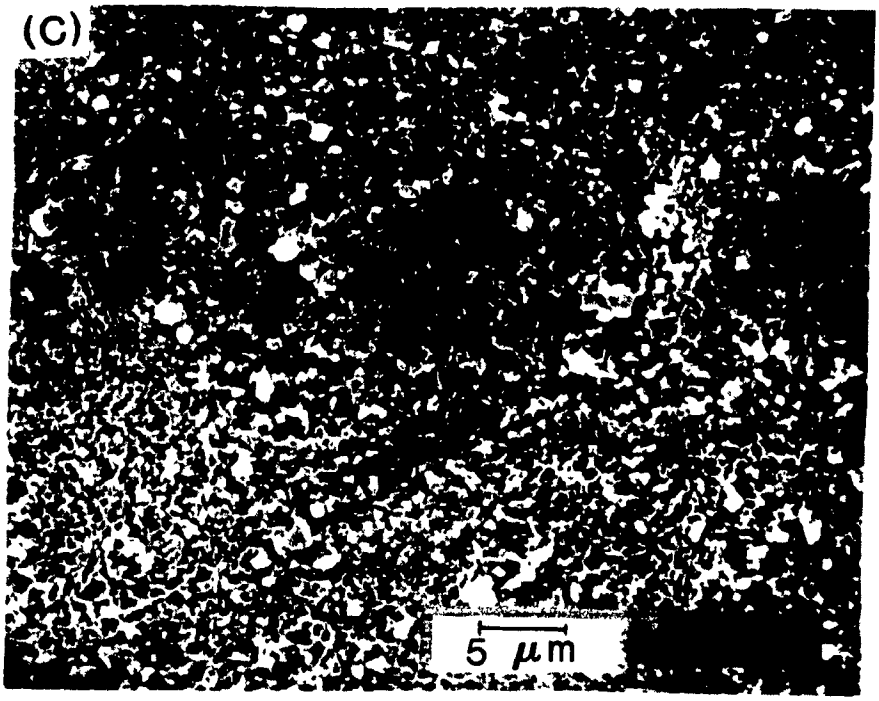

Figure 5.26: (C) Third layer - 0.1 μm pore size filter paper (i.e., layer furthest away from cake).

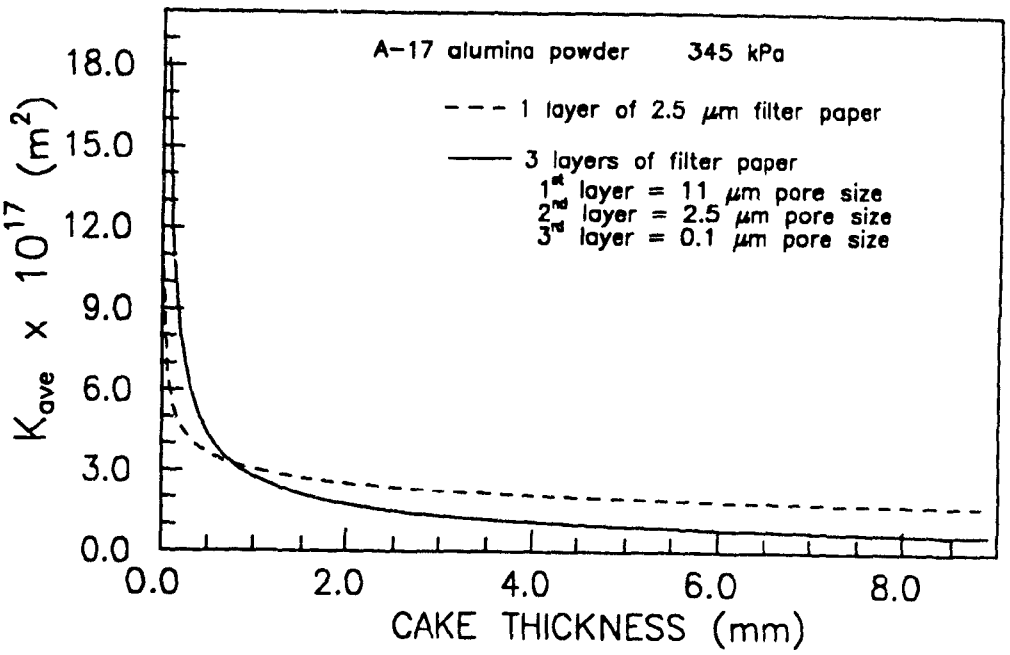

Figure 5.27: K_{ave} versus L. Three layers of 11 μm, 2.5 μm, and 0.1 μm filter paper used (A-17 slip, P = 345 kPa) Dashed curve - one layer of 2.5 μm filter paper.

the top layer of the filter medium The permeability results (see Figure 5.27) show that progressive clogging has occurred. In Figure 5.26 the slip was filter pressed for 2 hours. Slips were also pressed for shorter times to illustrate the continuous migration of particles through the top and middle filter paper layers. Figures 5.28 and 5 29 show top views of the middle and bottom paper layers for slips cast for one minute and 10 seconds, respectively Figures 5.28 and 5.29 show that particles have accumulated on the middle and bottom paper layers, however significantly more particle migration has occurred in Figure 5.26.

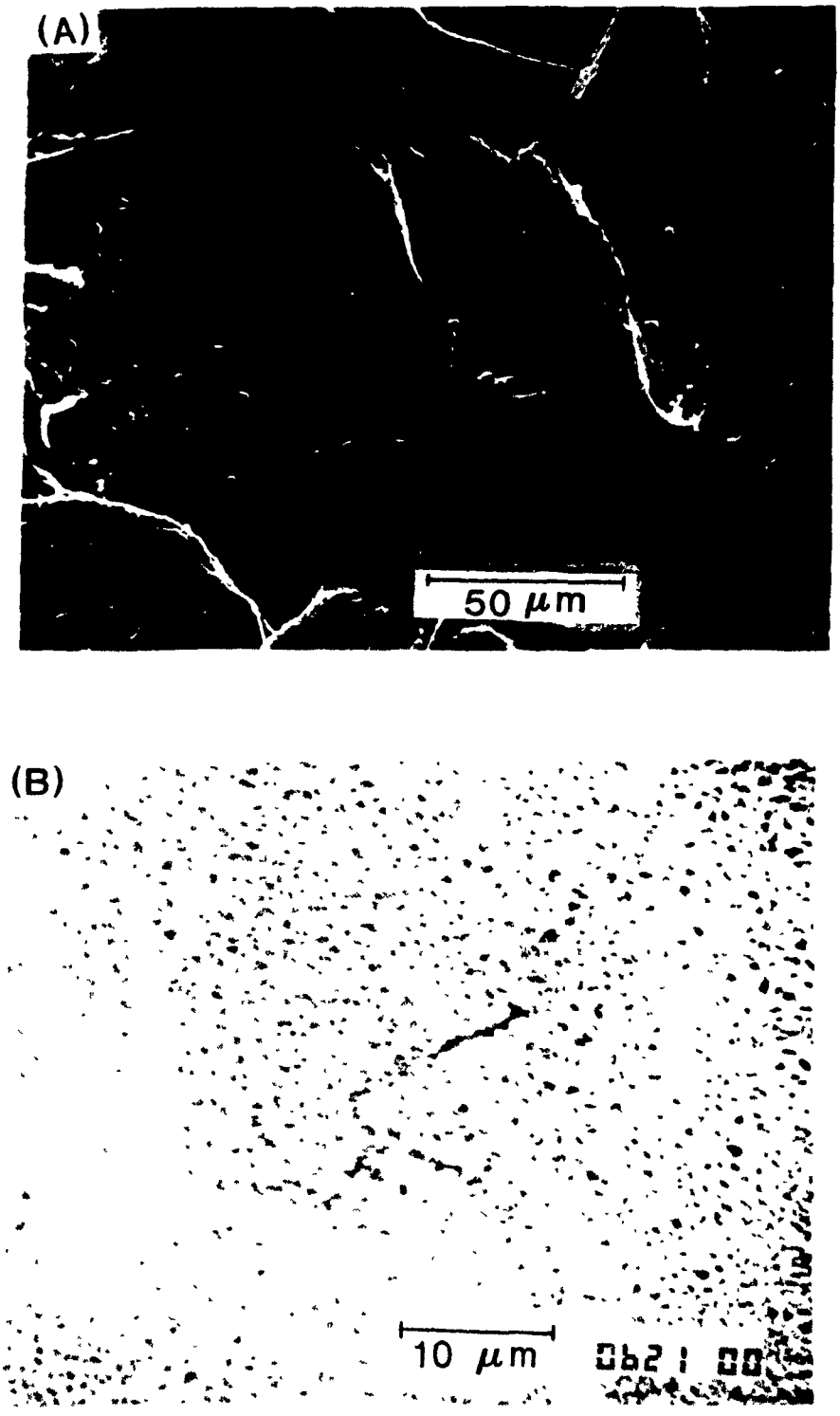

Figure 5.28: SEM of filter paper after being used to filter press (at 345 kPa) an A-17 slip for one minute. The top, middle and bottom filter paper layers had pore sizes of 11 μm, 2.5 μm and 0.1 μm, respectively. (A) Top view of the middle filter paper layer. (B) Top view of the bottom layer.

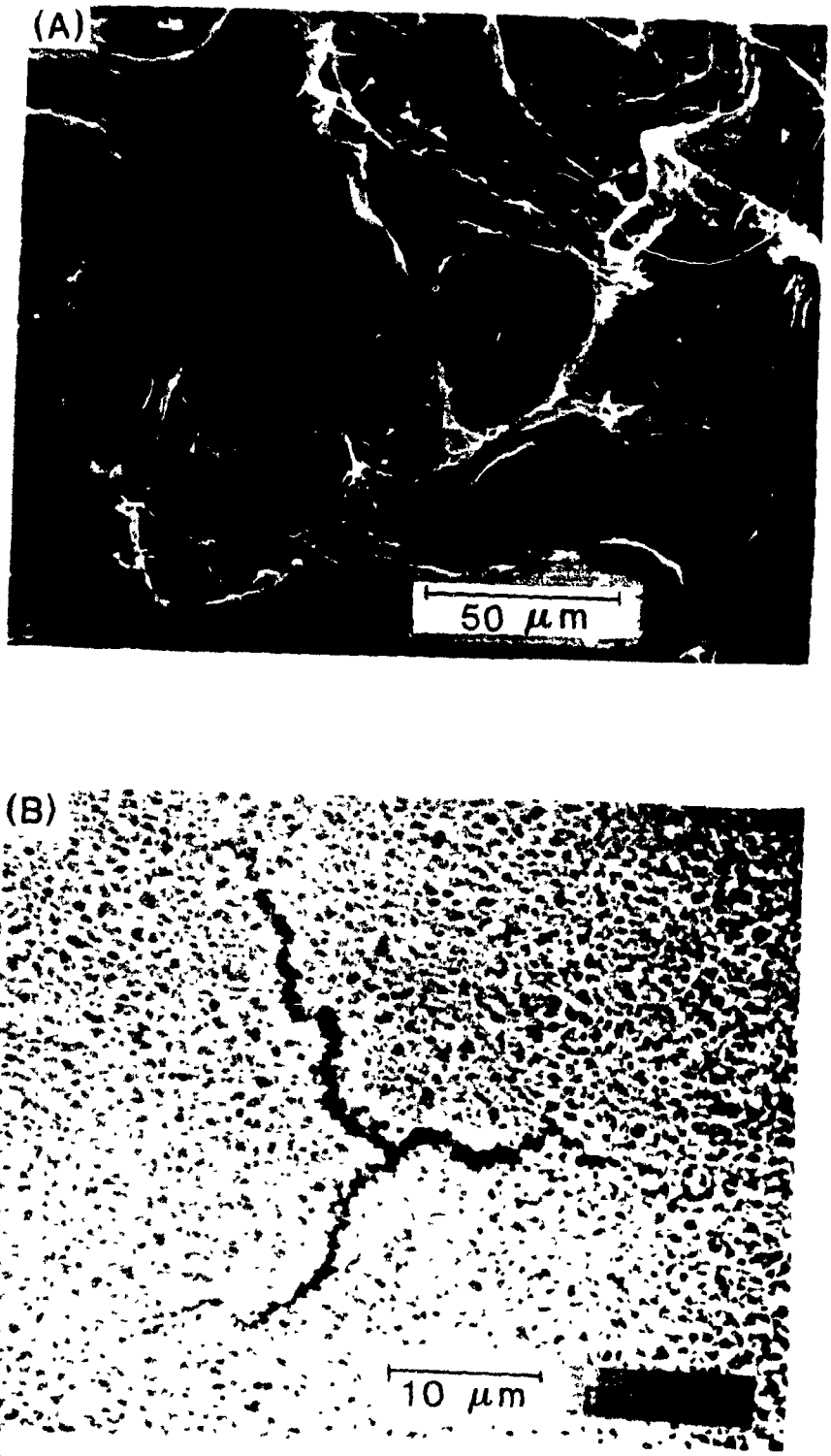

Figure 5.29. SEM of filter paper after being used to filter press (at 345 kPa) an A-17 slip for 10 seconds. The top, middle and bottom filter paper layers had pore sizes of 11 μm, 2.5 μm and 0.1 μm, respectively. (A) Top view of the middle filter paper layer. (B) Top view of the bottom layer.

Chapter 6

RANDOM TUBE MODEL TO SIMULATE FILTRATION

6.1 PERMEABILITY OF POROUS MEDIA

Darcy's law in Chapter 2 showed that the superficial velocity, q is proportional to the pressure gradient, dP_l/dx and inversely proportional to the viscosity, μ of the filtrate:

$$q = \frac{K}{\mu} dP_l/dx \tag{6.1}$$

where permeability, K is the proportionality constant and only depends on the structure of the porous medium. The above equation implies that resistance to flow is entirely due to viscous drag. Darcy's law has been found to be valid for laminar flow where the particle Reynolds number, $\Re$ is less than approximately 20 or for a modified Reynolds number, $\Re_m$ less than 2.[37, 75] The Reynolds number and modified Reynolds number are defined as:

$$\Re = \frac{d_p q \rho_f}{\mu} \tag{6.2}$$

and

$$\Re_m = \frac{\rho_f q}{\mu(1-\nu)S_o} \tag{6.3}$$

where d_p is the particle diameter, ρ_f is the density of the filtrate, ν is the porosity and S_o is the specific surface (i.e., surface area per unit volume of solid).

Reynolds number, $\Re$ is employed in the following equation to emphasize that the resistance to flow is entirely due to viscous drag:

$$C_f = \mathcal{F}\Re \tag{6.4}$$

where C_f is a constant and $\mathcal{F}$ is the friction factor:

$$\mathcal{F} = \frac{\mathrm{dP_l}}{\mathrm{dx}} \frac{\mathrm{d_p}}{\rho_\mathrm{f} \mathrm{q}^2} \tag{6.5}$$

From Darcy's law, it is found that K has units of $(length)^2$ and Equation (6.4) implies that K is proportional to the square of the particle diameter. However, other features of the porous media are also important. The Kozeny-Carman equation describes K in terms of the porosity, ν specific surface of the porous medium, S_o and the Kozeny constant, h:[75, 37, 76]

$$K = \frac{\nu^3}{h(1-\nu)^2 S_o^2} \tag{6.6}$$

If the porous media is an assembly of spheres then:

$$S_o = 6/d_p \tag{6.7}$$

and therefore,

$$K = \frac{\nu^3}{h(1-\nu)^2} \frac{d_p^2}{36} \tag{6.8}$$

The Kozeny constant, h is made up of two terms, a shape factor and the tortuosity and it is found in practice that h is approximately 5.0 for many different systems.[76] The Kozeny-Carman equation was first derived by assuming that the fluid flow through the

consolidated layer could be modeled as a bundle of capillary tubes using Poiseuille's Law modified in terms of a hydraulic radius and an assumed tortuosity of flow. An important limitation of the Kozeny-Carman equation is that the pores must be randomly distributed and be reasonably uniform.

Quite often filter cakes can have a distribution of pore sizes and an average pore size should not be used to describe the flow through filter cakes. Furthermore, experimental work has demonstrated that during the filtration of ceramic powders there is a certain unpredictability about the process even when a knowledge of the size distribution and the physical chemistry of the powder is available.

6.2 RANDOM TUBE MODEL

A computer model has been developed to simulate the filtration process. The filtration model takes into account variations in cake microstructures by using a two-dimensional network of tubes with different radii size distributions in a regular square lattice arrangement. An example of the network used in this study is shown in Figure 6.1. The network setup was first proposed by Leitzelement et al.[77] to model deep bed filtration. Deep bed filtration is an engineering process in which a large volume of liquid containing a small concentration of fine particles in a suspension is clarified by passage through a bed of granular material such as sand (e.g. water purification).

Fluid flow in the network can be calculated on a computer by solving a series of simultaneous equations derived by using a matrix expression for Darcy's law and

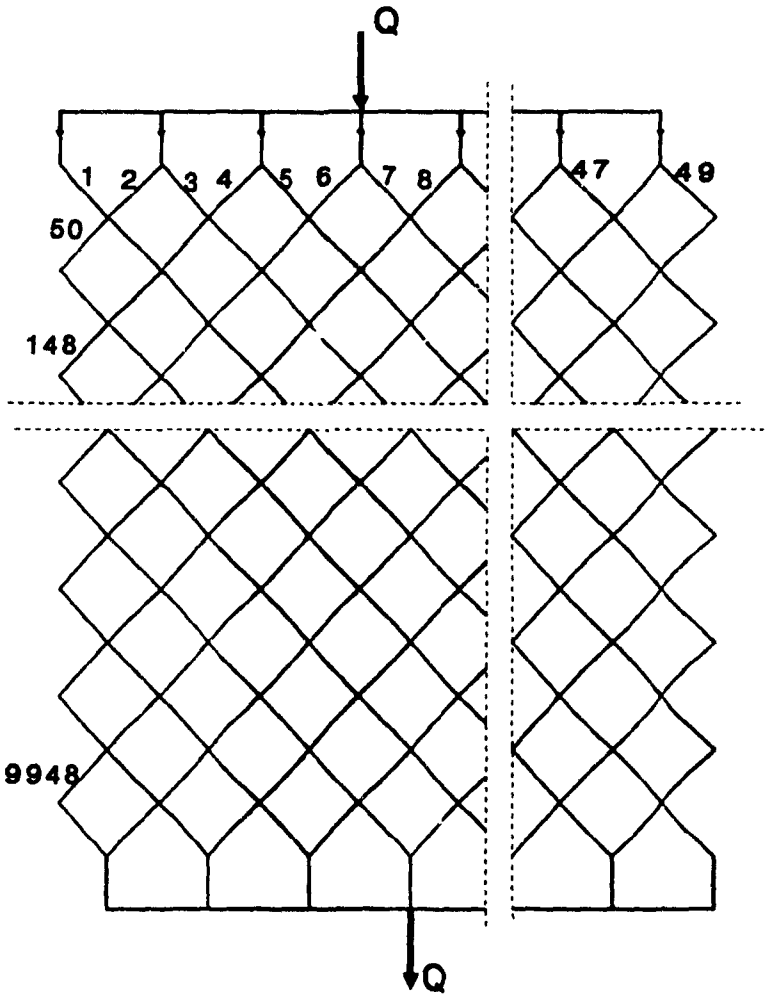

Figure 6.1: Two dimensional tube network.

applying electrical network theory:[77, 78]

$$[Q] = [Z]^{-1}[P] \tag{6.9}$$

where the column vector $[Q]$ contains the flows in all n loops in the network, $[P]$ matrix is a column vector containing the imposed pressure drop as the first element with all the other elements being zero and $[Z]$, a square $n \times n$ matrix, is an operator which acts as the resistance of the whole network.

The number of solutions required for the flow distribution in the tubes is equal to the total number of loops in the network. One can see that this method is feasible for a small network but the size of the network is limited by the RAM memory of the computer. For example, using a computer with 6 megabytes of memory, the largest network which can be handled is one that has 55 rows and 6 loops per row, a total of 715 tubes. This is a rather small network and is not sufficiently large to be representative of fluid flow through a cake.

An alternative approach using the Hardy-Cross Method[79, 80, 81] was chosen to solve the network.

6.2.1 HARDY-CROSS METHOD

The Hardy-Cross Method is a method of successive approximations based on satisfying the following conditions (see Figure 6.2): (1) At any node, the total inflow must equal the total outflow. This condition satisfies the continuity equation. (2) Between any two nodes the total pressure drop is independent of the path taken. Therefore, the sum of the pressure drops around each loop must be zero.

To solve the network, flows are initially assumed for each tube so that continuity is satisfied at each node. Then a successive computational procedure is used to correct

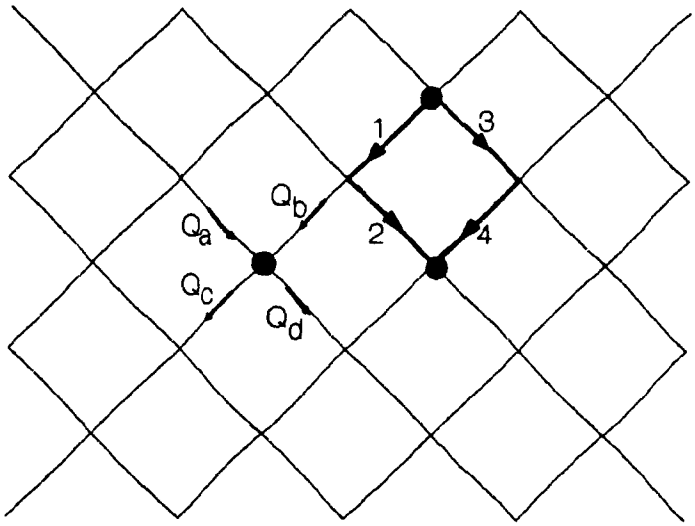

Figure 6.2: Flow conditions for the Hardy-Cross Method.

the assumed flows to satisfy condition (2).

Laminar flow through circular tubes is described by the Hagen-Poiseuille equation:

$$\Delta P = (\frac{8\mu L}{\pi R^4})Q \tag{6.10}$$

where μ is the viscosity of the filtrate, L the tube length, R tube radius, Q volumetric flow rate and ΔP is the pressure drop. Therefore, the flow resistance is proportional to L/R^4. To calculate flows in the network it has been assumed that the length of each tube is proportional to its radius. Thus, the flow resistance is proportional to $1/R^3$.

In any individual loop, the total pressure drop in the clockwise direction is the sum of pressure drops in all tubes that carry flow in the clockwise direction

(subscript cl) around the loop,

$$\Sigma \Delta P_{cl} = \Sigma C_n \frac{Q_{cl}}{R_{cl}^3} \tag{6.11}$$

where C_n is a constant. Similarly, the loss of head in the counterclockwise direction (subscript cc) is,

$$\Sigma \Delta P_{cc} = \Sigma C_n \frac{Q_{cc}}{R_{cc}^3}. \tag{6.12}$$

The difference between Equations (6.11) and (6.12) is the loop's closure error of the first trial. One must determine a flow correction ΔQ; which when subtracted from Q_{cl} and added to Q_{cc} will equalize the two pressure drops. Thus, ΔQ must satisfy the following equation:

$$\Sigma \frac{1}{R_{cl}^3}(Q_{cl} - \Delta Q) = \Sigma \frac{1}{R_{cc}^3}(Q_{cc} + \Delta Q). \tag{6.13}$$

From this relationship we may solve for ΔQ:

$$\Delta Q = \frac{(\frac{1}{R_{cl}^3})Q_{cl} - (\frac{1}{R_{cc}^3})Q_{cc}}{\frac{1}{R_{cc}^3} + \frac{1}{R_{cl}^3}}. \tag{6.14}$$

A second approximation is estimated for the flow distribution using ΔQ. These successive corrections are found for each loop in the entire network until ΔQ and the difference between ΔP_{cl} and ΔP_{cc} becomes negligibly small.

After having solved for the flows, the permeability of the network can then be calculated by applying Darcy's Law:

$$dP_l/dx = \frac{\mu q}{K}. \tag{6.15}$$

The permeability, K is normalized relative to the permeability of a network with all tubes having a tube radius of 1.0 μm, K_o:

$$K/K_o = \frac{1/\Delta P}{1/\Delta P_o} \tag{6.16}$$

where ΔP is the pressure drop across the network and ΔP_o is the pressure drop across a network with the same total inflow rate and same network grid size as for the network in question, but with all tubes in this network having a radius, R_o equal to 1 μm. The pressure drop, ΔP across the network was calculated along each column i and then averaged:

$$\Delta P = \frac{C_n}{I} \sum_{i=1}^{I} \sum_{j=1}^{J} \frac{1}{R_{ji}^3} Q_{ji} \tag{6.17}$$

where j is the tube layer, J is the total number of layers, I is the total number of columns and R_{ji} and Q_{ji} are the radius and flow rate, respectively of tube ji. The pressure drop, ΔP_o is equal to the following:

$$\Delta P_o = C_n J \frac{1}{R_o^3} Q_o \tag{6.18}$$

where Q_o is the flow rate through the tubes for a network with all the tubes having a radius, $R_o = 1.0 \mu m$. Therefore, the following expression is obtained for K/K_o:

$$\begin{aligned} K/K_o &= \frac{\Delta P_o}{\Delta P} \\ &= (IJ \frac{1}{R_o^3} Q_o)/(\sum_{i=1}^{I} \sum_{j=1}^{J} \frac{1}{R_{ji}^3} Q_{ji}) \\ &= (IJQ_o)/(\sum_{i=1}^{I} \sum_{j=1}^{J} \frac{1}{R_{ji}^3} Q_{ji}). \end{aligned} \tag{6.19}$$

The computer program is listed in Appendix A.

The main advantage of the Hardy-Cross Method is that large networks containing more than 10,000 tubes can be modeled using a microcomputer with only 640 kilobytes of RAM memory and thus this network size is more representative of flow through a porous cake. The Hardy-Cross Method, however due to its iterative approach to solve for the flows in the network still requires a lot of CPU time. Some of the computer programs that will be presented in later sections to describe the filtration process can take approximately three days to run on an IBM microcomputer with an 80386 processor. Because of the slow speed of the microcomputer and the large number of runs that were required most of the computer runs were performed on the CRAY X-MP (with 8 megabytes of memory and 2 processors) supercomputer located at the Dorval Weather Station. The CRAY solved the networks on the order of 200 times faster than compared to the 80386 microcomputer

6.3 RANDOM NUMBER GENERATOR

Tube radii of the network having the following size distribution functions were studied: (1) Gaussian (normal), (2) log-normal and (3) Rayleigh. A random number generator function was incorporated into the computer program. The random numbers were generated using the rejection method.[82] The rejection method requires choosing a finite comparison function, $f(x)$ that is everywhere greater than the probability distribution, $p(x)$ that one wishes to generate. It is essential to choose a comparison function whose indefinite integral is known analytically, and is also analytically invertible to give x as a function of the area under the comparison function to the left of x. Select a random uniform deviate between 0 and the total area, A_{tot} under $f(x)$ and use it to obtain a corresponding x_1. A second uniform deviate be-

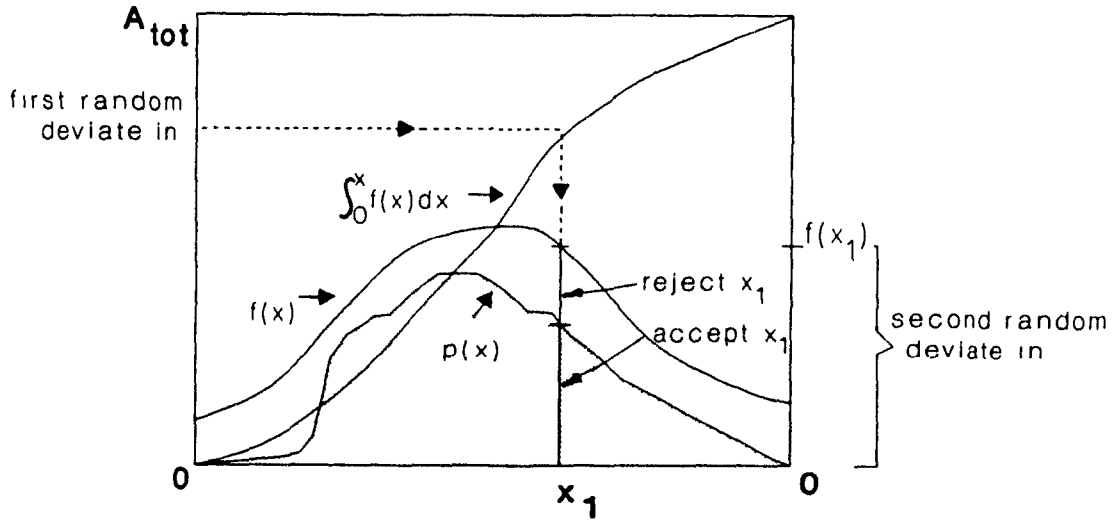

Figure 6.3: Rejection method for generating a random deviate x from a known probability distribution $p(x)$ that is everywhere less than some other function $f(x)$ (after Ref. 82).

tween 0 and $f(x_1)$ is selected to obtain the y_1 coordinate. Now, if $p(x_1)$ is greater than y_1 then the x_1 value is accepted. If $p(x_1)$ is less than y_1, the x_1 value is rejected and the selection process is repeated until the x_1 value is accepted. Figure 6.3 illustrates the procedure. To choose uniform random deviates between 0.0 and 1.0 a "portable" function routine based on the algorithm of Press[82] was used.

6.3.1 DISTRIBUTIONS

Random tube sizes were generated for the following three probability density functions:[83, 84]

$$Gaussian: p_g(x) = \frac{1}{\sigma\sqrt{2\pi}} \exp\left[-\frac{1}{2}\left(\frac{x-\mu_m}{\sigma}\right)^2\right] \quad -\infty < x < \infty \qquad (6.20)$$

where μ_m and σ are the mean and standard deviation, respectively, of the variate.

$$Log-normal: p_l(x) = \frac{1}{\sqrt{2\pi}\xi x}\exp\left[-\frac{1}{2}\left(\frac{\ln x - \lambda_m}{\xi}\right)^2\right] \quad 0 \le x < \infty \tag{6.21}$$

where λ_m and ξ are the mean and standard deviation, respectively, of $\ln x$.

$$Rayleigh \cdot p_r(x) = 2\alpha^2 x \exp(-\alpha^2 R^2) \quad x \ge 0 \tag{6.22}$$

where $\alpha^{-1} = \frac{2}{\sqrt{\pi}}\mu_m$ is a characteristic tube radius.

The comparison curve, $f(x)$ chosen for these distributions is:

$$f(x) = \frac{c_o}{1 + (x - x_o)^2/a_o^2} \tag{6.23}$$

where a_o, c_o and x_o are constants. The total area under this curve is:

$$\begin{aligned} A_{tot} &= \int_{-\infty}^{\infty} \frac{c_o a_o^2}{a_o^2 + (x - x_o)^2}\, dx \\ &= c_o a_o \tan^{-1}\left(\frac{x - x_o}{a_o}\right)\Big|_{-\infty}^{\infty} \\ &= c_o a_o \pi. \end{aligned} \tag{6.24}$$

Therefore,

$$\begin{aligned} c_o a_o \pi U &= c_o a_o \tan^{-1}\left(\frac{x - x_o}{a_o}\right)\Big|_{-\infty}^{x_1} \\ &= c_o a_o \left[\tan^{-1}\left(\frac{x_1 - x_o}{a_o}\right) + \frac{1}{2}\pi\right] \end{aligned} \tag{6.25}$$

where U is a uniform deviate between 0 and 1. Equation (6.25) is invertible to give

x_1 as a function of the area under $f(x)$ to the left of x_1:

$$x_1 = a_o \tan\left((U - 1/2)\,\pi\right) + x_o \tag{6.26}$$

Therefore, the x-coordinate of an area-uniform random point under $f(x)$ is given by Equation (6.26) or more simply if a phase shift of $1/2\pi$ is applied one can use the following equation:

$$x_1 = a_o \tan\left(\pi U\right) + x_o. \tag{6.27}$$

The constants a_o, c_o and x_o are chosen such that $f(x)$ is everywhere greater than $p(x)$. The ratio of accepted to rejected points is the ratio of the area under p to the area between p and f.

To verify that the random number generator gives good representations of the theoretical probability density functions, frequency histograms were generated using the random number generator. Figures 6.4, 6.5 and 6.6 show examples of frequency histograms along with the theoretical probability density curves. For each histogram, 2000 numbers were generated. The figures show that the random number generator generates numbers that fit the density function curves very well.

6.4 FLOW CALCULATIONS

The network model was analyzed with various tube size distributions. Figure 6.7 shows examples of a Gaussian, log-normal and a Rayleigh distribution, each with a mode = 1.0 μm. The permeabilities, K calculated for the three examples are all different and the reasons for this will be discussed in the following sections. The K values in the figure are given relative to the permeability of a network in which all

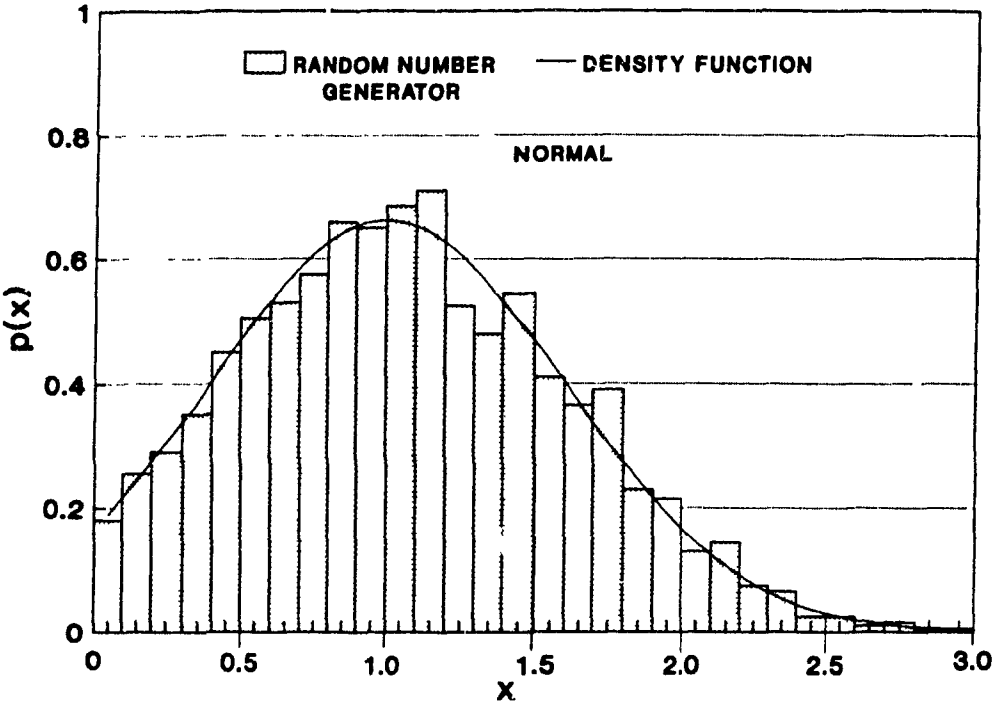

Figure 6.4: Frequency histogram generated using the random number generator and the theoretical probability density function curve for a Gaussian (normal) distribution ($\sigma = 0.6$, $\mu_m = 1.0$).

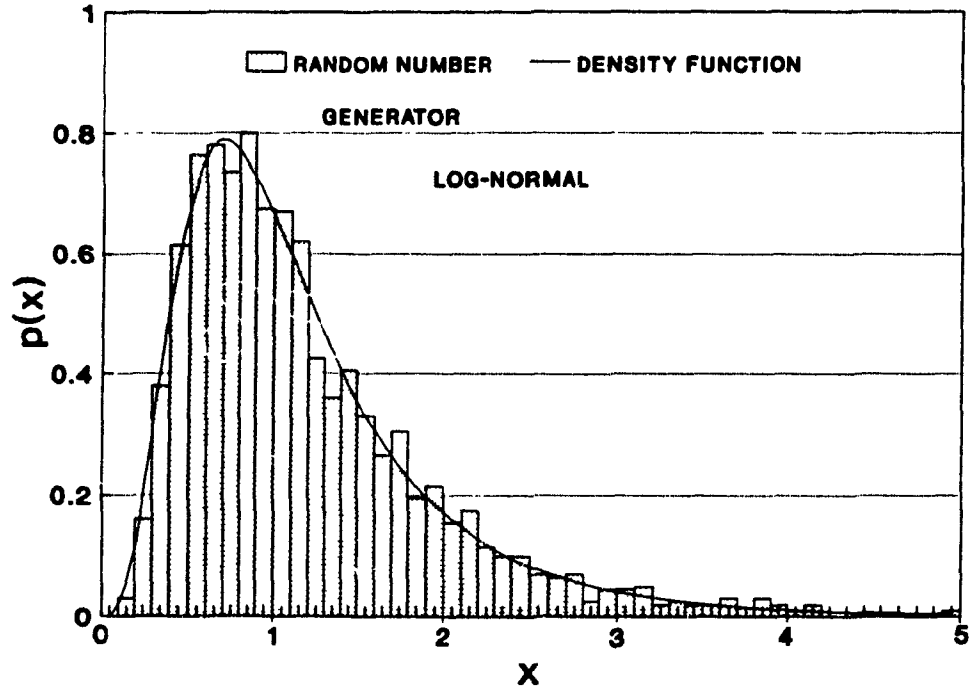

Figure 6.5: Frequency histogram generated using the random number generator and the theoretical probability density function curve for a log-normal distribution ($\xi = 0.6$, $\lambda_m = 0$).

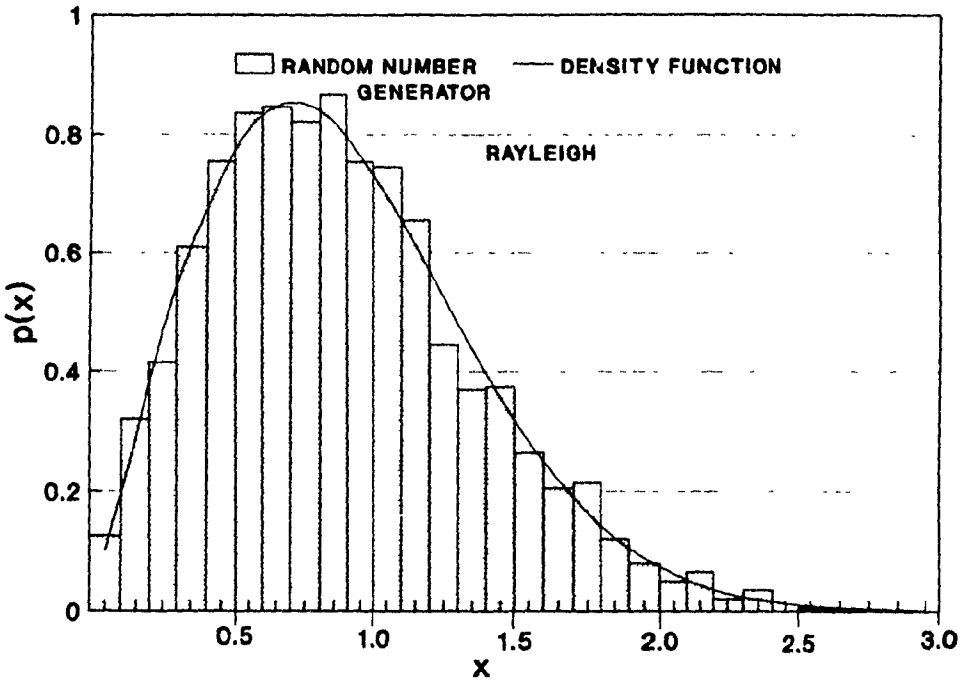

Figure 6.6: Frequency histogram generated using the random number generator and the theoretical probability density function curve for the Rayleigh distribution ($\alpha^{-1} = 1$).

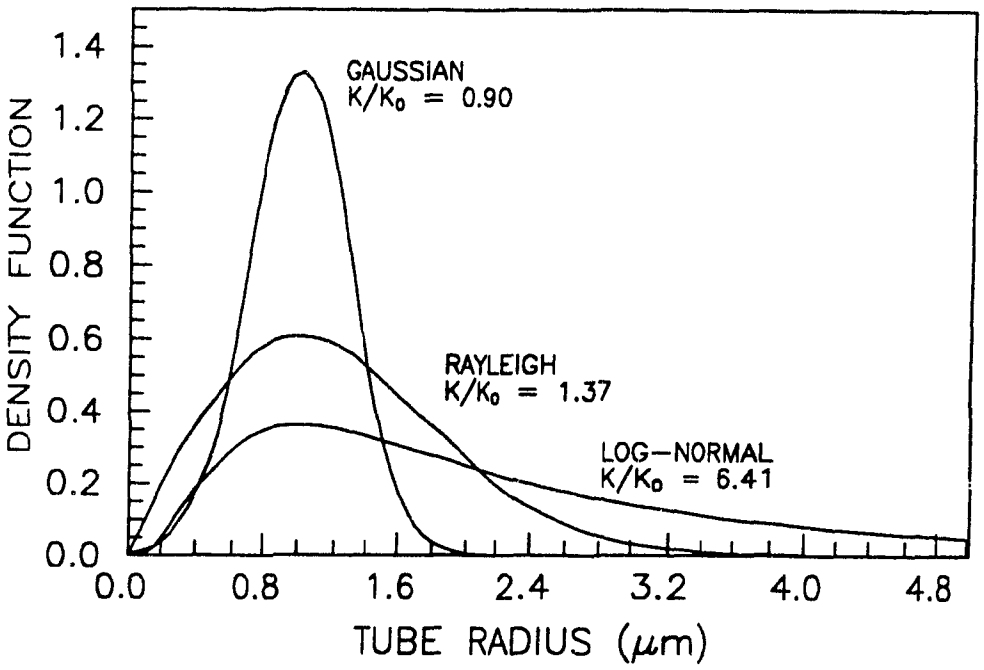

Figure 6.7: Permeabilities for networks with Gaussian, log-normal and Rayleigh tube size distributions (mode = 1 μm)

the tubes have a uniform size of 1.0 μm, K_o.

6.4.1 GAUSSIAN DISTRIBUTION

The tube radii of the networks were filled with Gaussian distributions. Each network had a modal and mean radius = 1.0 μm but different standard deviations. Negative tube radii occur for the distributions with standard deviations greater than 0.3. Therefore, tube radii were restricted to the range between 0.05 and 1.95 μm. By choosing this range, negative tube radii are avoided and the modal and mean tube size of 1.0 μm is still conserved (see Figure 6.8). Figure 6.9 is a graph of the dimensionless permeability, K/K_o versus the number of tubes in the network. The calculation for each K/K_o value was repeated 10 times and then averaged. A different seed number was used in the random number generator for each repeated

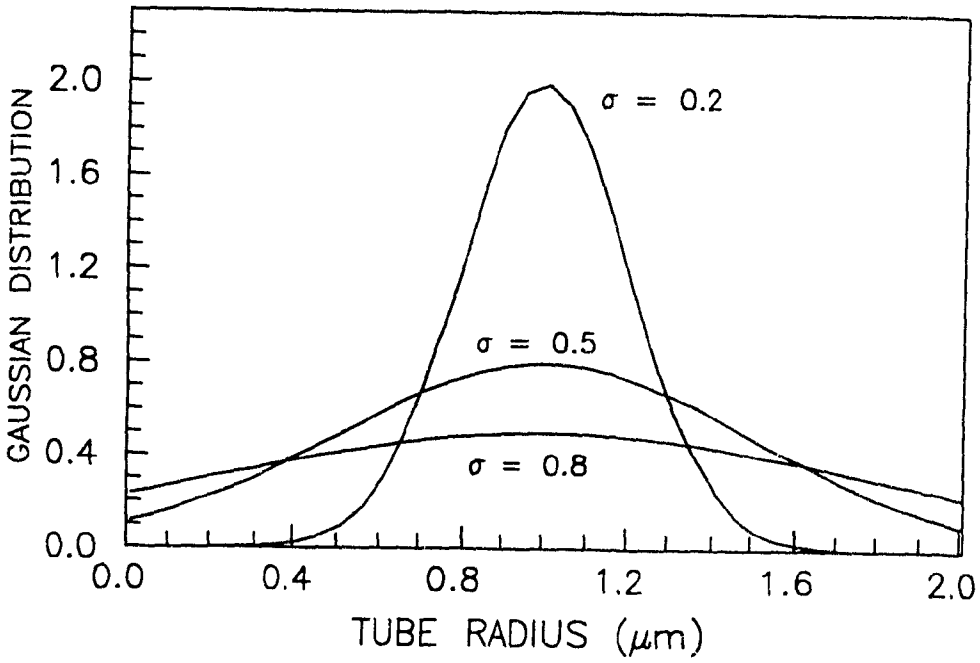

Figure 6.8: Gaussian probability density functions.

run. Figure 6.9 shows that the results for each standard deviation stabilizes only when more than approximately 2000 tubes are used in the network. Therefore, a network with at least 2000 tubes should be used to obtain meaningful results. Figure 6.9 also illustrates that the permeability values of a network for the same median pore size depends on the standard deviation of the pore size distribution. As the standard deviation of the distribution varies from 0 to 1.0, the permeability of the network decreases by a factor of 1.37.

It is interesting to note that the mean resistance of the tubes in the network, $\overline{1/R^3}$ is very different from the resistance to filtration of the network, K_o/K. Figure 6.10 shows graphs of K_o/K and $\overline{1/R^3}$ versus standard deviation for networks consisting of 199 rows and 49 tubes per row (i.e. 9751 tubes). The graph shows that $\overline{1/R^3}$ increases at a much greater rate than K_o/K with increase in standard deviation.

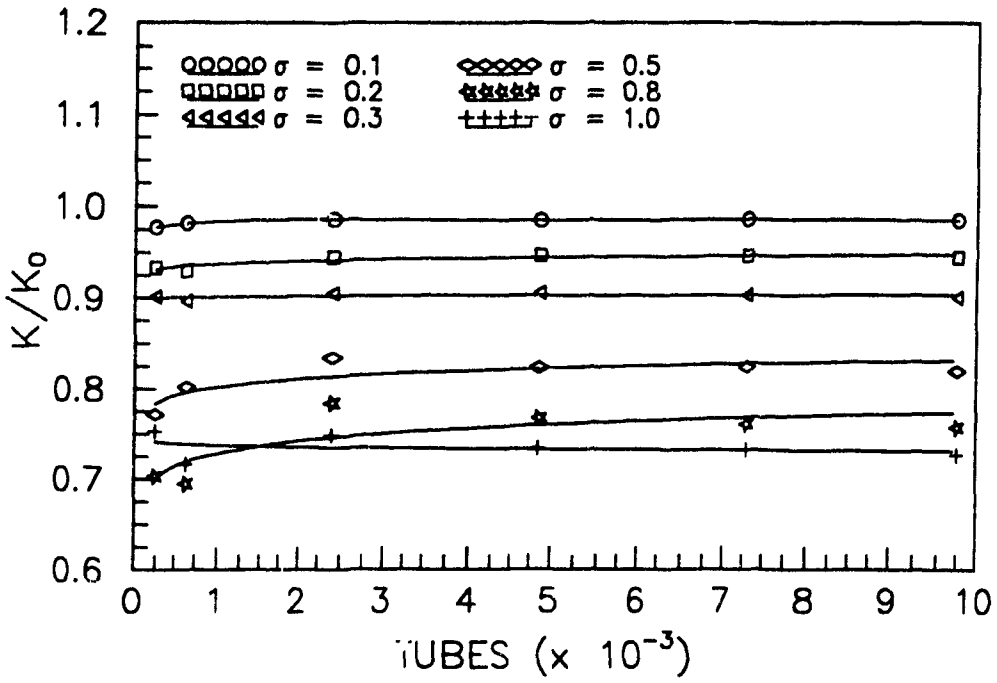

Figure 6.9: Permeability versus number of tubes for Gaussian tube radii distributions with different standard deviations ($\mu_m = 1.0$ μm).

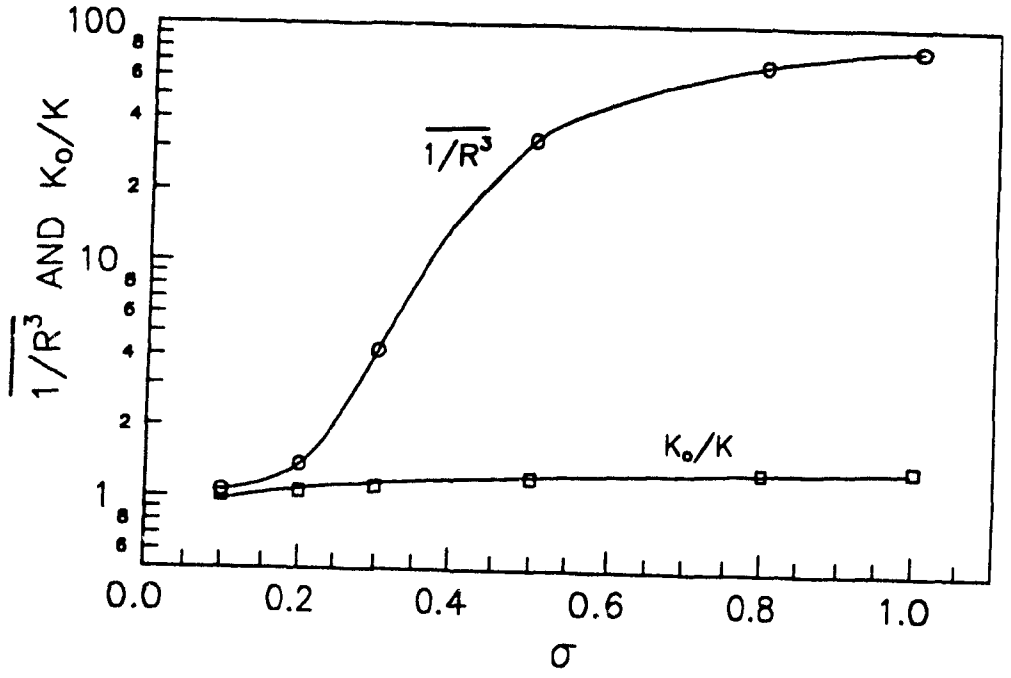

Figure 6.10: Curves of $\overline{1/R^3}$ and K_o/K versus standard deviation for Gaussian distributions. Networks consist of 199 rows and 49 tubes per row.

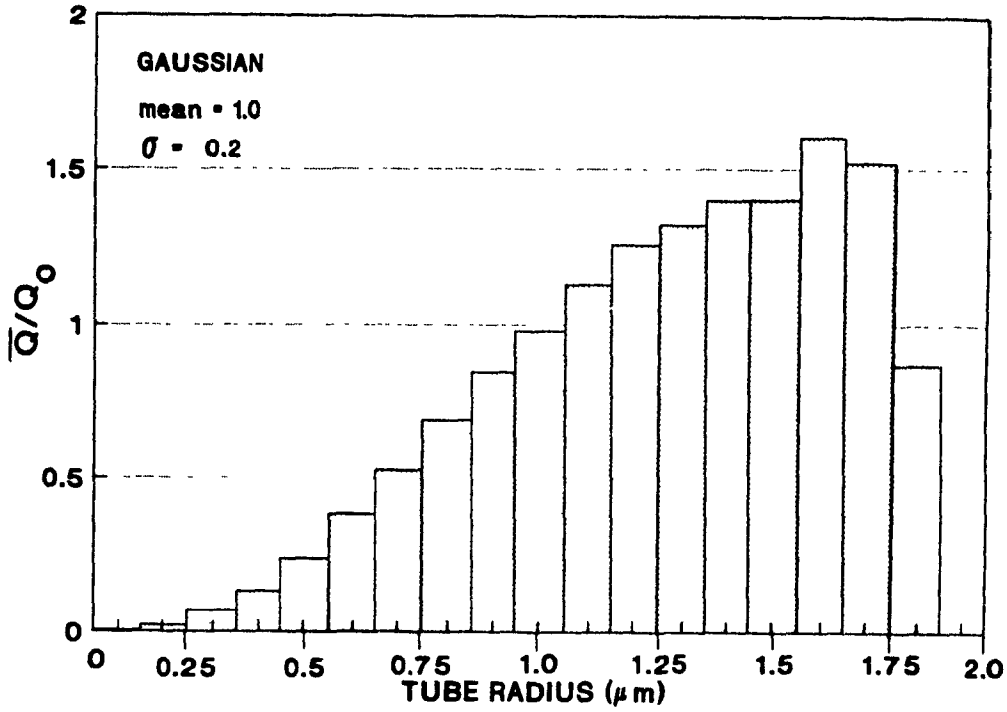

Figure 6.11: Histogram of the mean flow rates in a network with a Gaussian tube size distribution where $\mu_m = 1.0$ μm and $\sigma = 0.2$ (network size = 199 rows and 49 tubes per row).

Figures 6.11, 6.12, and 6.13 are histograms of the mean volumetric flow rate, $\overline{Q}$ through tubes in the networks for a given tube size class. The networks were filled with different Gaussian tube size distributions. The $\overline{Q}$ values in the figures are given relative to Q_o where Q_o is the volumetric flow rate in a tube if all tubes in the network had a uniform size of 1 μm. In general, as would be expected, the mean volumetric flow rate, $\overline{Q}$ increases with the tube radius. These network results are compared with $\overline{Q}/Q_o$ values for tube radii arranged in parallel in a single layer (see Figures 6.14 and 6.15). Figures 6.14 and 6.15 show histograms for Gaussian distributions with standard deviations of 0.2 and 1.0 with the tubes arranged in parallel. The results were calculated based on a flow resistance of L/R^4 where $L = 1.0$ μm and $1/R^3$ as was used in the network model since the model assumed L to be proportional to R. It is interesting to note that the $\overline{Q}/Q_o$ values for tubes arranged in parallel are smaller

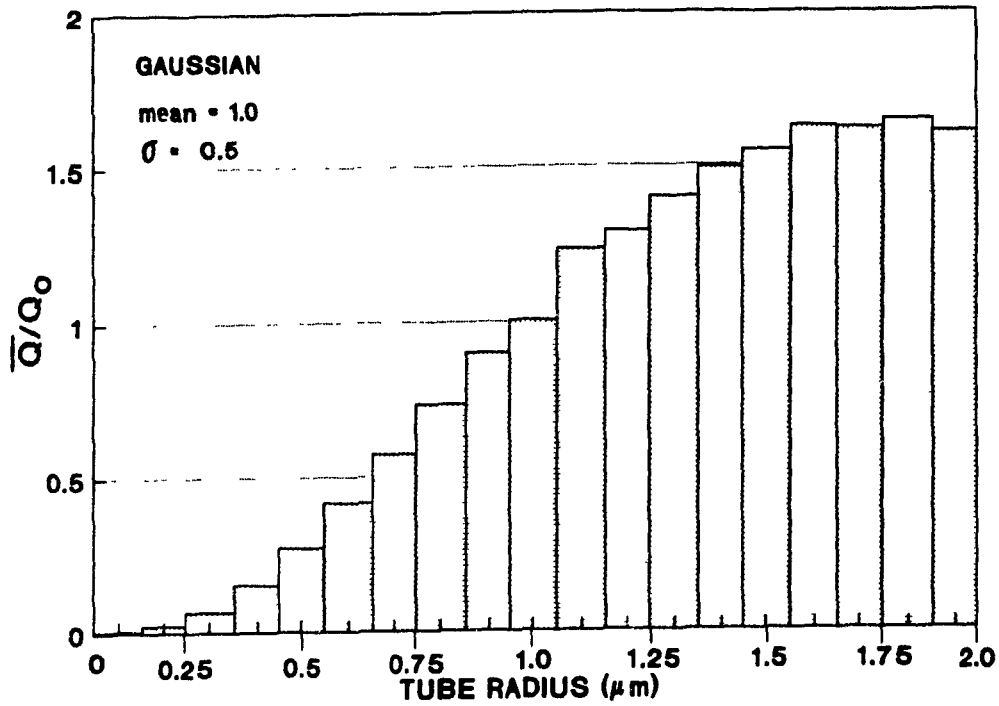

Figure 6.12: Histogram of the mean flow rates in a network with a Gaussian tube size distribution where $\mu_m = 1.0\ \mu$m and $\sigma = 0.5$ (network size = 199 rows and 49 tubes per row).

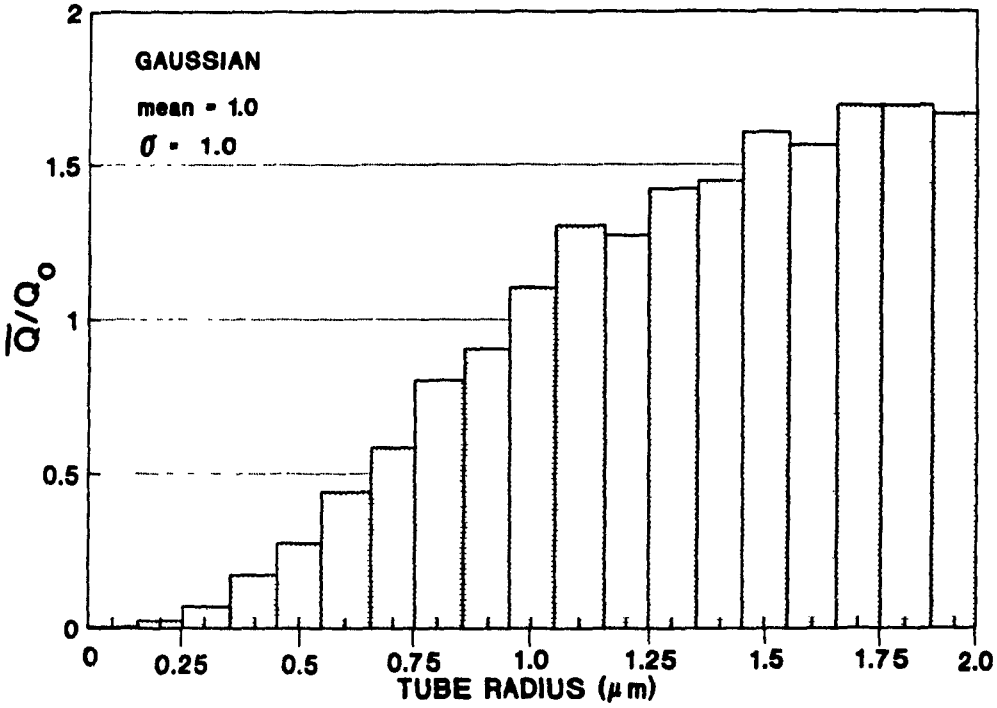

Figure 6.13: Histogram of the mean flow rates in a network with a Gaussian tube size distribution where $\mu_m = 1.0\ \mu$m and $\sigma = 1.0$ (network size = 199 rows and 49 tubes per row).

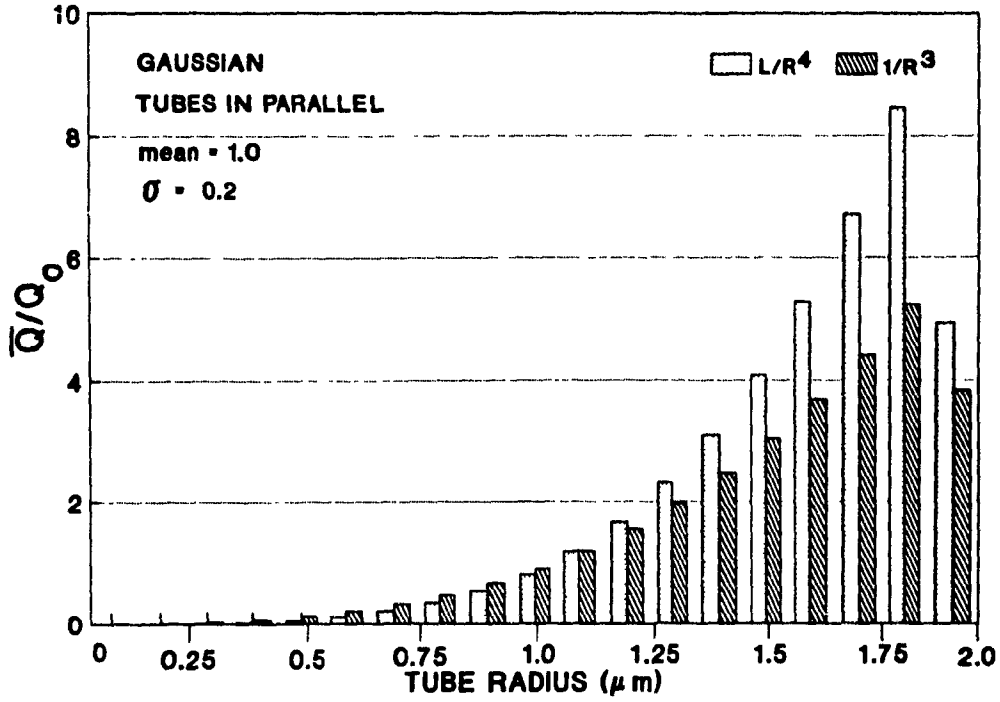

Figure 6.14: Histogram of mean tube flow rate for 9751 tubes arranged in parallel. The tubes have a Gaussian size distribution with $\mu_m = 1.0$ μm and $\sigma = 0.2$.

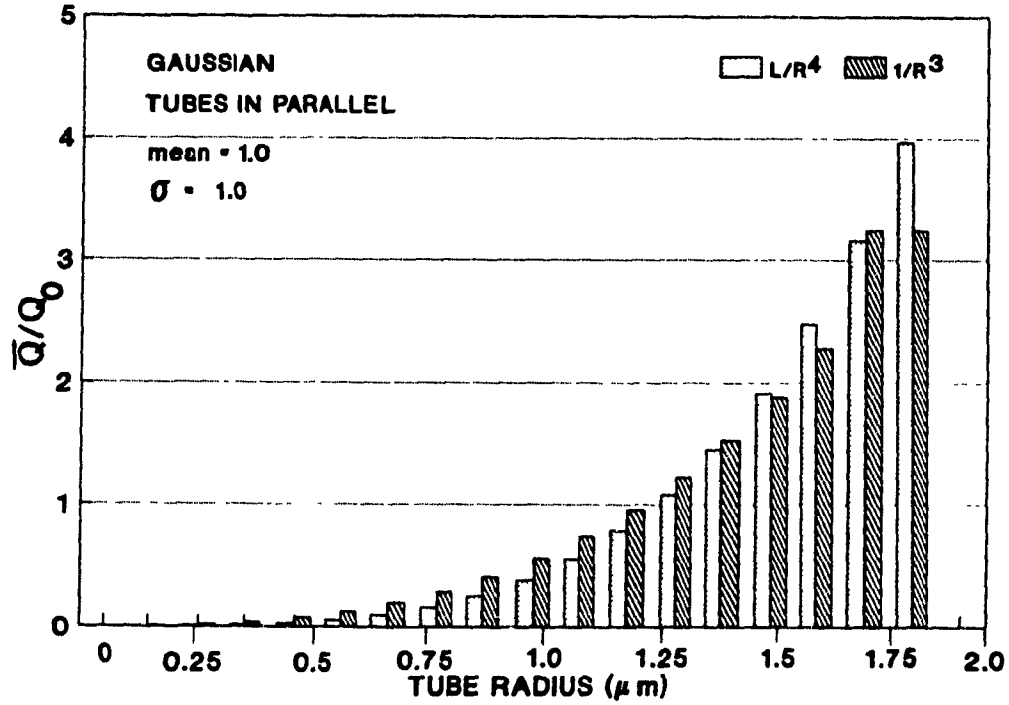

Figure 6.15: Histogram of mean tube flow rate for 9751 tubes arranged in parallel. The tubes have a Gaussian size distribution with $\mu_m = 1.0$ μm and $\sigma = 1.0$.

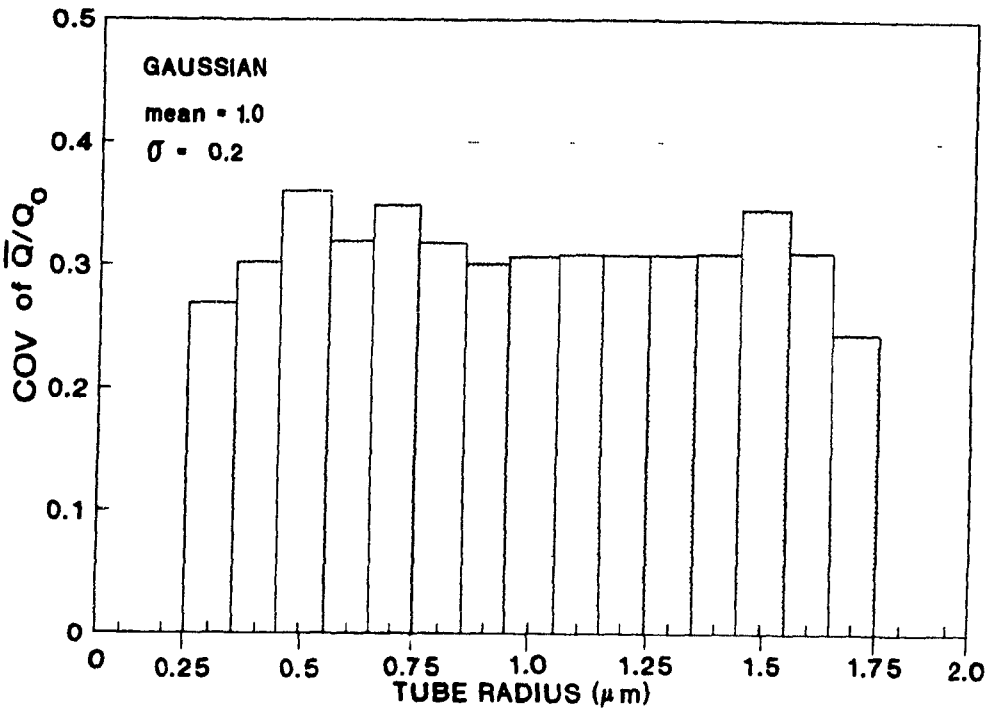

Figure 6.16: Histogram of coefficient of variation, COV of mean flow rate versus tube radius. Gaussian tube size distribution, $\mu_m = 1.0$ μm and $\sigma = 0.2$ (network size = 199 rows and 49 tubes per row).

in the small tubes and increase to much larger values in the large tubes compared to the results obtained in the network model. Again, these results illustrate that the pore size distribution and pore arrangement can significantly affect flow rates.

There can be large variations in the flow rates in the tubes for a given tube size. Figures 6.16, 6.17 and 6.18 are histograms of the coefficient of variation, COV of $\overline{Q}/Q_o$ versus tube radius. For a narrow tube size distribution ($\sigma = 0.2$), the COV versus tube radius histogram is quite uniform with a COV of about 0.3 (see Figure 6.16). With increase in the tube size distribution spread, the COV values increase. Furthermore, with a wide distribution the COV values are the greatest for the small tubes (see Figures 6.17 and 6.18). The distribution with a standard deviation of 1.0 has a COV of 1.4 for tubes between 0.05 and 0.15 μm and then tends to level off to about 0.85 with increase in tube size. These COV values are

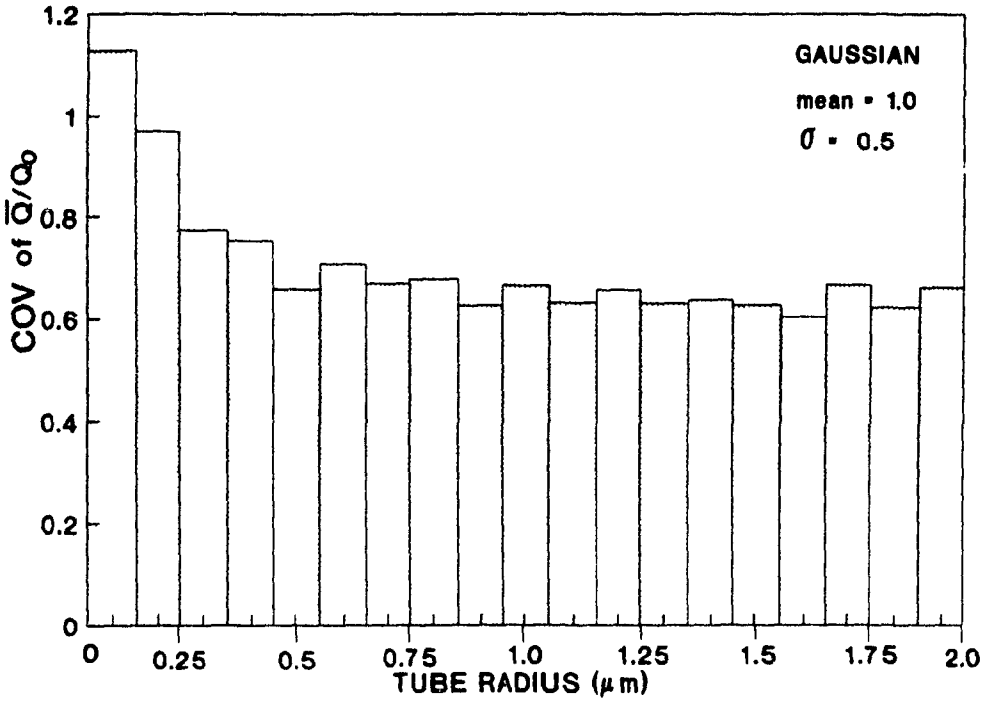

Figure 6.17: Histogram of coefficient of variation, COV of mean flow rate versus tube radius. Gaussian tube size distribution, $\mu_m = 1.0$ μm and $\sigma = 0.5$ (network size = 199 rows and 49 tubes per row).

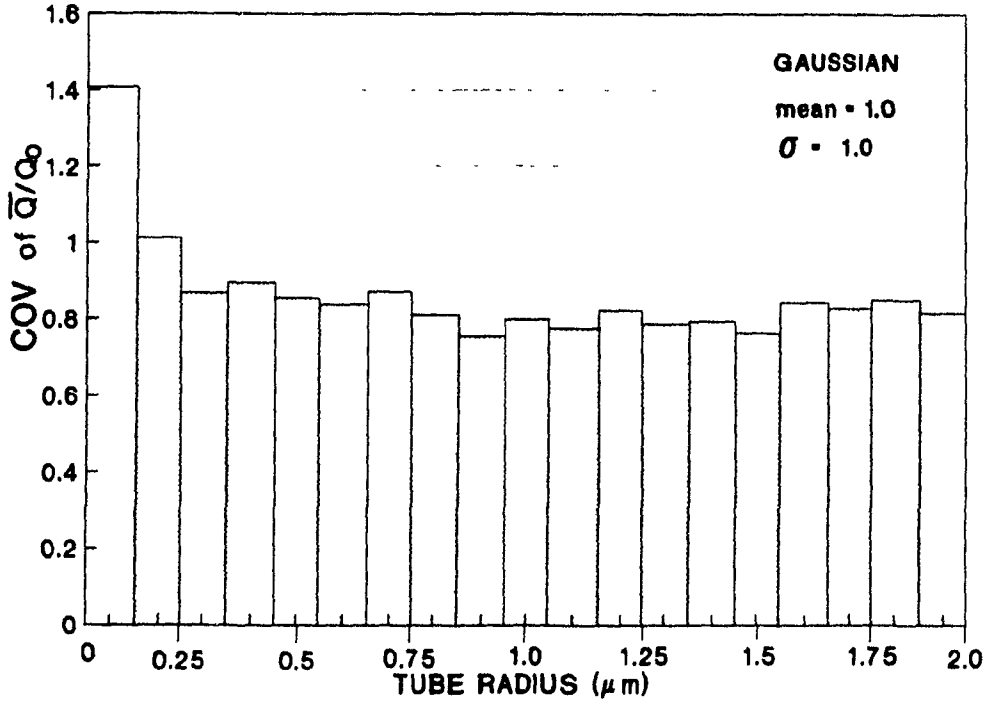

Figure 6.18: Histogram of coefficient of variation, COV of mean flow rate versus tube radius. Gaussian tube size distribution, $\mu_m = 1.0$ μm and $\sigma = 1.0$ (network size = 199 rows and 49 tubes per row).

significantly higher than found for a narrow distribution.

In general, flow through the larger pores are favoured, thereby reducing the effect of the high resistance to flow in the smaller pores, however the high COV values for wide tube size distributions show that some of the small tubes have fairly high flow rates causing high pressure drops in these tubes and therefore reducing the overall permeability of the network. The spread of the distribution in the network affects the flow pattern and in filtration theory it is insufficient to know only the average pore size or average pore resistance to flow. The configuration of the network must be included in the averaging procedure. The flow in a given tube depends not only on the size of the tube being considered but also on the size of the tubes around it.

6.5 LOG-NORMAL DISTRIBUTION

Often ceramic powders have log-normal size distributions. It has been found that the pore size distribution can be correlated to the particle size distribution for random-sphere packings. For a narrow particle size distribution the pore size distribution has a similar, if not wider, size distribution.[85] Under filtration conditions the log-normal distribution mimics the pore size distribution fairly well.[86, 87, 26]

Log-normal tube radii distributions, with different standard deviations, were used in the networks. The median of each distribution was determined so that the peaks of the distributions all occurred at 1.0 μm (see Figure 6.19). Figure 6.20 shows curves of K_o/K, the mean resistance, $\overline{1/R^3}$ and the resistance to flow calculated from the mean pore size, $1/\overline{R}^3$ versus the standard deviation of the ln (*tube radius*) for the log-normal distributions. Even though the curve for $\overline{1/R^3}$ is increasing, the K_o/K curve is decreasing. Furthermore, the graph shows that $1/\overline{R}^3$ decreases at a much

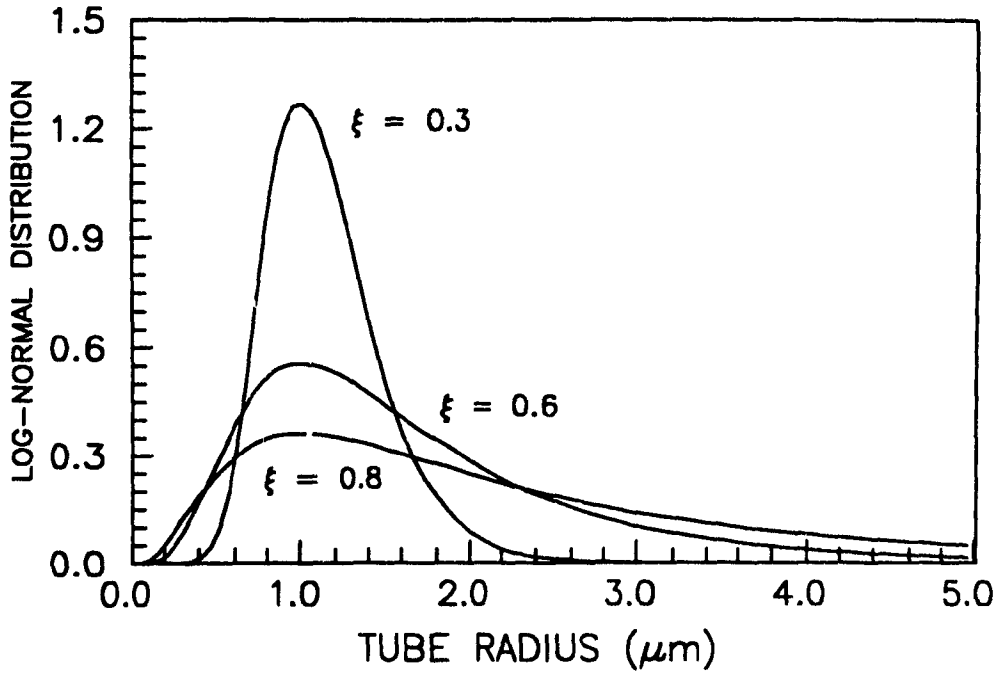

Figure 6.19: Log-normal probability density functions. Mode = 1.0 μm.

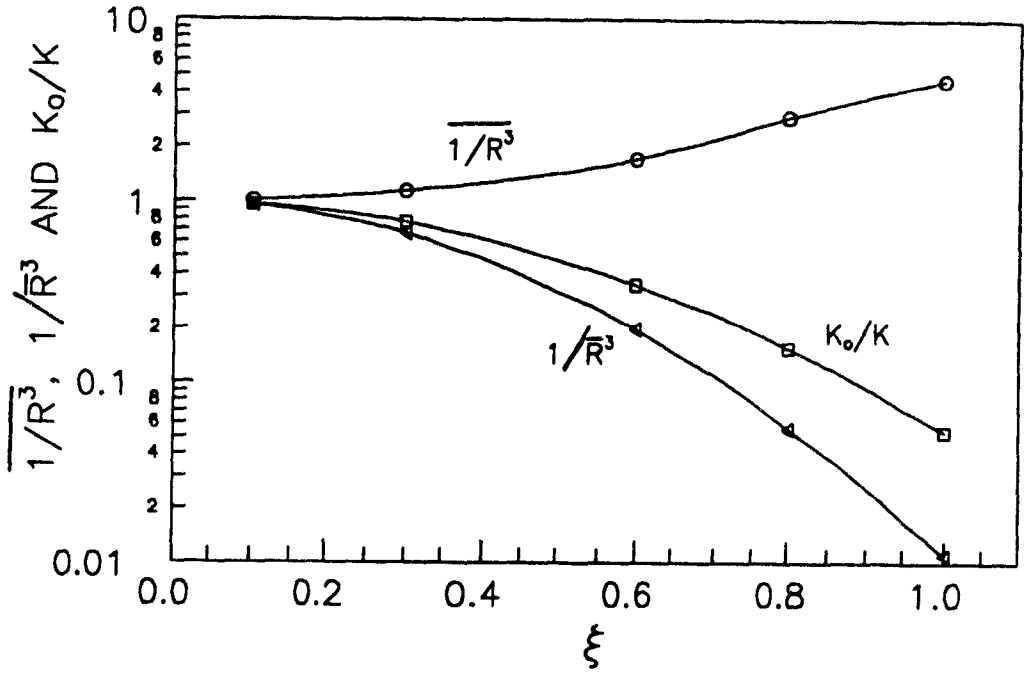

Figure 6.20: Curves of K_o/K, $\overline{1/R^3}$ and $1/\overline{R}^3$ versus the standard deviation of the ln(*tube radius*), ξ for log-normal distributions. Mode = 1.0 μm (network size = 199 rows and 49 tubes per row).

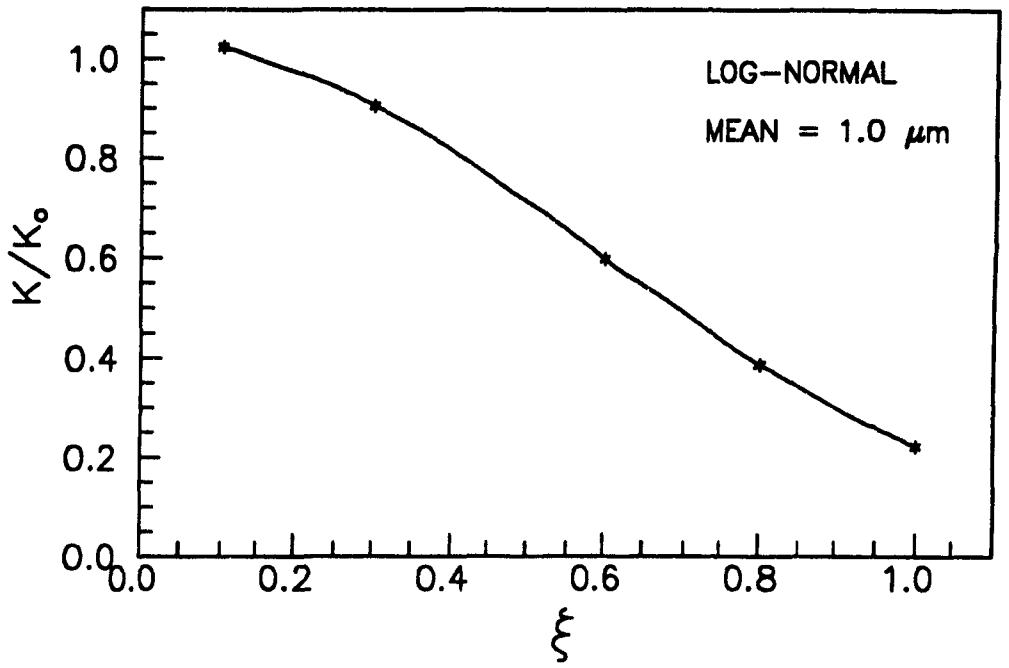

Figure 6.21: Permeability versus standard deviation of the ln (*tube radius*), ξ for log-normal distributions. Mean = 1.0 μm (network size = 199 rows and 49 tubes per row)

greater rate than K_o/K with increase in standard deviation. By introducing a few larger tubes to the network the filtration resistance is decreased substantially. On the other hand, as illustrated in Figure 6.20, introducing a few smaller tubes to the network still has a significant effect on the filtration resistance. Even though the K_o/K curve is decreasing due to larger tubes being introduced to the network the K_o/K values are still greater than the $1/\overline{R}^3$ values for a particular standard deviation due to the smaller pores.

Figure 6.21 is a graph of K/K_o versus standard deviation. The curve decreases with standard deviation. The distributions all had a mean tube radius = 1.0 μm (see Figure 6.22). With increase in standard deviation the modal tube size decreases. The mean tube size remains constant however with increase in standard deviation smaller tubes are introduced to the network and even though the larger tubes help

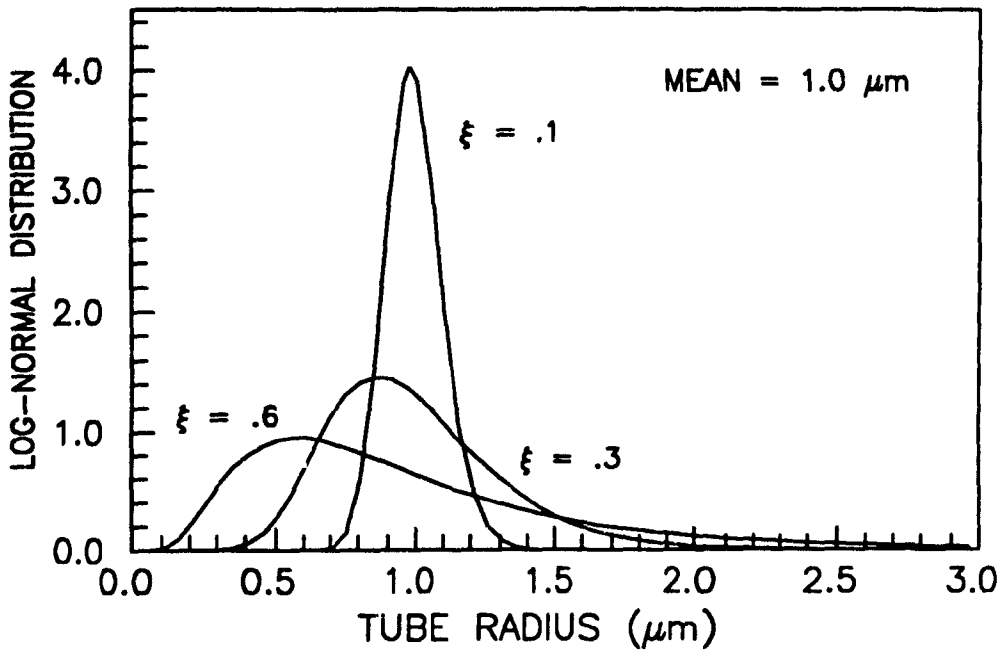

Figure 6.22: Log-normal probability density functions. Mean = 1.0 μm.

reduce the effect of the high resistance created by the small tubes it is not suffice to prevent the permeability of the network to drop. These results again emphasize that distributions of pore sizes cannot be simply accounted for by an average pore size.

Schilling and Aksay[26] have illustrated how processing parameters such as interparticle potential and particle size distribution affect the cake permeability and microstructure evolution throughout casting. As discussed in the literature review they found that well dispersed suspensions produced a bimodal pore size distribution reflecting the presence of first-generation agglomerates surrounded by second-generation pores. They suggested that densely packed individual particles form first-generation agglomerates, and aggregates of these first-generation agglomerates form larger second-generation agglomerates. A poorly dispersed suspension produced a cast that exhibited larger second-generation pores and a smoother distribution of pore sizes. The pore size distribution curves are shown in Figure 6.23. Due to the

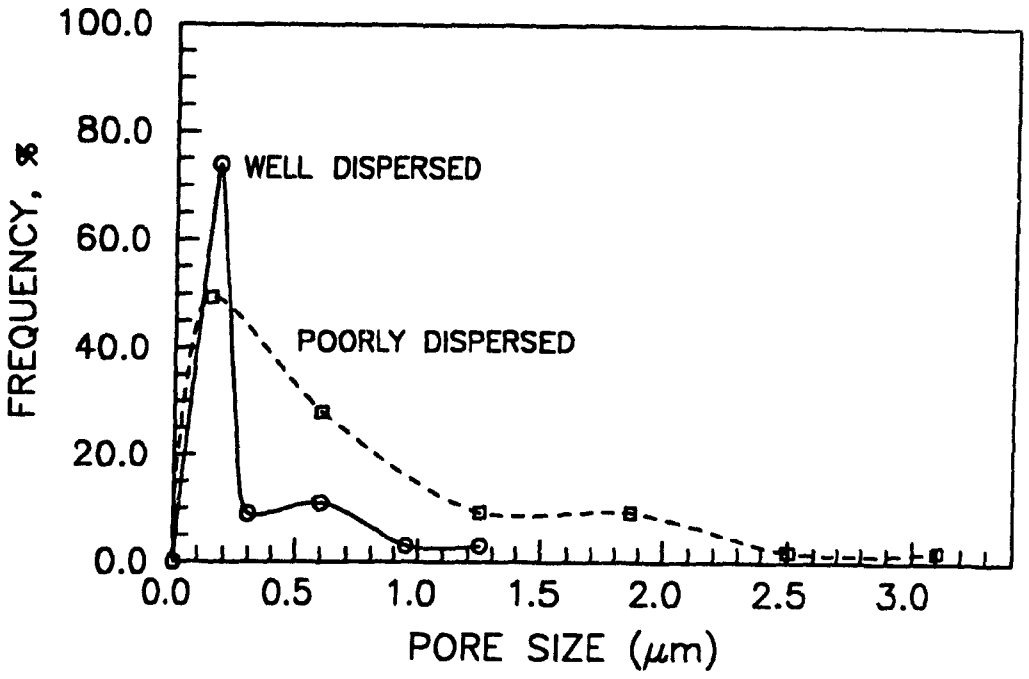

Figure 6.23: Pore size distributions for partially sintered slip cast alumina specimens prepared from well dispersed and poorly dispersed specimens (after Ref. 26).

larger second-generation pores the permeability of the cast prepared from the poorly dispersed suspension was found to be approximately 60 times greater than the permeability of the cast prepared from the well dispersed suspension. As shown earlier in Figure 6.20 as the standard deviation of the distribution increased, which simulates an increase in flocculation of a porous cake, the permeability increased.

The network model was used to study the effects that first and second-generation agglomerates have on permeability. Figure 6.24 shows two distributions both with a median tube radius = 1.0 μm, mean = 1.3 μm and maximum peaks occurring at 0.5 μm. The permeabilities however were found to be quite different for the two cases. The permeabilities, K/K_o were equal to 0.501 and .946 for curve (1) and (2), respectively. Curve (1) which produced the lower permeability had a greater proportion of first-generation agglomerates whereas curve (2) had a smooth distribution with

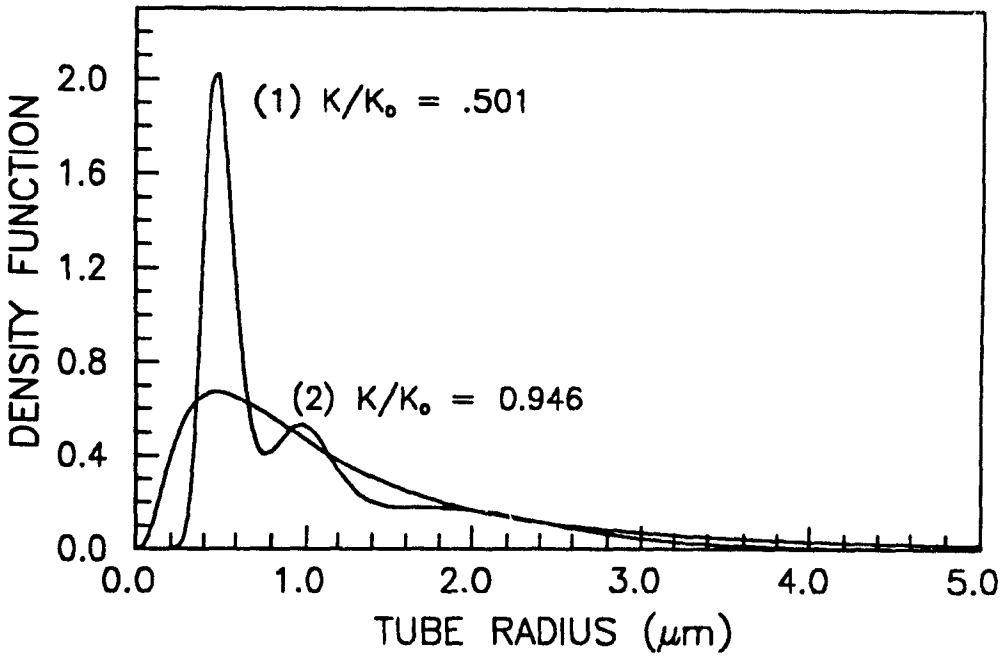

Figure 6.24. For both curves the median = 1.0 μm, mean = 1.3 μm and mode = 0.5 μm. Curve (1) simulates first and second generation agglomerates and curve (2) has a smooth but wider distribution.

a few larger pores. These results show that only minor variations in the pore size distribution are required to affect the permeability and this, in turn, influences the casting rate, as was shown experimentally by Schilling and Aksay.

6.6 BEHAVIOUR UNDER FIXED POROSITY CONDITIONS

As shown earlier by the Kozeny-Carman equation (refer to Equation (6.6)) the porosity of a porous medium affects the permeability. So far, the network permeability results presented in this thesis have been calculated based upon a fixed number of tubes in the network. However, by varying the pore size distributions and using a fixed number of tubes the total tube pore volume will vary and this will change the

porosity of the system.

In this section, permeability results for different pore size distributions will be presented. But, rather than the networks being comprised of a fixed total number of tubes the networks will have a constant pore volume.

6.6.1 METHODOLOGY

In order to obtain a fixed tube pore volume the following procedure is performed on a network with a fixed number of layers and tubes per layer:

(1) The total tube volume of network is calculated.

(2) Tubes are blocked off so flow can not pass through them.

(3) Tubes are blocked off until the volume of tubes remaining to participate in flow equals the desired fixed volume.

The computer programs use different schemes for choosing the tubes to be blocked off. The scheme chosen depends upon the number of tubes required to be blocked off. One program attempts to achieve the desired network volume by using the following scheme. Even numbered tubes at specified intervals are selected to be blocked off (see Figure 6.25). The interval at which the tubes are selected at is decreased until a sufficient number of tubes are blocked off. The smallest interval being every second tube in every second layer where the even number tubes in the first and last tube of each layer is not removed. If with this scheme an insufficient number of tubes are blocked off the following alternative scheme is employed. Four tubes that meet at a node are blocked off. The nodes are chosen at specified intervals (see Figure 6.26). If enough pipes are still not removed then this network volume is further reduced by removing 24 (or 112 if necessary) tubes that are concentrated around a node (see Figure 6.27). See Appendix B for a sample computer program listing.

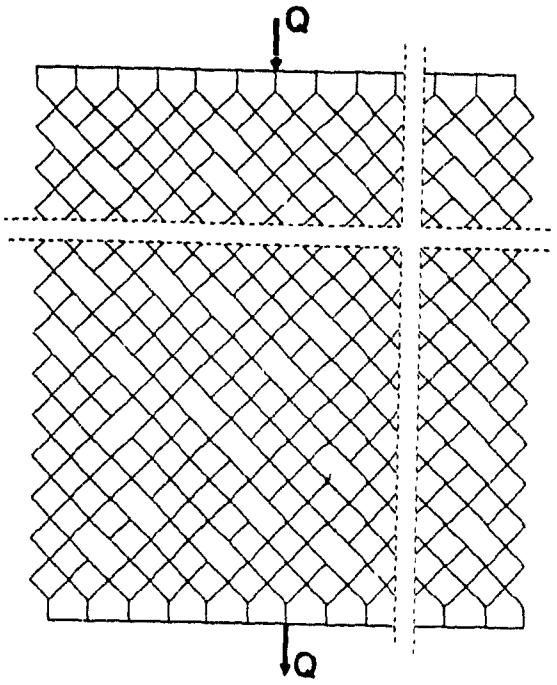

Figure 6.25: Even numbered tubes are blocked off to obtain the desired total network tube volume.

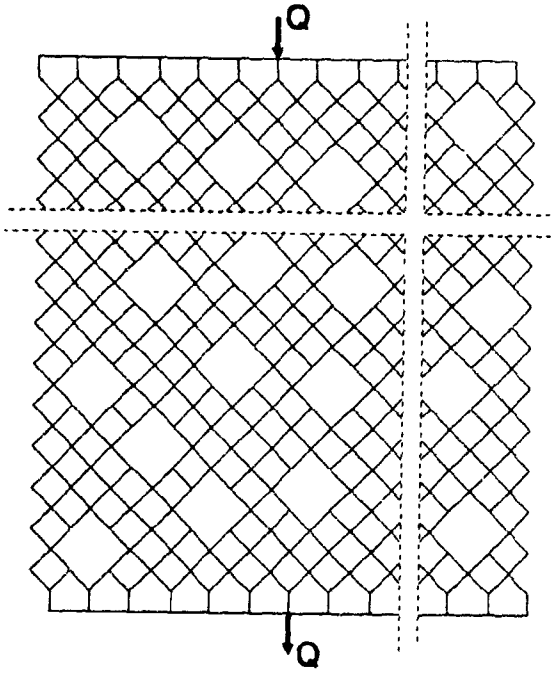

Figure 6.26: Four tubes that meet at a node are blocked off to obtain the desired total network tube volume.

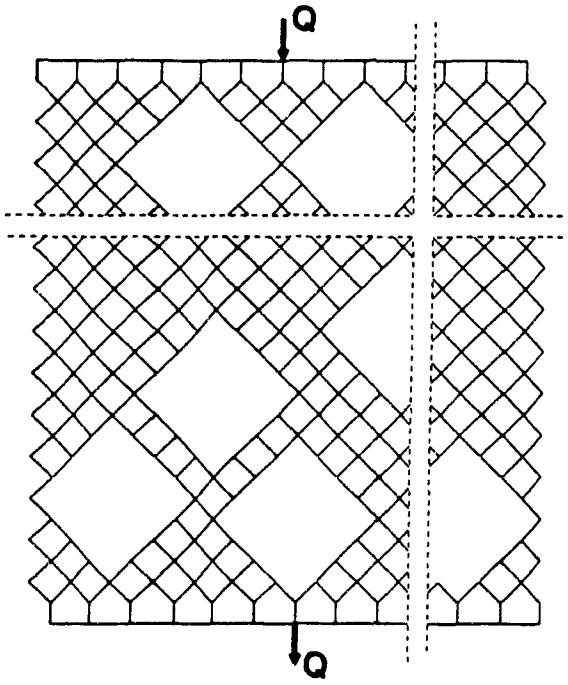

Figure 6.27: Twenty-four tubes that are concentrated around a node are blocked off.

6.6.2 RESULTS

Networks were filled with Gaussian tube radius distributions and the tube radii were restricted to the range between 0.05 and 1.95 μm. Tubes were blocked off until the network tube volume, V was equal to V_o where V_o is the volume if all tubes in the unblocked original network had a radius = 1.0 μm. Figure 6.28 is a graph of K/K_o versus standard deviation of the tube radius, σ. Again as in previous sections the calculation for each K/K_o value was repeated 10 times and then averaged. A different seed in the random number generator was used for each repeated run. Figure 6.28 also shows a graph of the percentage of tubes blocked off in the network versus standard deviation. With increase in standard deviation the percentage of tubes blocked off increases and K/K_o decreases. These permeability results are substantially lower than the results presented in Section 6.4.1 where the network model was based on a

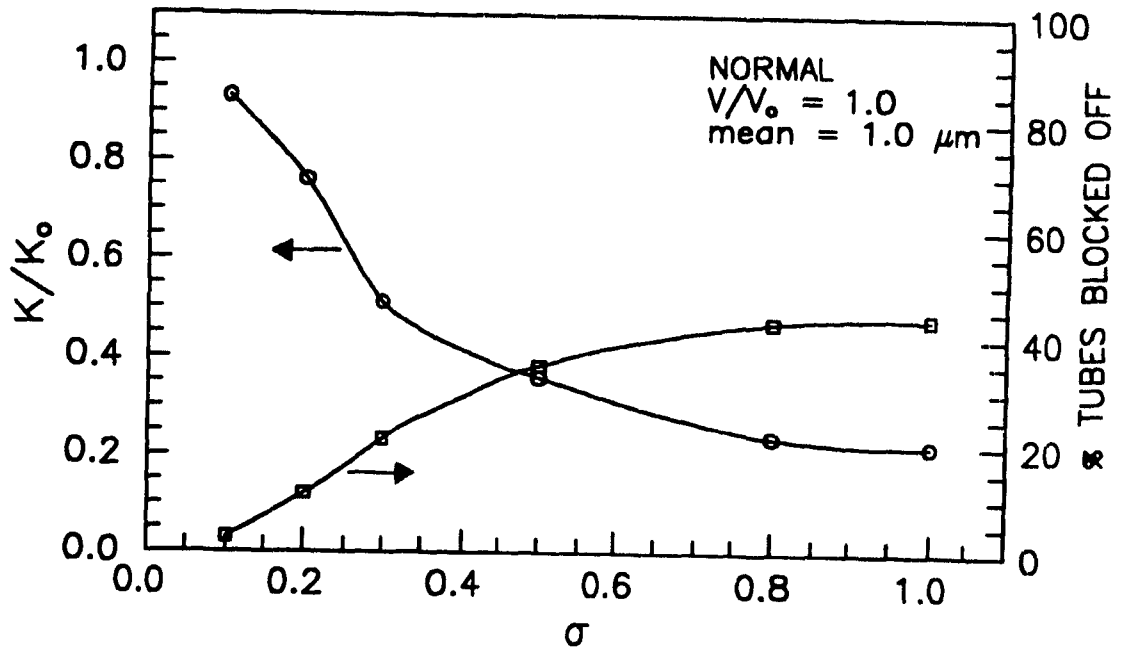

Figure 6.28: Graphs of permeability and percent of tubes blocked off in the network versus standard deviation of the tube radius, σ for Gaussian (normal) distributions (network size = 49 rows and 49 tubes per row).

constant number of tubes rather than on a constant network volume. As more and more tubes are blocked off with increase in standard deviation of the tube radius, inevitably more and more tubes will be connected in series. Therefore, the smaller tubes will play an important role in determining the permeability of the network.

Networks were also filled with log-normal tube size distributions. The networks all had values of $V/V_o = 1.0$. Figure 6.29 is a graph of K/K_o versus the standard deviation of the ln (*tube radius*), ξ where the radii were restricted to values less than 3.0 μm. The log-normal distributions would have a median = 1.0 μm if there was no restriction on the maximum tube size. The graph shows that there is a large reduction in permeability with increase in standard deviation.

Figure 6.30 shows graphs of K/Ko versus standard deviation for two types of log-normal distributions. For curve (1), the distribution had a modal value equal to

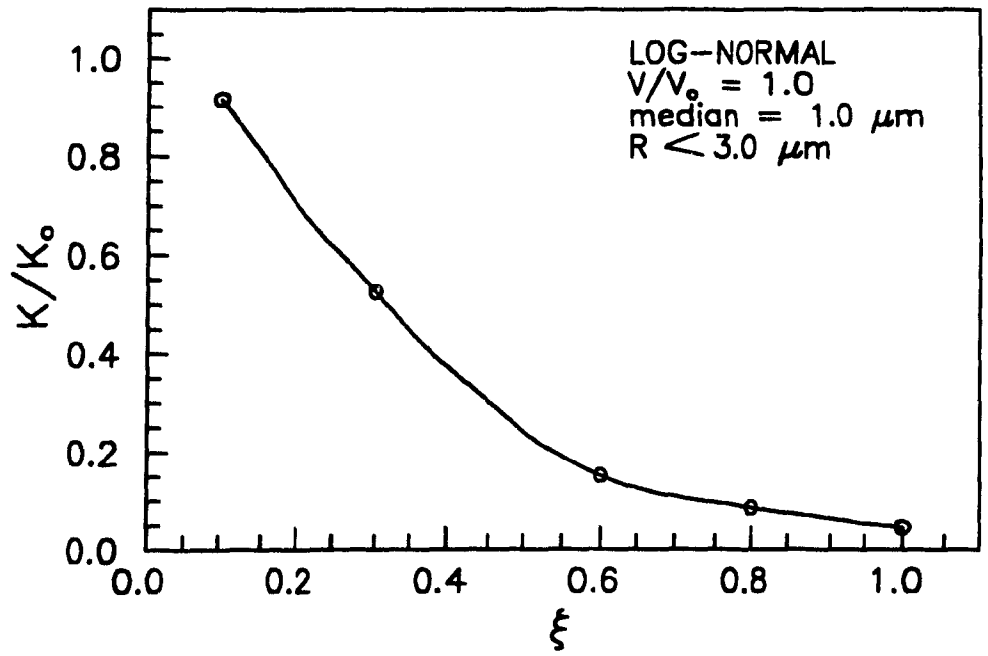

Figure 6.29: Permeability versus standard deviation of the ln(*tube radius*), ξ for log-normal tube radius distributions. Median = 1.0 μm (network size = 99 rows and 49 tubes per row).

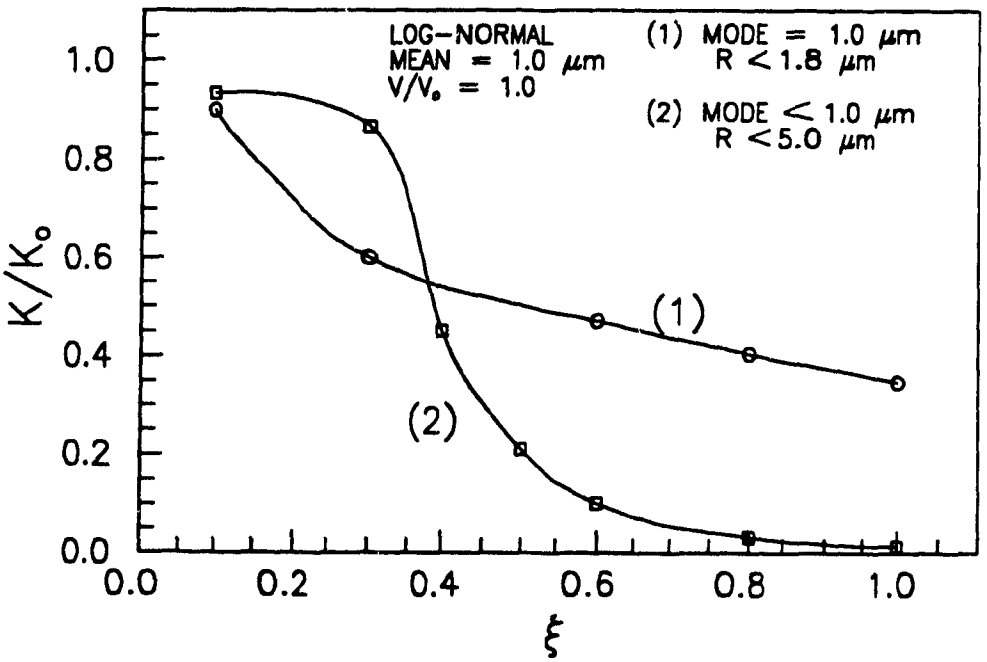

Figure 6.30: Permeability versus standard deviation of the ln(*tube radius*), ξ for log-normal tube radius distributions. Mean = 1.0 μm (network size = 99 rows and 49 tubes per row).

1.0 μm, average radius of 1.0 μm and tubes were restricted to radii less than 1.85 μm. For curve (2), the average radius was 1.0 μm and tubes were restricted to radii less than 5.0 μm. The modal value for curve (2) decreases with standard deviation. Again, Figure 6.30 shows that the permeability decreases with increase in standard deviation. Figure 6.30 shows, however that the reduction in permeability is much greater for curve (2) even though the distributions for both curves had an average radius = 1.0 μm. This is a result of the wider distribution and decrease in the modal value with increase in standard deviation for curve (2)

The permeability results demonstrate that for a given porosity the permeability results can differ greatly depending upon the pore size distribution.

Figure 6.31 is a graph of K/K_o versus V/V_o for log-normal distributions with different standard deviations where the average radius = 1.0 μm. As would be expected K/K_o increases with V/V_o and for a given V/V_o value, K/K_o drops with increase in the standard deviation.

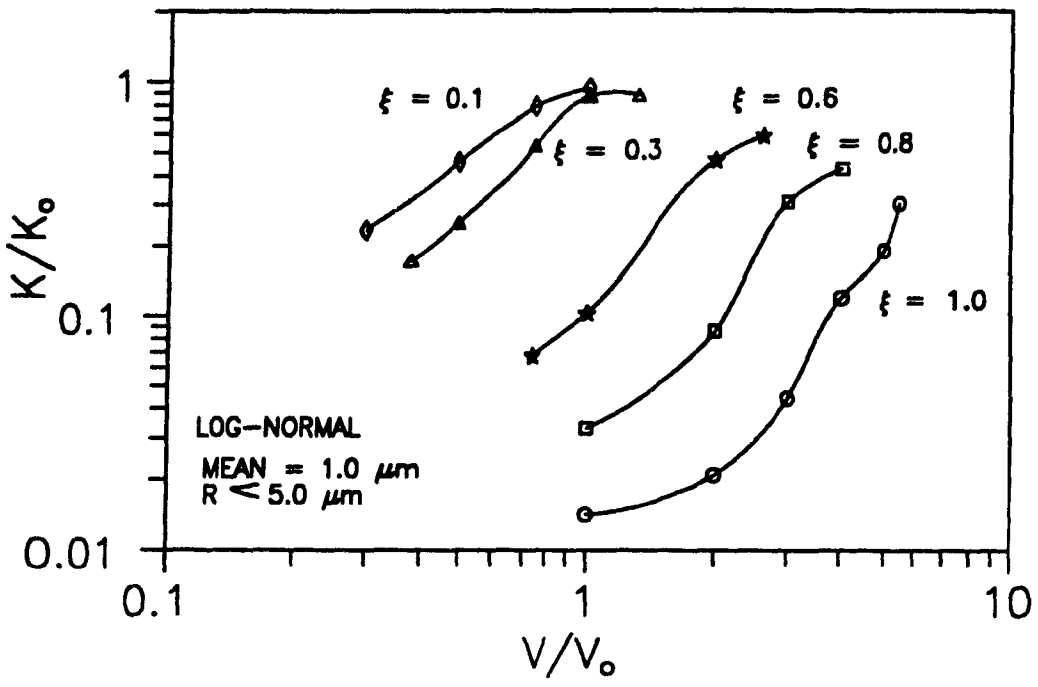

Figure 6.31: Permeability versus V/V_o for log-normal distributions with a mean tube radius = 1.0 μm (network size = 99 rows and 49 tubes per row).

Chapter 7

RANDOM TUBE MODEL OF CLOGGING DURING FILTRATION

During slip casting and filter pressing it has often been assumed that there is no motion of fine particles within the cake as it builds up with time. In other words, the particles are deposited layer upon layer with no relative motion between them.

Experimental work demonstrates that fine particles can be carried along with the filtrate and deposited within the cake and/or filter medium thereby clogging and reducing the permeabilities of the porous media. This in turn will affect the rate of cake growth as well as the density and porosity of the cake

Permeability reduction due to clogging can occur if: (1) particles larger in size than a given pore size are trapped by the pore thus reducing its area and/or (2) as a result of fine particles depositing on the pore walls and gradually reducing the pore radii (see Figure 7.1).

A computer model consisting of a network of tubes with a log-normal tube size distribution was developed to simulate the cake build-up process taking into account the clogging effects. The model will illustrate that minor changes in the pore size distribution due to clogging can significantly affect its permeability and casting rate.

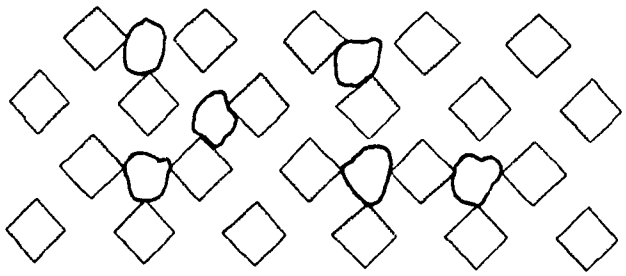

(1) - Pores trap particles larger than the pore openings.

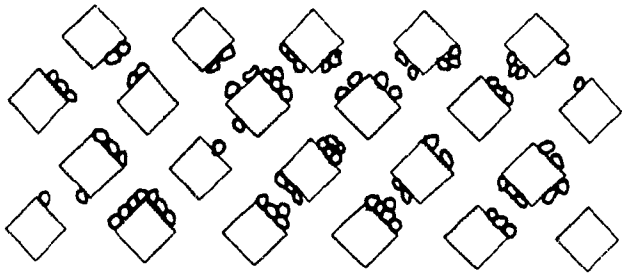

(2) - Fine particles deposit on pore walls and gradually reduce the pore radii.

Figure 7.1: Schematic illustration of porous medium clogging.

7.1 CAKE BUILD-UP MODEL

To simulate the cake build-up process, initially a fixed number of rows and loops per row are used in the network to represent a unit cake layer. The fluid flow and the permeability in the network is calculated using the same algorithm as was used in Section (6.2.1). Then additional tubes are added to the network and the fluid flows through the tubes and permeability of the network are again calculated. The process continues with more and more tubes being added to the network to simulate the cake build-up process (see Figure 7.2).

If no clogging occurs the permeability, K should be constant with increase in network length as shown in Figure 7.3. The K values are given relative to the permeability of a network with all tubes having a uniform size of 1.0 μm, K_o. The tube radii of the network were filled with a log-normal distribution having a standard deviation, ξ equal to 0.6 and a median=1.0 μm. Computer runs were carried out using six rows by 49, 101 and 201 tubes per row as a unit cake layer. The curves tend to become constant after approximately three layers. The graph shows that the computer model is accurate except in the very early stages (i.e. less than three layers) due to the small number of tubes in the network. The model will be further developed in the following sections to account for clogging during filtration. A unit layer consisting of six rows and 49 tubes per row will be used in the following models.

7.2 PROGRESSIVE CLOGGING DUE TO DEPOSITION ON PORE WALLS

The rates of deposition of particles within a porous medium are determined by the forces of interaction between the porous medium (i.e. cake and filter medium),

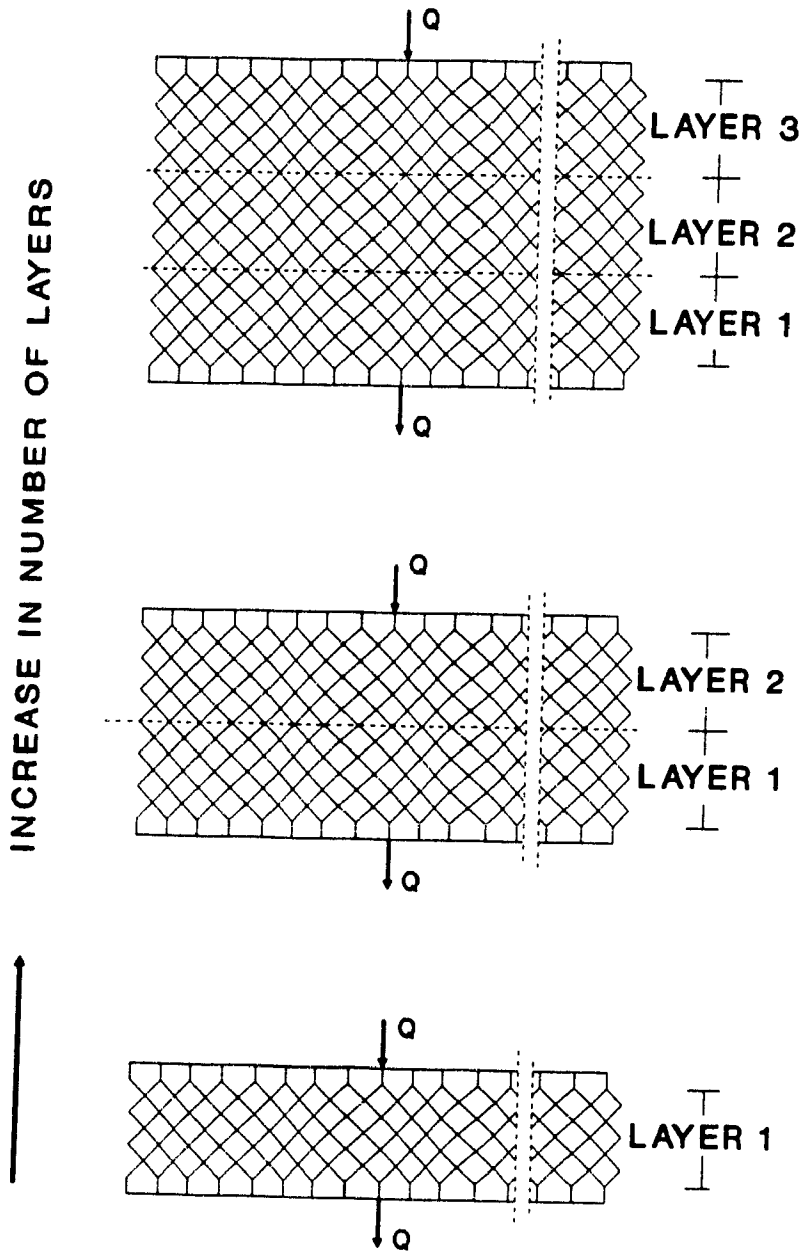

Figure 7.2: Schematic illustration of the network model simulating the cake build-up process.

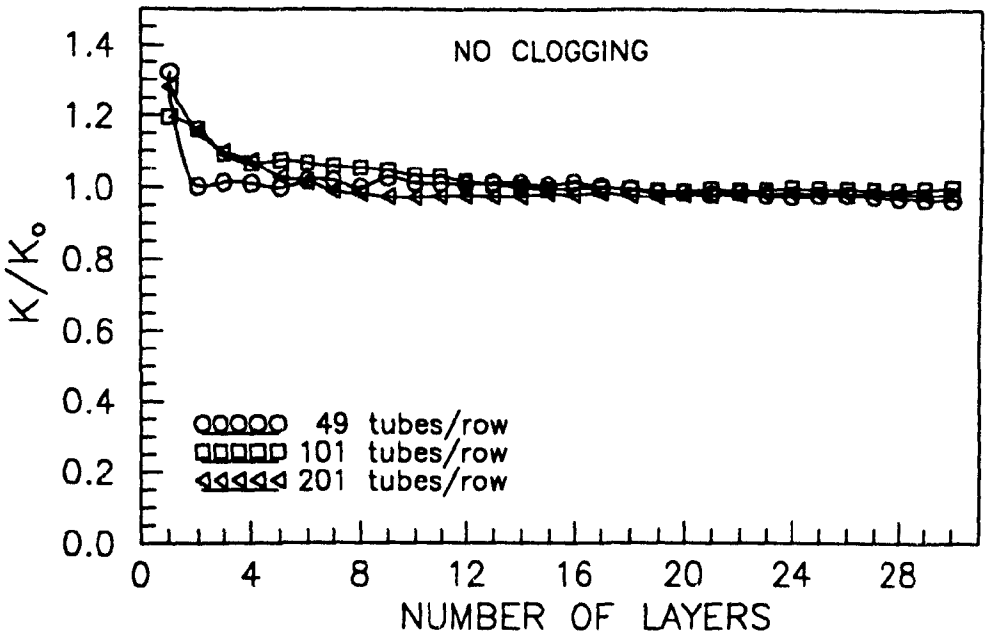

Figure 7.3: Permeability versus number of layers. No clogging.

the carrier fluid, and the suspended particles.[88] Such interaction occurs due to:

1. London-van der Waals attraction,
2. Double-layer repulsion, and
3. Hydrodynamic forces.

Adsorption of colloidal particles in porous media is very sensitive to the type of interaction between the electrostatic double layers surrounding the particles and the porous medium. Furthermore, this sensitivity depends, in addition, on the convective field that carries the particles.[89] The case where the forces of interaction are completely attractive or where there is no appreciable energy barrier ($V_{act} < 10kT$) will be used in the model.

When the forces of interaction are completely attractive the dominant resistance to particle transfer lies in the diffusion boundary layer. The particle flux to

the capillary surface is provided by the perfect sink solution derived by Levich for Poiseuille flow,[90]

$$j' = 0.67\rho D\left(\frac{2u_r}{DRl_p}\right)^{1/3} \tag{7.1}$$

where u_r is the mean fluid velocity in a pore of radius R, and l_p is the distance along the pore. The derivation of equation (7.1) is given in Appendix C. The number of particles per pore volume, ρ is defined as:

$$\rho = \text{number of particles}/\pi R^2 L \tag{7.2}$$

where L is the length of the pore. The diffusion constant, D is given by:

$$D = \frac{kT}{f} \tag{7.3}$$

where k is the Boltzmann's constant = 1.3805×10^{-23} J/K, T is the absolute temperature and f is a friction coefficient. For spheres:

$$f = 6\pi\mu r \tag{7.4}$$

where r is the particle radius. The diffusion constant, D is the proportional to $1/r$:

$$D = \frac{2.161 \times 10^{-19}}{r} \quad (m^2/sec) \tag{7.5}$$

when T = 298 K. Equation (7.1) can be integrated over the pore surface area to obtain the fraction of suspended particles depositing per second:

$$\lambda = \int_0^L \frac{2}{3}\rho D\left(\frac{2u_r}{DR}\right)^{1/3} l_p^{-1/3}(2\pi R)dl_p$$

$$= \frac{4}{3}\rho D\left(\frac{2u_r}{DR}\right)^{1/3} l_p^{2/3} \cdot \frac{3}{2} \cdot \pi R\Big|_0^l$$

$$\lambda = \frac{2D(2u_r L^2/DR)^{1/3}}{RL} \tag{7.6}$$

The fraction of suspended particles depositing per pore, λ' is given by:

$$\lambda' = \lambda L/u_r. \tag{7.7}$$

The fraction of suspended particles depositing per second increases with interstitial velocity. However, it is suggested that there exists a critical velocity, u_c such that particles of size r can no longer adhere to the walls of the pores in the filter cake.[91] Hydrodynamic forces in the direction perpendicular to the flow, F_H, will exist for non-spherical particles. It is assumed that the upper bound of this force is equal to that in the flow direction and is given by:[91]

$$F_H = 1.7 \times 6\pi\mu r u_r. \tag{7.8}$$

When F_H reaches a critical value F^*, the particles of size r can no longer deposit on the surface. The dominant force in adhesion is the London-van der Waals force of attraction.[92] Using the flatplate-sphere system, the London-van der Waals force, F_A, can be represented by:

$$F_A = \frac{-H_A r}{6d_o^2} \tag{7.9}$$

where d_o is the distance of closest approach. Typically, the Hamaker constant, H_A is of the order of 10^{-19} - 10^{-21} J.[93, 94] The particles are slightly separated from the pore wall due to the adsorbed electrolyte and therefore the distance of closest approach is generally about 4-10 Å.[92, 95] For smooth surfaces Visser[94] found that the shear

force F^* needed to dislodge a particle was equal to the London-van der Waals force. Therefore u_c is given by:

$$u_c = H_A/(192\mu d_o^2) \tag{7.10}$$

In the computer model values of 1.5×10^3, 15×10^3 and 150×10^3 μm/sec were used.

As a first approximation it is reasonable to assume that u_c is independent of particle size. However, the situation in a filter cake is more complex than considered here in this analysis. The fluid velocity is zero at the pore surface and increases as one moves away from the surface towards the middle of the pore. Larger particles protrude further into the flow and are therefore acted on by faster moving fluid. This implies that the deposition of large particles will decrease before that of small ones.

The model only considers the London-van der Waals forces of attraction and hydrodynamic forces. The model does not take into account the effect of double-layer forces. Rajagopalan and Tien[96] have shown that as long as the double-laver forces are not too large, it is safe to ignore them.

Another weakness of the model is that it takes no account of deposited particles being dislodged, despite the fact that experimental studies of deep bed filtration indicate that this can occur in porous media.[97, 98, 99] Despite the weaknesses of the model, the results are still very useful in illustrating how porous media clogging can affect the slip casting and filter pressing processes.

7.2.1 COMPUTER MODEL

Initially as each cake layer is added to the model the flow through all the pipes in the network is determined. Then suspended particles are introduced to the model. With each additional layer added to the network, fine particles are entrained with the fluid in this top layer.

The number of suspended particles per pore is proportional to the flow volume and no particles percolate through pipes with backflow. Applying Darcy's law for one dimensional laminar flow through the porous medium, the filtration velocity, q is given by:

$$\frac{Q}{A} = q = dP_l/dx\frac{K}{\mu} \tag{7.11}$$

where Q is the volumetric flow rate and A is the cross-sectional area of the medium. If cake and filter medium clogging is ignored and a uniform porosity of the cake is assumed, K will be constant and therefore:

$$q \propto 1/L \tag{7.12}$$

However, if clogging occurrs the permeability will change with increase in length:

$$q = \frac{G_c}{L}(K_{(b-1)}/K_o) \tag{7.13}$$

where G_c is a constant, b is the number of cake layers and $K_{(b-1)}$ is the permeability of the network with $(b-1)$ layers. The values for G_c used in the network model were chosen so that the filtration velocities are in the range of the filtration velocities experimentally measured while filter pressing alumina slips.

Alumina suspensions, with a volume solids loading, $\epsilon_{sl} = 0.39$, filter pressed at 275 kPa (40 psi) and using filter paper with an average pore size of 0.1 μm as the filter medium had permeabilities in the range of 3.5×10^{-17} m^2. The experimentally measured filtration velocity,

$$q = \frac{KP}{\mu L} \tag{7.14}$$

was found to be in the range of $9.7 \times 10^3/L$ μm/sec where L is given in μm. Due to

the resistance of the filter paper there is a limiting maximum filtration velocity. The filter paper has a permeability, $K_m = 4.5 \times 10^{-16}$ m^2 and a thickness, $L_m = 120$ μm. Therefore with $P = 275$ kPa the filtration velocity of water through the filter paper is equal to 1.03×10^3 μm/sec. Setting this velocity equal to q in equation (7.14) we find an equivalent minimum cake thickness equal to 9.4 μm. In the computer model, the thickness of each cake layer, ΔL, was fixed at 10 μm. Values for G_c between 50 μm^2/sec and 1×10^5 μm^2/sec were chosen to explore a range of filtration velocities.

The velocity through each tube, $u(i)$ is calculated by applying the following equation:

$$u(i) = q\frac{Q(i)A_pN}{Q_{inf}A(i)\nu} \tag{7.15}$$

where ν is the porosity, Q_{inf} is the total network inflow rate, N is the number of tubes per network row, A_p is the average tube area, and $A(i)$ and $Q(i)$ is the area and flow rate of tube i, respectively. A porosity of 0.42 was used in the model.

If $u(i)$ is greater than u_c then all the suspended particles in tube i are transported through the tube. If $u(i)$ is less than u_c then the number of particles deposited in tube i is:

$$N_{dep} = \lambda'\phi(b)Q(i)/Q_{ave} \tag{7.16}$$

where $\lambda' \leq 1$, $\phi(b)$ is the average number of suspended particles per pore in layer b and Q_{ave} is the average tube volumetric flow rate. The volume of particles deposited on the pore wall is equal to the reduction in the volume of the tube radius. The tube radii are allowed to be reduced to a negligibly small but finite value of 0.05 μm to simplify the network computations. Therefore, a limit is imposed on the volume of fines depositing in a pore.

Once the tube radii have been reduced due to particle deposition, the permeability of the clogged network is then solved. Then an additional layer is added to the

network and the process is repeated until the network has a total of 30 layers. The volume of fines that percolate through a layer is the volume of fines that is entrained with the fluid in the layer below it when the process is repeated with an additional layer added to the network.

One can realize that particles are continuously flowing through and/or being deposited within each layer. Furthermore, it is possible for some of the percolating particles to make their way to the bottom layer. Two situations were studied: (1) the migrating particles that make their way to the bottom layer are free to filter out along with the fluid (i.e. no clogging due to the filter medium) and (2) the particles which make their way to the bottom layer are arrested in this layer. Often if a fine pore sized filter medium is used, fine particles passing through the cake will be stopped at the cake/medium interface.

7.3 MODEL FOR CLOGGING DUE TO PORES TRAPPING PARTICLES

With this model the suspended particles can pass through pipes that are larger than the size of the suspended particles, r_s and a fraction of the particles will be trapped by a portion of pores smaller than r_s. It is assumed that a particle, once trapped, blocks a pore. The clogged pore is reduced to a negligibly small but finite value of 0.05 μm to simplify the network computation.

Initially, as an additional cake layer is added to the model the flow through all the tubes in the network is determined. Then suspended particles are introduced to the model. Fine particles are entrained with the fluid in the top layer. The volume of migrating particles that pass through a layer without being trapped is stored and this

volume of particles is entrained with the fluid in the layer below it when the process is repeated with an additional layer added to the network.

The number of suspended particles per tube is proportional to the flow volume. The volume of small tubes (i.e. tubes smaller than r_s) in layer b that is clogged is given by the following equation:

$$V(b)_{sc} = V(b)_{sus}\frac{Q(b)_{so}}{Q(b)_{tot}} \tag{7.17}$$

where $Q(b)_{so}$ is the summation of the positive volumetric flow rates of unclogged small pores in layer b, $Q(b)_{tot}$ is the summation of the total positive volumetric flow rates of all the pores in layer b and $V(b)_{sus}$ is the volume of suspended particles in layer b. Small tubes in a layer are clogged at random until the sum of the volume reduction of the small clogged tubes in layer b equals $V(b)_{sc}$. After the permeability of the clogged network is solved an additional layer is added to the network and the process is repeated until the network has a total of 30 layers.

This model as does the model for progressive clogging due to particle deposition on pore walls examines the following two situations: (1) the migrating particles that make their way to the bottom layer are free to filter out along with the fluid and (2) the particles which make their way to the bottom layer are arrested in this layer.

7.4 RESULTS FOR CLOGGING DUE TO PARTICLE DEPOSITION

Network permeabilities were calculated for networks clogging due to fine particles depositing on the pore walls. The tube radii of the networks were filled with a log-normal distribution with a standard deviation (of the ln (*tube radius*)) equal to

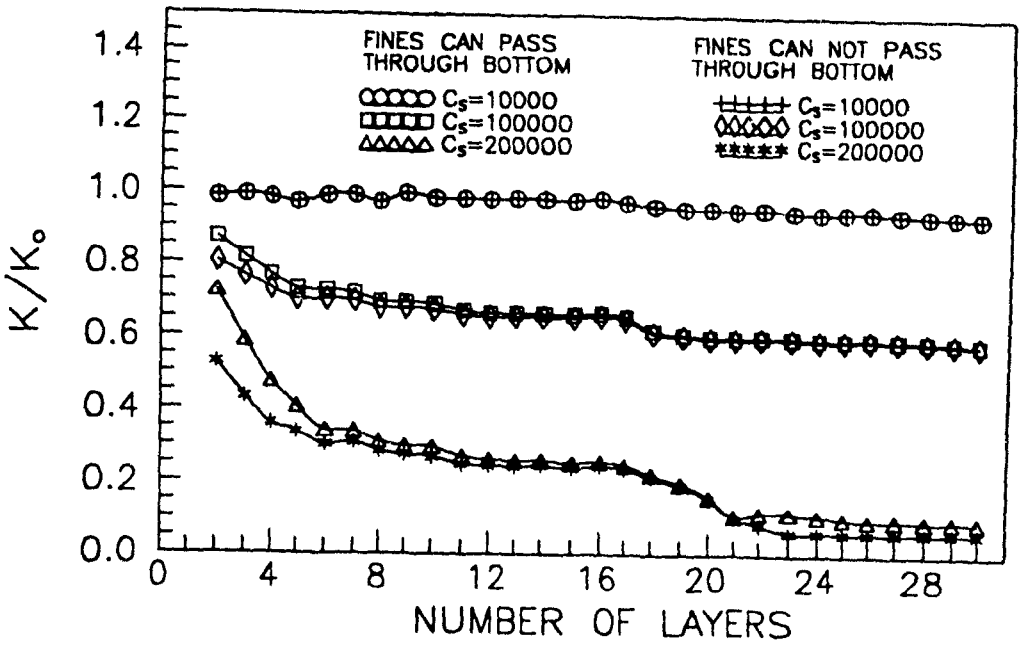

Figure 7.4: Permeability versus number of layers in network, r_s = 0.01 μm and $q_i = 500/L$ μm/sec.

0.6 and a median of 1.0 μm. The unit cake layer length, ΔL, was set at 10 μm (see section (7.2.1)).

Three suspended particle concentrations, C_s (i.e., average number of suspended particles per pore) were studied. The concentrations were determined so that the average number of suspended particles would fill 1 %, 10 %, and 20 % of the volume of a pore with a radius of 1 μm.

Figures 7.4 to 7.7 are graphs of K/K_o versus the number of cake layers. The critical velocity, u_c, was set at 15 x 10^3 μm/sec.

In Figure 7.4, the suspended particles had radii of 0.01 μm and an initial superficial velocity, q_i, equal to $500/L$ μm/sec. Two conditions were examined: (1) the migrating particles that make their way to the cake bottom were free to filter out with the fluid (i.e., no clogging due to the filter medium) and (2) the particles that migrate to the cake bottom were arrested in the bottom layer. With increase in

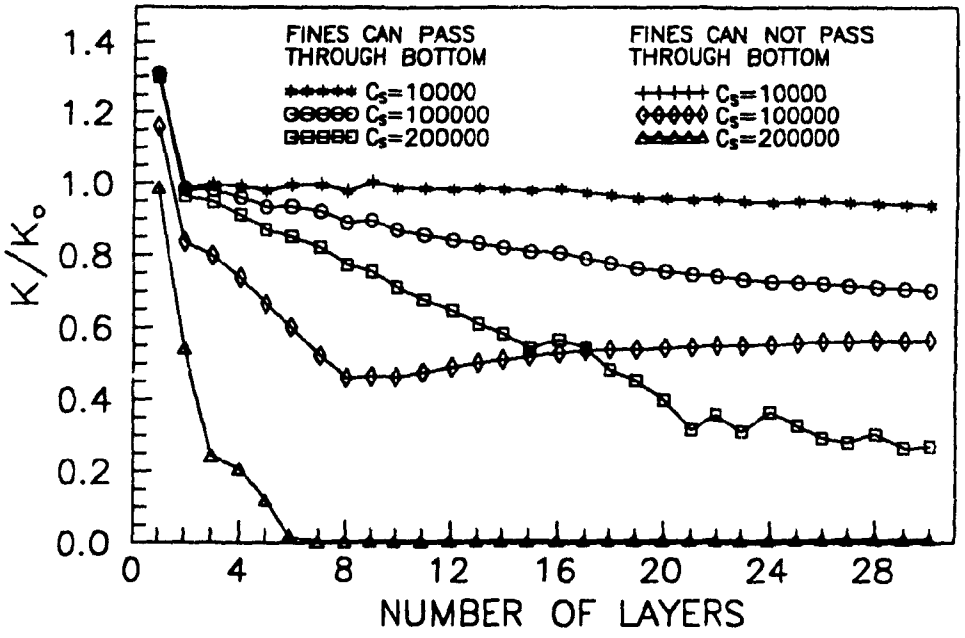

Figure 7.5: Permeability versus number of layers in network, $r_s = 0.01$ μm and $q_s = 10 \times 10^3/L$ μm/sec.

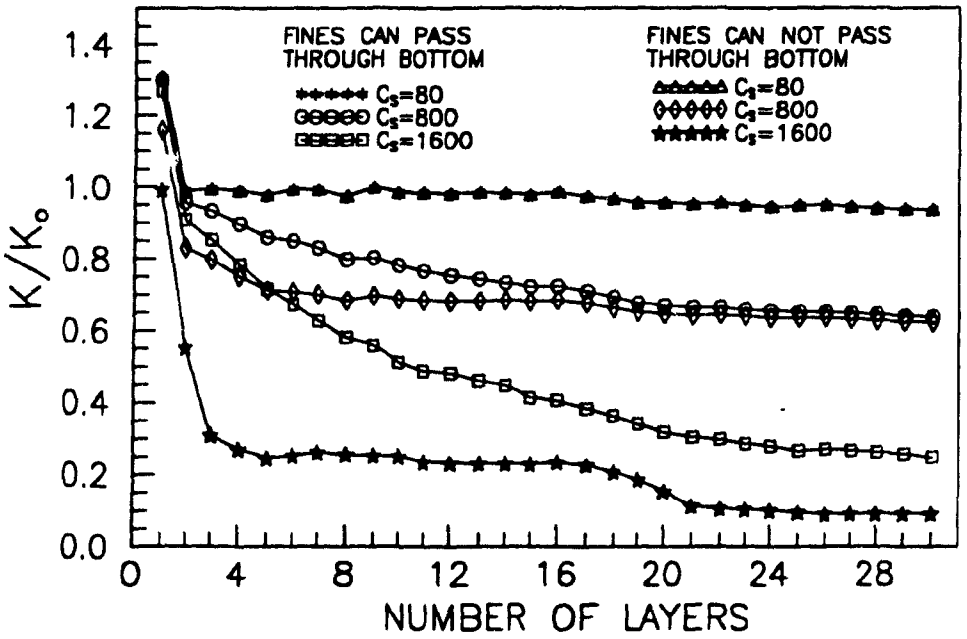

Figure 7.6: Permeability versus number of layers in network, $r_s = 0.05$ μm and $q_s = 500/L$ μm/sec.

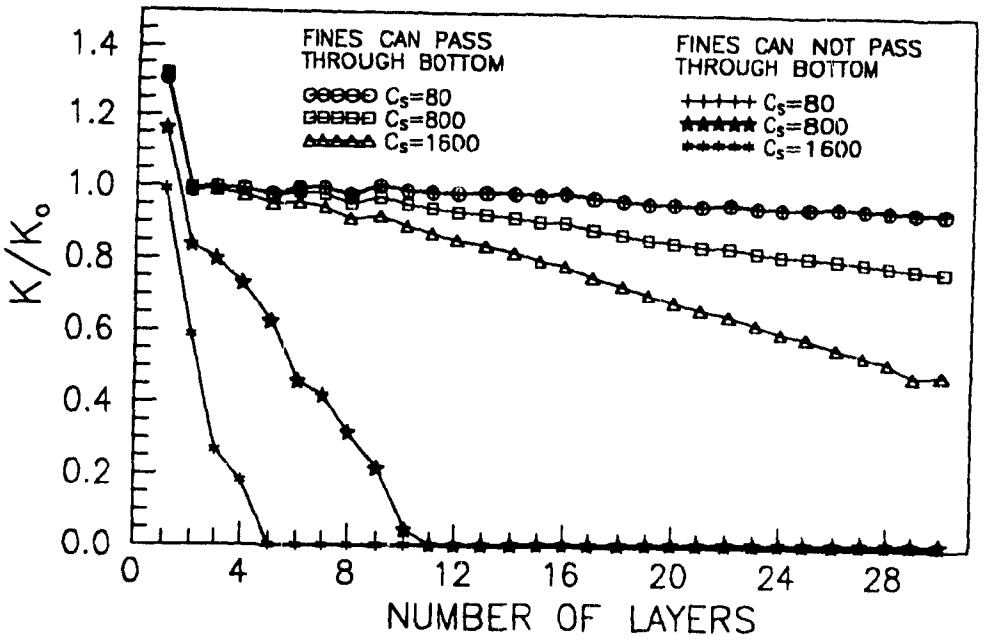

Figure 7.7: Permeability versus number of layers in network, $r_s = 0.05$ μm and $q_i = 10 \times 10^3/L$ μm/sec.

suspended particle concentration, C_s (i.e., average number of suspended particles per pore) K decreases. The additional effect in reducing K due to particles being arrested at the bottom layer is nil at a low C_s and only minor at the highest concentration of suspended particles.

The conditions for the permeability results presented in Figure 7.5 are the same as for Figure 7.4 except that the initial superficial velocity is 20 times greater (i.e., $q_i = 10 \times 10^3/L$ μm/sec). Again, as in Figure 7.4, the additional effect of reducing K due to particles being arrested at the bottom layer is nil at a low C_s. However, at the higher suspended particle concentrations, the additional effect in reducing K due to particles being arrested at the bottom layer is very significant. These results demonstrate that clogging at the cake bottom due to the filter medium can be very detrimental to the filtration rate. With the higher superficial velocity being used in the model, one observes that the cake bottom and filter medium can become clogged

very rapidly if there is a high concentration of suspended particles. In the very early stages of filtration, the filtration velocity is high and therefore many of the suspended fine particles will be transported to the cake bottom-filter medium interface. In the initial stages, many pores at the cake bottom are free and therefore the rate of clogging is high. The permeability decreases rapidly. There appears to be a critical number of clogged pores that causes the permeability to decrease sharply and then once severe clogging has occurred the permeability levels off.

In Figure 7.6, $q_i = 500/L$ μm/sec and $r_s = 0.05$ μm. Again, as in the previous graphs, the permeability of the network decreases with C_s. There is no additional reduction in K due to clogging of the bottom cake layer when $C_s = 80$. The additional effect in reducing K due to particles being arrested in the bottom layer increases with C_s. The drop off in K due to clogging of the cake bottom is not as dramatic as in Figure 7.5 and the permeabilities for the cases where particles are free to pass through the cake bottom are higher than in Figure 7.4. The radii of the fines are larger than for the results presented in the previous two graphs, therefore more of the fines will be migrating through the pores rather than depositing on the pore surfaces for a given flow velocity. However, the drop off in K due to the fines being arrested at the cake bottom is not as dramatic as in Figure 7.5. With the lower velocity more particles are deposited in the upper layers of the network and less are transported to the bottom layer.

In Figure 7.7, $q_i = 10 \times 10^3/L$ μm/sec and the radii of the suspended particles are 0.05 μm. These results also show that a higher velocity causes a rapid and dramatic drop off in K due to particles being arrested at the cake bottom. For the cases where the fines were not arrested at the cake bottom, the drop off in K was less than in the previous graphs due to the larger radii of the fines (0.05 μm) and higher

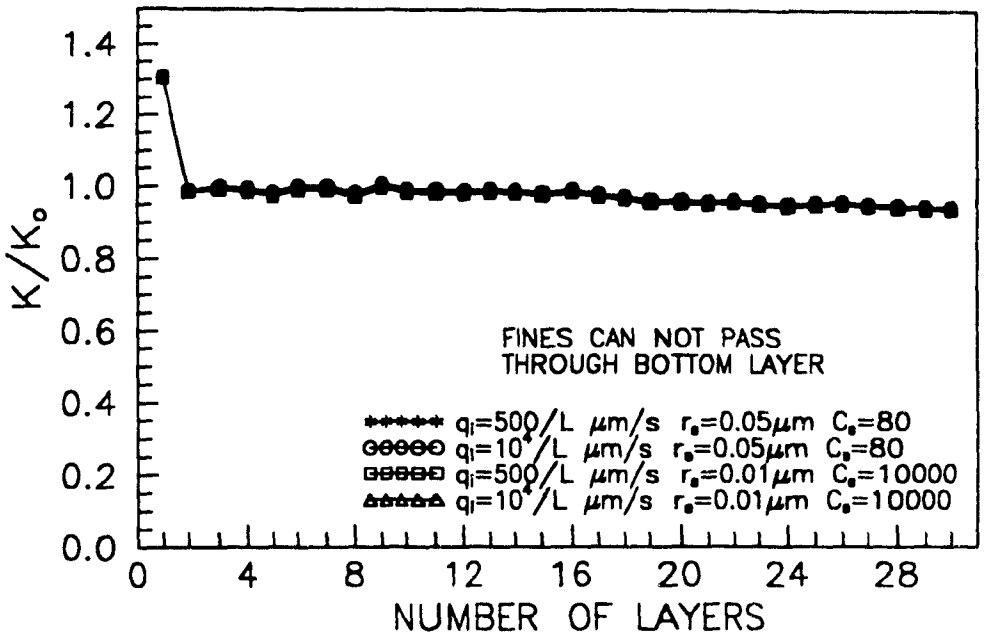

Figure 7.8: Permeability versus number of layers in network, C_e = 80 and 10000.

velocity.

Figures 7.8-7.13 illustrate the effects that q_i and the radii of the fines have on the permeability. In Figures 7.8-7.10 fines are prevented from passing through the bottom layer whereas in Figures 7.11-7.13 fines are free to pass through the bottom layer. In summary, Figures 7.9 and 7.10 show that the greater velocity ($q_i = 10\times10^3/L$ μm/sec) and larger fines (0.05 μm) cause the permeability to drop rapidly and dramatically due to clogging of the bottom layer. Figures 7.12 and 7.13 show that the smaller velocity ($q_i = 500/L$ μm/sec) and the smaller suspended particle radius (0.01 μm) causes clogging to occur more within the cake as it increases in thickness. Figures 7.8 and 7.11 show that at a low suspended particle concentration the deposition of fines on the pore walls has very little effect in reducing K.

The effects that the different initial filtration velocities, q_i and critical velocities, u_c have on the clogging of the network was analyzed. Figures 7.14 and 7.15 are

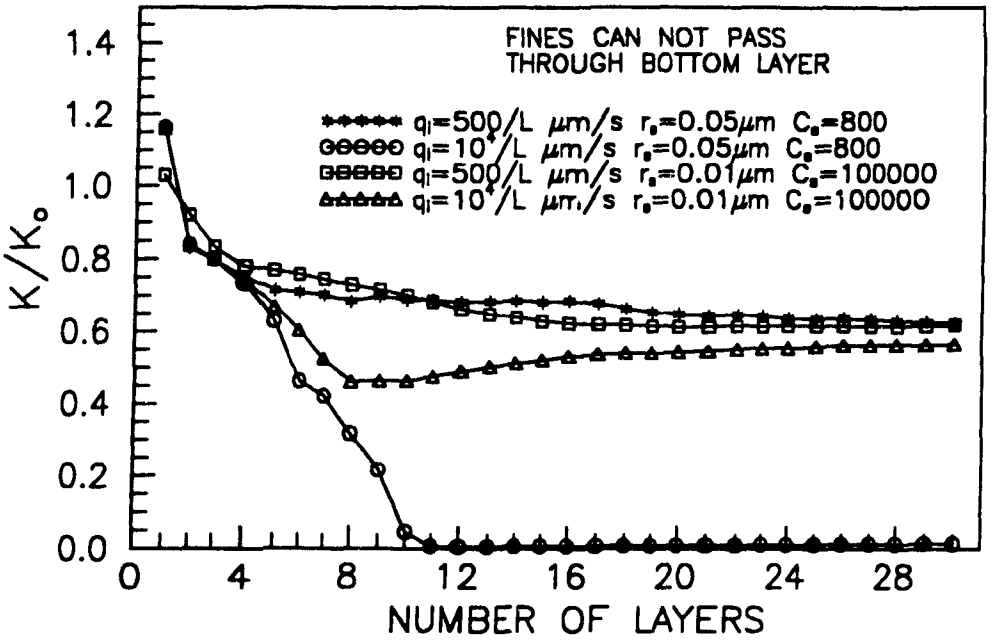

Figure 7.9: Permeability versus number of layers in network, C_s = 800 and 100000.

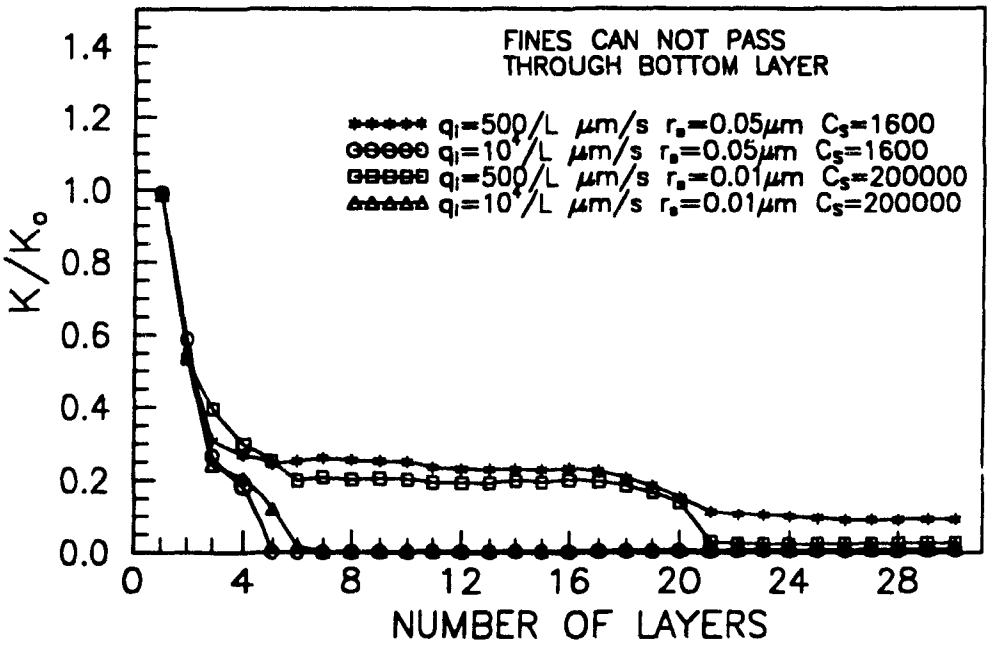

Figure 7.10: Permeability versus number of layers in network, C_s = 1600 and 200000.

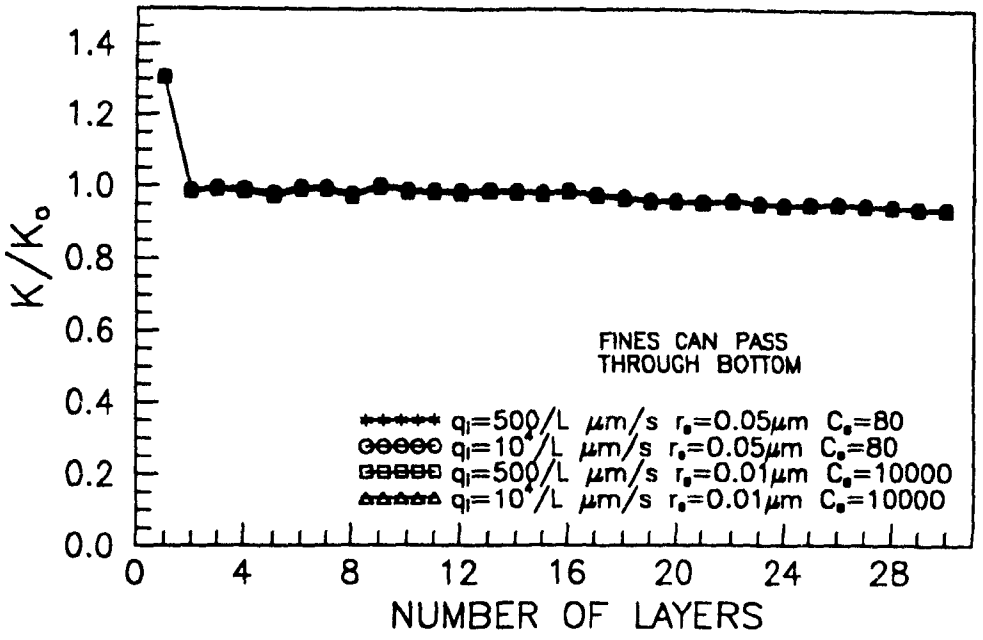

Figure 7.11: Permeability versus number of layers in network, C_s = 80 and 10000.

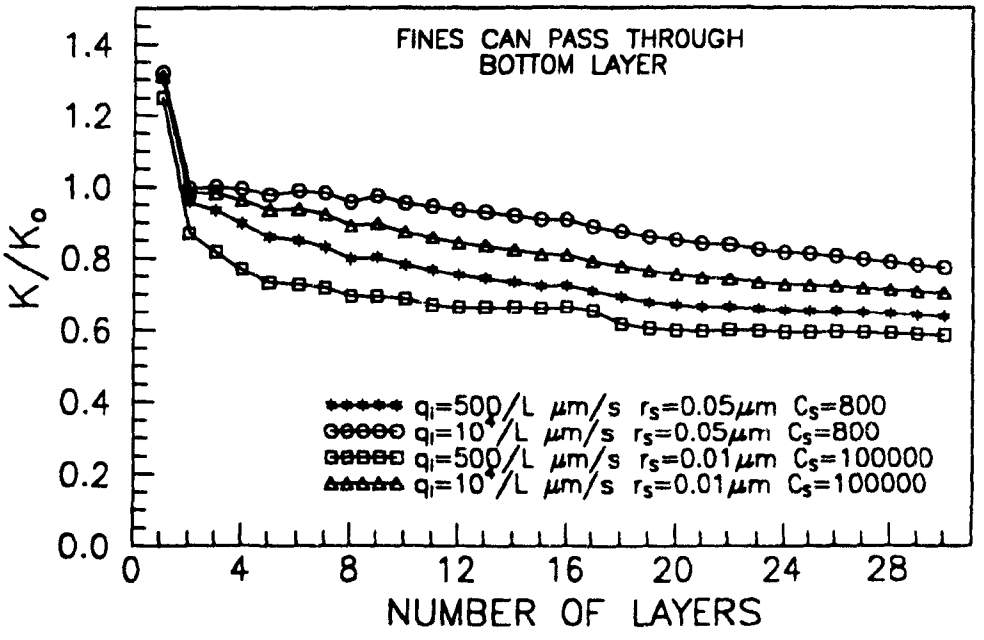

Figure 7.12: Permeability versus number of layers in network, C_s = 800 and 100000.

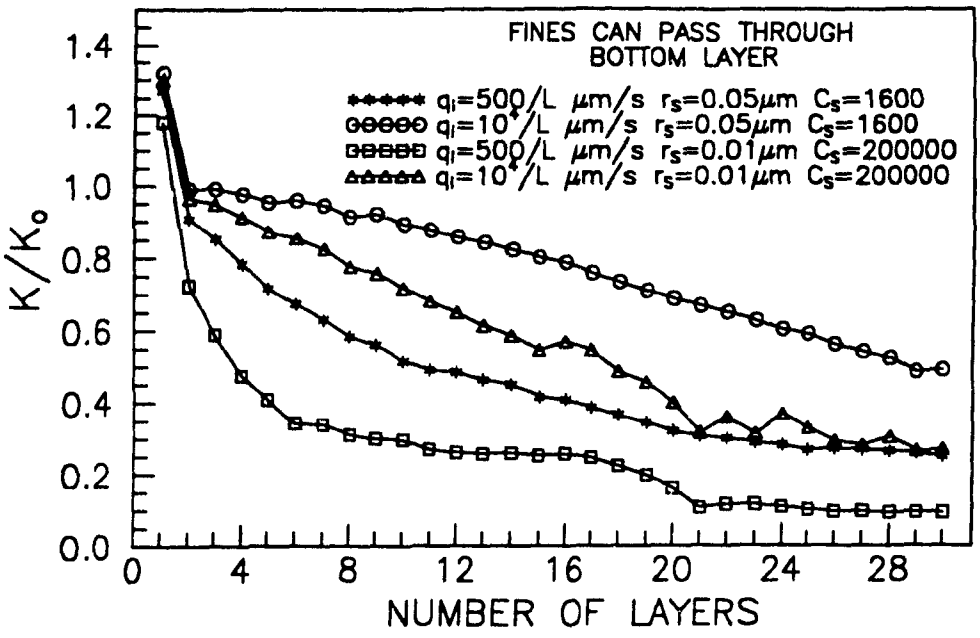

Figure 7.13: Permeability versus number of layers in network, C_s = 1600 and 200000.

graphs of K/K_o versus number of layers. The fines had a radius of 0.05 μm and C_s = 800. The fines were prevented from passing through the bottom layer. The critical velocity, u_c, was set at 1.5×10^3 μm/sec, 15×10^3 μm/sec and 150×10^3 μm/sec for both Figure 7.14 and 7.15. In Figure 7.14 filtration velocities of $50/L$ μm/sec, $500/L$ μm/sec and $5000/L$ μm/sec were used. In Figure 7.15 velocities 20 times greater than in Figure 7.14 were used. For both graphs, u_c had very little effect on the permeability results. However, in Figure 7.14 there is a sharp drop off in K for $q_i = 5 \times 10^3/L$ μm/sec and in Figure 7.15 the sharp drop off in K occurs for $q_i = 10 \times 10^3/L$ μm/sec and $100 \times 10^3/L$ μm/sec. These results show that at high values of q_i many of the suspended particles can percolate right through the cake and therefore clog the bottom layer.

In Figures 7.16 and 7.17, the fines had a radius of 0.01 μm and C_s = 100000. The velocities in Figure 7.17 were 20 times greater than in Figure 7.16. In Figure 7.16

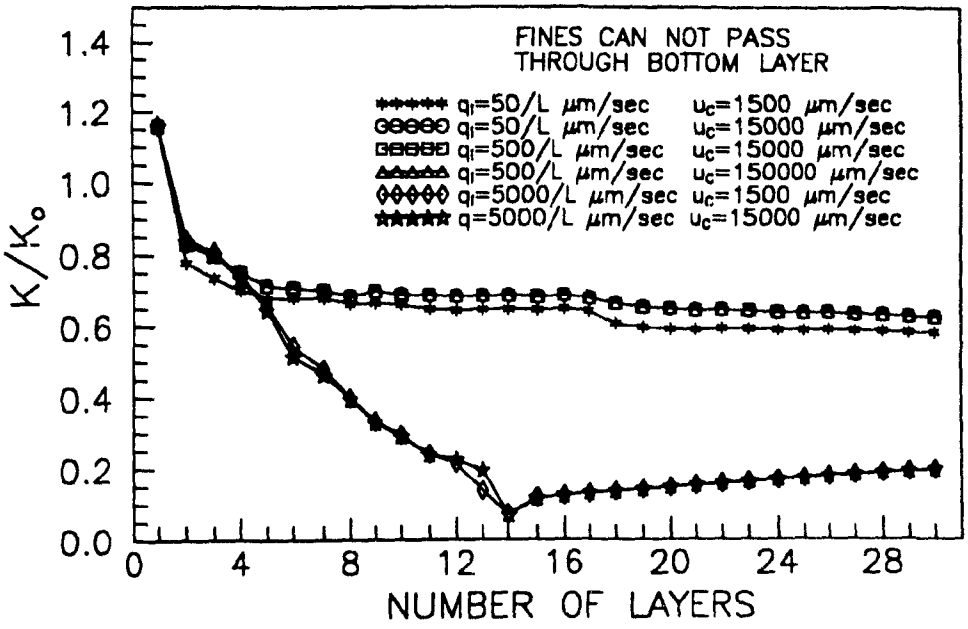

Figure 7.14: Permeability versus number of layers in network, $r_s = 0.05$ μm and $C_s = 800$.

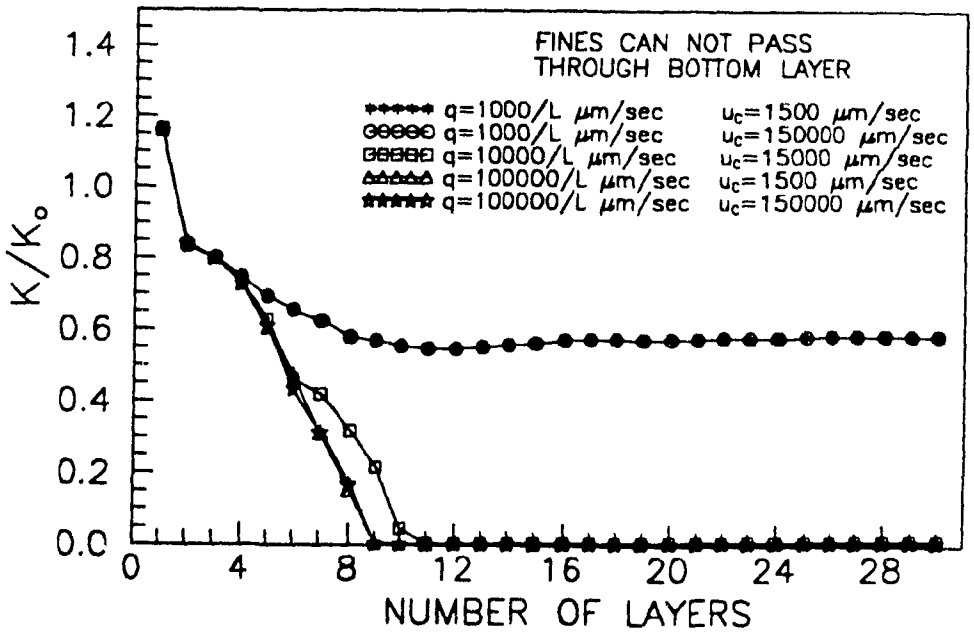

Figure 7.15: Permeability versus number of layers in network, $r_s = 0.05$ μm and $C_s = 800$.

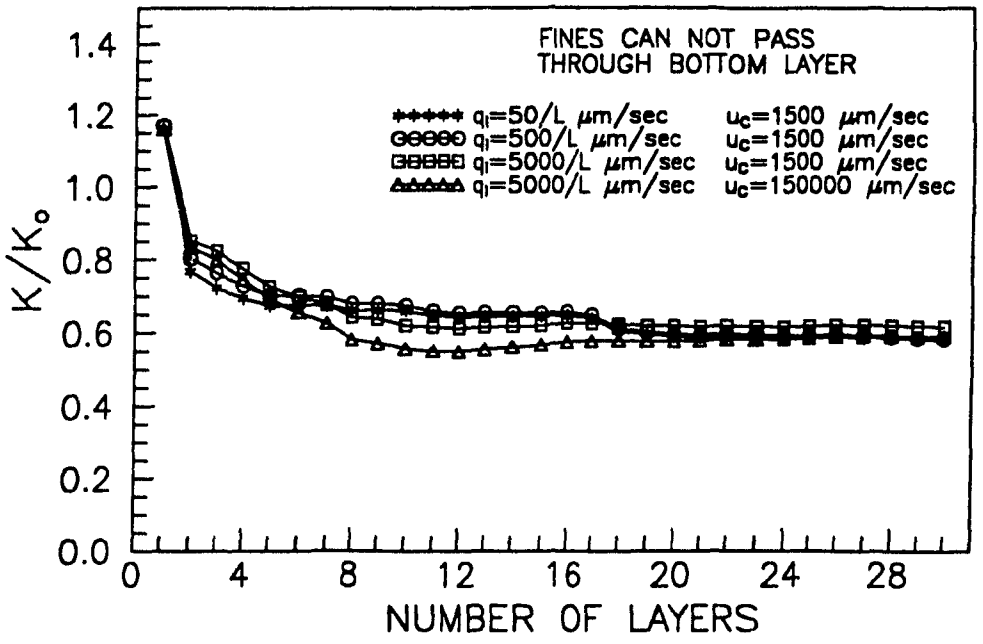

Figure 7.16: Permeability versus number of layers in network, $r_s = 0.01$ μm and $C_s = 100000$.

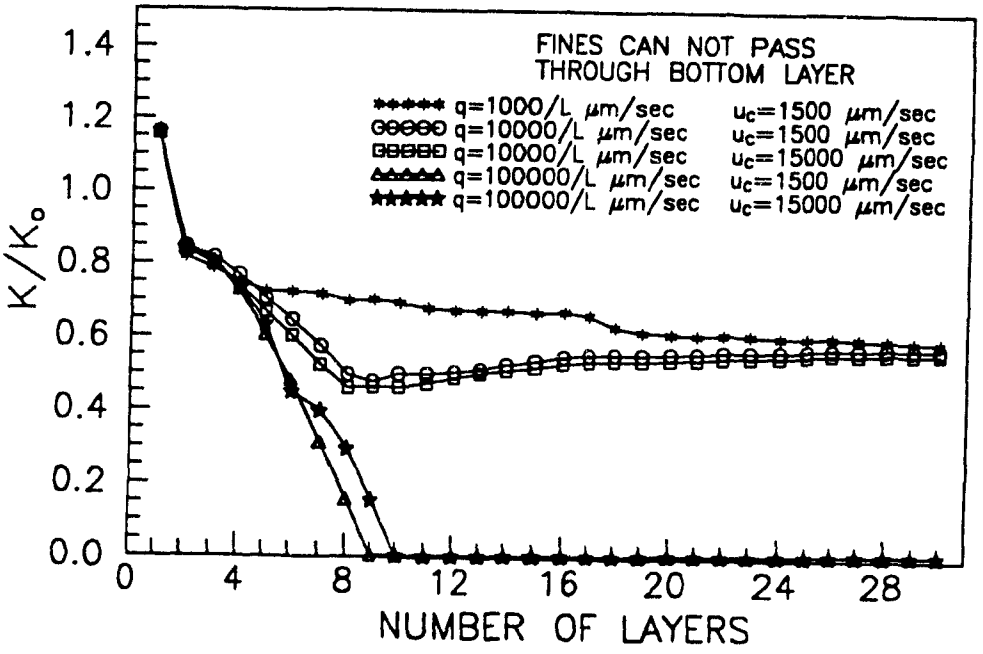

Figure 7.17: Permeability versus number of layers in network, $r_s = 0.01$ μm, $C_s = 100000$.

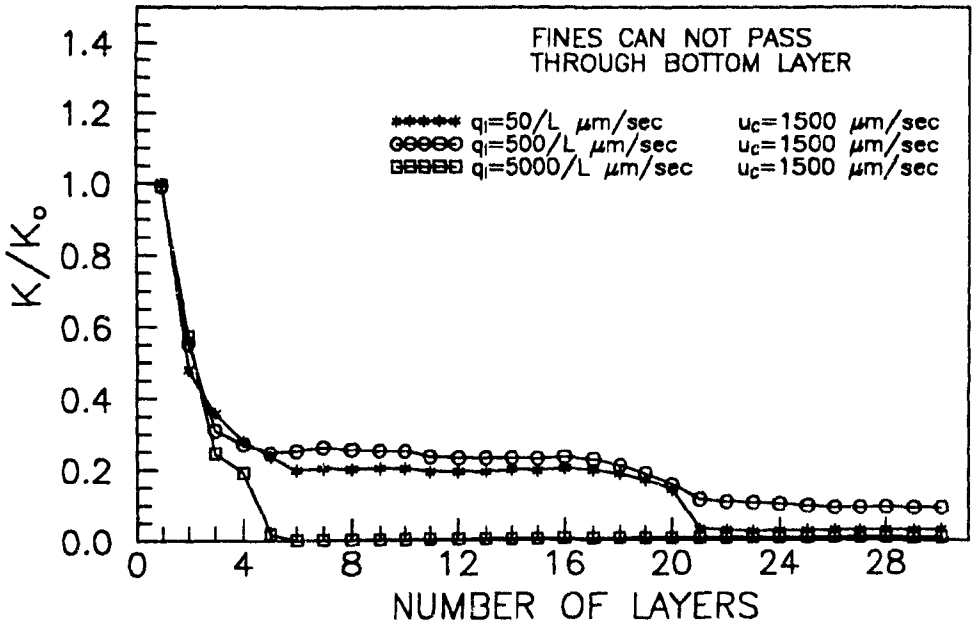

Figure 7.18: Permeability versus number of layers in network, $r_s = 0.05$ μm and $C_s = 1600$.

there was no dramatic decrease in K. However, in Figure 7.17, at the highest filtration velocity ($q_t = 100 \times 10^3/L$ μm/sec) there was a sharp decrease in K. Comparing Figures 7.16 and 7.17 with Figures 7.14 and 7.15 one can observe that the reduction in K was more severe due to the coarser suspended fines (0.05 μm). These coarser fines adhere less to the tube walls and therefore more percolate to the cake bottom and clog the bottom layer. The filtration conditions in Figures 7.18-7.21 are similar to the conditions used in Figures 7.14-7.17 aside from using higher suspended particle concentrations, C_s. The concentrations were fixed at 1600 and 200000 for fines with radii of 0.05 μm and 0.01 μm, respectively. With these higher C_s values there is a more rapid and greater drop off in K.

The situation where the suspended particles are free to filter out of the cake bottom was also analyzed for different values of u_c and q_t. Figure 7.22 confirms that K decreases with decrease in q_t. As q_t decreases more particles deposit on the tube

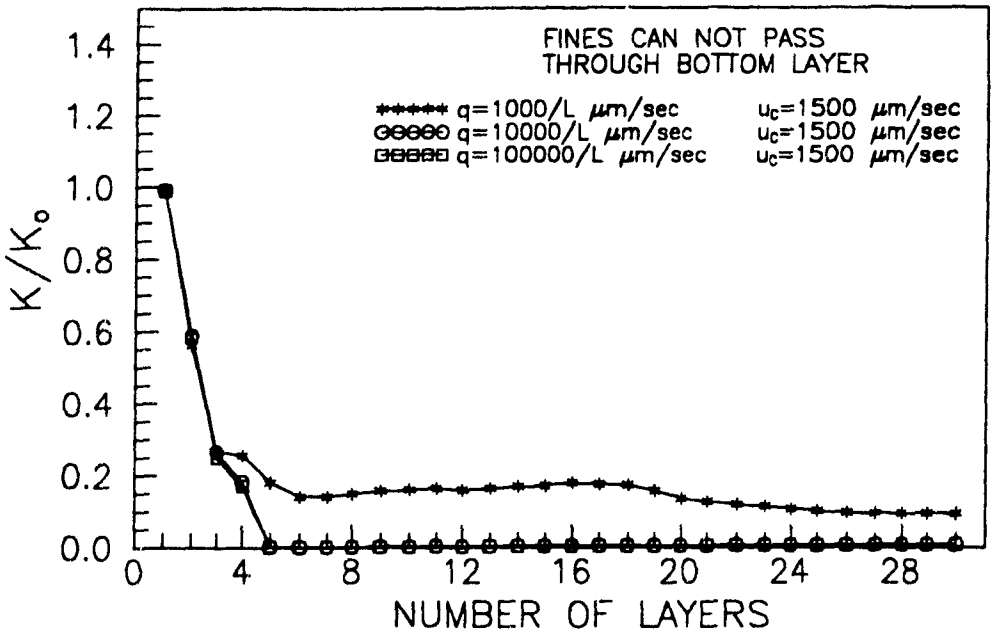

Figure 7.19: Permeability versus number of layers in network, $r_s = 0.05$ μm, $C_s = 1600$.

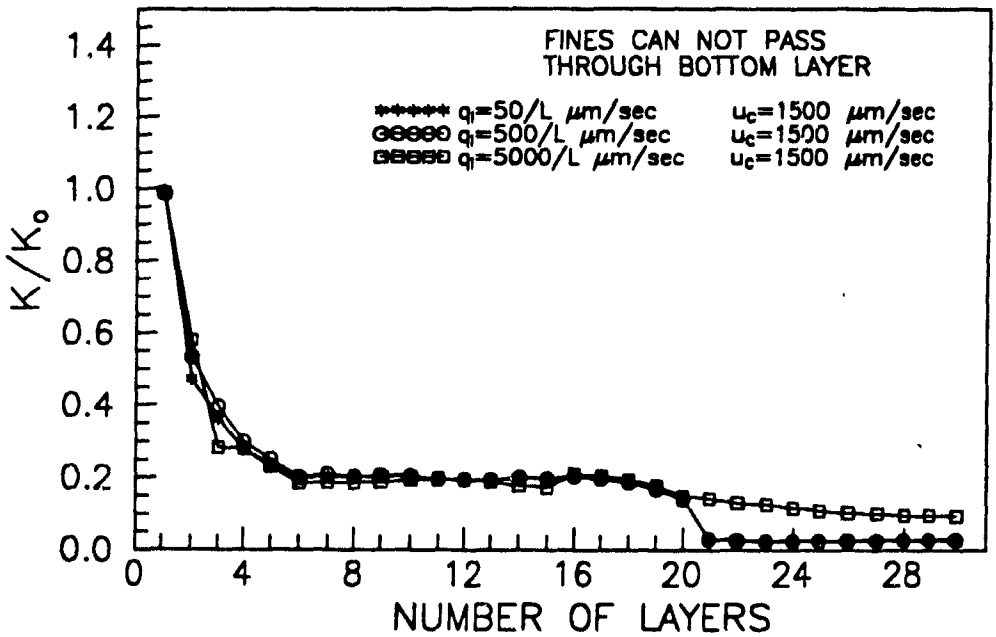

Figure 7.20: Permeability versus number of layers in network, $r_s = 0.01$ μm and $C_s = 200000$.

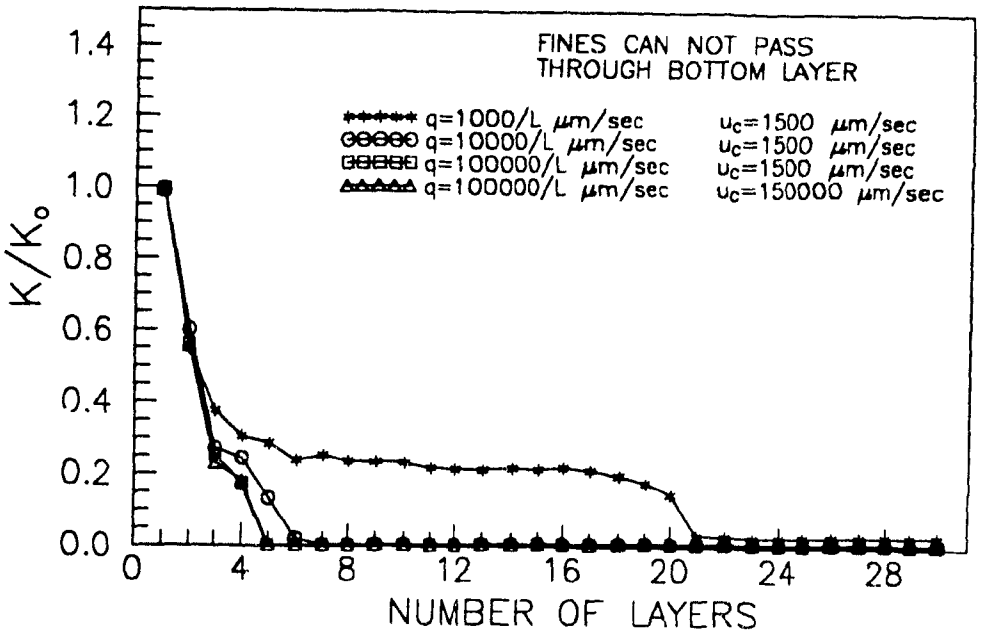

Figure 7.21: Permeability versus number of layers in network, $r_s = 0.01$ μm, $C_s = 200000$.

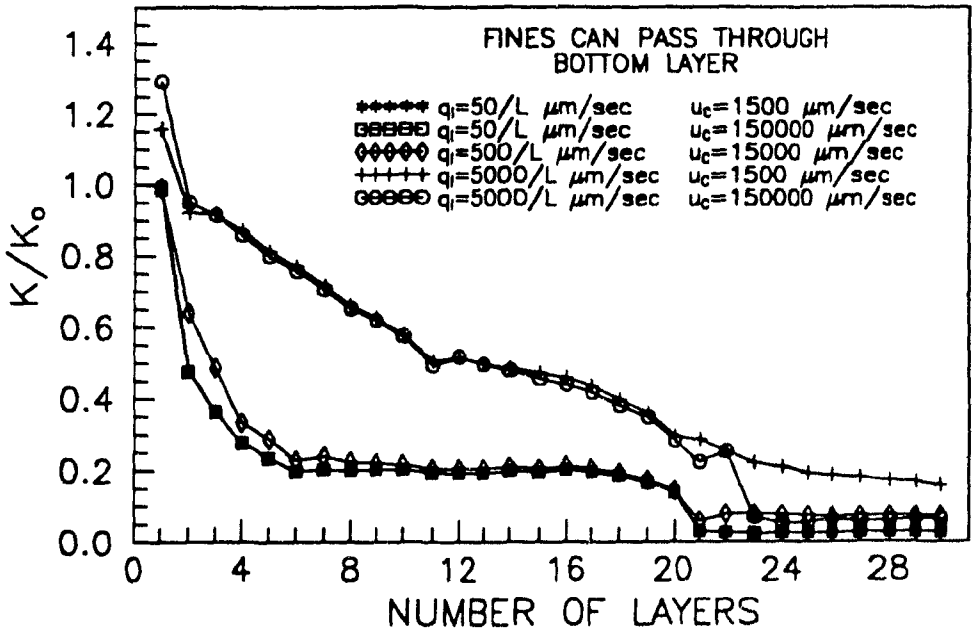

Figure 7.22: Permeability versus number of layers in network, $r_s = 0.01$ μm and $C_s = 200000$.

walls and clog the network. It is interesting to note that at a high q_i ($5000/L$ μm/sec), the permeability results are affected by u_c. After 21 layers, there was a sharp decrease in K for the two curves with $u_c = 15000$ μm/sec and 150000 μm/sec but not for the curve with $u_c = 1500$ μm/sec. With a low u_c and high q_i some of the particles are prevented from depositing on the pore walls.

The permeability results illustrate that the networks can be severely clogged due to particles depositing on the tube walls and reducing the tube radii. The reduction in tube volume during clogging was analyzed. As each layer of tubes is added to the network and before particle deposition occurs, the tube volume of this additional layer, V_{op} is calculated. Then, after particle deposition occurs, the tube volume for each layer, V_{cl} in the network is recalculated. The ratio of the unclogged tube volume, V_{cl} to V_{op} was calculated as the network increased in length.

Figures 7.23-7.27 are graphs of V_{cl}/V_{op} versus number of layers. Six curves are shown on each graph. The results are plotted for a network consisting of 5, 10, 15, 20, 25 and 30 layers. The suspended particles had a radius of 0.01 μm and $C_s = 200000$.

In Figures 7.23 and 7.24, $q_i = 500/L$ and $10 \times 10^3/L$ μm/sec, respectively. For both Figures the particles were prevented from passing through the bottom layer. In Figure 7.23, V_{cl}/V_{ol} is fairly constant with the top most layer having a slightly higher V_{cl}/V_{op} value (i.e., less clogging). With $q_i = 500/L$ μm/sec most of the particles deposit in the upper layers of the network. In Figure 7.24 however, the tube volume reduction is significantly higher in the first (i.e., bottom) layer. With this higher velocity ($q_i = 10 \times 10^3/L$ μm/sec), during the build-up of the first 5 and even 10 layers a significant volume of the fine particles percolates through the network and deposits in the bottom layer causing a dramatic drop in K. After the first 10 layers have been formed an insignificant amount of particles percolate to the bottom layer.

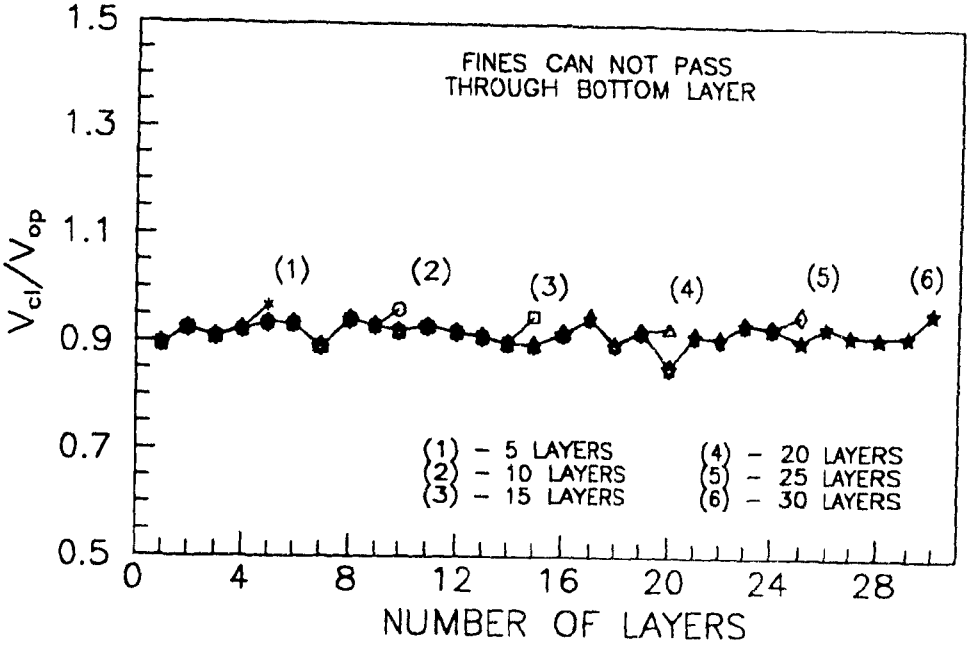

Figure 7.23: Graph shows fraction of original tube volume of layer available for flow after particle deposition has occurred ($q_i = 500/L$ μm/sec, $u_c = 15 \times 10^3$ μm/sec, $r_s = 0.01$ μm and $C_s = 200000$).

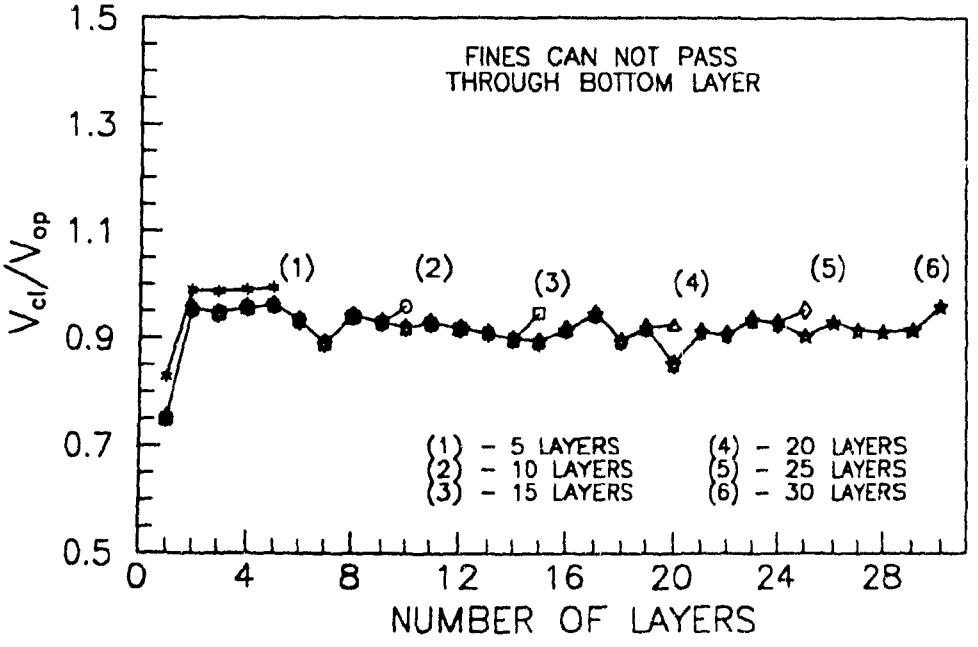

Figure 7.24: Graph shows fraction of original tube volume of layer available for flow after particle deposition has occurred ($q_i = 10 \times 10^3/L$ μm/sec, $u_c = 15 \times 10^3$ μm/sec, $r_s = 0.01$ μm and $C_s = 200000$).

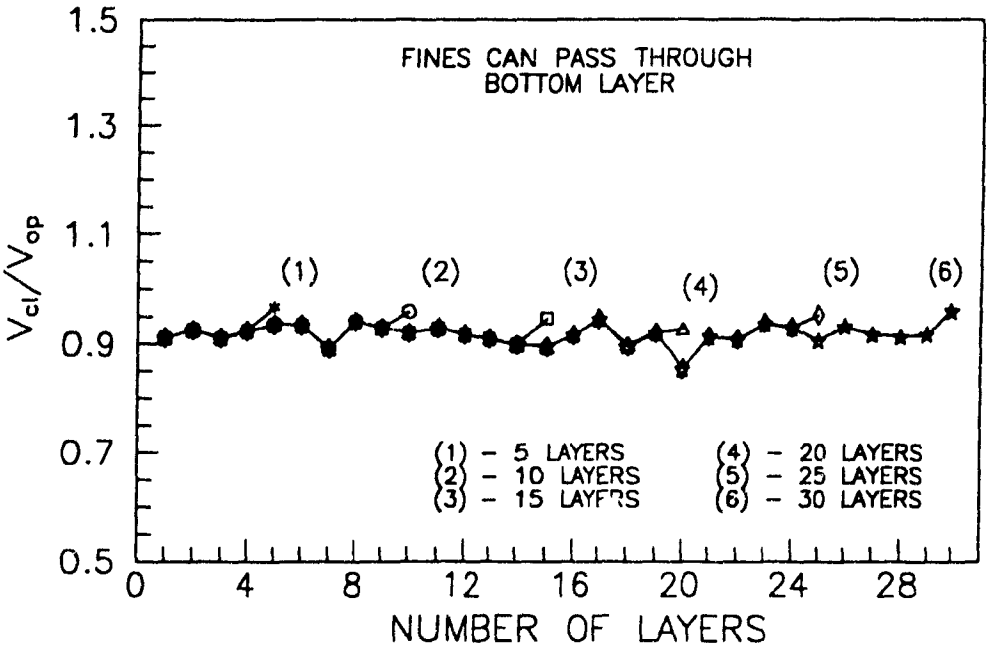

Figure 7.25: Graph shows fraction of original tube volume of layer available for flow after particle deposition has occurred ($q_i = 500/L$ μm/sec, $u_c = 15 \times 10^3$ μm/sec, $r_s = 0.01$ μm and $C_s = 200000$).

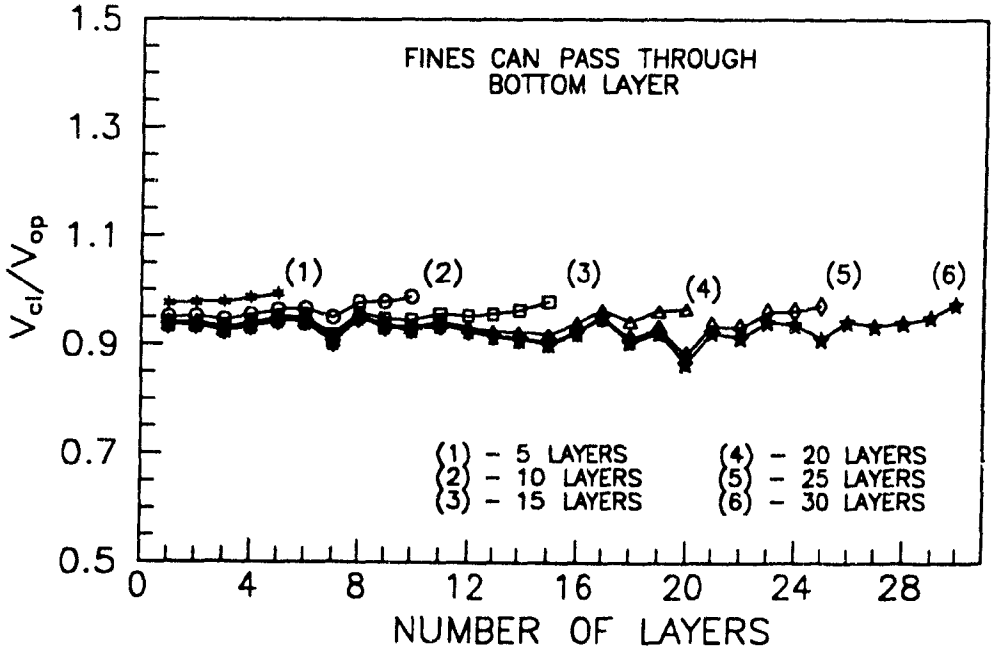

Figure 7.26: Graph shows fraction of original tube volume of layer available for flow after particle deposition has occurred ($q_i = 10 \times 10^3/L$ μm/sec, $u_c = 15 \times 10^3$ μm/sec, $r_s = 0.01$ μm and $C_s = 200000$).

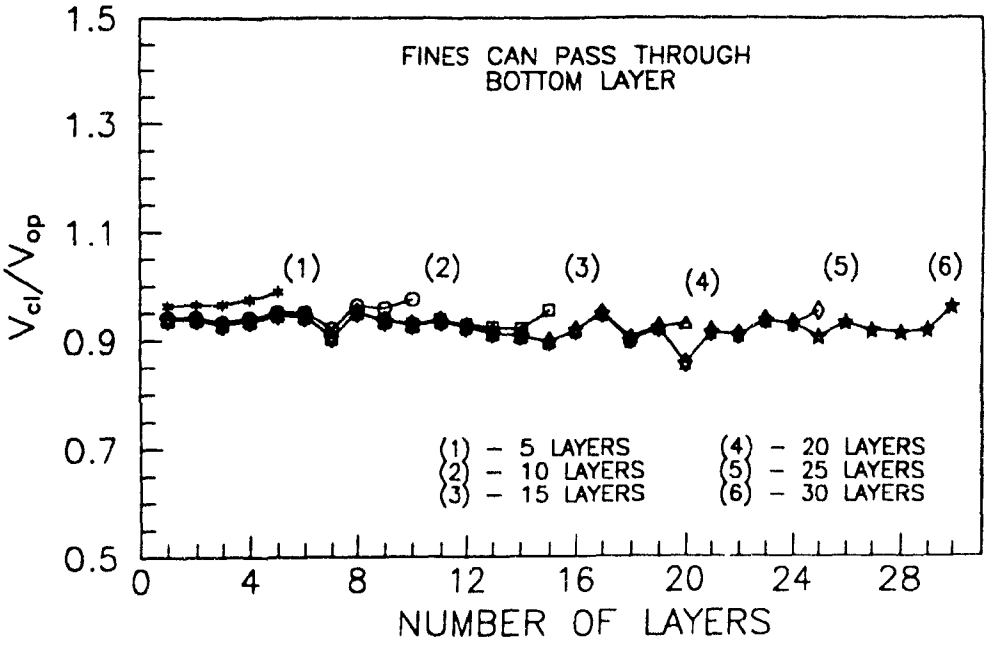

Figure 7.27: Graph shows fraction of original tube volume of layer available for flow after particle deposition has occurred ($q_t = 5 \times 10^3/L$ μm/sec, $u_c = 150 \times 10^3$ μm/sec, $r_s = 0.01$ μm and $C_s = 200000$).

In Figures 7.25-7.27 the particles that percolate to the bottom layer are free to filter out with the filtrate. In Figure 7.25 where $q_t = 500/L$ μm/sec, again the curves are fairly constant due to most of the particles depositing in the upper network layers. In Figure 7.26 where $q_t = 10 \times 10^3$ μm/sec, V_{cl}/V_{op} decreases in the bottom layers (i.e., first couple of layers) as the network increases in its number of layers. Particles are depositing in the entire network length and some are being transported right through the network and filtering out with the filtrate.

In Figure 7.22 where $r_s = 0.01$ μm, $C_s = 200000$ and the particles can pass through the bottom layer the decrease in K is more gradual at the higher filtration velocity ($q_t = 5 \times 10^3/L$ μm/sec). The graph of V_{cl}/V_{op} versus number of layers for this case is shown in Figure 7.27. The results show that the V_{cl}/V_{op} values decrease for the curves with network lengths of 5, 10 and 15 layers. The high velocities were initially filtering some of the particles out of the network and depositing the rest

throughout the network.

Figures 7.23-7.27 show that the V_{cl}/V_{op} values are near 0.9, however in the earlier graphs it was shown that sometimes the permeability can drop by more than a factor of 100 due to clogging. Therefore, these V_{cl}/V_{op} results illustrate that only a small reduction in pore volume is required to cause severe clogging.

7.5 RESULTS FOR CLOGGING DUE TO PORES TRAPPING PARTICLES

Network permeabilities were calculated for networks that clogged as a result of tubes trapping particles larger than the tube openings. Three volume concentrations of suspended particles, C_v = 0.005, 0.01 and 0.05 were studied. The volume concentration, C_v is defined as the volume of flowing particles in a layer per total pore volume of the layer.

Figures 7.28-7.30 are graphs of K/K_o versus the number of layers in the networks. The tube radii of the networks were filled with log-normal distributions with ξ = 0.6 and a median of 1 μm. In Figures 7.28, 7.29 and 7.30 tubes with radii smaller than r_s = 0.4 μm, 0.6 μm and 0.8 μm could be clogged, respectively. The suspended particles that make their way to the cake bottom were free to filter out with the fluid. The results show that for a small r_s (= 0.4 μm) the clogging of these small pipes have very little effect in reducing K. As expected, for a larger r_s (= 0.8 μm) clogging can significantly reduce K. The larger r_s the greater the effect C_v has on decreasing K.

In Figures 7.31-7.33 the bottom layer arrests the particles that migrate to the bottom of the network. All other conditions are similar to the ones in Figures 7.28-7.30, respectively. The drop in K is most severe for the case where r_s = 0.4 μm.

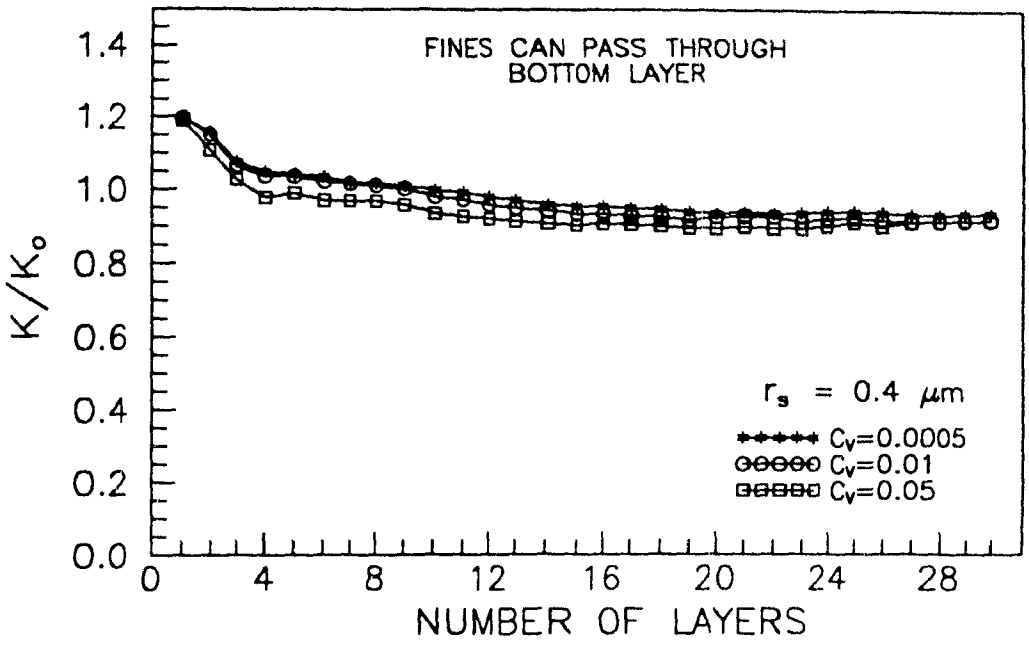

Figure 7.28: Permeability versus number of layers in network, $r_s = 0.4\ \mu m$.

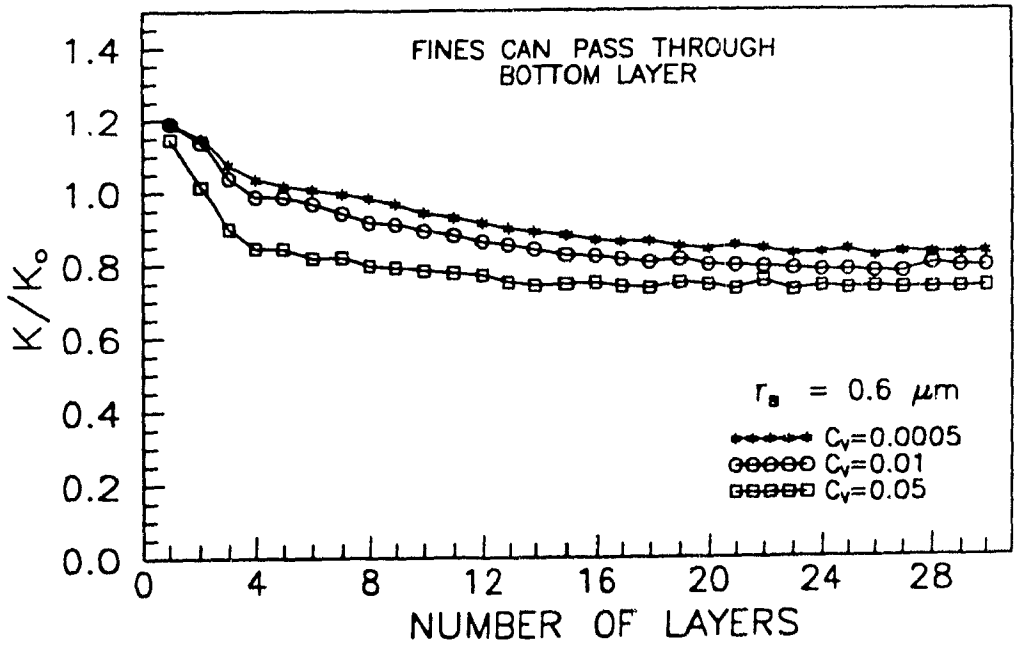

Figure 7.29: Permeability versus number of layers in network, $r_s = 0.6\ \mu m$.

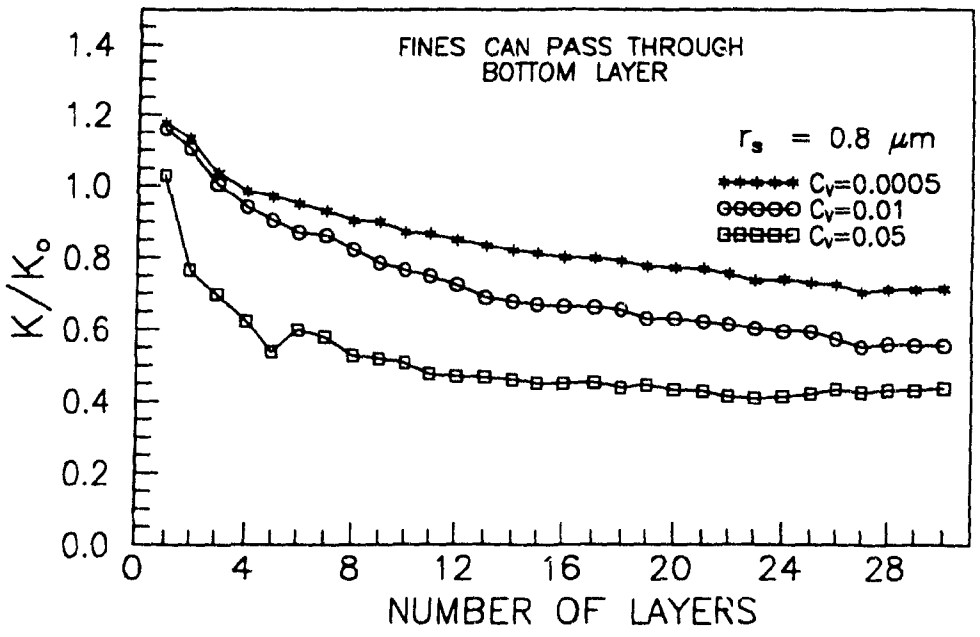

Figure 7.30: Permeability versus number of layers in network, r_s = 0.8 μm.

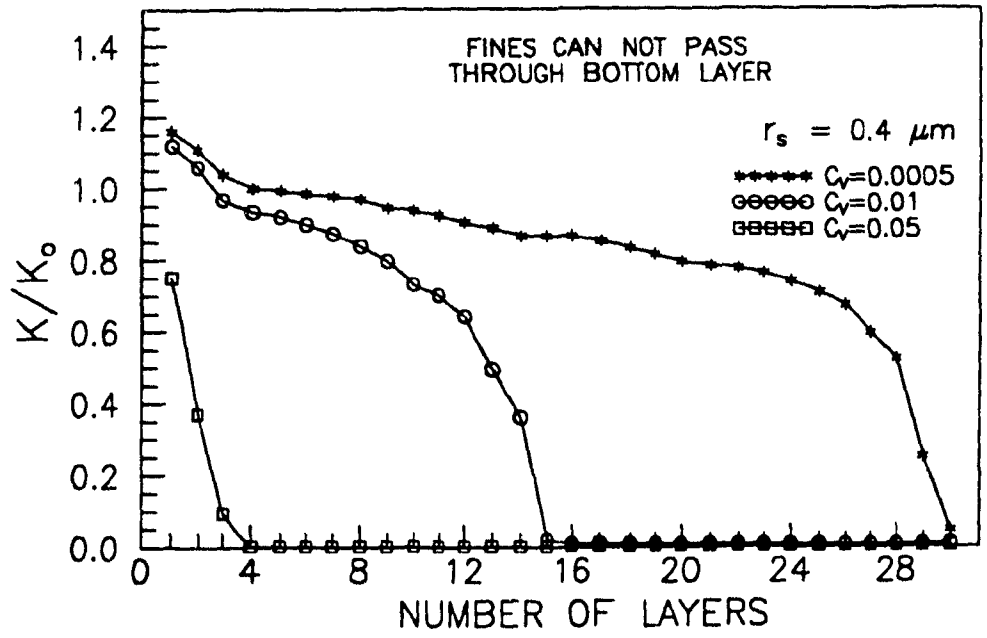

Figure 7.31: Permeability versus number of layers in network, r_s = 0.4 μm.

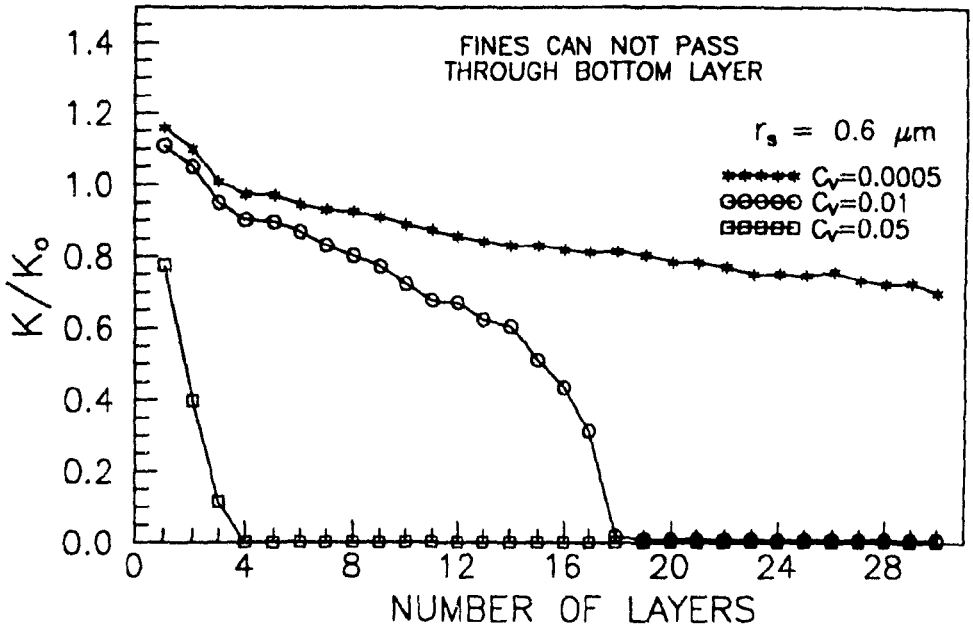

Figure 7.32: Permeability versus number of layers in network, $r_s = 0.6$ μm.

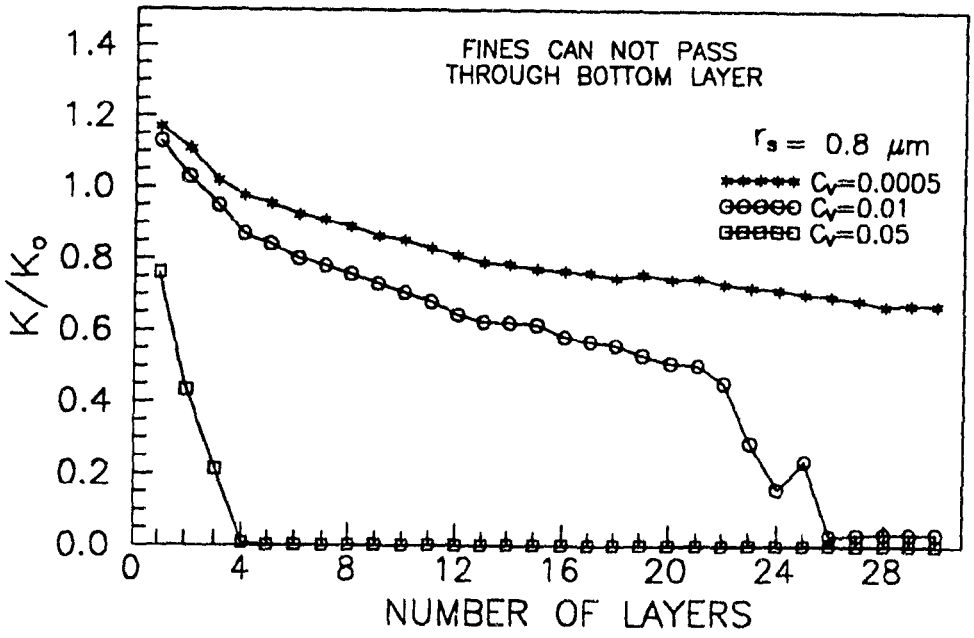

Figure 7.33: Permeability versus number of layers in network, $r_s = 0.8$ μm.

With decrease in r_s, more particles will percolate to the bottom layer and severely clog it. In the initial stages there are still many open pores in the bottom layer and the rate of clogging is high. The reduction in permeability is rapid and drastic. Once the bottom layer is severely clogged, the permeability levels off with increase in the number of layers. The extremely low permeability of the bottom layer controls the permeability of the network.

With a higher r_s (= 0.8 μm) more of the particles are retained throughout the network rather than percolating to the bottom layer. At a high C_v (= 0.05) severe clogging of the bottom layer still occurs, but at lower concentrations the reduction in permeability is more gradual due to progressive clogging throughout the network length. At a higher C_v (= 0.05) the severe clogging of the bottom layer occurs but at lower concentrations the reduction in permeability is more gradual due to progressive clogging throughout the network length.

In Figures 7.34 and 7.35, the standard deviation of the ln (*tube radius*), ξ = 0.4 and 0.8, respectively. Tube radii smaller than 0.6 μm could be clogged. The suspended particles were free to pass through the bottom layer. In Figure 7.34 very little clogging occurred due to the narrow tube size distribution. Therefore, most of the suspended particles percolated right through the network. In Figure 7.35, more clogging occurred due to the wide tube size distribution. With increase in ξ the modal tube size decreases and therefore the suspended particles block more tubes.

In Figures 7.36 and 7.37 the suspended particles were prevented from passing through the bottom layer. All other conditions were similar to the ones in Figures 7.34 and 7.35, respectively. In Figure 7.36, the decrease in K is only severe at the concentration, C_v = 0.05. However, in Figure 7.37 where the network has a wide tube size distribution the clogging is rapid and severe for all suspended particle concentrations.

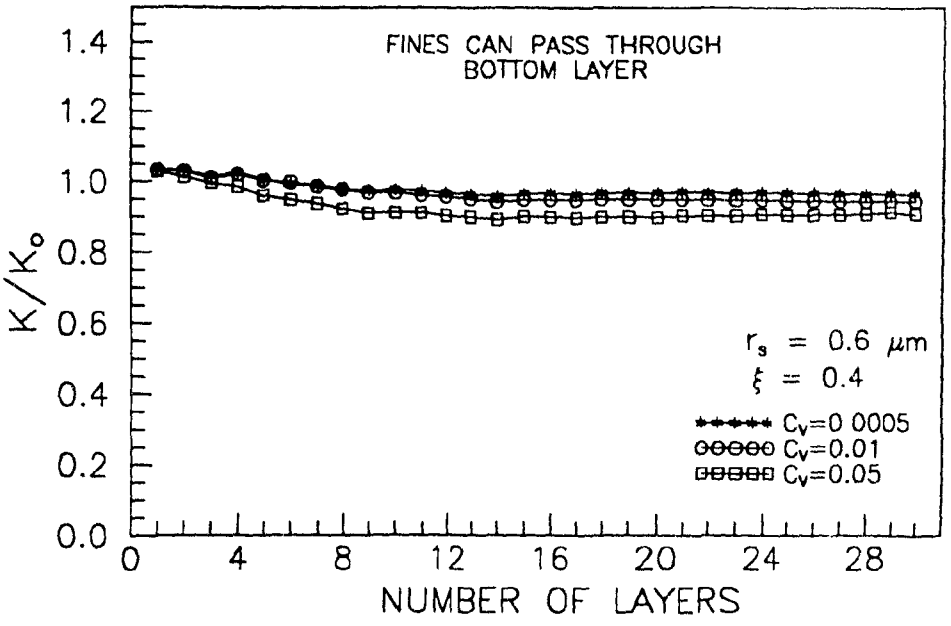

Figure 7.34: Permeability versus number of layers in network, $\xi = 0.4$.

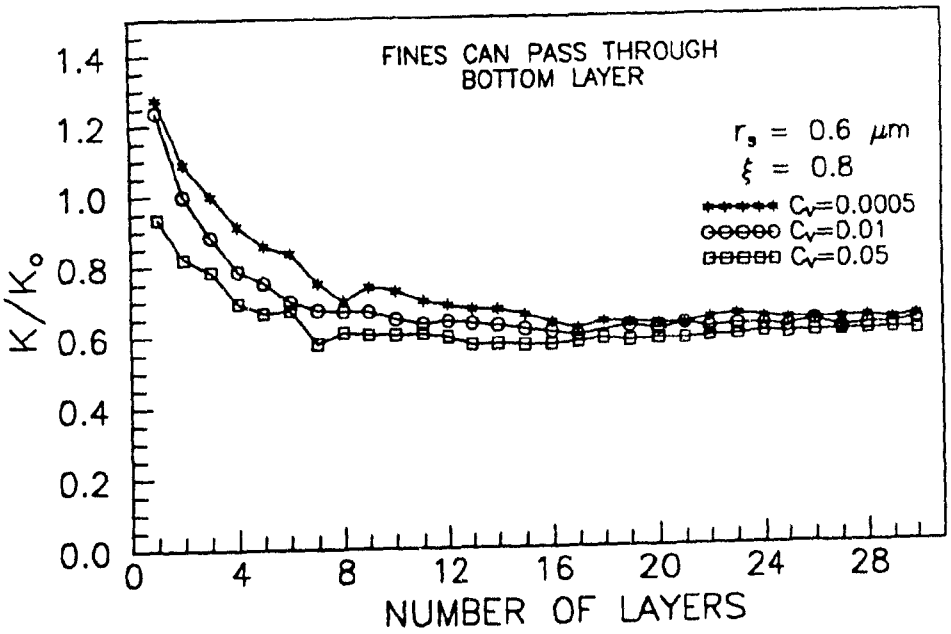

Figure 7.35: Permeability versus number of layers in network, $\xi = 0.8$.

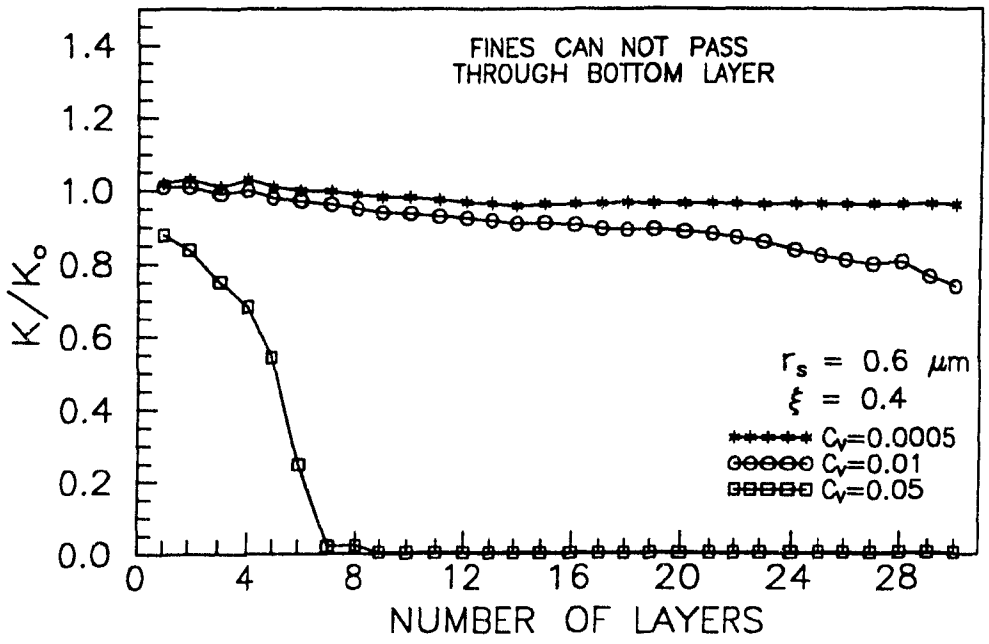

Figure 7.36: Permeability versus number of layers in network, $\xi = 0.4$.

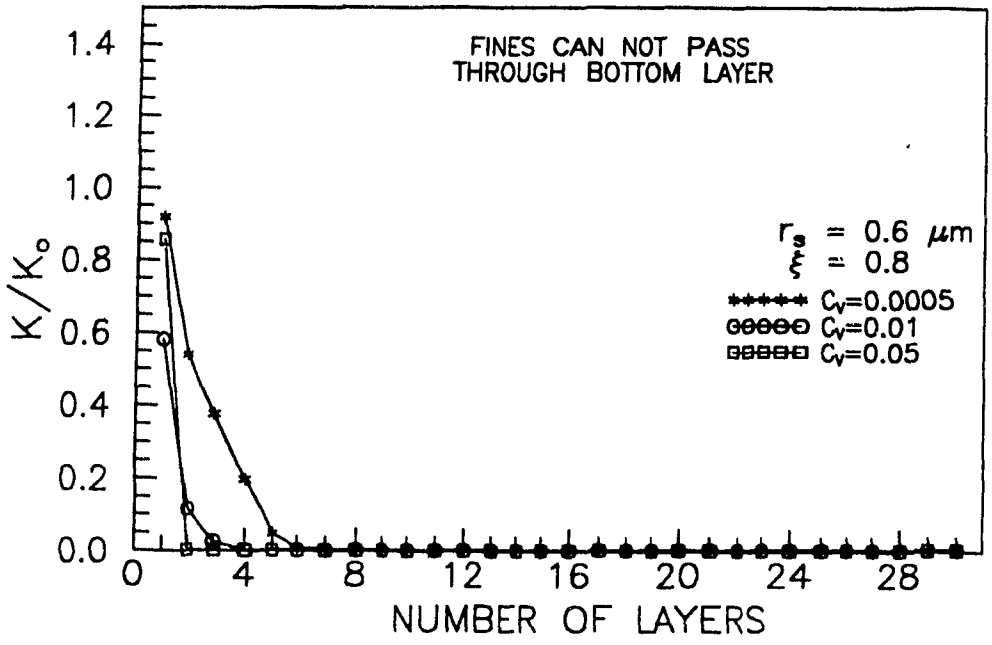

Figure 7.37: Permeability versus number of layers in network, $\xi = 0.8$.

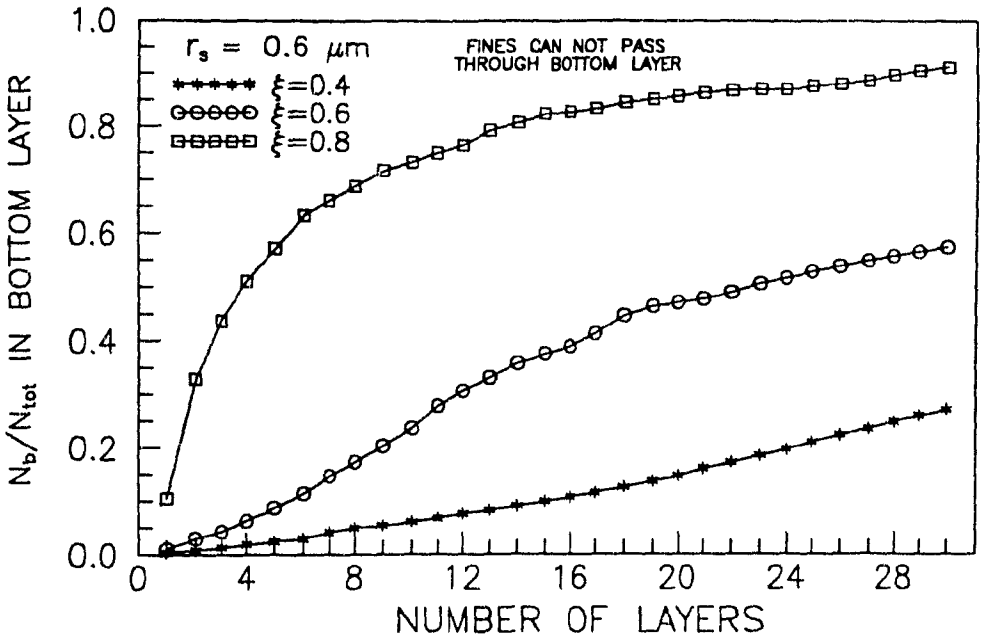

Figure 7.38: Fraction of clogged tubes in the bottom layer versus number of layers in network.

In general, the higher flow rates are in the larger tubes and the lower flow rates are in the smaller tubes. Therefore, with a wide tube size distribution the larger tubes transport larger volumes of suspended particles than the smaller tubes. Even though suspended particles block the smaller tubes the high flow rates in the larger tubes transport many of the suspended particles to the bottom layer resulting in severe clogging of the bottom layer. With a narrow tube size distribution the flow distribution is also narrow. As a result, the clogging of the bottom layer is slower with a narrow distribution than compared to a wide distribution Figure 7.38 is a graph of the fraction of clogged tubes in the bottom layer versus the total number of layers in the network. The curves show that for $\xi = 0.4$, the tube clogging in the bottom layer is much slower and far less severe compared to the results for $\xi = 0.8$.

In both cases where (1) the suspended particles can pass through the bottom layer and (2) the suspended particles are prevented from passing through the bottom

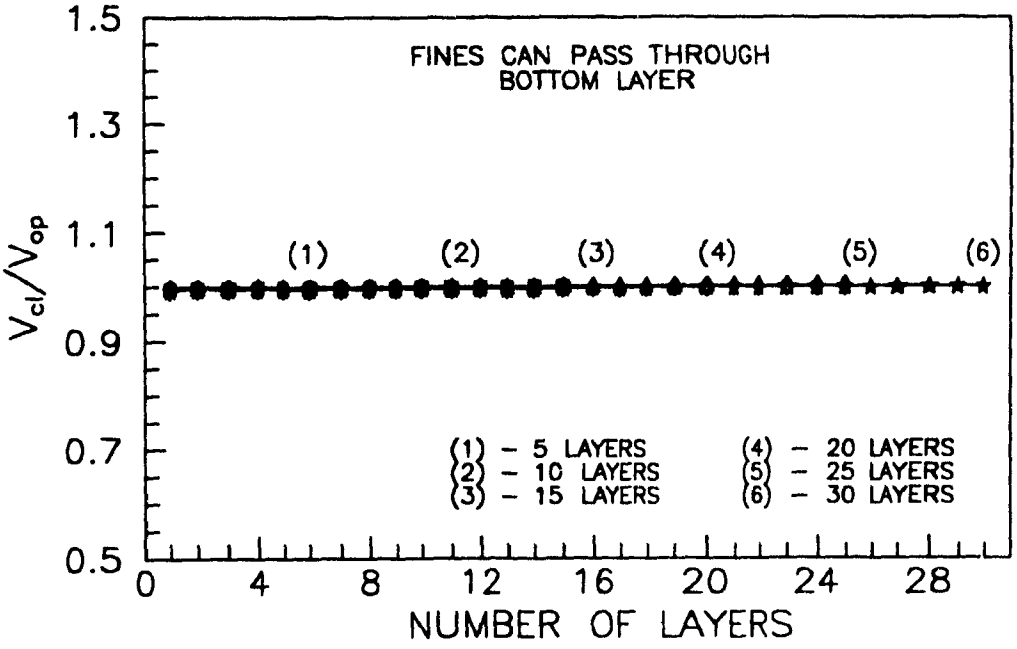

Figure 7.39: Fraction of original tube volume of a layer available for flow after particle deposition ($r_s = 0.6$ μm, $C_v = 0.01$ and $\xi = 0.4$).

layer the permeability reduction due to tube clogging increases with the standard deviation of the tube size. The reduction in tube volume during clogging was analyzed. Figures 7.39-7.44 are graphs of V_{cl}/V_{op} versus number of layers where V_{cl} is the tube volume of a layer during clogging and V_{op} is the tube volume of a layer before clogging occurs. The results are plotted for a network consisting of 5, 10, 15, 20, 25 and 30 layers. In Figures 7.39-7.41 the suspended particles are free to pass through the bottom layer. The volume concentration, $C_v = 0.01$ and $r_s = 0.6$ μm. The tube size standard deviation, $\xi = 0.4$, 0.6 and 0.8 for Figures 7.39, 7.40 and 7.41, respectively. For all three figures, V_{cl}/V_{op} is nearly constant with increase in network size and is close to 1.0. In Figures 7.42-7.44 the conditions are the same as for Figures 7.39-7.41 except that the suspended particles are prevented from passing through the bottom layer. The results for the three figures are very similar. The tube volume of the bottom layer decreases with increase in the network length. The tube volume of the

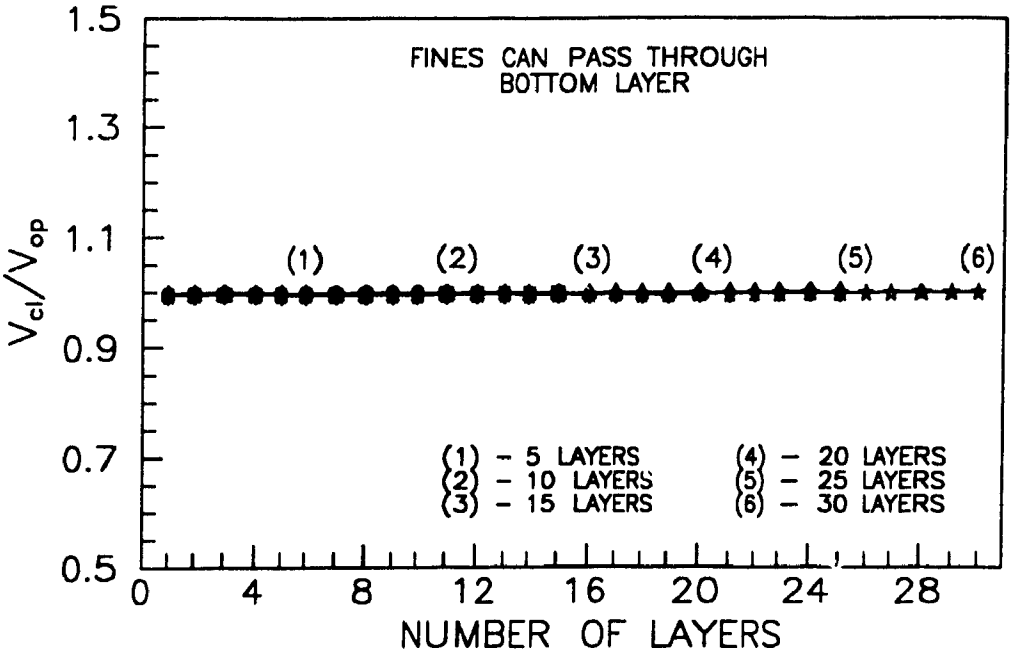

Figure 7.40: Fraction of original tube volume of a layer available for flow after particle deposition ($r_s = 0.6\ \mu$m, $C_v = 0.01$ and $\xi = 0.6$).

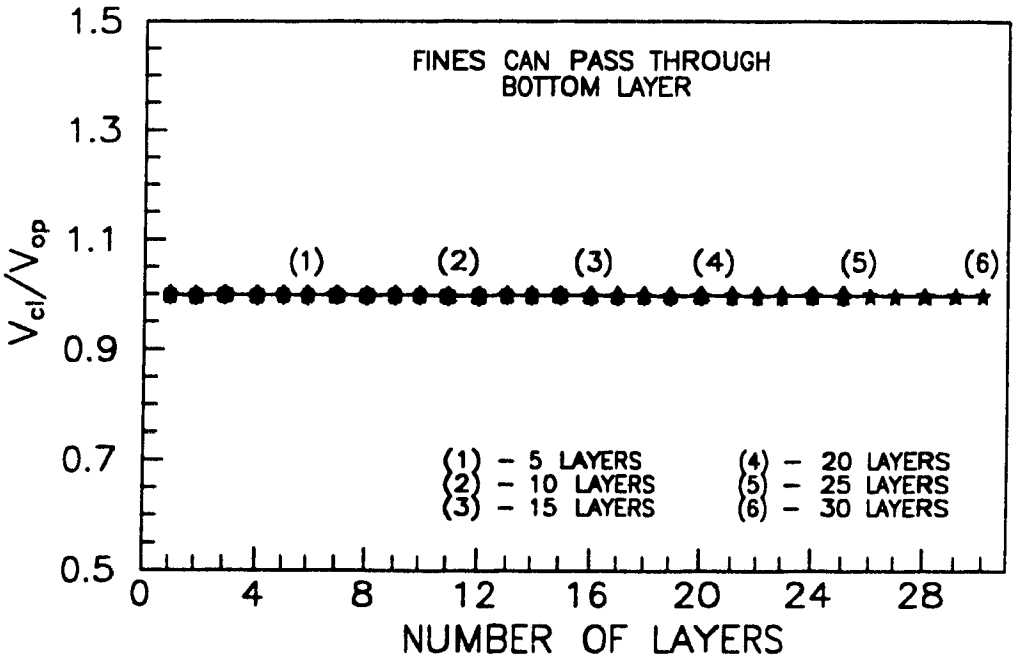

Figure 7.41: Fraction of original tube volume of a layer available for flow after particle deposition ($r_s = 0.6\ \mu$m, $C_v = 0.01$ and $\xi = 0.8$).

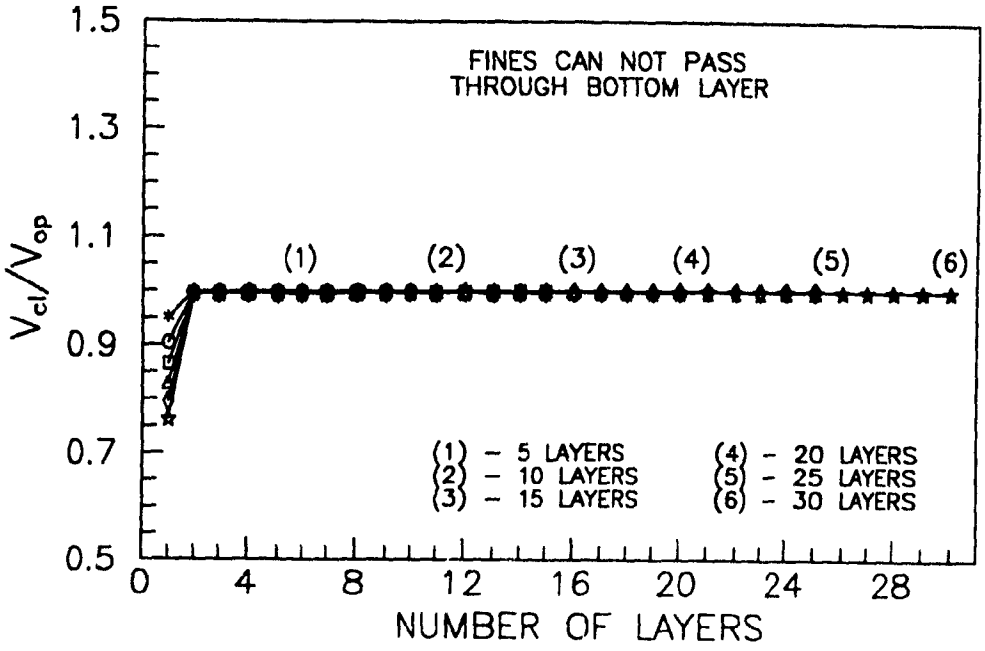

Figure 7.42: Fraction of original tube volume of a layer available for flow after particle deposition ($r_s = 0.6$ μm, $C_v = 0.01$ and $\xi = 0.4$).

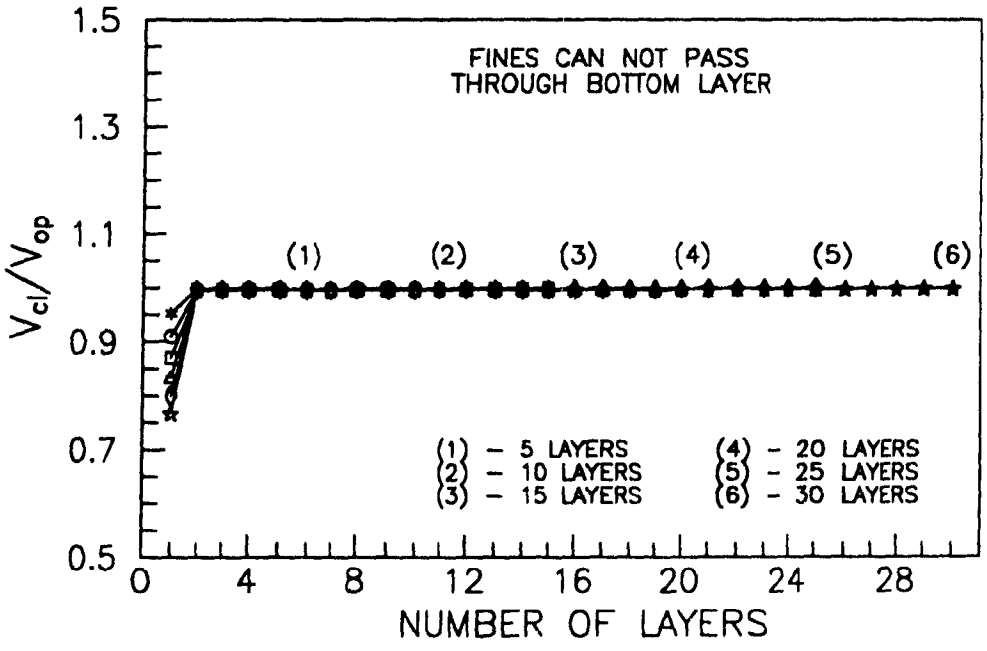

Figure 7.43: Fraction of original tube volume of a layer available for flow after particle deposition ($r_s = 0.6$ μm, $C_v = 0.01$ and $\xi = 0.6$).

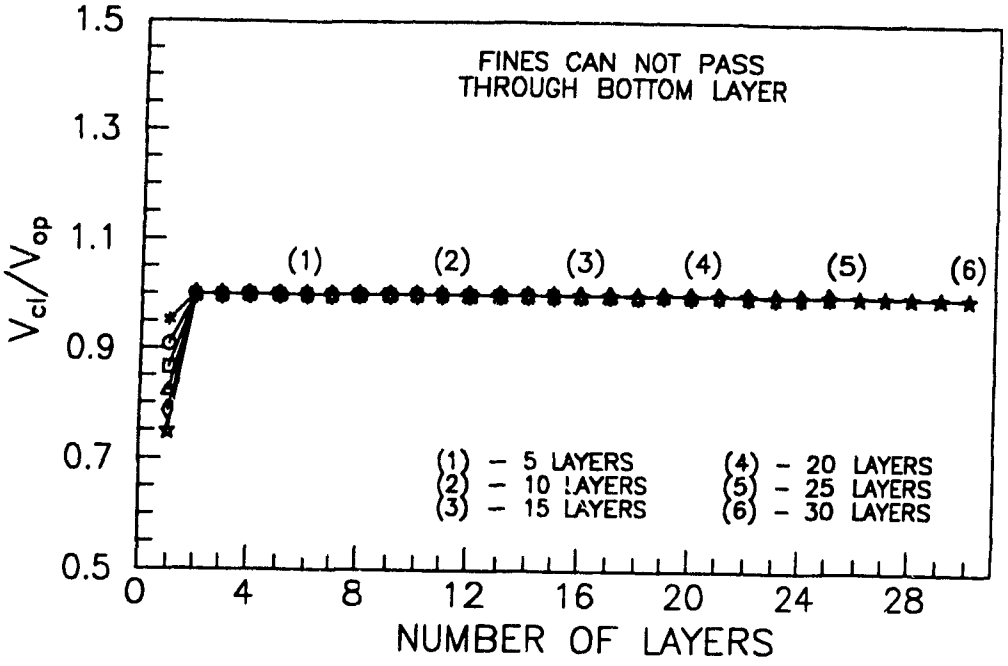

Figure 7.44: Fraction of original tube volume of a layer available for flow after particle deposition ($r_s = 0.6$ μm, $C_v = 0.01$ and $\xi = 0.8$).

layers above the bottom layer are quite constant and are close to 1.0. Though the tube volume results are very similar for different tube size standard deviations the permeability results are very different. These findings can be explained by analyzing the number of tubes that are clogged with change in ξ.

After each layer of tubes is added to the network, the number of tubes that are blocked due to trapping of suspended particles is recorded. The ratio of the number of blocked tubes in the layer, N_b to the number of tubes in the layer, N_{tot} was calculated as the network increased in length.

Figures 7.45-7.50 are graphs of N_b/N_{tot} versus number of layers where $C_v = 0.01$ and $r_s = 0.6$ μm. Again, the results are plotted for a network consisting of 5, 10, 15, 20, 25 and 30 layers. In Figures 7.45-7.47 the tube size standard deviation, ξ is equal to 0.4, 0.6 and 0.8, respectively. The suspended particles were free to pass through the bottom layer. These three figures show that the rate of pore blocking

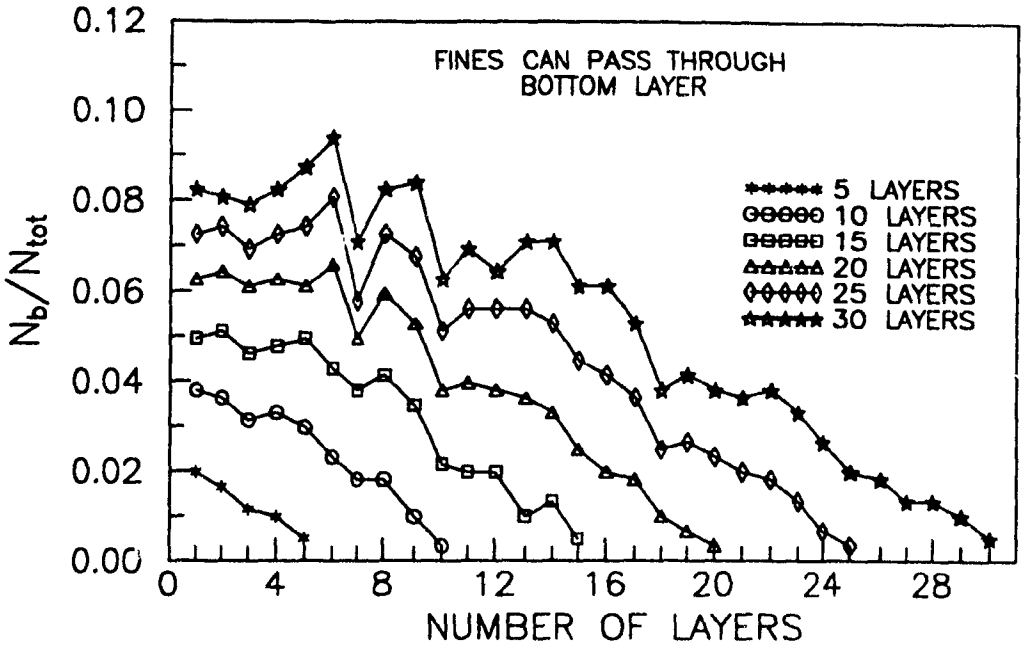

Figure 7.45: Graph of fraction of clogged tubes per layer for networks consisting of different numbers of total layers ($r_s = 0.6$ μm, $C_v = 0.01$, ξ =0.4).

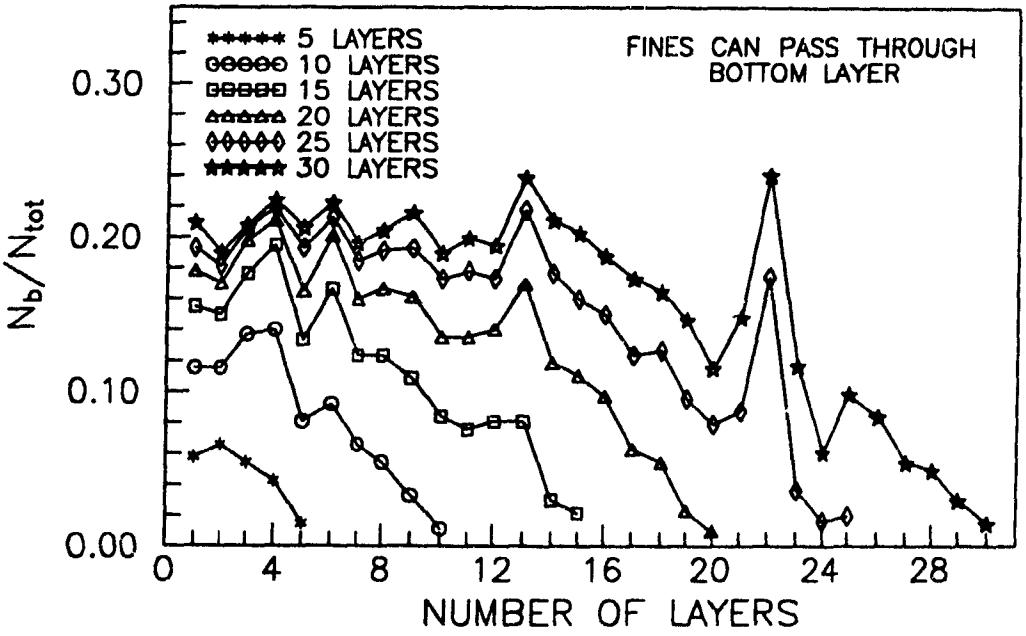

Figure 7.46: Graph of fraction of clogged tubes per layer for networks consisting of different numbers of total layers ($r_s = 0.6$ μm, $C_v = 0.01$, ξ =0.6).

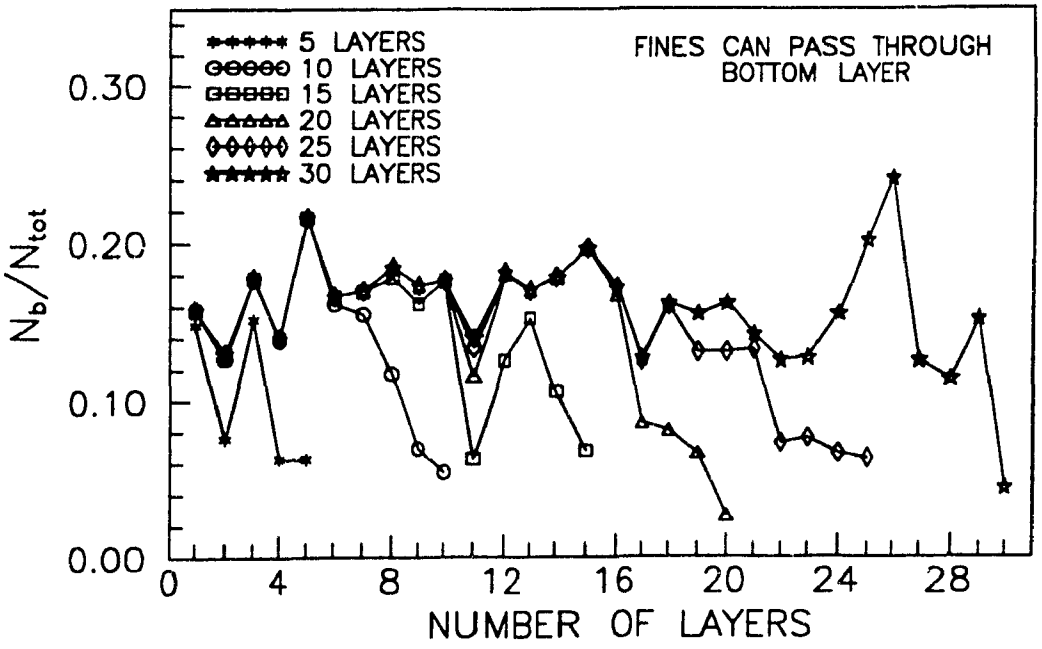

Figure 7.47: Graph of fraction of clogged tubes per layer for networks consisting of different numbers of total layers ($r_s = 0.6$ μm, $C_v = 0.01$, ξ =0.8).

increases with ξ. In Figure 7.45 where $\xi = 0.4$, N_b increases from the top layer to the bottom layer (i.e., layer 1) and more tubes are progressively blocked with increase in the network length. In Figure 7.47 on the other hand, where the network has a wide tube size distribution ($\xi = 0.8$) the results are more dispersed. The six curves in this figure are very similar except for the first few top layers of each curve. These results show that clogging of the tubes smaller than $r_s = 0.6$ μm occurs rapidly and is far less gradual as compared to Figure 7.45. With increase in ξ, clogging had little effect in reducing the tube volume. However, N_b increased substantially accounting for the decrease in permeability with increase in ξ. The conditions in Figures 7.48-7.50 are the same as in Figures 7.45-7.47, respectively, except that the suspended particles are prevented from passing through the bottom layer. The curves in Figures 7.48-7.50 are similar to the ones in Figures 7.45-7.47, respectively. However, the bottom layer (i.e., layer 1) in each curve has a greater number of clogged tubes. Referring back to the

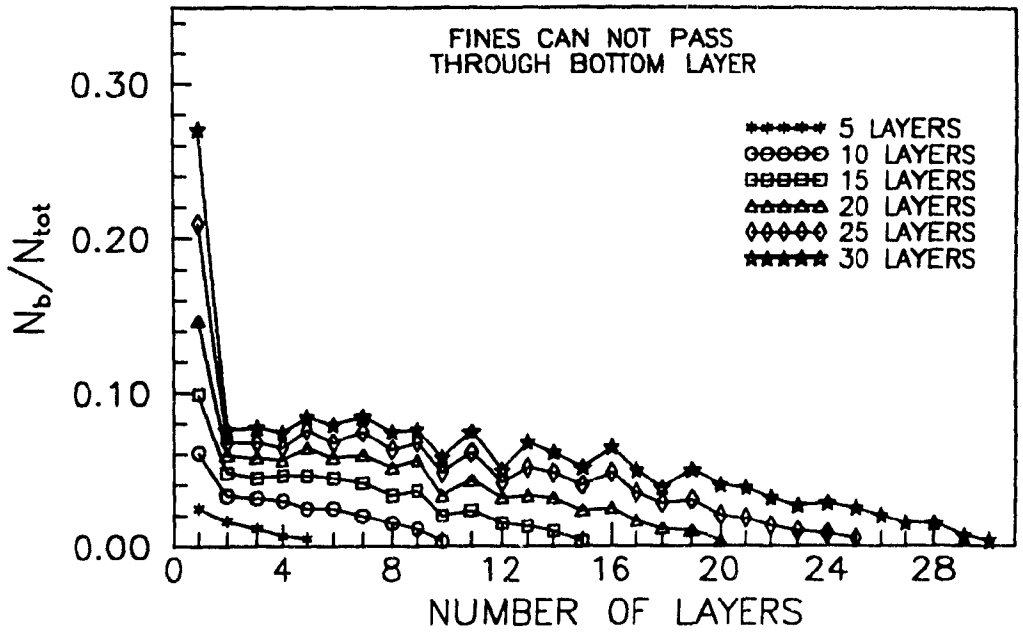

Figure 7.48: Graph of fraction of clogged tubes per layer for networks consisting of different numbers of total layers ($r_s = 0.6\ \mu$m, $C_v = 0.01$, ξ =0.4)

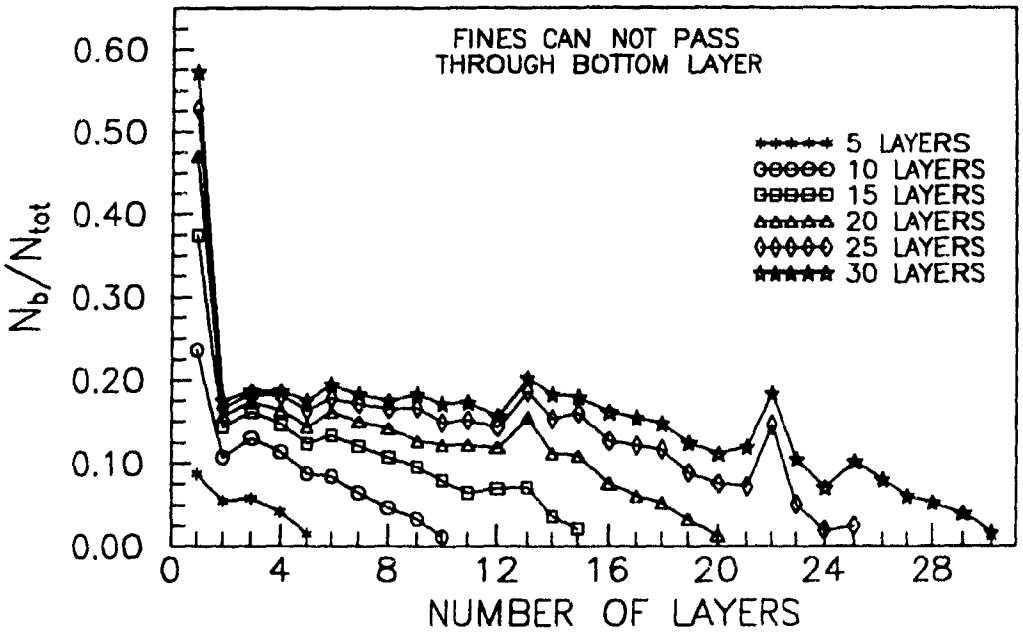

Figure 7.49: Graph of fraction of clogged tubes per layer for networks consisting of different numbers of total layers ($r_s = 0.6\ \mu$m, $C_v = 0.01$, ξ =0.6).

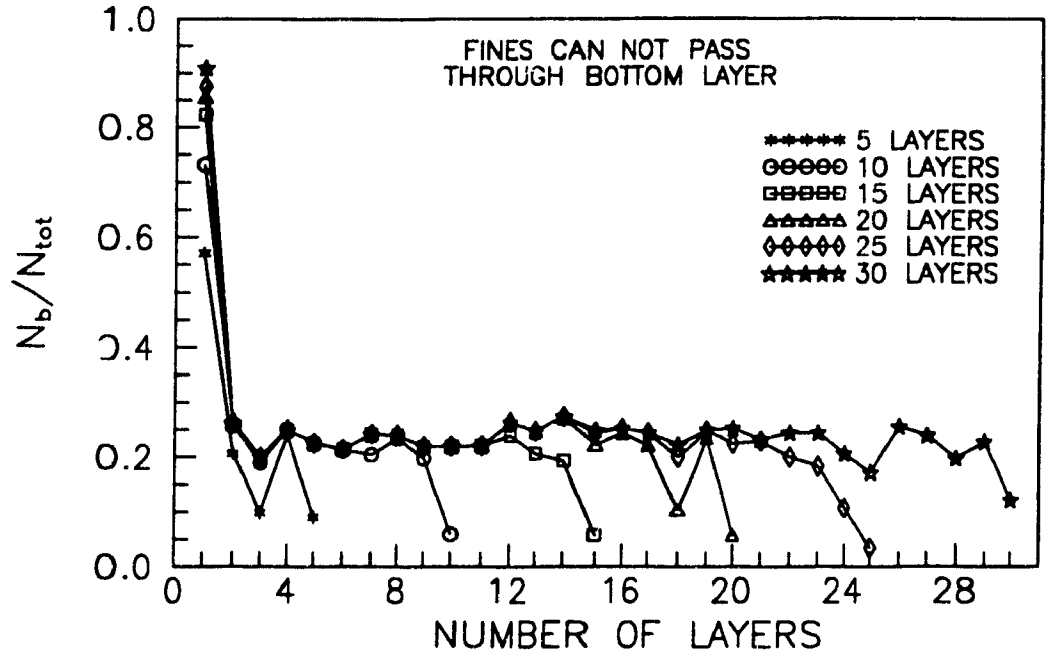

Figure 7.50: Graph of fraction of clogged tubes per layer for networks consisting of different numbers of total layers ($r_s = 0.6$ μm, $C_v = 0.01$, ξ =0.8).

permeability results it was shown that for the conditions where $C_v = 0.01$, $r_s = 0.6\mu$m and where the fine particles were prevented from passing through the bottom layer for $\xi = 0.4$ (see Figure 7.36) the decrease in K was very gradual and only dropped to $K/K_o = 0.74$ for a network consisting of 30 layers. For $\xi = 0.6$ (see Figure 7.32) there was a sharp decrease in K between networks with 14 and 18 layers followed by a levelling off at approximately $K/K_o = 0.01$. For $\xi = 0.8$ (see Figure 7.37), K decreased rapidly down to $K/K_o = 0.002$ for the first 4 layers. It appears that there is some critical N_b/N_{tot} value that causes a drastic drop in permeability. This critical phenomena can be explained by percolation theory.

7.5.1 PERCOLATION THEORY

Percolation theory deals with the effects of varying, in a random system, the richness of interconnections present. An important aspect of the percolation model

Table 7.1: Applications of percolation theory (after Ref. 100).

PHENOMENON	TRANSITION
Flow of liquid in a porous medium	Local/extended wetting
Spread of disease in a population	Containment/epidemic
Communication or resistor networks	Disconnected/connected
Conductor-insulator composite materials	Insulator/metal
Composite superconductor-metal materials	Normal.superconducting
Discontinuous metal films	Insulator/metal
Stochastic star formation in spiral galaxies	Nonpropagation/propagation
Quarks in nuclear matter	Confinement/nonconfinement
Thin helium films on surfaces	Normal/superfluid
Metal-atom dispersions in insulators	Insulator/metal
Dilute magnets	Para/ferromagnetic
Polymer gelation, vulcanization	Liquid/gel
The glass transition	Liquid/glass

is the presence of a sharp phase transition at which long-range connectivity suddenly disappears. This percolation transition, which occurs with decreasing connectedness makes percolation a natural model for describing a diversity of phenomena.[100] Table 7.1 lists some physical situations to which percolation ideas have been applied.

As an example of a percolation process consider the electrical network experiment illustrated in Figure 7.51. The electrical network is represented by a very large square-lattice network of unit conductors (bonds). The bonds are then randomly cut until there is no electrical conduction between the two bounding electrodes. There exists a sharp transition at which the long-range connectivity of the system disappears. This basic transition, which occurs abruptly as the composition of the system is varied constitutes the percolation threshold. In this example the percolation threshold corresponds to the disappearance of the electrical conduction between the two bounding electrodes. Starting with all conducting bonds present in the network and then randomly cutting bonds, the current, I_c drops as more and more bonds are cut as indicated by the curve in the lower part of Figure 7.51. Denoting the fraction of un-

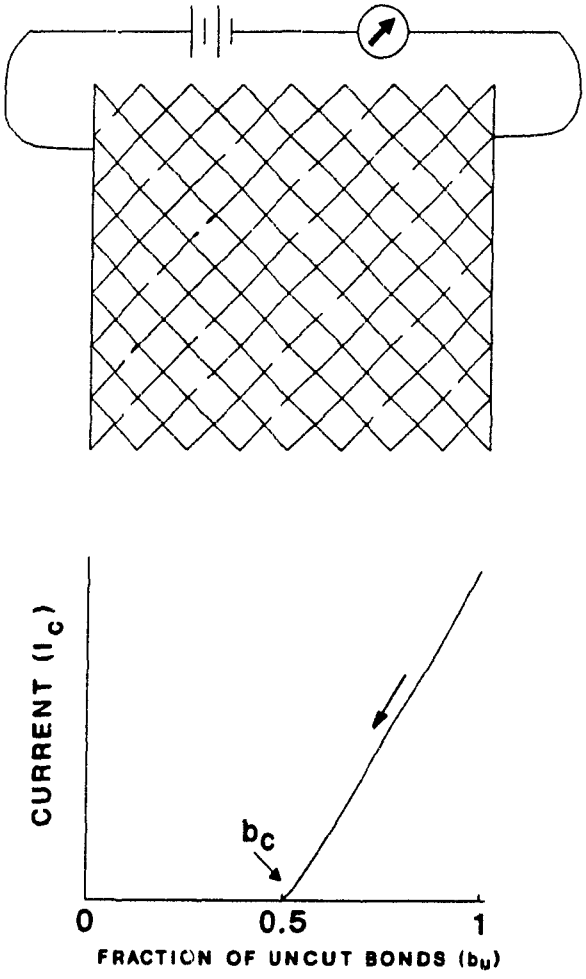

Figure 7.51: Network is randomly cut until there is no electrical conduction between the two bounding electrodes (after Ref. 100).

cut bonds remaining as b_u, $I_c(b_u)$ continues to decrease as b_u decreases until a critical bond concentration, denoted as b_c, is reached at which point the current I_c vanishes. For $b_u < b_c$, there exists no connected path of conducting bonds that traverse the network from one electrode to the other. A well-defined b_u at which, with decreasing b_u, the electrical network becomes an open circuit requires a very large network. The distance L between the electrodes must greatly exceed the bond length l_b: $(L/l_b) \gg 1$. For a finite system, repeated experiments will yield a spread of observed thresholds which bracket b_c. It is known that $b_c = 0.5$ is the value of the percolation threshold for bond percolation on a square lattice. The percolation threshold is known exactly for a few other two-dimensional lattice arrangements, but not for any lattices in three (or higher) dimensions.

There is a variation in b_c from one lattice arrangement to another due to the sensitivity of b_c to the local structure. The more highly connected a lattice or in other words, the higher the coordination number the lower is the concentration of unblocked bonds needed to sustain long-range connectivity. Lattices in higher dimensions are more highly connected than those in lower dimensions and therefore the trend is to decreasing b_c with increasing dimensionality.

The above example is termed bond percolation. A network is composed of sites (intersections between bonds) and bonds (connections between sites). There are two basic types of percolation processes on networks: bond percolation and site percolation. In bond percolation, each bond is either connected (which occurs with probability p) or disconnected (which occurs with probability (1-p)). In site percolation, each bond is considered to be connected and it is the sites that carry the random-connectivity character of the structure. Each site is either connected (unblocked) or disconnected (blocked), with probabilities p and 1-p, respectively.

Table 7.2: Bottom layer values of N_b/N_{tot} for networks of critical lengths, L_c.

ξ	r_s	L_c	C_v	N_b/N_{tot}
0.4	0.6	10	0.05	0 558
0.6	0.4	4	0.05	0.393
	0.6	19	0.01	0.464
		4	0.05	0.487
	0.8	4	0.05	0.517
0.8	0.6	6	0.005	0.442
		4	0.01	0.510
		2	0.05	0.586

In 1957 the mathematician J. M. Hammersley provided the original motivation for the use of the term percolation for the connectivity threshold by considering the passage of a fluid through a network of channels, with some channels being randomly blocked (disconnected).

In essence, our random tube network model describing clogging due to suspended particles blocking tube openings is a bond-percolation process. The permeability results showed that there is some critical ratio of the number of tubes blocked in the layer to the total number of tubes in the layer, N_b/N_{tot}, that causes a drastic drop in permeability. Table 7.2 lists bottom layer values of N_b/N_{tot} for different values of ξ, C_v and r_s. The N_b/N_{tot} values were calculated for a critical network length, L_c. The critical network length, L_c is defined as the number of layers at which point there is a sharp drop in K. The N_b/N_{tot} values are near 0.5 as is predicted by percolation theory for a square lattice network. As stated earlier, $b_c = 0.5$ in the limit $(L/l_b) \rightarrow \infty$. Since a unit layer in the network only has six rows of tubes there was a spread of N_b/N_{tot} values that bracket 0.5. The bottom layer was the only layer that was critically blocked whereas the upper layers were much less clogged. However, the critical clogging of the bottom layer controlled the permeability of the network due to its severe drop in K.

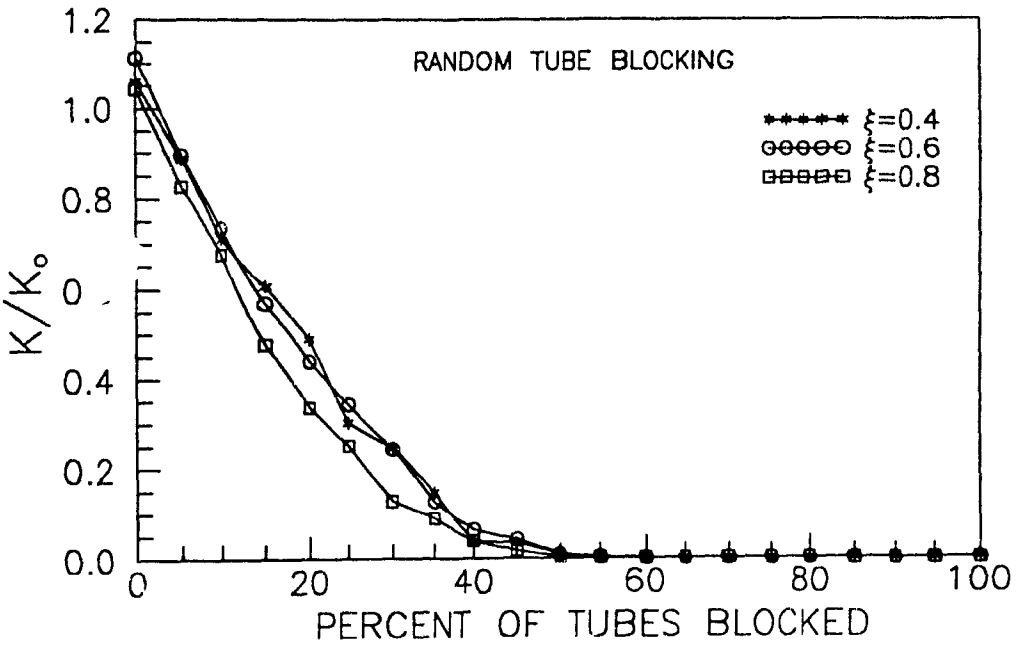

Figure 7.52: Permeability versus percent of randomly blocked tubes (network size = 49 rows and 49 tubes per row).

To further illustrate this percolation phenomena, networks consisting of 49 rows and 49 tubes per row were filled with log-normal tube size distributions with $\xi = 0.4$, 0.6 and 0.8 Tube radii were blocked randomly. The radii of the blocked tubes were reduced to 0.05 μm, a negligibly small but finite size to simplify network computations. Figure 7.52 is a graph of K/K_o versus percent of blocked tubes in the network. These results show that the percolation threshold is at approximately 0.5 as predicted by theory.

7.6 PORE SIZE REDUCTION AND PORE BLOCKING

Network permeabilities were calculated for networks clogging due to the combined effect of: (1) tubes trapping particles larger than the tube openings and (2)

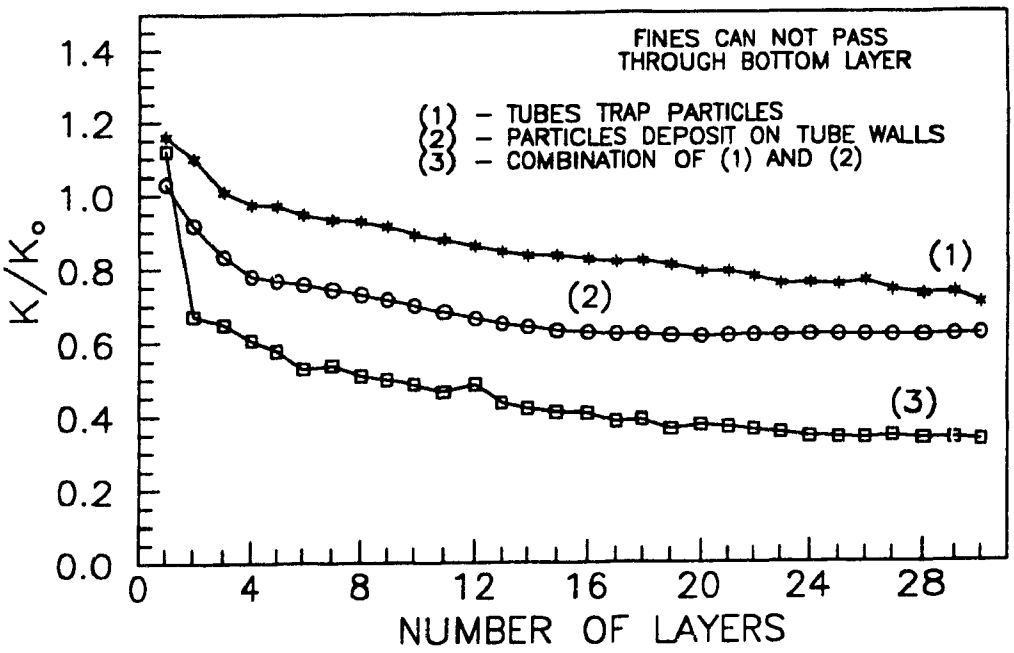

Figure 7.53: Permeability versus number of layers in network. Curve - (1) $C_v = 0.005$, $r_s = 0.6$ μm. Curve - (2) $C_s = 100000$, $r_s = 0.01$ μm and $q_t = 500/L$ μ/sec.

fines depositing on the tube walls. The tube radii of the networks were filled with log-normal distributions with $\xi = 0.6$ and a median of 1 μm. The suspended particles were prevented from passing through the bottom layer. The computer program is listed in Appendix D.

Figures 7.53-7.56 are graphs of K/K_o versus number of layers in the network. Tubes smaller than 0.6 μm could be blocked and 0.01 μm fines could deposit on the tube walls. The fine suspended particle concentration, $C_s = 100000$. The critical velocity, u_c, for the fine suspended particles was set at 15×10^3 μm/sec. In Figures 7.53 and 7.54, $C_v = 0.005$ and $q_t = 500/L$ μm/sec and 10×10^3 μm/sec, respectively. The length of the network, L, is given in μm. In Figures 7.55 and 7.56, $C_v = 0.01$ and $q_t = 500/L\mu$m/sec and 10×10^3 μm/sec, respectively. In Figures 7.54 and 7.56, tube size reduction due to particle deposition was greater than in Figures 7.53 and

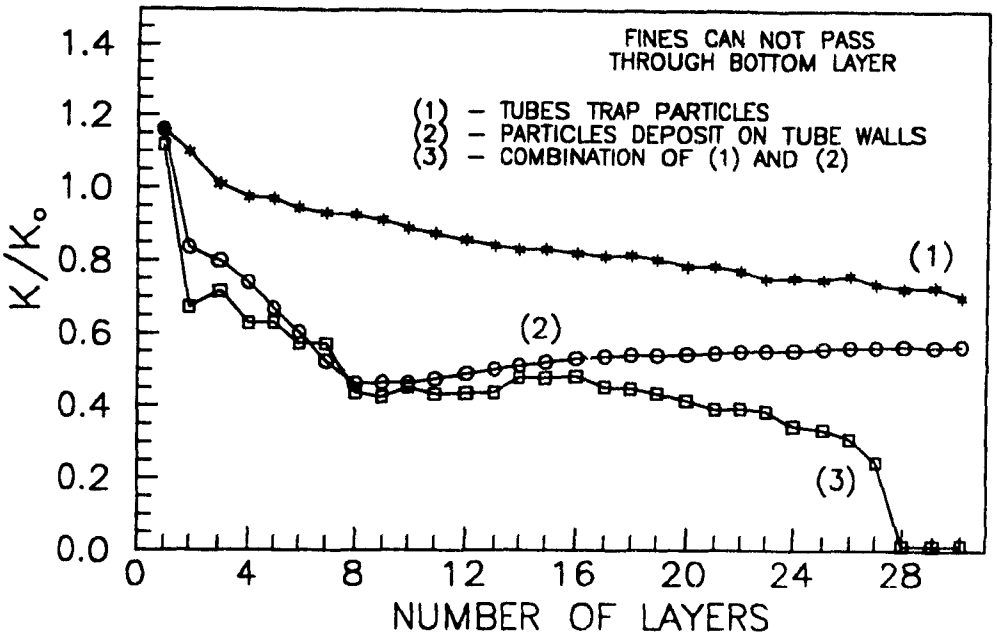

Figure 7.54: Permeability versus number of layers in network. Curve - (1) $C_v = 0.005$, $r_s = 0.6$ μm. Curve - (2) $C_s = 100000$, $r_s = 0.01$ μm and $q_i = 10 \times 10^3$ μm/sec.

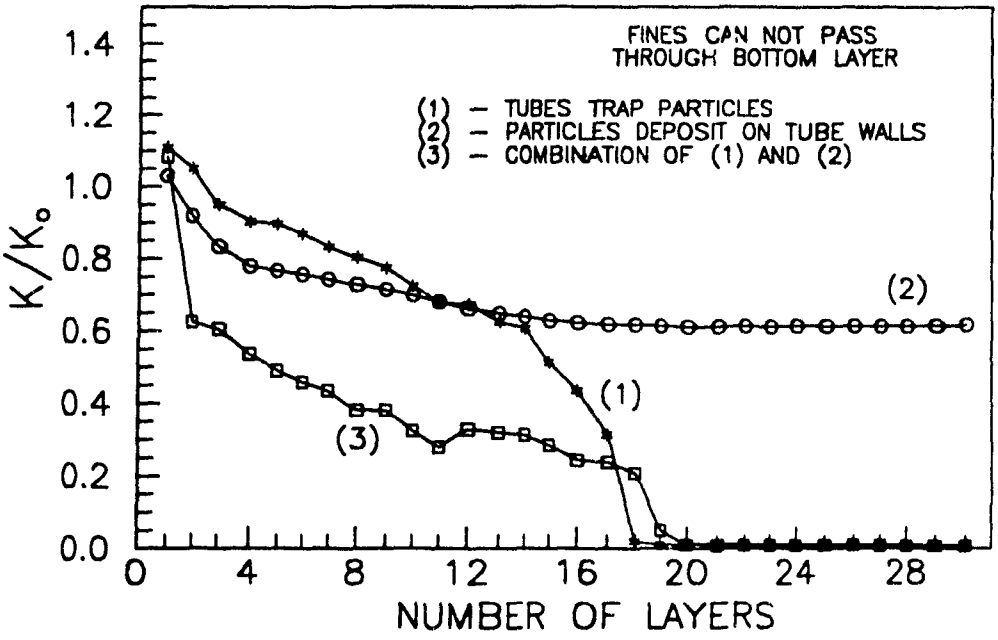

Figure 7.55: Permeability versus number of layers in network. Curve - (1) $C_v = 0.01$, $r_s = 0.6$ μm. Curve - (2) $C_s = 100000$, $r_s = 0.01$ μm and $q_i = 500/L$ μm/sec.

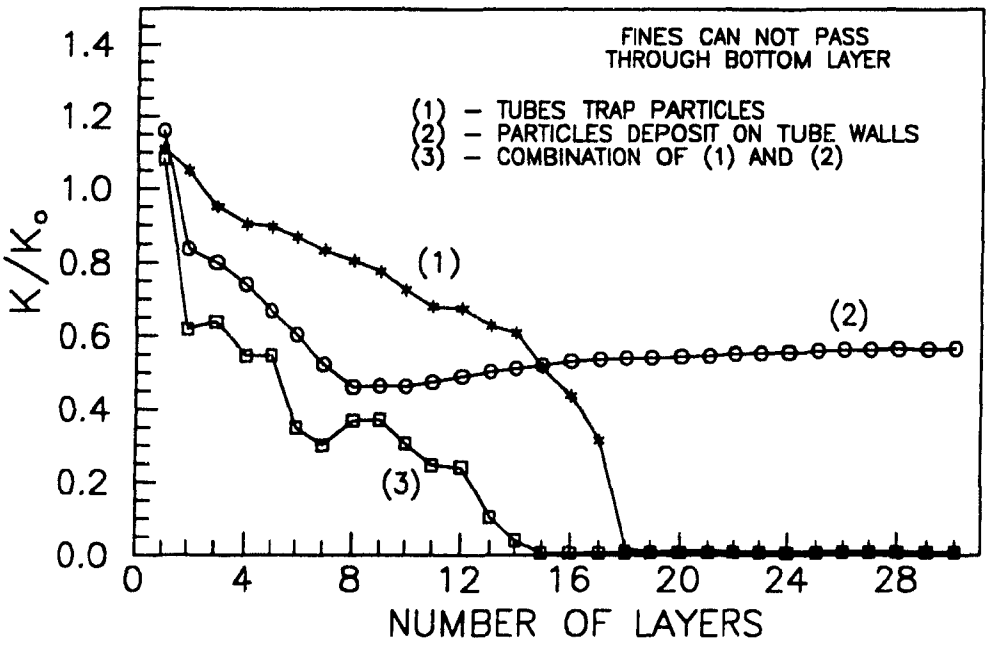

Figure 7.56: Permeability versus number of layers in network. Curve - (1) $C_v = 0.01$, $r_s = 0.6$ μm. Curve - (2) $C_s = 100000$, $r_s = 0.01$ μm and $q_i = 10 \times 10^3/L$ μm/sec.

7.55, respectively. In Figure 7.54 the added effect of tube size reduction due to tube blocking caused a sharp drop off in K to occur at the critical network layer number, $L_c = 28$, whereas for the pore blocking and pore reduction curves there was no sharp drop off in K. In Figure 7.56, $L_c = 18$ for the tube blocking curve. The added effect of tube size reduction due to tube blocking however caused L_c to decrease to 15. These results again illustrate that there is a critical number of blocked pores that cause a sharp drop in K.

Chapter 8

SUMMARY AND CONCLUSIONS

It is essential to acquire a better understanding of the filtration mechanics involved in filtration processes so that the advanced ceramic industry can reliably reproduce high strength products with complex shapes. In particular, the industry is concerned with forming a green body with maximum particle packing and uniformity so that minimum shrinkage and minimum porosity will result during sintering and densification.

Slip casting and filter pressing experiments were carried out to study how the growth rate of thickness and the microstructure of the cake are affected by various processing parameters. The properties of the ceramic suspensions greatly affect the filtration process, therefore it was important to control the rheology of the suspensions. A coarse (C-71FG), a fine (A-16SG) and a mixture of these coarse and fine alumina powders were used for the rheological study and filtration experiments.

The viscosity measurements showed that for a given solids loading, the viscosity of the slip decreases with increasing concentration of deflocculant. After a minimum in viscosity is reached (i.e., maximum deflocculation), a levelling off, followed by a gradual increase in viscosity occurs. At maximum deflocculation, the A-16SG slips were shear thinning and the C-71FG slips were shear thickening. The slips that contained a 50/50 mixture of the A-16SG and C-71FG powder were initially shear thinning with an increase in the shear rate, reached a minimum viscosity, and then

began to shear thicken slightly. Shear thinning is a characteristic of a flocculated slip whereas shear thickening can be attributed to the solids having a tight packing arrangement.

Filtration experiments showed that slips containing a mixture of C-71FG and A-16SG powder produced higher cake green densities at all solids loadings compared to the C-71FG or A-16SG slips. For the A-16SG slips the cake green densities decreased and the cake thickness growth rate increased with the solids loading of the slip due to increased flocculation.

The microstructure of the plaster of Paris mold plays a vital role in the slip casting process because it is the pore structure of the mold that provides the capillary suction pressure and therefore affects the growth rate of the cake. It was shown that with increase in the plaster/water ratio the mold density and suction pressure increased but the mold permeability decreased. A-16SG slips were cast using molds prepared with different plaster/water ratios. The cake thickness growth rate only increased very slightly with increase in plaster/water ratio. As the suction pressure increases with plaster/water ratio, the fraction of pressure utilized to overcome flow resistance in the mold becomes more important at the higher plaster/water ratios thereby negating the increase in pressure available for cake formation.

As the cake thickness increases with casting time fine particles can be carried along with the filtrate and deposited within the cake and/or filter medium thereby clogging and reducing the permeabilities of the porous media. SEM micrographs confirm that fine particles can migrate to the cake bottom and accumulate there. SEM micrographs also show that some of the fines can pass through the filter medium, depending upon the ratio of particle size to medium pore size. Surface area measurements, likewise, showed that a higher concentration of fine particles can accumulate

at the cake bottom. When cake and/or filter medium clogging occurs the permeability of the system will vary with cake thickness and therefore the traditional filtration equations that assume a constant cake and filter medium permeability are not valid.

A computer model consisting of a network of tubes with a random tube size distribution was developed to simulate the filtration process and account for porous medium clogging. Flow through the network was solved using the Hardy-Cross Method. The results of the model also emphasize that porous media with the same average pore size and porosity but with different pore size distributions can have very different permeabilities and therefore permeability can not be defined in terms of an average pore size.

The model considered clogging to occur by two means: (1) as a result of fine particles depositing on the pore walls and gradually reducing the pore radii and (2) by pores trapping particles larger than the pore openings. The model showed that the permeability of porous media can decrease gradually with increase in clogging but then at a critical ratio of the number of clogged pores in a layer, N_b to the total number of pores in the layer, N_{tot} a drastic drop in permeability occurs. This critical phenomena was explained by percolation theory. An important aspect of percolation theory is the presence of a sharp phase transition at which long-range connectivity suddenly disappears. In essence, the model that incorporates clogging due to suspended particles blocking tube openings is a bond-percolation process The critical N_b/N_{tot} values calculated for the networks were near 0.5 as predicted by percolation theory for a square lattice network.

The reduction in network tube volume during clogging was also analyzed. The ratio of the clogged tube volume, V_{cl} to the unclogged tube volume, V_{op} for each network layer was calculated as the network increased in length. It was shown that

depending upon the tube size distribution, with V_{cl}/V_{op} values as high as 0.95 the permeability still decreased by more than a factor of 100 compared to an unclogged network. Filtration experiments and the network model results showed that cake permeability can vary as a function of cake thickness and from run to run due to minor changes in the local and overall cake microstructures.

STATEMENT OF ORIGINALITY

Filtration casting behaviour of ceramic suspensions is an area still not fully understood. The filtration experiments that were carried out to explore how particle sizes, particle size distributions and solids volume fractions of slips affect the growth rates and the green densities of the filter cakes have given further insight into the filtration forming processes. This is the first time that the plaster of Paris mold microstructure, density, permeability, suction pressure and the effects that all these mold properties have on the slip casting process were analyzed as a function of the plaster/water ratio used to form the mold.

Surface area measurements as well as SEM analysis of longitudinal cross-sections of filter paper and cakes were novel approaches used to find evidence of cake and filter medium clogging. A computer model consisting of a two-dimensional network of tubes with a random size distribution was developed to simulate the increase in cake thickness during the filtration process. The model analyzed the effects that the tube size distribution, porosity and clogging had on the permeability of porous media. Clogging was modelled based upon two assumptions: (1) particles larger in size than a given pore size were trapped by the pore thus reducing its area and/or (2) as a result of fine particles depositing on the pore walls and gradually reducing the pore radii. The Hardy-Cross Method was incorporated into the program to solve for the flows in the network tubes. The advantage of this approach compared to solving series of simultaneous equations is that large networks could easily be modelled. For example 10000 tubes could be modelled using less than 640 kilobytes of RAM memory and

thus the larger the network size the more representative the model is of flow through a filter cake. The results of the model show that an analogy can be made between porous media clogging and percolation theory.

REFERENCES

1. I. J. McColm and N. J. Clark, *Forming, Shaping and Working of High-Performance Ceramics* (New York: Chapman and Hall, 1988), pp. 1-67.

2. F. F. Lange, "Approach to Reliable Powder Processing," in *Ceramic Transactions Volume 1 Ceramic Powder Science II*, eds. Gary L. Messing, Edwin R. Fuller, Jr., Hans Hausner (Westerville, Ohio: The American Ceramic Society Inc., 1988), pp. 1069-83.

3. P Rado, "Slip-casting of Non-clay Materials," *Trans. Brit. Ceram. Soc.*, **72** [7] 291-97 (1973).

4. D. W. Richerson, *Modern Ceramic Engineering* (New York: Marcel Dekker Inc., 1982), pp. 149-95.

5. W D. Kingery, *Introduction to Ceramics* (New York: John Wiley & Sons Inc , 1960), pp. 33-56.

6. F. H. Norton, *Elements of Ceramics , 2nd edn.* (Massachusetts: Addison-Wesley Publishing Company, 1974), pp. 92-112.

7 O. J. Whittemore, Jr., "Particle Compaction," in *Ceramic Processing Before Firing*, eds. G.Y. Onoda, Jr. and L.L. Hench (New York, John Wiley & Sons Inc., 1978), pp. 343-53.

8. J.S. Reed and R.B. Runk, "Dry Pressing," in *Treatise on Materials. Science and Technology Volume 9 Ceramic Fabrication Processes*, ed. Franklin F. Y. Wang (New York: Academic Press Inc., 1976), pp. 71-93.

9. R. R. Rowlands, "A Review of the Slip Casting Process," *Ceramic Bulletin*, **45** [1] 16-19 (1966)

10. P. H. Dal and W. J. H. Berden, "The Capillary Action of Plaster Moulds," in *Science of Ceramics, Vol.4*, ed. G.H. Stewart (London, UK: The British Ceramic Society, 1968), pp. 113-31.

11. D. S. Adcock and I. C. McDowall, "The Mechanism of Filter Pressing and Slip Casting," *J. Am. Ceram. Soc.*, **40** [10] 355-62 (1957).

12. P. H. Dal and W. Deen, "The Forming of Ceramic Bodies During the Slip Casting Process," in *Proceedings of the Sixth International Ceramic Congress, Weisbaden* (Deutsche Keramische Gesellschaft, 1958), pp. 219-42.

13. I. A. Aksay and C. H. Schilling, "Mechanics of Colloidal Filtration," in *Advances in Ceramics, Volume 9, Forming of Ceramics*, eds. J. A. Mangels and G.L. Messing (Columbus, Ohio: American Ceramic Society, 1984), pp. 85-93.

14. Bernard Mulroy, "Casting and the Mechanics of the Casting Process," *Ceramics*, **23** [284] 14-21 (1972).

15. W. Ryan and W. E. Worrall, "Casting-Experiments with Fireclays," *Trans. Brit. Ceram. Soc.*, **60** 540-555 (1961).

16. Y. Shiraki, "Casting Properties of Pottery Body due to Specific Base-Exchange Cations Studies on Slip Casting (VIII)," *J. Ceram. Ass. Japan*, **72**, 57-62 (1964).

17. A. L. Johnsom and F. H. Norton, "Fundamental Study of Clay: III, Casting as a Base-Exchange Phenomenon," *J. Am. Ceram. Soc.*, **25** [12] 336-44 (August 1, 1942).

18. K. Bridger and M. Massuda "Principles of Slip Casting/ Pressure Filtration," in *Ceramic Transactions Volume 12 Ceramic Powder Science III*, eds. Gary L. Messing, Shin-ichi Hirano, Hans Hausner (Westerville, Ohio: The American Ceramic Society Inc., 1990), pp. 507-19.

19. W. D. Kingery, H. Bowen and D. Uhlmann, *Introduction to Ceramics, 2nd ed.* (New York: John Wiley & Sons Inc., 1976), pp. 448-509.

20. W. D. Kingery, "Densification During Sintering in the Presence of a Liquid Phase. I. Theory," in *Journal of Applied Physics*, **30**, 301-6 (1959).

21. R. Pampuch, R., *Ceramic Materials* (New York: American Elsevier Publishing Company Inc., 1976), pp. 119-50.

22. I. B. Cutler, "Active Powders," in *Ceramic Processing Before Firing*, eds. G.Y. Onoda, Jr. and L.L. Hench (New York: John Wiley & Sons Inc., 1978), pp. 21-29.

23. E. Barringer, N. Jubb, B. Fegley, R. L. Pober and H. K. Bowen, "Processing Monosized Powders," in *Ultrastructure Processing of Ceramics, Glasses, and Composites*, eds. L.L. Hench, and D.R. Ulrich (New York: John Wiley & Sons Inc., 1984), pp. 315-33.

24. I. A. Aksay, "Microstructure Control Through Colloidal Consolidation," in *Advances in Ceramics, Volume 9, Forming of Ceramics*, eds. J. A. Mangels and G. L. Messing (Columbus, Ohio: American Ceramic Society, 1984), pp. 94-103.

25. J. W. Halloran, "Agglomerates and Agglomeration in Ceramic Processing", in *Ultrastructure Processing of Ceramics, Glasses and Composites*, eds. L. L. Hench. and D. R. Ulrich (New York: John Wiley & Sons Inc., 1984), pp. 404-17.

26. C. H. Schilling and I. A. Aksay, "Slip Casting of Advanced Ceramics and Composites,"in *Transactions of the Canadian University-Industry Council on Advanced Ceramics, Third Workshop*, ed. P. S. Nicholson (Montreal, Quebec: Canadian University-Industrial Council on Advanced Ceramics, 1987), pp. 2-22.

27. J. Th. G. Overbeek, "Recent Developments in the Understanding of Colloid Stability," *J. Colloid. Int. Sci.*, **58** [2] 408-22 (1977).

28. I. A. Aksay and C. H. Schilling, "Colloidal Filtration Route to Uniform Microstructures," in *Ultrastructure Processing of Ceramics, Glasses, and Composites*, eds. L.L. Hench and D.R. Ulrich (New York: John Wiley & Sons Inc., 1984), pp. 439-47.

29. H. R. Kruyt, *Colloid Chemistry* (Amsterdam: Elsevier Publishing Company, 1952), pp. 264-266.

30. D. J. Shaw, *Introduction to Colloid and Surface Chemistry* (Boston, Massachusetts: Butterworth & Co. Publishers Ltd., 1970), pp. 157-74.

31. B. Jirgensons, *Colloid Chemistry* (New York: John Wiley & Sons Inc., 1954), pp. 118-24.

32. T. G. M. Van de Ven, "VI. Double Layer Interactions," *Class Notes*, McGill University, Montreal, 1986.

33. T. G. M. Van de Ven, "V. The Electrical Double Layer," *Class Notes*, McGill University, Montreal, 1986.

34. T. G. M. Van de Ven, "XII. Electrokinetic Phenomena," *Class Notes*, McGill University, Montreal, 1986).

35. P. C. Hiemenz, *Principles of Colloid and Surface Chemistry* (New York: Marcel Dekker Inc., 1977).

36. T. G. M. Van de Ven, "VII. Polymer-Colloid Interactions," *Class Notes*, McGill University, Montreal, 1986).

37. P. C. Carman, "Fundamental Principles of Industrial Filtration," *Trans. Inst. Chem. Engrs. (Londom)*, **16**, 168-88 (1938).

38. H. Darcy, "Determination of the Laws of Flow of Water Through Sand", *Appendix to Histoire des Fontaines Publiques de Dijon*, pp. 590-95 (1856); translated by J. R. Crump, *Fluid/Particle Separation Journal*, **2** [1] 33-35 (1989).

39. E. Deeg, "Slip Casting, a Diffusion Problem," *Ber. dtsch. keram. Ges.*, **30** [16] 129-38 (1953); *Ceramic Abstr.*, November 1953, p. 194a.

40. A. Dietzel and H. Mostetzky, "Mechanism of Dewatering of a Ceramic Slip by Plaster Mold: I, Experimental Investigation of Diffusion Theory of Slip-Casting Process," *Ber. dtsch. keram. Ges.*, **33** [1] 7-18 (1956); "II, Calculation of Diffusion Coefficient of Slip Water in Cast and in Slip - Proving of Extended Theory of Three-Phase System Plaster-Cast-Slip, *Ber. dtsch keram. Ges.*, **33** [2] 47-52 (1956); "III, Penetration of Slip Water into Plaster Mold as a Wetting Problem - Pore Size Distribution, Criticism of Pressure Diffusion Method, *Ber. dtsch. keram. Ges.*, **33** [3] 73-85; (1956) "IV, X-Ray Definition of Texture of Cast", *Ber. dtsch. keram. Ges.*, **33** [4] 115-18 (1956); *Ceramic Abstr.*, September 1956, p. 193b.

41. F. M. Tiller and C. Tsai, "Theory of Filtration of Ceramics: I, Slip Casting," *J. Am. Ceram Soc.*, **69** [12] 882-87 (1986).

42. F.M. Tiller and R. Chow, "Clogging Phenomena in Filtration of Liquefied Coal," *Chem Eng. Prog.*, **77**, 61-8 (1981).

43. F. M. Tiller and H. Cooper, "The Role of Porosity in Filtration: Part V. Porosity Variations in Filter Cakes," *A.I.Ch.E. Journal*, **8** [4] 445-49 (1962).

44. F.M. Tiller and J.R. Crump, "Solid-Liquid Separation: An Overview," *Chem Eng. Progr.*, **77** [10] pp. 65-75 (1977).

45. F.M. Tiller, J.R. Crump and F. Ville, "A Revised Approach to the Theory of Cake Filtration," in *Fine Particles Processing, 2*, ed. P. Somasundaran (New York: Amer Inst. Min. Met. Pet Eng. Inc., 1980), pp. 1549-82.

46. F.M. Tiller and T.C. Green, "Role of Porosity in Filtration IX: Skin Effect with Highly Compressible Materials," *A.I.Ch.E. Journal*, **19** [6] 1266-69 (1973).

47. F.M. Tiller and W. Leu, "Basic Data Fitting in Filtration," *Journal of the Chinese Institute of Chemical Engineers*, **11** 61-70 (1980).

48. F.M. Tiller and W. Lu, "The Role of Porosity in Filtration VIII: Cake Nonuniformity in Compression-Permeability Cells," *A.I.Ch.E. Journal*, **18** [3] 569-72 (1972).

49. F.M. Tiller and M. Shirato, "The Role of Porosity in Filtration: VI. New Definition of Filtration Resistance," *A.I.Ch.E. Journal*, **10** [1] 61-67 (1964).

50. Wenfang Leu and Frank M. Tiller, "Experimental Study of the Mechanism of Constant Pressure Cake Filtration: Clogging of Filter Media," *Separation Science and Technology*, **18** [12 & 13] 1351-69 (1983).

51. Alcoa Chemicals Division, *Product Data Calcined Aluminas*, Bauxite, AR, 1988.

52. Alcan Chemicals, *Product Data Aluminas C-70 series*, Cleveland, Ohio, 1986.

53. W. M. Flock, "Bayer-Processed Aluminas," in *Ceramic Processing Before Firing*, eds. F. Y. Onoda, Jr. and L. L. Hench (New York, John Wiley & Sons Inc., 1978), pp. 85-103.

54. A. L. Stuijts and G. J. Oudemans, "Ceramic Forming Methods," in *The Proc. of the British Ceramic Society, No. 3* (Stoke-on-trent, England: British Ceramic Society, 1965), pp. 81-99.

55. P. J. Anderson and P. Murray, "Zeta Potentials in Relation to Rheological Properties of Oxide Slips," *J. Am. Ceram. Soc.*, **42** [2] 70-74 (February 1959).

56. W. E. Hauth, Jr., "Behavior of the Alumina-Water System," *J. Physical and Colloidal Chemistry*, **54**, 142-56 (1950).

57. W. E. Hauth, Jr., "Slip Casting of Aluminum Oxide," *J. Am. Ceram. Soc.* **32** [12] 394-98 (1949).

58. E. Dörre, H. Hübner, *Alumina Processing, Properties, and Applications* (Berlin. Springer-Verlag 1984), pp. 235-37.

59. W. Dawihl, E. Dörre, "Adsorption Behaviour of High-Density Alumina Ceramics Exposed to Fluids," *Evaluation of Biomaterials*, eds. George D. Winter, Jean L. Leray and Klaas de Groot (Chichester: John Wiley & Sons Ltd , 1980), pp. 239-45.

60. G. Y. Onoda, Jr., "The Rheology of Organic Binder Solutions," in *Ceramic Processing Before Firing*, eds. G. Y Onoda, Jr. and L L Hench (New York: John Wiley & Sons, 1978), pp. 235-51.

61. M. D. Sacks, "Properties of Silica Suspensions and Cast Bodies," *Am. Ceram. Soc. Bull*, **63** [12] 1510-15 (1984).

62. J. W. Halloran, "Role of Powder Agglomerates in Ceramic Processing," in *Advances in Ceramics, Volume 9, Forming of Ceramics*, eds J. A. Mangels and G.L. Messing (Columbus, Ohio: American Ceramic Society, 1984), pp 67-75.

63. W. E. Worrall, "Flow Properties of Acid-deflocculated Alumina Slips," *Trans. Brit. Ceram. Soc.*, **62**, 659-72 (1963).

64. S. G. Maguire and William Brodie, "Gelation Rate Index and Cast Quality," *Ceram. Eng. and Sci. Proc.*, **2**, 917-29 (1981).

65. J. E. Funk, "Slip Casting and Casters," in *Advances in Ceramics, Volume 9, Forming of Ceramics*, eds. J. A. Mangels and G.L. Messing (Columbus, Ohio: American Ceramic Society, 1984), pp. 76-84.

66. P. M. Heertjes, "Filtration," *Trans. Instn. Chem. Engrs.*, **42**, 266-74 (1964).

67. J. Hermia, "Constant Pressure Blocking Filtration Laws - Application to Power-Law Non-Newtonian Fluids," *Trans. Instn. Chem. Engrs*, **60**, 183-87 (1982).

68. A. Rushton and I. Hassan, "The Effect of Media Structure on Pore Bridging and Blocking," in *International Symposium on Recent Developments in Filter Media and Their Applications* (Bruges, Belgium, September 1980), pp. 1.3.1-1.3.20.

69. F. F. Notebaert, D. A. Wilms and A. A. Van Haute, "A New Deduction With a Larger Application of The Specific Resistance to Filtration of Sludges," *Water Research*, **9**, 667-73 (1975).

70. P. R. Karr and T. M. Keinath, "Limitations of the Specific Resistance and CST Tests for Sludge Dewatering," *Filtration & Separation*, **15**, 543-44 (November/December 1978).

71. R. C. P. Cubbon and E. G. Walker, " The Rheological Properties of Suspensions of Potters Plaster in Water. A New Quality Control Test," *Trans. J. Br. Ceram. Soc.*, **80**, 97-104 (1981).

72. A. Dinsdale, "The Effect of Heat on Plaster," *Trans. Brit Ceram. Soc.*, **52**, 614-31 (1953).

73. C. M. Lambe, "Preparation and Use of Plaster Molds," in *Ceramic Fabrication Processes*, ed. W. D. Kingery (New York: John Wiley & Sons, 1958), pp.31-40.

74. R. F. Craig, *Soil Mechanics 3rd edition* (Berkshire, England: Van Nostrand Reinhold Co. Ltd., 1983), pp.40-43.

75. J. Dodds and M. Leitzelement, "The Relation Between the Structure of Packing Particles and Their Properties," in *Physics of Finely Divided Matter*, eds. N. Boccara and M. Daoud (Berlin: Springer-Verlag, 1985), p.56-75.

76. P. C. Carman, *Flow of Gases Through Porous Media* (New York: Academic Press Inc., 1956).

77. M. Leitzelement, P. Maj, J.A. Dodds and J.L. Greffe, "Deep Bed Filtration in a Network of Random Tubes," in *Solid-Liquid Separation*, Ed. J. Gregory (New York: Ellis Horwood, 1984), pp. 273-96.

78. J. Dodds, G. Baluais and D. Leclerc,"Filtration Processes," in *Disorder and Mixing*, eds. E. Guyon, J. Nadal and Y. Pomeau (Dordrecht, The Netherlands: Kluwer Academic Publishers, 1988), pp. 163-83.

79. N. H. C. Hwang, "Water Flow in Pipes and Pipe Networks," in *Fundamentals of Hydraulic Engineering Systems* (Englewood Cliffs, New Jersey: Prentice-Hall Inc., 1981), pp. 86-97.

80. W. Li, "Steady Incompressible Flow in Pipes," in *Fluid Mechanics in Water Resources Engineering* (Boston, Massachusetts: Allyn and Bacon Inc., 1983), pp. 61-72.

81. V. L. Streeter and E. B. Wylie, "Steady Closed-Conduit Flow," in *Fluid Mechanics 8th Edition* (New York: McGraw-Hill Inc., 1985), pp. 446-59.

82. William H. Press, *Numerical Recipes: the Art of Scientific Computing* (New York: Cambridge University Press, 1986).

83. Alfredo H-S. Ang and Wilson H. Tang, *Probability Concepts in Engineering Planning and Design Volume 1 Basic Principles* (New York: John Wiley & Sons Inc., 1975).

84. Muhammad Sahimi, Barry D. Hughes, L.E. Scriven and H. Ted Davis, "Dispersion in Flow through Porous Media-I. One-Phase Flow," *Chemical Engineering Science*, **41** [8] 2103-22 (1986).

85. R. M. German, "Pore Size and Shape," in *Particle Packing Characteristics* (Princeton, New Jersey: Metal Powder Industries Federation, 1989), pp. 298-300.

86. Y. Oguri and E. Hattori, "Preparation of Translucent SiO_2 Glass From Monosized Particles," in *Ceramic Transactions, Vol. 1, Ceramic Powder Science II.*, eds. G.L. Messing, E.R. Fuller Jr. and H. Hausner (Westerville, Ohio: The American Ceramic Society, 1988), pp. 701-8.

87. F. G. R. Gauthier and S. C. Danforth, "Packing of Bimodal Mixtures of Colloidal Silica," in *Ceramic Transactions, Vol. 1, Ceramic Powder Science II.*, eds. G. L. Messing, E. R. Fuller Jr. and H. Hausner (Westerville, Ohio: The American Ceramic Society, 1988), pp. 709-15.

88. M. M. Sharma and Y. C. Yortsos, "Transport of Particulate Suspensions in Porous Media: Model Formulation," *AIChE Journal* **83** [2] 428-48 (October 1981).

89. Raj Rajagopalan and Jong S. Kim, "Adsorption of Brownian Particles in the Presence of Potential Barriers: Effect of Different Modes of Double-Layer Interaction," *Journal of Colloid and Interface Science* **101** [1] 214-24 (September 1984).

90. V. G. Levich, *Physicochemical Hydrodynamics* (Englewoo Cliffs, New Jersey: Prentice-Hall Inc., 1962), pp. 112-16.

91. R. I. Mackie, R. M. W. Horner and R. J. Jarvis, "Dynamic Modeling of Deep-Bed Filtration," *AIChE Journal*, **33** [11] 1761-75 (November 1987).

92. K. C. Khiler and H. S. Fogler, "The Existence of a Critical Salt Concentration for Particle Release," *Journal of Colloid and Interface Science*, **101** [1] 214-24 (September 1984).

93. T. G. M. Van de Ven, "IV. Van Der Waals Forces," *Class Notes*, Montreal, McGill University, 1986.

94. J. Visser, "On Hamaker Constants: A Comparison Between Hamaker Constants and Lifshitz - Van Der Waals Constants", *Advan. Colloid Interface Sci.*, **3**, 331-63 (1972).

95. B. Dahneke, "Kinetic Theory of the Escape of Particles from Surfaces," *Journal of Colloid and Interface Science*, **50** [1] 89-107 (January 1975).

96. R. Rajagopalan and C. Tien, "Single Collector Analysis of Collection Mechanisms in Water Filtration," *The Canadian Journal of Chemical Engineering*, **55**, 246-55 (June 1977).

97. A. C. Payatakes, H. Y. Parks and J. Petrie, "A Visual Study of Particle Deposition and Reentrainment during Depth Filtration of Hydrosols with a Polyelectrolyte, " *Chem. Eng. Sci* . **36**. 1319-35 (1981).

98. A. Maroudas and P. Eisenklam, "Clarification of Suspensions. A Study of Particle Deposition on Granular Media," *Chem. Eng. Sci.*, **20**, 867-73 (1965).

99. H. C. Pendse, C. Tien, R. M. Turian and R. Rajagopalan, "Dispersion Measurements in Clogged Filter Beds - A Diagnostic Study of the Morphology of Particle Deposition," *A.I.Ch.E. Journal*, **24**, 473-84 (1978).

100. Richard Zallen, "Physics of Amorphous Solids," (New York: Wiley-Interscience, 1983), pp. 135-83.

Appendix A

COMPUTER PROGRAM FOR RANDOM TUBE NETWORK MODEL

```
C
C      ************************************************************
C      *              RANDOM TUBE NETWORK MODEL                   *
C      *                                                          *
C      *  PROGRAM CALCULATES THE PERMEABILITY OF THE NETWORK.     *
C      *                                                          *
C      *  PROGRAM NAME = HARDYDEC.FOR                             *
C      * ************************************************************
C
C           EL = # OF ELEMENTS/ROW
C            N = TOTAL # OF LOOPS
C          TEL = TOTAL # OF ELEMENTS
C         ROWS = # OF ROWS
C        LOOPS = # OF LOOPS/ROW
C         TOLQ = ERROR TOLERANCE FOR Q
C         TOLH = ERROR TOLERANCE FOR HEAD LOSS
C        Q_INT = Q INFLOW
C         IDUM = SEED FOR RANDOM NUMBER GENERATOR
C      PERMEAB = PERMEABILITY
C
C
      REAL R(20000), Q(20000),SUMH,SUMZ,QDELTA,QINT
      REAL LOSSAVE
      INTEGER RRUN,LOK,ROWS,LOOPS,EL,N,TEL,LO
      COMMON ICOUNT
C
      do 2000 icount = 1,2
         if (icount .eq. 1) then
            rows=200
            loops=24
C     RESULTS ARE WRITTEN TO FILE = "RESULT_1"
      open (1,file= 'RESULT_1')
      write (1,*) 'file = RESULT_1'
      write(1,*)'program name = HARDYDEC.FOR'
      write (1,*)'LOGNORMAL DISTRIBUTION'
      write (1,*)'std=0.6 median=1'
      write(1,*)'Xo=1.0  Ao=0.5  Co=3.0'
      write(1,*)'x=0.5*tan(pi*randx)+1.0'
        endif
      if (icount .eq. 2) then
         close (1, status= 'keep')
         rows=200
         loops=24
       open (2,file= 'RESULT_2')
       write (2,*) 'file=RESULT_2 same as RESULT_1 except'
       write (2,*) 'LOGNORMAL  STD = 1.0   MEDIAN = 1.0'
```

```
          write (2,*) 'Xo=0.4  Ao=0.8 Co=2.0'
         endif
C
            RRUN=0
            LOK = 0
            QINT = 1
            EL = 2*LOOPS +1
            N= LOOPS*(ROWS-2)
            TEL = (ROWS-1)*EL
            TOLQ= 0.00001
            TOLH=10000
          write (icount,*)'rows= ',rows,' loops= ',loops
          write (icount,*)'tolq = ',tolq, '  tolh = ',tolh
C
C         THE NETWORK IS SOLVED 10 TIMES EACH TIME USING
C         A DIFFERENT SEED
               do 1900 ll=1,10
                  write (*,*) 'run  cycle ',ll,icount
                 rrun=0.
             idum=-100*ll
             iidum=idum
C          FUNCTION "RLOGNOR" IS USED TO ASSIGN TUBE RADII WITH
C          A LOGNORMAL SIZE DISTRIBUTION
            DO 100 I=1,TEL
                R(i)= RLOGNOR(IDUM)
100         CONTINUE
            DO 200 I=1,EL
               Q(I)=QINT/EL
200         CONTINUE
            DO 500 I=2,(ROWS-1)
                 IF ((MOD(I,2)) .EQ. 0) THEN
                     DO 300 J=((I-1)*EL+1),(I*EL-2),2
                           JJ=J+1
                            K=J-EL
                           KK=K+1
                           Q(J)=.5*(Q(K)+Q(KK))
                           Q(JJ)=Q(J)
300                  CONTINUE
                          J=i*EL
                          K=J-EL
                          Q(J)=Q(K)
                  ELSE
                     J=(I-1)*EL+1
                     K=J-EL
                     Q(J)=Q(K)
                      DO 400 J=((I-1)*EL+2),((I)*EL),2
```

```
                              JJ=J+1
                               K=J-EL
                              KK=K+1
                              Q(J)=.5*(Q(K)+Q(KK))
                              Q(JJ)=Q(J)
400                        CONTINUE
                         ENDIF
500                    CONTINUE
C
C
550                     continue
C              START BALANCING
C                LOK = NUMBER OF LOOPS BALANCED
                     LOK=0
                      do 600 I=1,(EL-2),2
                          J=I+1
                          SUMH=(-1/(R(I)**3))*Q(I)
                          SUMZ=1/(R(I)**3)
                          SUMH=SUMH+(1/(R(J)**3))*Q(J)
                          SUMZ=SUMZ+1/(R(J)**3)
                          QDELTA=SUMH/SUMZ
                          Q(I)=Q(I)+QDELTA
                          Q(J)=Q(J)-QDELTA
                    IF ((ABS(QDELTA).lt.TOLQ).AND.(ABS(SUMH).lt.TOLH)) THEN
                           LOK=LOK+1
                    ENDIF
600                     CONTINUE
                     if (rows .gt. 3) then
                          ı=2
                          do 700 lo = 1,n
                               j=ı+el
                              sumh=(-1/(r(i)**3))*q(i)+(-1/(r(j)**3))*q(j)
                              sumz=1/(r(i)**3)+1/(r(j)**3)
                              k=i+1
                              jj=j+1
                              sumh=sumh+(1/(r(k)**3))*q(k)+(1/(r(jj)**3))*q(jj)
                              sumz=sumz+1/(r(k)**3)+1/(r(jj)**3)
                              qdelta=sumh/sumz
                              q(i)=q(i)+qdelta
                              q(j)=q(j)+qdelta
                              q(jj)=q(jj)-qdelta
                              q(k)=q(k)-qdelta
                         if ((abs(qdelta).lt.tolq).and.(abs(sumh).lt.tolh))then
                              lok=lok+1
                         endif
                    if ((mod(lo,loops).eq.0).and.(mod((lo/loops),2).eq.0))then
```

```
                    i=i+4
              else
                    i=i+2
            endif
700       continue
            endif
              if (mod(rows,2) .eq. 0) then
                do 800 i=(tel-el+2),(tel-1),2
                     j=i+1
                     sumh=(-1/(r(i)**3))*q(i)
                     sumz=1/(r(i)**3)
                     sumh=sumh+(1/(r(j)**3))*q(j)
                     sumz=sumz+1/(r(j)**3)
                     qdelta=sumh/sumz
                     q(i)=q(i)+qdelta
                     q(J)=q(j)-qdelta
               if ((abs(qdelta).lt.tolq).and.(abs(sumh).lt.tolh)) then
                   lok=lok+1
                 endif
800             continue
               endif
                if (mod(rows,2).gt.0 ) then
                  do 900 i=(tel-el+1),(tel-2),2
                     j=i+1
                     sumh=(-1/(r(i)**3))*q(i)
                     sumz=1/(r(i)**3)
                     sumh=sumh+(1/(r(j)**3))*q(j)
                     sumz=1/(r(j)**3)
                     qdelta=sumh/sumz
                     q(i)=q(i)+qdelta
                     q(j)=q(j)-qdelta
              if ((abs(qdelta).lt.tolq).and.(abs(sumh).lt.tolh)) then
                       lok=lok+1
                   endif
900               continue
               endif
                rrun =rrun+1
                 if ((lok .lt. (n+2*loops)).and.(rrun .lt. 3000)) then
                    go to 550
                else
                   write (icount,*) 'it took ',rrun,' iterations'
                   headloss=0.
               do 1100 j=1,el
                  do 1000 i=j,tel,el
                    headloss=headloss+(1/(r(i)**3))*q(i)
1000                continue
```

```
1100          continue
                  lossave=headloss*el/(rows-1)/el
                  permeab=1./(lossave)
        write (icount,*) 'seed ',iidum,' k ',permeab
              endif
1900         continue
2000        continue
             end
c
c                  LOGNORMAL RANDOM NUMBER GENERATOR
                     function rlognor(idum)
                        real median
                        common icount
                   if (icount .eq. 1) then
                       std=0.6
                       xo=1.0
                       ao=0.5
                       co=3.0
                       median=1.0
                    endif
                    if (icount .eq. 2) then
                       std=1.0
                       xo=0.4
                       ao=0.8
                       co=2.0
                       median=1.o
                    endif
10                        randx=ran1(idum)
                    if((randx .ge. .494).and.(randx.le..54))then
                            go to 10
                    endif
                    xx=ao*tan(3.14159265*randx)+xo
                    yy=ran1(idum)*co
                    yy=yy/(1 +((xx-xo)**2)/(ao*ao))
                    if (xx .le. 0.0) then
                        go to 10
                    endif
                 px =(1.0/(sqrt(2*3.14159265)*std*xx))
                 px =px*exp((-.5*(log(xx)-log(median))**2)/(std**2))
c
                  if (px .ge. yy) then
                      rlognor = xx
                  else
                     go to 10
                  endif
               return
```

```
      end
C
      function ran1(idum)
         dimension s(97)
         integer ma,ia1,ic1,m2,ia2,ic2,m3,ia3,ic3
         m1=259200
        ia1=7141
        ic1=54773
         m2=134456
        ia2=8121
        ic2=28411
         m3=243000
        ia3=4561
        ic3=51349
        data iff /0/
        if (idum .lt. 0 .or. iff .eq. 0) then
              iff=1
              ix1=mod(ic1-idum,m1)
              ix1=mod(ia1*ix1 +ic1,m1)
              ix2=mod(ix1,m2)
              ix1=mod(Ia1*ix1+ic1,m1)
              ix3=mod(ix1,m3)
              do 11 j=1,97
                   ix1=mod(ia1*ix1+ic1,m1)
                   ix2=mod(ia2*ix2+ic2,m2)
                   s(j)=(float(ix1)+float(ix2)/m2)/m1
11                continue
                  idum = 1
            endif
            ix1=mod(ia1*ix1+ic1,m1)
            ix2=mod(ia2*ix2+ic2,m2)
            ix3=mod(ia3*ix3+ic3,m3)
            j=1+(97*ix3)/m3
            if (j .gt. 97 .or. j .lt. 1) then
                write(*,*) 'error'
            endif
            ran1=s(j)
            s(j)=(float(ix1)+float(ix2)/m2)/m1
            return
            end
```

Appendix B

COMPUTER PROGRAM FOR RANDOM TUBE NETWORK MODEL WITH A FIXED NETWORK TUBE VOLUME

```
C
C       ************************************************** *
c       *  RANDOM TUBE NETWORK MODEL WITH A FIXED NETWORK    *
C       *       TUBE VOLUME (i.e. CONSTANT POROSITY)         *
C       *                                                    *
C       *  PROGRAM BLOCKS OFF TUBES SO FLOW CAN NOT PASS     *
C       *  THROUGH THEM.  EITHER 4, 8 OR 16 TUBES THAT       *
C       *  MEET AT A NODE ARE BLOCKED OFF UNTIL THE VOLUME   *
C       *  OF UNBLOCKED TUBES EQUALS THE DESIRED FIXED       *
C       *  VOLUME.  THE TUBE BLOCKING SCHEME CHOSEN DEPENDS  *
C       *  UPON THE REDUCTION IN TUBE VOLUME REQUIRED.  THE  *
C       *  PERMEABILITY OF THE NETWORK IS THEN CALCULATED.   *
C       *                                                    *
C       *  PROGRAM NAME = VOLUME.FOR                         *
C       ****************************************************
C
C            EL = # OF ELEMENTS/ROW
C             N = TOTAL # OF LOOPS
C           TEL = TOTAL # OF ELEMENTS
C          ROWS = # OF ROWS
C         LOOPS = # OF LOOPS/ROW
C          TOLQ = ERROR TOLERANCE FOR Q
C          TOLH = ERROR TOLERANCE FOR HEAD LOSS
C          QINT = Q INFLOW
C          IDUM = SEED FOR RANDOM NUMBER GENERATOR
C       PERMEAB = PERMEABILITY
C
C
        REAL R(26200), Q(26200),SUMH,SUMZ,QDELTA,QINT
        REAL LOSSAVE
        INTEGER RRUN,LOK,ROWS,LOOPS,EL,N,TEL,lo
        COMMON ICOUNT
C
        do 2000 icount = 1,3
           write(*,*)'icount = ',icount
           if (icount .eq. 1) then
              rows=200
              loops=24
C       RESULTS ARE WRITTEN TO FILE = "VOLUME_1"
        open (1,file= 'VOLUME_1')
        write (1,*) 'file = VOLUME_1    '
        write (1,*) 'program name = VOLUME.FOR'
        write (1,*) 'PIPES REDUCED 4,8 AND 16 AT ONCE'
        write (1,*)'LOGNORMAL distribution'
        WRITE (1,*) 'VOL RED. = 1*(ROWS-1)*EL'
        write (1,*)'std=0.6 median=0.8353   no minimum R '
```

```
      write (1,*) 'Xo=0.46   Ao=0.5   Co=3.0'
      write (1,*) 'x=0.5*tan(pi*randx) + 0.460'
        endif
      if (icount .eq. 2) then
         close (1, status= 'keep')
         rows=200
         loops=24
       open (2,file= 'VOLUME_2')
       write (2,*) 'file = VOLUME_2 same as VOLUME_1 except'
       write (2,*)'lognormal std=0.8 Xo=1. Ao=1.3 Co=1.'
       write (2,*)'median=1.896480879  peak=1.0'
       write (2,*)'if r>2*median another is chosen  '
      endif
      if (icount .eq. 3) then
          close (2,status='keep')
          rows=200
          loops=24
         open (3,file= 'VOLUME_3')
         write (3,*) 'file=VOLUME_3 same as VOLUME_1 except'
         write(3,*)'lognormal std=1.0 Xo=1.0 Ao=1.3 Co=1.'
         write(3,*)'median=2.718281828   peak=1.0'
         write(3,*)'if r>2*median another is chosen'
      endif
c
         RRUN=0
         LOK = 0
         qint = 1
         EL = 2*LOOPS +1
         N= LOOPS*(ROWS-2)
         TEL = (ROWS-1)*EL
         TOLQ= 0.00001
         TOLH=10000
         IXX=16
       write (icount,*)'rows= ',rows,' loops= ',loops
       write (icount,*)'tolq = ',tolq, '  tolh = ',tolh
c
C       THE NETWORK IS SOLVED 10 TMES EACH TIME USING
C       A DIFFERENT SEED
            do 1900 ll=1,10
               write (*,*) 'run  cycle ',ll,icount
              rrun=0.
         idum=-100*ll
         iidum=idum
         volume=0.0
c     FUNCTION "RLOGNOR" IS USED TO ASSIGN TUBE RADII
C     WITH A LOGNORMAL DISTRIBUTION
```

```
              DO 100 I=1,TEL
                  R(i)= RLOGNOR(IDUM)
100           CONTINUE
c
C
C       CALCULATING AVERAGE RADIUS AND TOTAL VOLUME
                RAD=0.
                DO 110 I=1,TEL
                    RAD=R(I)+RAD
110             CONTINUE
                AVERAGE=RAD/TEL
                WRITE(ICOUNT,*)'AVERAGE ',AVERAGE
                WRITE(*,*)'AVERAGE ',AVERAGE
                DO 120 I=1,TEL
                   VOLUME=VOLUME+R(I)**3.
120             CONTINUE
                write(icount,*)'volume ',volume
C
                 ired = 0
c         IRED = NUMBER OF PIPE REDUCTIONS
                 volred=volume
c
c       NOTE: PIPE RADIUS IS BEING CHANGE TO PIPE RESISTANCE
C
           do 150 i=1,tel
               r(i) = 1./(r(i)**3.)
150        continue
c
             DO 200 I=1,EL
                Q(I)=qint/EL
200          CONTINUE
c
c       NEED TO FIND OUT HOW MANY PIPES NEED TO TAKEN OUT
C
             IX=16
220          CONTINUE
             volred = VOLUME
             IRED=0.
             IX=IX-2
             DO 280 I=2,(ROWS-2),2
                 DO 250 J=((I-1)*EL+1),(I*EL-2),2
                   IF ((MOD(J,IX).EQ.0).AND.(I.LE.(ROWS-2))
     +              .AND.(J.NE.(1+(I-1)*EL)).AND.(MOD(J,EL).NE.0))THEN
                       volred=volred-1/R(J)
                       IRED=IRED+1
                   ENDIF
```

```
250             CONTINUE
280           CONTINUE
              IF ((volred.GT.1*(ROWS-1)*EL).and. (ix.ne.2)) THEN
                  GO TO 220
              ENDIF
              if ((volred.le. 1*(rows-1)*el).and.(ix.ge.2))then
                 write(icount,*)'ix ired ',ix,ired
                 write(icount,*)'USE PROGRAM "UNI2HAR.FOR" INSTEAD'
                 goto 2000
              endif
c
c       TRYING DIFFERENT PORE REDUCTION SCHEMES
C
C
C         INTIALIZING THE Q'S
C
          DO 282 I=(el+1),TEL
              Q(I)=1.
282       CONTINUE
C
               IF ((IX .EQ. 2) .AND.(volred.GT.1*(ROWs-1)*EL))THEN
                 IXX=6
285               CONTINUE
                 volred=VOLUME
                 IRED=0
                 IXX=IXX-2
                   DO 295 I=2,(ROWS-2),4
                     DO 290 J=((I-1)*EL+1),(I*EL-2),2
                       IF ((MOD(J,IXX).EQ.0).AND.(I.LE.(ROWS-2))
     +                   .AND.(J.NE.(1+(I-1)*EL))
     +                   .AND.(MOD(J,EL).NE.0)) THEN
                           JA=J-1
                           JB=J-1+EL
                           JC=J+EL
                           volred=volred-1./R(J)-1./R(JA)
     +                          -1/R(JB)-1/R(JC)
                            IRED=IRED+4
                       ENDIF
290                  CONTINUE
295                CONTINUE
             IF ((volred .GT.1*(ROWS-1)*EL).AND.(IXX.NE.4)) THEN
                   GO TO 285
             ENDIF
             IF (volred .LT.1*(ROWS-1)*EL)THEN
                    ICHOICE=2
                    write(icount,*)'ichoice = 2'
```

```
                ENDIF
               ENDIF
            IF((IXX.EQ.4).AND.(volred.GT.1*(ROWS-1)*EL)) THEN
                  volred=VOLUME
                  IRED=0
               DO 310 I=2,(ROWS-3),4
                  DO 300 J=((I-1)*EL+3),(I*EL-2),4
                       JA=J-1
                       JB=J-1+EL
                       JC=J+EL
                       volred=volred-1/R(J)-1/R(JA)-1/R(JB)-1/R(JC)
                      Q(j)=0.
                      q(ja)=0.
                      q(jb)=0.
                      q(jc)=0.
                       IRED=IRED+4
300               CONTINUE
310            CONTINUE
c
C
                    IF(volred .LT.1*(ROWS-1)*EL) THEN
                        ICHOICE=3
                        write(icount,*)'ichoice = 3'
                    ENDIF
                         k=3
                        imered=ired
                        volnew=volred
                  while ((volnew .gt.(1*(rows-1)*el)).and.(k.ge.2))
                         k=k-1
                         volnew=volred
                         ired=imered
                    DO 330 I=4,(ROWS-3),4*k
                       DO 320 J=((I-1)*EL+5),(I*EL-2),4
                            JA=J-1
                            JB=J-1+EL
                            JC=J+EL
                            q(j)=0.
                            q(ja)=0.
                            q(jb)=0.
                            q(jc)=0.
                    volnew=volnew-1/R(J)-1/R(JA)-1/R(JB)-1/R(JC)
                    IRED=IRED+4
320                    CONTINUE
330                 CONTINUE
          endwhile
c
```

```
                    i=4
            while((volnew .gt.(1*(rows-1)*el)).and.(i.le.(el-5)))
                 q(i)=0.
                 q(i+1)=0.
                 ired=ired+2
                 volnew=volnew-1/r(i)-1/r(i+1)
                 i=i+4
           endwhile
c
            if(mod(rows,2).eq.0)then
                  i=(rows-2)*el+3
               elseif(mod((rows-1),4).eq.0)then
                  i=(rows-2)*el+4
               elseif(mod((rows-3),4).eq.0)then
                  i=(rows-2)*el+2
               else
                  write(*,*) 'something is wrong'
                  write(icount,*) 'something is wrong '
            endif
            while((volnew.gt.(1*(rows-1)*el)).and.(i.le.(tel-2)))
                 q(i)=0.
                 q(i+1)=0.
                 ired=ired+2
                 volnew=volnew-1/r(i)-1/r(i+1)
                 i=i+4
            endwhile
c
            ihad=0
            do 332 i=1,tel
               if(q(i) .ne. 0.)then
                  ihad=ihad+1
               endif
332          continue
             write(*,*)'ired  ihad ',ired,ihad
c
C       CASE WHERE 8 PIPES ARE REMOVED AT A TIME
             IEIGHT=0
             volend=volnew
             kab=4
             imered=ired
            while(volnew.gt.(1*(rows-1)*el+20).and.(kab.ge.2))
                 IEIGHT=1
                 kab=kab-1
                 ired=imered
                 volend=volnew
                 do 340 i=2,(rows-7),8*kab
```

```
                  do 335 j=i*el+5,((i+1)*el-5),8
                     q(j)=0.
                     q(j+el+1)=0.
                     q(j+el+2)=0.
                     q(j+3)=0.
                     q(j+2*el+1)=0.
                     q(j+2*el+2)=0.
                     q(j+3*el)=0.
                     q(j+3*el+3)=0.
                     volend=volend-1./r(j)-1./r(j+el+1)
     +               -1./r(j+el+2)-1./r(j+3)-1./r(j+2*el+1)
     +               -1./r(j+2*el+2)-1./r(j+3*el)-1./r(j+3*el+3)
                      ired=ired+8
335               continue
340            continue
            endwhile
                  volnew=volend
                  ihad=0
                  do 342 i=1,tel
                     if(q(i) .ne.0.)then
                        ihad=ihad+1
                     endif
342               continue
                  write(*,*)'volnew ired ihad ',volnew,ired,ihad
c
               kka=3
               imered=ired
               volend=volnew
               while ((volend.gt.(1*(rows-1)*el+20)).and.
     +               (kka.ge.2))
                  kka=kka-1
                  ired=imered
                  volend=volnew
                  do 355 i=6,(rows-7),8*kka
                    do 350 j=(i*el+9),((i+1)*el-5),8
                     q(j)=0.
                     q(j+el+1)=0.
                     q(j+el+2)=0.
                     q(j+3)=0.
                     q(j+2*el+1)=0.
                     q(j+2*el+2)=0.
                     q(j+3*el)=0.
                     q(j+3*el+3)=0.
                     volend=volend-1./r(j)-1./r(j+el+1)
     +               -1./r(j+el+2)-1./r(j+3)-1./r(j+2*el+1)
     +               -1./r(j+2*el+2)-1./r(j+3*el)-1./r(j+3*el+3)
```

```
                    ired=ired+8
350               continue
355             continue
              endwhile
                    volnew=volend
                    write(*,*)'volnew ired ',volnew,ired
                  ihad=0
                 do 360 i=1,tel
                   if(q(i) .gt. 0.)then
                     ihad=ihad+1
                   endif
                  i2had=ihad
360             continue
                  WRITE(ICOUNT,*)'8 VOLNEW IRED IHAD KAB KKA ',VOLNEW,
     +                 IRED,IHAD,KAB,KKA
c
c       CASE WHERE 16 PIPES ARE REMOVED AT A TIME
                  ISIXTEEN=0
                  KHH=3
                  IMERED=IRED
                  VOLEND=VOLNEW
                WHILE((VOLEND.GT.(1*(ROWS-1)*EL+100)).AND.(KHH.GE.2))
                  ISIXTEEN=1
                  KHH=KHH-1
                  IRED=IMERED
                  VOLEND=VOLNEW
                  DO 400 I=4,(ROWS-13),16*KHH
                      DO 390 J=((I)*EL+11),((I+1)*EL-11),16
                           JA=J
                        DO 365 JINT=1,8
                          Q(JA)=0.
                          VOLEND=VOLEND-1/R(JA)
                          IRED=IRED+1
                          JA=JA+EL+1
365                     CONTINUE
                        JA=J+7
                        DO 367 JINT=1,8
                          Q(JA)=0.
                          VOLEND=VOLEND-1/R(JA)
                          IRED=IRED+1
                          JA=JA+EL-1
367                     CONTINUE
390                   CONTINUE
400                CONTINUE
                 WRITE(*,*) '16 PIPES VOLEND IRED KHH ',VOLEND,IRED,KHH
                  ENDWHILE
```

```
                VOLNEW=VOLEND
C
          WRITE(ICOUNT,*)'16 PIPES AT ONCE VOLNEW IRED KHH ',VOLNEW,
     +      IRED,KHH
            KHI=3
            IMERED=IRED
            VOLEND=VOLNEW
            WHILE((VOLEND .GT.(1*(ROWS-1)*EL+120)).AND.(KHI.GE.2))
                KHI=KHI-1
                VOLEND=VOLNEW
                IRED=IMERED
                DO 430 I=12,(ROWS-13),16*KHI
                  DO 425 J=I*EL+19,(I+1)*EL-11,16
                      JA=J
                    DO 410 JINT=1,8
                      Q(JA)=0.
                      VOLEND=VOLEND-1/R(JA)
                      IRED=IRED+1
                      JA=JA+EL+1
410                 CONTINUE
                    JA=J+7
                    DO 415 JINT=1,8
                      Q(JA)=0.
                      VOLEND=VOLEND-1/R(JA)
                      IRED=IRED+1
                      JA=JA+EL-1
415                 CONTINUE
425               CONTINUE
430             CONTINUE
              ENDWHILE
                VOLNEW=VOLEND
          WRITE(ICOUNT,*)'16 VOLNEW IRED KHI I8 I16 ',VOLNEW,IRED,KHI
     +           ,IEIGHT,ISIXTEEN
c
c         PUTTING PIPES BACK IN
                ik=0
C         NOTE : BE CAREFUL NOT TO DUPLICATE PUTTING BACK PIPES
C                THAT HAVE ALREADY BEEN PUT BACK  I.E. IF IK=24
C                AND I=IK,(ROWS-3),4  THINGS WOULD BE DUPLICATED
          IF (ISIXTEEN .EQ. 0 .AND. IEIGHT .EQ. 0.) THEN
          while(volnew.lt.(1*(rows-1)*el-20.).and.(ik.lt.(rows-3-8))
     +           .and. (ik .le. (el-9-8)))
                ik=ik+8
             do 435 i=ik,(rows-3),20
                do 433 j=((i-1)*el+5+ik),(i*el-2),16
                    q(j)=1.
```

```
                    q(j-1)=1.
                    q(j-1+el)=1.
                    q(j+el)=1.
                  volnew=volnew+1./r(j)+1./r(j-1)+1./r(j-1+el)
     +                    +1./r(j+el)
                    ired=ired-4
433               continue
435             continue
                ENDWHILE
               endIF
            WRITE(ICOUNT,*)'VOLRED IRED K IXX ik ',VOLNEW,IRED,K,IXX,ik
                ihad=0
              do 440 i=1,tel
                 if(q(i).gt.0.)then
                      ihad=ihad+1
                 endif
440            continue
C
          ENDIF
                  IF(volred.LT.1*(ROWS-1)*EL)THEN
                      ICHOICE=4
                      write(icount,*)'ichoice = 4'
                  ENDIF
C
c
c      REINITIALIZE FIRST ROW OF Qs
              IONE=0
            DO 443 I=1,EL
                IF(Q(I).NE.0)THEN
                   IONE=IONE+1
                ENDIF
443         CONTINUE
            DO 447 I=1,EL
               IF(Q(I).NE.0)THEN
                   Q(I)=QINT/IONE
               ENDIF
447         CONTINUE
C
            do 500 i=2,(rows-1),2
                do 450 j=((i-1)*el+1),(i*el-2),2
                   if((q(j).eq.0).and.(q(j+1).ne.0))then
                       q(j+1)=q(j-el+1)+q(j-el)
                   endif
                   if((q(j).ne.0).and.(q(j+1).eq.0.))then
                      q(j)=q(j-el)+q(j-el+1)
                   endif
```

```
                    if((q(j).ne.0).and.(q(j+1).ne.0))then
                      q(j)=0.5*(q(j-el)+q(j-el+1))
                      q(j+1)=q(j)
                    endif
450              continue
                    q(i*el)=q((i-1)*el)
                 IF(MOD(ROWS,2).EQ.0)THEN
                    q(i*el+1)=q((i-1)*el+1)
                 do 470 j=(i*el+2),((i+1)*el-1),2
                    if((q(j).eq.0).and.(q(j+1).ne.0))then
                        q(j+1)=q(j-el+1)+q(j-el)
                    endif
                    if((q(j).ne.0).and.(q(j+1).eq.0))then
                       q(j)=q(j-el)+q(j-el+1)
                    endif
                    if((q(j).ne.0).and.(q(j+1).ne.0))then
                      q(j)=0.5*(q(j-el)+q(j-el+1))
                      q(j+1)=q(j)
                    endif
470              continue
                 ELSE
                   WRITE(*,*)'CHOOSE "ROWS" MULTIPLE OF 2'
                 ENDIF
500              continue
c
570                 continue
c
c       NOTE: WHEREVER YOU SEE R( ) IT IS = 1./(PIPE RADIUS)**3.
C
c          START BALANCING
                   LOK=0
c                  BALANCING FOR 1ST LAYER OF LOOPS
                   do 600 I=1,(EL-2),2
                       J=I+1
                     if(q(i).ne.0 .and. q(j).eq.0)then
                        sumh=-r(i)*q(i)-r(i+el+1)*q(i+el+1)
                        sumz=r(i)+r(i+el+1)
                        sumh=sumh+r(j+2)*q(j+2)+r(j+el+1)*q(j+el+1)
                        sumz=sumz+r(j+2)+r(j+el+1)
                        qdelta=sumh/sumz
                        q(i)=q(i)+qdelta
                        q(i+el+1)=q(i+el+1)+qdelta
                        q(j+2)=q(j+2)-qdelta
                        q(j+el+1)=q(j+el+1)-qdelta
                        if((abs(qdelta).lt.tolq).and.
     +                          (abs(sumh).lt.tolh))then
```

```
                        lok=lok+1
                      endif
                    endif
                  if((q(i).eq.0).and.(q(j).ne.0))then
                        lok=lok+1
                  endif
                  if((q(i).ne.0).and.(q(j).ne.0))then
                       SUMH=-R(I)*Q(I)
                       SUMZ= R(I)
                       SUMH=SUMH+ R(J)*Q(J)
                       SUMZ=SUMZ+ R(J)
                       QDELTA=SUMH/SUMZ
                       Q(I)=Q(I)+QDELTA
                       Q(J)=Q(J)-QDELTA
                         IF ((ABS(QDELTA).lt.TOLQ).AND.
     +                            (ABS(SUMH).lt.TOLH))THEN
                            LOK=LOK+1
                         ENDIF
                   endif
600                CONTINUE
C
                 if (rows .gt. 3) then
                     i=2
C               BALANCING FOR ALL THE LOOPS
                do 700 lo=1,n
                 j=i+el
                  if(q(i).eq.0 .or. q(i+1).eq.0) then
                        lok=lok+1
                  elseif((q(i).ne.0.).and.(q(i+1).ne.0).and.
     +              (q(i+el).eq.0.).and.(lo.le.loops*(rows-3)))
     +                 then
                    IF(Q(I+2*EL-1).NE.0.)THEN
                      j=i-1+el
                      js=j+el
                      jss=js+el+1
                      sumh=-r(i)*q(i)-r(j)*q(j)-r(js)*q(js)
     +                          -r(jss)*q(jss)
                      sumz=r(i)+r(j)+r(js)+r(jss)
                      k=i+1
                      jj=k+1+el
                      jk=jj+el
                      jkk=jk+el-1
                      sumh=sumh+r(k)*q(k)+r(jj)*q(jj)+r(jk)*q(jk)
     +                              +r(jkk)*q(jkk)
                      sumz=sumz+r(k)+r(jj)+r(jk)+r(jkk)
                      qdelta=sumh/sumz
```

```
                    q(i)=q(i)+qdelta
                    q(j)=q(j)+qdelta
                    q(js)=q(js)+qdelta
                    q(jss)=q(jss)+qdelta
                    q(k)=q(k)-qdelta
                    q(jj)=q(jj)-qdelta
                    q(jk)=q(jk)-qdelta
                    q(jkk)=q(jkk)-qdelta
                  if((abs(qdelta).lt.tolq).and.(abs(sumh).lt.tolh))then
                      lok=lok+1
                  endif
               ENDIF
C
C              IF THIS ELSEIF STATEMENT IS TRUE THEN LOOP IN
C              BOTTOM LAYER IS BALANCED
               elseif((q(i).ne.0.).and.(q(i+1).ne.0.).and.
     +               (q(i+el).eq.0.).and.(lo.gt.loops*(rows-3)))then
                        lok=lok+1
C
               elseif((q(i).ne.0.).and.(q(i+1).ne.0.).and.
     +              (q(i+el).ne.0.).and.(q(i+1+el).ne.0.))then
                    sumh=-r(i)*q(i)-r(i+el)*q(i+el)
                    sumh=sumh+r(i+1)*q(i+1)+r(i+1+el)*q(i+1+el)
                    sumz=r(i)+r(i+el)+r(i+1)+r(i+1+el)
                    qdelta=sumh/sumz
                    q(i)=q(i)+qdelta
                    q(i+el)=q(i+el)+qdelta
                    q(i+1)=q(i+1)-qdelta
                    q(i+1+el)=q(i+1+el)-qdelta
                    if((abs(qdelta).lt.tolq).and.(abs(sumh)
     +                                  .lt.tolh))then
                         lok=lok+1
                    endif
                ENDIF
c
c         THIS IS FOR THE CASE WHERE 8 PIPES ARE REMOVED AT A TIME
               IF((Q(I).NE.0.).AND.(Q(I+1).NE.0.).AND.
     +  (MOD(LO,LOOPS).GE.2).AND.(LO.LT.LOOPS*(ROWS-9)).AND.
     +    (MOD(LO,LOOPS).LE.(LOOPS-2)))THEN
                    IF(Q(I+2*EL-1).EQ.0..AND.Q(I+4*EL-3).NE.0.)THEN
                      J=I-1+EL
                      JA=J-1+EL
                      JB=JA-1+EL
                      JC=JB+EL
                      JD=JC+EL+1
                      JE=JD+EL+1
```

```
                        JF=JE+EL+1
C
                        JG=I+2+EL
                        JH=JG+1+EL
                        JI=JH+1+EL
                        JJ=JI+EL
                        JK=JJ+EL-1
                        JL=JK+EL-1
                        JM=JL+EL-1
                        SUMH=-R(I)*Q(I)-R(J)*Q(J)-R(JA)*Q(JA)-R(JB)*Q(JB)
     +                   -R(JC)*Q(JC)-R(JD)*Q(JD)-R(JE)*Q(JE)-R(JF)*Q(JF)
                        SUMZ=R(I)+R(J)+R(JA)+R(JB)+R(JC)+R(JD)
     +                         +R(JE)+R(JF)
                        SUMH=SUMH+R(I+1)*Q(I+1)+R(JG)*Q(JG)+R(JH)*Q(JH)
     +                    +R(JI)*Q(JI)+R(JJ)*Q(JJ)+R(JK)*Q(JK)
     +                    +R(JL)*Q(JL)+R(JM)*Q(JM)
                        SUMZ=SUMZ+R(I+1)+R(JG)+R(JH)+R(JI)+R(JJ)
     +                    +R(JK)+R(JL)+R(JM)
                        QDELTA=SUMH/SUMZ
                        Q(I)=Q(I)+QDELTA
                        Q(J)=Q(J)+QDELTA
                        Q(JA)=Q(JA)+QDELTA
                        Q(JB)=Q(JB)+QDELTA
                        Q(JC)=Q(JC)+QDELTA
                        Q(JD)=Q(JD)+QDELTA
                        Q(JE)=Q(JE)+QDELTA
                        Q(JF)=Q(JF)+QDELTA
                        Q(I+1)=Q(I+1)-QDELTA
                        Q(JG)=Q(JG)-QDELTA
                        Q(JH)=Q(JH)-QDELTA
                        Q(JI)=Q(JI)-QDELTA
                        Q(JJ)=Q(JJ)-QDELTA
                        Q(JK)=Q(JK)-QDELTA
                        Q(JL)=Q(JL)-QDELTA
                        Q(JM)=Q(JM)-QDELTA
                        IF((ABS(QDELTA).LT.TOLQ).AND.(ABS(SUMH)
     +                        .LT.TOLH))THEN
                            LOK=LOK+1
C                         WRITE(*,*)'8 PIPES LO LOK ',LO,LOK
                        ELSE
C                         WRITE(*,*)' QDELTA  LO 8 PIPES ',QDELTA,LO
                        ENDIF
                      ENDIF
                    ENDIF
C
C          CASE WHERE 16 PIPES ARE REMOVED AT A TIME
```

```
                IF((Q(I).NE.0.).AND.(Q(I+1).NE.0).AND.
     +           (MOD(LO,LOOPS).GE.4).AND.(MOD(LO,LOOPS).LE.(LOOPS-4))
     +           .AND.(LO.LT.(LOOPS*(ROWS-16))))THEN
                 IF((Q(I+2*EL-1).EQ.0).AND.Q(I+4*EL-3).EQ.0.)THEN
                     SUMH=0.
                     SUMZ=0.
                     IA=I
                     DO 610 JINT=1,8
                        SUMH=SUMH-R(IA)*Q(IA)
                        SUMZ=SUMZ+R(IA)
                        IA=IA+EL-1
610                  CONTINUE
                     IA=I+8*EL-7
                     DO 615 JINT=1,8
                        SUMH=SUMH-R(IA)*Q(IA)
                        SUMZ=SUMZ+R(IA)
                        IA=IA+EL+1
615                  CONTINUE
                     IA=I+1
                     DO 620 JINT=1,8
                        SUMH=SUMH+R(IA)*Q(IA)
                        SUMZ=SUMZ+R(IA)
                        IA=IA+EL+1
620                  CONTINUE
                     IA=I+8*EL+8
                     DO 625 JINT=1,8
                        SUMH=SUMH+R(IA)*Q(IA)
                        SUMZ=SUMZ+R(IA)
                        IA=IA+EL-1
625                   CONTINUE
                     QDELTA=SUMH/SUMZ
                        IA=I
                     DO 630 JINT=1,8
                        Q(IA)=Q(IA)+QDELTA
                        IA=IA+EL-1
630                  CONTINUE
                     IA=I+8*EL-7
                     DO 635 JINT=1,8
                        Q(IA)=Q(IA)+QDELTA
                        IA=IA+EL+1
635                  CONTINUE
                     IA=I+1
                     DO 640 JINT=1,8
                        Q(IA)=Q(IA)-QDELTA
                        IA=IA+EL+1
640                  CONTINUE
```

```
                    IA=I+8*EL+8
                    DO 645 JINT=1,8
                       Q(IA)=Q(IA)-QDELTA
                       IA=IA+EL-1
645                 CONTINUE
                    IF((ABS(QDELTA).LT.TOLQ).AND.(ABS(SUMH)
     +                 .LT. TOLH))THEN
                         LOK=LOK+1
C                    WRITE(*,*)'16 PIPES LOK LO ',LOK,LO
                    ENDIF
                  ENDIF
                ENDIF
c
              if((mod(lo,loops).eq.0).and.
     +             (mod((lo/loops),2).eq.0))then
                     i=i+4
              else
                     i=i+2
              endif
700         continue
            endif
C
              if (mod(rows,2) .eq. 0) then
                do 800 i=(tel-el+2),(tel-1),2
                     j=i+1
                     if((q(i).ne.0).and.(q(j).eq.0.))then
                        sumh=-r(i)*q(i)-r(i-el+1)*q(i-el+1)
                        sumz=r(i)+r(i-el+1)
                        sumh=sumh+r(j+2)*q(j+2)+r(i-el+2)*q(i-el+2)
                        sumz=sumz+r(j+2)+r(i-el+2)
                        qdelta=sumh/sumz
                        q(i)=q(i)+qdelta
                        q(i-el+1)=q(i-el+1)+qdelta
                        q(j+2)=q(j+2)-qdelta
                        q(i-el+2)=q(i-el+2)-qdelta
                        if((abs(qdelta).lt.tolq).and.
     +                       (abs(sumh).lt.tolh))then
                              lok=lok+1
                        endif
                     endif
                     if((q(i).eq.0.).and.(q(j).ne.0.))then
                          lok=lok+1
                     endif
              if((q(i).ne.0.).and.(q(j).ne.0.))then
                     sumh=-r(i)*q(i)
                     sumz= r(i)
```

```
                    sumh=sumh+ r(j)*q(j)
                    sumz=sumz+ r(j)
                    qdelta=sumh/sumz
                    q(i)=q(i)+qdelta
                    q(J)=q(j)-qdelta
                 if((abs(qdelta).lt.tolq).and.(abs(sumh).lt.tolh))then
                    lok=lok+1
c                   WRITE(*,*)'LOK  LAST ROW ',LOK
                  else
c                  write(*,*)'qdelta  sumh',qdelta,sumh
                  endif
               endif
800           continue
             endif
C
                if (mod(rows,2).gt.0 ) then
                  do 900 i=(tel-el+1),(tel-2),2
                     j=i+1
                     if((q(i).ne.0.).and.(q(j).eq.0))then
                        sumh=-r(i)*q(i)-r(i-el+1)*q(i-el+1)
                        sumz=r(i)+r(i-el+1)
                        sumh=sumh+r(j+2)*q(j+2)+r(i-el+2)*q(i-el+2)
                        sumz=sumz+r(j+2)+r(i-el+2)
                        qdelta=sumh/sumz
                        q(i)=q(i)+qdelta
                        q(i-el+1)=q(i-el+1)+qdelta
                        q(j+2)=q(j+2)-qdelta
                        q(i-el+2)=q(i-el+2)-qdelta
                        if((abs(qdelta).lt.tolq).and.
     +                      (abs(sumh).lt.tolh))then
                           lok=lok+1
                         endif
                      endif
                      if((q(i).eq.0.).and.(q(j).ne.0.))then
                              lok=lok+1
                      endif
                    if((q(i).ne.0.).and.(q(j).ne.0.))then
                      sumh=-r(i)*q(i)
                      sumz= r(i)
                      sumh=sumh+ r(j)*q(j)
                      sumz=sumz + r(j)
                      qdelta=sumh/sumz
                      q(i)=q(i)+qdelta
                      q(j)=q(j)-qdelta
                          if (abs(qdelta).lt.tolq) then
                            lok=lok+1
```

```
                    endif
                endif
900           continue
            endif
C
              rrun =rrun+1
          IF ((lok.lt.(n+2*loops)).and.(rrun.lt.3000))then
C               ALL LOOPS ARE STILL NOT BALANCED
                go to 570
          ELSE
               write (icount,*) 'it took ',rrun,' iterations'
C
C              NOW CALCULATE PERMEABILITY
               headloss=0.
               iave=0
                DO 1050 J=1,EL
                  IF (Q(J) .NE. 0.)THEN
                    IAVE=IAVE+1
                    IHEAD=J
                    DO 1000 I=1,(ROWS-1)
                       IF(Q(IHEAD) .NE. 0.)THEN
                          HEADLOSS=HEADLOSS +R(IHEAD)*Q(IHEAD)
                       ENDIF
                       IF(Q(IHEAD).EQ.0..AND.MOD(IHEAD,2).EQ.0)THEN
                         IHEAD=IHEAD+1
                         IF (Q(IHEAD).EQ.0.)THEN
                           WRITE(ICOUNT,*)'Q SHOULD NOT EQ 0'
                         ENDIF
                         HEADLOSS=HEADLOSS+R(IHEAD)*Q(IHEAD)
                       ENDIF
                       IF(Q(IHEAD).EQ.0..AND.MOD(IHEAD,2).NE.0.)THEN
                          IHEAD=IHEAD-1
                          HEADLOSS=HEADLOSS+R(IHEAD)*Q(IHEAD)
                          IF(Q(IHEAD).EQ.0.)THEN
                            WRITE(ICOUNT,*)'Q SHOULD NOT EQ 0'
                          ENDIF
                        ENDIF
                          IHEAD=IHEAD+EL
1000                  CONTINUE
                    ENDIF
1050             CONTINUE
                 lossave=headloss*el/(rows-1)/iave
                 permeab=1/(lossave)
       write(icount,*) 'seed ',iidum,' lossave ',lossave,' k ',permeab
c
c      VOLUME IS THE TOTAL PORE VOLUME BEFORE ANY PIPES ARE REMOVED
```

```
c
      write (icount,*)'volume = ',volume,' reduced volume = ',volnew
      write (icount,*)'ixx=   ired iave ',ixx,ired,iave
        ENDIF
C
1900     CONTINUE
2000    CONTINUE
        write (*,*)'PROGRAM TERMINATED'
        END
c
c
c               LOGNORMAL RANDOM NUMBER GENERATOR
                  function rlognor(idum)
c
c               rayleigh number generator
c                 function rayleigh(idum)
C
C                NORMAL DISTRIBUTION  MEDIAN = 1.0
c                 function rnormal(idum)
c
                    real median
                    integer tel
                    common iCOUNT,tel
              if (icount .eq. 1) then
                   std=0.6
                   xo=0.46
                   ao=0.5
                   co=3.0
                   MEDIAN=0.8353
                   RMIN=10000.
              endif
              if(icount .eq. 2) then
                    std=0.8
                    xo=1.0
                    ao=1.3
                    co=1.0
                    median=1.896480879
                    rmin=1.896480879*2.
              endif
C
10                    randx=ran1(idum)
                   if ((randx .ge. .494) .and. (randx .le. .54)) then
                       go to 10
                   endif
                     xx=AO*tan((3.141592654)*randx)+XO
                      yy=ran1(idum)*CO
```

```
                yy=yy/(1 +((xx-xo)**2)/(AO*AO))
               if((xx.le.0.0).or. (xx .gt. rmin))then
                   go to 10
               endif
      px=(1.0/(sqrt(2*3.141592654)*STD*xx))
      hyy=-.5*(log(xx)-log(median))**2
      hyy=hyy/(std**2)
      px=px*exp(hyy)
         if (px .ge. yy) then
              rlognor = xx
         else
            go to 10
         endif
      return
      end
c
      function ran1(idum)
         dimension s(97)
         integer ma,ia1,ic1,m2,ia2,ic2,m3,ia3,ic3
         m1=259200
        ia1=7141
        ic1=54773
         m2=134456
        ia2=8121
        ic2=28411
         m3=243000
        ia3=4561
        ic3=51349
        data iff /0/
       2 if (idum .lt. 0 .or. iff .eq. 0) then
               iff=1
               ix1=mod(ic1-idum,m1)
               ix1=mod(ia1*ix1 +ic1,m1)
               ix2=mod(ix1,m2)
               ix1=mod(Ia1*ix1+ic1,m1)
               ix3=mod(ix1,m3)
               do 11 j=1,97
                    ix1=mod(ia1*ix1+ic1,m1)
                    ix2=mod(ia2*ix2+ic2,m2)
                    s(j)=(float(ix1)+float(ix2)/m2)/m1
11                 continue
                  idum = 1
             endif
             ix1=mod(ia1*ix1+ic1,m1)
             ix2=mod(ia2*ix2+ic2,m2)
             ix3=mod(ia3*ix3+ic3,m3)
```

```
      j=1+(97*ix3)/m3
      if (j .gt. 97 .or. j .lt. 1) then
          write(*,*) 'error'
      endif
      ran1=s(j)
      s(j)=(float(ix1)+float(ix2)/m2)/m1
      return
      end
```

Appendix C

DERIVATION OF PERFECT SINK SOLUTION OF PARTICLE FLUX TO THE TUBE SURFACE

The general equation of convective diffusion is given by:

$$\frac{\partial \rho}{\partial t} + (\vec{u}\,\nabla)\rho = D\nabla^2\rho \tag{C.1}$$

where the gradient, $\nabla = \left(\frac{\partial}{\partial x}, \frac{\partial}{\partial y}, \frac{p}{\partial z}\right)$ and the Laplacian, $\nabla^2 = \frac{\partial^2}{\partial x} + \frac{\partial^2}{\partial y} + \frac{\partial^2}{\partial z}$. The concentration, ρ is defined as the number of particles per tube volume, D is the Diffusion constant and u is the velocity.

The Poiseuille velocity profile is given by:

$$u = u_o(1 - \frac{r^2}{R^2}) \tag{C.2}$$

where $u_o = (R^2\Delta P)/(4\mu l_p)$ is the maximum velocity at the axis of the tube ($r = 0$), ΔP is the pressure drop o. - the distance l_p and R is the tube radius. Since the velocity distribution is a paraboloid of revolution, its volume is one-half that of its circumscribing cylinder; therefore the average velocity,

$$u_r = u_o/2. \tag{C.3}$$

Diffusion occurs over small distances from the wall, where $r \approx R$. Therefore, by introducing a new variable,

$$y = R - r, \tag{C.4}$$

Equation (C.2) can be approximated by:

$$u \approx u_o \frac{2y}{R}. \tag{C.5}$$

For our problem the equation of convective diffusion takes the form:

$$\frac{2u_o}{R} y \frac{\partial \rho}{\partial x} = D \frac{\partial^2 \rho}{\partial y^2} \tag{C.6}$$

where x is the distance along the tube. The boundary conditions for the maximum diffusional flux are :

$$\begin{aligned} &\rho \rightarrow \rho_o \quad as \quad y \rightarrow \infty \\ &\rho = 0 \quad\quad at \quad y = 0. \end{aligned} \tag{C.7}$$

Equation (C.6) is solved by introducing the dimensionless quantity:

$$\psi = \left(\frac{u_o}{DR}\right)^{1/3} \frac{y}{x^{1/3}}. \tag{C.8}$$

Therefore,

$$\begin{aligned} \frac{\partial \rho}{\partial x} &= \frac{\partial \rho}{\partial \psi} \cdot \frac{\partial \psi}{\partial x} \\ &= \frac{-y}{3x^{4/3}} \left(\frac{u_o}{DR}\right)^{1/3} \cdot \frac{\partial \rho}{\partial \psi} \end{aligned} \tag{C.9}$$

and,

$$\begin{aligned} \frac{\partial \rho}{\partial y} &= \frac{\partial \rho}{\partial \psi} \cdot \frac{\partial \psi}{\partial y} \\ &= \frac{\psi}{y} \frac{\partial \rho}{\partial \psi} \end{aligned} \tag{C.10}$$

and,

$$\begin{aligned} \frac{\partial^2 \rho}{\partial y^2} &= \frac{\partial}{\partial \psi} \left[\frac{\psi}{y} \frac{\partial \rho}{\partial \psi} \right] \cdot \frac{\partial \psi}{\partial y} \\ &= \left(\frac{\psi^2}{y^2} \right) \frac{\partial^2 \rho}{\partial \psi^2}. \end{aligned} \tag{C.11}$$

Substitute equations (C.9) and (C.11) into equation (C.6):

$$\frac{\partial^2 \rho}{\partial \psi^2} + \frac{2}{3} \psi^2 \frac{\partial \rho}{\partial \psi} = 0. \tag{C.12}$$

To solve for ρ integrate the following:

$$\begin{aligned} \int \frac{\partial(\partial \rho / \partial \psi)}{\partial \rho / \partial \psi} &= \int -\frac{2}{3} \psi^2 \partial \psi \\ \ln\left(\frac{\partial \rho}{\partial \psi}\right) &= -\frac{2}{9} \psi^3 + constant \\ \int \partial \rho &= \int_0^{\psi} B \exp\left(-2/9\psi^3\right) \partial \psi \\ \rho &= \int_0^{\psi} B \exp\left(-2/9\psi^3\right) \partial \rho + D \end{aligned} \tag{C.13}$$

where B and D are constants of integration. By applying the boundary conditions (equation (C.7)) we find:

$$\begin{aligned} B &= \rho_o / \textstyle\int_o^{\infty} \exp\left(-2/9\psi^3\right) \partial \rho \\ D &= 0. \end{aligned} \tag{C.14}$$

Therefore,

$$\rho = \frac{\rho_o \int_0^{\psi=(u_o/DR)^{1/3}y/x^{1/3}} \exp(-2/9\psi^3)\partial\psi}{\int_o^\infty \exp(-2/9\psi^3)\partial\psi}. \tag{C.15}$$

The diffusional flux to the wall of the tube is given by:

$$\begin{aligned} j' &= D\left(\frac{\partial\rho}{\partial y}\right)_{y=0} \\ &= \frac{D\rho_o}{x^{1/3}}\left(\frac{2u_r}{DR}\right)^{1/3}\frac{1}{\int_0^\infty \exp(-2/9\psi^3)\partial\psi} \\ &= \frac{D\rho_o}{x^{1/3}}\left(\frac{2u_r}{DR}\right)^{1/3}\cdot\frac{(0.23)^{1/3}}{0.89} \\ &= 0.67\rho_o D\left(\frac{u_r}{DRx}\right)^{1/3}. \end{aligned} \tag{C.16}$$

Appendix D

COMPUTER PROGRAM FOR SIMULATION OF FILTRATION PROCESS

```
C
C     ****************************************************************
C     *              SIMULATION OF FILTRATION PROCESS                *
C     *                                                              *
C     *   PROGRAM SIMULATES THE CAKE BUILD-UP PROCESS AND TAKES      *
C     *   INTO ACCOUNT THE CLOGGING EFFECTS.  CLOGGING IS            *
C     *   INCORPORATED BY TWO MEANS: (1) FINE PARTICLES DEPOSITING   *
C     *   ON THE TUBE WALLS AND GRADUALLY REDUCING THE TUBE RADII    *
C     *   AND (2) TUBES TRAPPING PARTICLES LARGER THAN THE PORE      *
C     *   OPENINGS.  SUSPENDED PARTICLES ARE PREVENTED FROM          *
C     *   PASSING THROUGH THE BOTTOM LAYER.  THE PERMEABILITY IS     *
C     *   CALCULATED AS THE NETWORK INCREASES IN LENGTH.             *
C     *                                                              *
C     *   PROGRAM NAME = BIGSMNEW.FOR                                *
C     ****************************************************************
C
C           EL = # OF ELEMENTS/ROW
C            N = TOTAL # OF LOOPS
C          TEL = TOTAL # OF ELEMENTS
C         ROWS = # OF ROWS
C        LOOPS = # OF LOOPS/ROW
C         TOLQ = ERROR TOLERANCE FOR Q
C         TOLH = ERROR TOLERANCE FOR HEAD LOSS
C         QINT = Q INFLOW
C            A = RADIUS OF FINES (um)
C         IDUM = SEED FOR RANDOM NUMBER GENERATOR
C      PERMEAB = PERMEABILITY
C       ILAYER = # OF CAKE LAYERS
C      NUMPART = INITIAL AVERAGE NUMBER OF SUSPENDED
C                FINE PARTICLES IN TUBE
C      CONSVEL = SUPERFICIAL VELOCITY OF FILTRATE (um/sec)
C      VELCRIT = CRITICAL VELOCITY (um/sec)
C       LENGTH = CAKE LAYER THICKNESS (um)
C         FINE = TUBES SMALLER THAN "FINE" CAN BE CLOGGED
C  PARTICLE(ICAKE) = (VOLUME OF FLOWING PARTICLES IN LAYER
C                     ICAKE)/(TOTAL PORE VOLUME IN LAYER ICAKE)
C         CLOG = FRACTION OF SMALL PARTICLES THAT WILL CLOG
C                THE SMALL PIPES
C
C
      REAL R(20000), Q(20000),SUMH,SUMZ,QDELTA,qint,lossnor
      real lossave,VOL(20000),qcrit,volexc,rr(20000)
      REAL SMALL(1000),partnew(500),particle(500),brvol(200)
      real perconew(1000),percolate(200),srvol(200)
      real permeab,a,perco,POREVOL,length,velocity
      real big(1000),perm(100),kold
```

```
      real absmend(100),alittle(100),aclog(100),aneg(100)
      INTEGER RRUN,LOK,ROWS,LOOPS,EL,N,TEL,lo
      integer ipipe(20000),bsm
      common icount
C
      do 2400 icount = 1,2
         if (icount .eq. 1) then
            a = 0.01
            rows=7
            loops=24
C     RESULTS ARE WRITTEN TO FILE = "CLOG_1"
      open (1,file= 'CLOG_1')
      write (1,*) 'file = CLOG_1   program = BIGSMNEW.FOR'
      write (1,*) 'simulates experiments, units in microns'
      WRITE (1,*)'CLOGGING DUE TO DEPOSITION OF FINES AND'
      WRITE (1,*) 'PORE BLOCKING DUE TO TUBES TRAPPING PARTICLES'
      write (1,*) 'particles can NOT pass through bottom layer'
      write (1,*) 'cake steps = 200 um & 10 um FINES = 0.01 um'
      write (1,*) 'superficial v=10E+3/L um/sec '
      write (1,*) 'velcrit = 15E+3 um/sec numpart=100000'
      write (1,*)'LOGNORMAL distribution'
      write (1,*)'std=0.6 median=1.0   rlognorm=r  '
      write (1,*)'r < 0.6 can be clogged'
      write (1,*) 'Xo=1.00  Ao=0.5   Co=3.0'
      write (1,*) 'x=0.5*tan(pi*randx) + 1.00'
        endif
      if (icount .eq. 2) then
         close (1, status= 'keep')
         a = 0.05
         rows = 7
         loops =24
       open (2,file= 'CLOG_2')
       write (2,*) 'CLOG_2 same as CLOG_1 except'
       write(2,*) 'fine particles = 0.05 um'
      endif
C
        do 2350 ichange =1,2
           if(ichange .eq. 1)then
              length = 200.
           elseif (ichange .eq. 2)then
              length = 10
           endif
         ilayer=30
C        THERE ARE 6 ROWS/LAYER
         rows=7
         loops=24
```

```
              qint = 1
              numpart=100000
              consvel=10e+3/length
              velcrit=15e+3
              TOLH=10000
              fine=0.6
              A=0.01
              rave=1.0
            write (icount,*)'rows= ',rows,' loops= ',loops
            write (icount,*)'delta length = ',length
C
C           THE NETWORK IS SOLVED 3 TIMES EACH TIME USING
C           A DIFFERENT INITIAL "PARTICLE(ICAKE)" VALUE
                  do 2300 ll=1,3
                     kold=1.0
                     ib=0
                     rows=7
                     loops=24
                     write (*,*) 'run  cycle ',ll,icount
                    rrun=0.
                    lok=0
                    qbig=0.0
                    bsm=0
                    ibigend=1
                    ismaend=1
                    ib1=0
                    el=2*loops+1
                    n=loops*(rows-2)
                    tel=(rows-1)*el
                    idum = -100
               iidum=idum
               area=0.0
C
C              FUNCTION "RLOGNOR" IS USED TO ASSIGN TUBE RADII
C              WITH A LOGNORMAL SIZE DISTRIBUTION
               DO 100 I=1,TEL*ilayer
                   R(i)= RLOGNOR(IDUM)
                   area=area+r(i)**2
                   ipipe(i)=0
100            CONTINUE
C
C          AVAREA = AVERAGE AREA PER ROW
               avarea=area/((rows-1)*ilayer)
C
C        NOTE: PIPE RADIUS IS BEING CHANGED TO PIPE RESISTANCE
            do 150 i=1,tel
```

```
                r(i) = 1./(r(i)**3.)
150          continue
C
          DO 2200 ICAKE =1,ilayer
             qint=1.0
             tolq=qint*.001/el
               DO 200 I=1,EL
                  Q(I)=qint/EL
200            CONTINUE
C
C
               DO 500 I=2,(ROWS-1)
                    IF ((MOD(I,2)) .EQ. 0) THEN
                        DO 300 J=((I-1)*EL+1),(I*EL-2),2
                              JJ=J+1
                               K=J-EL
                              KK=K+1
                              Q(J)=.5*(Q(K)+Q(KK))
                              Q(JJ)=Q(J)
300                     CONTINUE
                             J=1*EL
                             K=J-EL
                             Q(J)=Q(K)
                      ELSE
                         J=(I-1)*EL+1
                         K=J-EL
                         Q(J)=Q(K)
                          DO 400 J=((I-1)*EL+2),((I)*EL),2
                                JJ=J+1
                                 K=J-EL
                                KK=K+1
                                Q(J)=.5*(Q(K)+Q(KK))
                                Q(JJ)=Q(J)
400                       CONTINUE
                      ENDIF
500                CONTINUE
C
C
C            NOTE: WHEREVER YOU SEE R( ) IT IS = 1./(PIPE RADIUS)**3.
C
C            START BALANCING
C
C
               IBALANCE = 1
               irepeat = 1
540            continue
```

```
                irepeat = 1+irepeat
C
C      NOTE: I REPEAT THE BALANCING SCHEME AFTER I DEPOSIT SOME OF
C             THE PARTICLES IN THE CAKE LAYERS
C
          rrun=0.0
550          CONTINUE
C
                 LOK=0
                  do 600 I=1,(EL-2),2
                      J=I+1
                      SUMH=-R(I)*Q(I)
                      SUMZ= R(I)
                      SUMH=SUMH+ R(J)*Q(J)
                      SUMZ=SUMZ+ R(J)
                      QDELTA=SUMH/SUMZ
                      Q(I)=Q(I)+QDELTA
                      Q(J)=Q(J)-QDELTA
               IF ((ABS(QDELTA).lt.TOLQ).AND.(ABS(SUMH).lt.TOLH)) THEN
                        LOK=LOK+1
               ENDIF
600                CONTINUE
C
C
                if (rows .gt. 3) then
                     i=2
                     do 700 lo = 1,n
                          j=i+el
                         sumh=-r(i)*q(i) - r(j)*q(j)
                         sumz= r(i)+ r(j)
                         k=i+1
                         jj=j+1
                         sumh=sumh+ r(k)*q(k) + r(jj)*q(jj)
                         sumz=sumz+ r(k) + r(jj)
                         qdelta=sumh/sumz
                         q(i)=q(i)+qdelta
                         q(j)=q(j)+qdelta
                         q(jj)=q(jj)-qdelta
                         q(k)=q(k)-qdelta
                 if ((abs(qdelta).lt.tolq).and.(abs(sumh).lt.tolh)) then
                         lok=lok+1
                 endif
               if ((mod(lo,loops).eq.0).and.(mod((lo/loops),2).eq.0)) then
                         i=i+4
                 else
                         i=i+2
```

```
            endif
700       continue
            endif
C
              if (mod(rows,2) .eq. 0) then
               DO 800 i=(tel-el+2),(tel-1),2
                     j=i+1
                     sumh=-r(i)*q(i)
                     sumz= r(i)
                     sumh=sumh+ r(j)*q(j)
                     sumz=sumz+ r(j)
                     qdelta=sumh/sumz
                     q(i)=q(1)+qdelta
                     q(J)=q(j)-qdelta
               if ((abs(qdelta).lt.tolq).and.(abs(sumh).lt.tolh)) then
                   lok=lok+1
               endif
800            continue
              endif
C
               if (mod(rows,2).gt.0 ) then
                 do 900 i=(tel-el+1),(tel-2),2
                    j=1+1
                    sumh=-r(i)*q(i)
                    sumz= r(1)
                    sumh=sumh+ r(j)*q(j)
                    sumz=sumz + r(j)
                    qdelta=sumh/sumz
                    q(1)=q(1)+qdelta
                    q(j)=q(j)-qdelta
                    if((abs(qdelta).lt.tolq).and.(abs(sumh).lt.
     +                    tolh)) then
                       lok=lok+1
                    endif
900              continue
              endif
C
               rrun =rrun+1
C
C
C
C     ********************************************************
C     ********************************************************
        if ((lok .lt. (n+2*loops)).and.(rrun .lt. 3000)) then
             go to 550
        else
```

```
            write (icount,*) 'it took ',rrun,' iterations'
C
C
C          ********************************************
           if (ibalance .eq. 1) then.
              TOTALVOL=0.0
C         NOTE: I'M ASSUMING # OF SUSPENDED PARTICLES/PORE IS
C               PROPORTIONAL TO flow volume
C
C        NOTE: FIND AVERAGE FLOW VOLUME
              QSUM=0.0
              DO 940 I=(TEL-(EL*6)+1),TEL
                 QSUM=QSUM+Q(I)
940           CONTINUE
                 QAVE=QSUM/(EL*6)
C
              VOLSMALL=0.0
              QSMALL=0.0
              QTOTAL=0.0
              ineg=0
              JSM=0
              DO 950 I=(TEL-(EL*6)+1),TEL
               IF((R(I)**(-1./3.).LT.fine).and.(q(i).ge.0.))THEN
                       JSM=JSM + 1
                       QSMALL=QSMALL + Q(i)
                       VOLSMALL=VOLSMALL+(1./R(I))-0.05**3.
                       SMALL(JSM)=I
                   ElSE
                       if((icake.eq.1).and.(q(i).ge.0.))then
                          if(r(i)**(-1./3.).ge.fine)then
                              bsm=bsm+1
                              qbig=qbig+q(I)
                              big(bsm)=i
                           endif
                        endif
                     ENDIF
                    if(q(i).ge.0.)then
                      qtotal=qtotal+q(i)
                elseif((q(i).lt.0.).and.(r(i)**(-1./3.).ge..051))then
                    ineg=ineg+1
               endif
950           CONTINUE
C
C
                  FRACSMALL=QSMALL/QTOTAL
C
```

```
C       PARTICLE = (VOLUME OF FLOWING PARTICLES IN LAYER ICAKE)/(TOTAL
C                           PORE VOLUME IN LAYER ICAKE)
C                 I'M ARBITRARILY CHOOSING IT
C
            if(ll.eq.1)then
                PARTICLE(icake) = 0.005
                  if(icake .ge. 2)then
                   particle(icake-1)=0.005
                  endif
               elseif(ll .eq. 2)then
                  particle(icake)=0.01
                     if(icake .ge. 2)then
                        particle(icake-1)=0.01
                     endif
               elseif(ll .eq. 3)then
                  particle(icake)=0.05
                     if(icake .ge. 2)then
                        particle(icake-1)=0.05
                     endif
               endif
                   WRITE(ICOUNT,*)'PARTICLE(ICAKE) ',PARTICLE(ICAKE)
                      CLOG = FRACSMALL*PARTICLE(icake)
C                        CLOG = FRACTION OF SMALL PARTICLES THAT WILL
C                               CLOG THE SMALL PIPES
C
                         VOLUME = 0.0
               DO 980 I=(TEL-(EL*6)+1),TEL
                     VOLUME=VOLUME + 1/R(I)
980            CONTINUE
                     VOLCLOG = CLOG*VOLUME
               if(icake.eq.1)then
                   volbot=(particle(icake)-clog)*volume
                endif
C
          WRITE(ICOUNT,981) VOLUME
981       format('TOP LAYER CAKE VOLUME',f18.7)
C
C       RANDOMLY CHOOSE SMALL PIPE TO CLOG
C
          VOLRED=0.0
          clogbot=volbot
          ib=0
          IF (VOLCLOG .GT. (VOLSMALL))THEN
              DO 1020 IK = 1,JSM
                 IA=SMALL(IK)
                 VOLCLOG=VOLCLOG-(1./R(IA))**(1./3.)+ 0.05**3
```

```
                R(IA)=1./(0.05**3)
                ipipe(ia)=1
1020          CONTINUE
               ib=jsm
C              WRITE(*,*)' JSM = # OF SMALL PIPES ',JSM
             if(icake .gt.1)then
               partnew(icake-1)=PARTICLE(icake)+VOLCLOG/VOLUME-clog
             endif
           ELSE
1022           if(volclog .gt. 0.)then
                 IJS=JSM*RAN1(IDUM) + 1
                     IA=SMALL(IJS)
                    IF(ipipe(ia).eq.0)THEN
                         VOLCLOG=VOLCLOG-(1./R(IA))+0.05**3
                         R(IA)=1./(0.05**3)
                         ipipe(ia)=1
                         ib=ib+1
                    ENDIF
                   go to 1022
                endif
               if(icake.eq.1)then
                    excess=0.0
                    ib1=ib+ib1
               VOLBOT=VOLBOT+VOLCLOG
               clogbot=volbot
               qadd=0.0
               DO 1030 IX=1,bsm
                     IL=BIG(IX)
                  if(q(il).ge.0.)then
                    VOLDEP=VOLBOT*Q(IL)/QBIG
                    qadd=qadd+q(il)
                  else
                    voldep=0.0
                  endif
                    IF (VOLDEP .LT. 0.008)THEN
                       EXCESS=VOLDEP+excess
                    ENDIF
                    IF(((VOLDEP+EXCESS).LE.(1./R(IL)-1.25E-4))
     +                .AND. (VOLDEP.GE.0.008))THEN
                         CLOGBOT=CLOGBOT-VOLDEP-EXCESS
                         R(IL)=1./(1./R(IL)-VOLDEP-EXCESS)
                         EXCESS=0.0
                    ELSEIF((VOLDEP+EXCESS).GT.(1./R(IL)-1.25E-4))THEN
C                        WRITE(ICOUNT,*)'PIPE IS TOO SMALL 1030'
                         EXCESS=VOLDEP-1./R(IL)+1.25E-4 +excess
                         clogbot=clogbot-1./r(il)+1.25e-4
```

```
                        r(il)=8000.
                        ib1=ib1+1
                    ENDIF
1030              CONTINUE
                endif
C
C
             if (icake .gt. 1)then
               partnew(icake-1)=PARTICLE(icake)-CLOG
             endif
           ENDIF
C          WRITE(ICOUNT,*)' JSM = # SMALL & # CLOGGED & # neg ',
C     +     JSM,IB,ineg
             if(icake .eq. 1)then
C              write(icount,*)'# of big pipes in bottom layer ',bsm
             endif
C
              brvol(icake)=0.0
              do 1040 ia=(tel-(el*6)+1),tel
                   brvol(icake)=brvol(icake)+1/r(ia)
1040          continue
C             write(icount,*)'brvol(icake) = ',brvol(icake)
C
C
C          CLOGGING DUE TO FINE PARTICLES
C            NOTE: I'M ASSUMING # OF SUSPENDED PARTICLES/PORE IS PROPORTIONAL
C                  TO FLOW VOLUME. THE FINE PARTICLES DO NOT ENTER PORES THAT
C                  HAVE BEEN CLOGGED DUE THE BIG PARTICLES
C
C            NOTE:  FIND AVERAGE FLOW VOLUME. I'M ONLY USING PORES THAT HAVE
C                   NOT BEEN CLOGGED BY THE BIG PARTICLES.
C
C
                 QSUM=0.0
                 Ipos=0
                 percolate(icake)=numpart
C
              if (icake .ge. 2)then
C               NOTE: USE NEXT STATEMENT BECAUSE LATER ON IN
C                     PROGRAM "PERCOLATE(icake-j+1)" IS "PERCOSUM"
                percolate(icake-1)=numpart*el*6
              endif
C
                 srvol(icake)=0.0
                 DO 1045 I=(TEL-(EL*6)+1),TEL
                    IF((ipipe(i).eq.0).and.(q(i).ge.0.))THEN
```

```
                    QSUM=QSUM+Q(I)
                    Ipos=ipos+1
                  ENDIF
1045            CONTINUE
C
C
C        PERCO = # OF FINES THAT ARE DEPOSITED IN LAYER
C     PERCOSUM = SUM OF FINES THAT PERCOLATE THROUGH LAYER
C       SUMDEP = SUM OF FINES THAT ARE DEPOSITED IN LAYER
C    DIFFUSION = DIFFUSION CONSTANT (um^2/sec)
C         KOLD = PERMEABILITY CALCULATED FOR NETWORK
C                WITH (ICAKE-1) LAYERS
C
C
                    QAVE=QSUM/Ipos
                    percolate(icake)=percolate(icake)*el*6/ipos
                    PERCOSUM=0.0
                    SUMDEP=0.0
                    DIFFUSION=0.2161/A
                    do 1047 i=(tel-(el*6)+1),tel
C
                    IF(ipipe(i).eq.0)THEN
                          velocity=(consvel*avarea*q(i))/
     +                    (icake*0.42*(r(I)**(-2./3.)))
                          velocity=velocity*kold
                            if (velocity.lt.0. .or. velocity.ge.
     +                          velcrit)then
                              perco=0.0
                              volperco=0.0
                                if(q(i).gt.0.)then
                        percosum=percosum+(percolate(icake)*q(i)/qave)
                                endif
                           endif
C
                           if(velocity.gt.0.0 .and. velocity.lt.
     +                          velcrit)then
                              perco=(2**(4./3.))*percolate(icake)
     +                           *(diffusion**(2./3.))
                          perco=perco*(velocity**(-2./3.))*(r(i)**(2./9.))
                              if(perco .gt. percolate(icake))then
                                  perco=percolate(icake)*(Q(I)/QAVE)
                               else
                                  perco=perco*(Q(I)/QAVE)
                                  percosum=percosum+(percolate(icake)
     +                                    *q(i)/qave-perco)
                               endif
```

```
                              sumdep=sumdep+perco
                          endif
C
                          volperco=perco*(a**3.)
C
C
C                         NEW PIPE RESISTANCE
C                         SMALLEST RADIUS THAT TUBE CAN BE REDUCED
C                           TO = 0.05 um
C
                          if (1./r(i) .le. volperco) then
                              percosum=percosum+(volperco-1/r(i)
     +                                    +1.25E-4)/(a**3)
                              r(i)=8000.
C                             PIPE VOLUME SMALLER THAN VOLPERCO
                              srvol(icake)=srvol(icake)+1/r(i)
                          else
                              R(I)=1./(1./R(I) - volPERCO)
                              srvol(icake)=srvol(icake)+1/r(i)
                          endif
C
C           WRITE (ICOUNT,*) 'TOTAL # OF PERCOLATING and '
C           write(icount,*) 'deposited particles from cake layer'
C           WRITE (ICOUNT,*) ICAKE,percosum,sumdep
C
                               deposited=sumdep
                     ELSE
                               srvol(icake)=srvol(icake)+1/r(i)
                     ENDIF
C
1047        continue
C
              if (icake .gt. 1)then
                perconew(icake-1)=percosum/(6*el)
C               write(*,*)'perconew(icake-1) ',perconew(icake-1)
C               write(icount,*)'perconew(icake-1) ',perconew(icake-1)
              endif
C
C
            if(icake .eq. 1)then
              qtot=0.0
              srvol(icake)=0.0
              do 1048 i=1,el*6
                 if((q(I).ge.0.).and.(r(i).le.7999.9))then
                    qtot=qtot+q(i)
                 endif
```

```
1048          continue
C
C
C           SUSPENDED PARTICLES CAN NOT PASS THROUGH BOTTOM LAYER
C           SMEXC = EXCESS VOLUME OF "FINES" THAT NEED TO BE
C                   DEPOSITED IN BOTTOM LAYER
C          DEPBOT = VOLUME FINES DEPOSITED IN BOTTOM LAYER
C          DEPSMA = VOLUME FINES DEPOSITED IN TUBE "I" IN BOTTOM LAYER
C
              smexc=0.0
              depbot=percosum*(a**3)
              do 1049 i=1,el*6
                    if((q(i).ge.0.).and.(r(i).le.7999.9))then
                       depsma=percosum*(a**3.)*q(i)/qtot
                    else
                       depsma=0.0
                    endif
                    if((depsma+smexc).le.((1./r(i))-1.25e-4))then
                       depbot=depbot-depsma-smexc
                       r(i)=1./((1./r(I))-depsma-smexc)
                       smexc=0.0
                    elseif((depsma+smexc).gt.((1./r(i))-1.25e-4))then
C                      write(icount,*)'pipe is too small'
                       smexc=depsma-(1./r(i))+1.25e-4+smexc
                       depbot=depbot-1./r(i)+1.25e-4
                       r(i)=8000.
                     endif
                  srvol(icake)=srvol(icake)+1./r(i)
1049            continue
              endif
C
C
C
C           ISMAEND = # OF UNCLOGGED TUBES IN BOTTOM LAYER
C
          IF (ICAKE .GE. 2) THEN
C
C             WHEN ALL TUBES ARE CLOGGED IN BOTTOM LAYER THEN
C             LAYER ABOVE BOTTOM LAYER BECOMES NEW CAKE BOTTOM
              if(ismaend .eq. 0)then
                  iend=icake-1
               else
                  iend=icake
               endif
C
               DO 1095 J=2,Iend
```

```
                volume=0.0
                volsmall=0.0
                QSMALL=0.0
                QTOTAL=0.0
                JSM=0
                qbig=0.0
                bsm=0
                ineg=0
                iclog=0
          DO 1050 I=(TEL-(EL*6*J)+1),(TEL-(EL*6*(J-1)))
             IF((R(I)**(-1./3.).LT.fine).AND.R(I)**(-1./3.)
     +                    .GT. 0.051)THEN
                         if(q(i).ge.0.)then
                           JSM=JSM + 1
                           QSMALL= QSMALL + Q(I)
                           SMALL(JSM)=I
                           volsmall=volsmall+(1./r(i))-0.05**3.
                         endif
              ELSE
                if((j.eq.iend).and.(r(i)**(-1./3.).gt. fine))then
                   if(q(i).ge.0.)then
                       bsm=bsm+1
                       qbig=qbig+q(i)
                       big(bsm)=i
                    endif
                endif
             ENDIF
C
          if((q(i).lt.0.).and.(r(i)**(-1./3.)).gt..051)then
                     ineg=ineg+1
                endif
                if((j.eq.iend).and.(r(i)**(-1./3.)).lt.0.051)then
                    iclog=iclog+1
                endif
                  if(q(i).ge.0.)then
                     QTOTAL=QTOTAL + Q(I)
                  endif
                     volume=volume+1/r(i)
1050          CONTINUE
C
              if(j.eq.iend)then
                    itotbsm=bsm
              endif
C
                    FRACSMALL=QSMALL/QTOTAL
                    CLOG=FRACSMALL*PARTICLE(icake-j+1)
```

```
                    VOLCLOG=CLOG*VOLUME
C
                  IF(jsm .eq.0) then
                    if((icake-j).gt.0)then
                      partnew(icake-j)=particle(icake-j+1)
                    endif
                  ELSEIF(VOLCLOG .GT.(VOLSMALL))THEN
                       DO 1060 IK =1,JSM
                           IA=SMALL(IK)
                           VOLCLOG=VOLCLOG-(1./R(IA))+0.05**3.
                           R(IA)=1./(0.05**3)
                           ipipe(ia)=1
1060                   CONTINUE
                       if(j.eq.iend)then
                           ib1=ib1+jsm
                       endif
                       if((icake-j).gt.0)then
                            PARTnew(icake-j)=PARTICLE(icake-j+1)
     +                        +volclog/volume - clog
                       endif
                   ELSEIF(VOLCLOG .LT. (VOLSMALL))THEN
1062                    if(volclog .gt. 0.)then
                            IJS=JSM*RAN1(IDUM)+1
                            IA=SMALL(IJS)
                            IF (ipipe(ia).eq.0)THEN
                               VOLCLOG=VOLCLOG-(1./R(IA))+0.05**3.
                               R(IA)=1./(0.05**3)
                               ipipe(ia)=1
                               if(j.eq.icake)then
                                   ib1=ib1+1
                               endif
                            ENDIF
                            go to 1062
                       endif
                       if((icake-j).gt.0)then
                          PARTnew(icake-j)=PARTICLE(icake-j+1)-CLOG
                       endif
                  ENDIF
C
C
                  if(ibigend .eq.0)then
                       is=(el*6+1)
                       ie=is+itotbsm-1
                       iy=2
                       ifinish=icake-1
                   else
```

```
                        is=1
                        ie=itotbsm
                        iy=1
                        ifinish=icake
                     endif
C
                     if(j.eq.ifinish)then
                        volbot=(particle(iy)-volclog/volume)*volume
                        volbot=(particle(iy)-clog)*volume+volclog+excess
                        clogbot=volbot
                        excess=0.0
C
                        DO 1070 ix=is,ie
                           IL=BIG(IX)
                           if(q(il).ge.0.)then
                                VOLDEP=VOLBOT*Q(IL)/QBIG
                           else
                                voldep=0.
                           endif
                           IF (VOLDEP .LT. 0.008)THEN
                                EXCESS=VOLDEP +excess
                           ENDIF
                           IF(((VOLDEP+EXCESS).LE.(1./R(IL)-1.25E-4))
     +                          .AND. (VOLDEP.GE.0.008))THEN
                               CLOGBOT=CLOGBOT-VOLDEP-EXCESS
                               R(IL)=1./(1./R(IL)-VOLDEP-EXCESS)
                               EXCESS=0.0
                           ELSEIF((VOLDEP+EXCESS).GT.(1./R(IL)
     +                             -1.25E-4)) THEN
                               ib1=ib1+1
                               EXCESS=VOLDEP-1./R(IL)+1.25E-4 +excess
                               clogbot=clogbot-1./r(il)+1.25e-4
                               r(il)=8000.
                           ENDIF
1070                    CONTINUE
C
                     ENDIF
C
C
                  brvol(icake-j+1)=0.0
                  do 1075 ia=(tel-(el*6*j)+1),(tel-(el*6*(j-1)))
                        brvol(icake-j+1)=brvol(icake-j+1)+1/r(ia)
1075              continue
C
                     srvol(icake-j+1)=0.0
                     Qsum=0.0
```

```
                    ime=0
                      do 960 i=(tel-(el*6*j)+1),(tel-(el*6*(j-1)))
                            if((ipipe(i).eq.0).and.(q(i).ge.0.))then
                               Qsum=Qsum+Q(I)
                            endif
960                   continue
C
                  sumvolperco=0.0
                  sumdep=0.0
                  percosum=0.0
C
C         FROM EXPERIMENTS FOUND SUPERFICIAL VELOCITY (i.e. consvel)
C         APPROX. = 10.E+3/LENGTH (um/sec)
C         USE POROSITY = 0.42
C
           do 970 i=((tel-el*6*j)+1),(tel-(el*6*(j-1)))
C
              if(ipipe(i) .eq.0)then
                 velocity= (consvel*avarea*q(i))/(icake
     +                     *0.42*(r(i)**(-2./3.)))
                 velocity=velocity*kold
                    if(velocity.lt.0. .or. velocity.ge.velcrit)then
                        perco =0
                        volperco=0.
                        IF(Q(I) .GT. 0.)THEN
                          percosum=percosum+(percolate(icake-j+1)
     +                                  *q(i)/qsum)
                        ENDIF
                    endif
                    if(velocity.ge.0. .and. velocity.lt. velcrit)then
                       perco=(2**(4./3.))*(diffusion**(2./3.))
                       perco=perco*(velocity**(-2./3.))*(r(i)**(2./9.))
                       perco=perco*percolate(icake-j+1)*Q(I)/Qsum
C                      write (icount,*)'velocity PERCO ',velocity,perco
                       sumdep=sumdep+perco
                       if(perco .gt. percolate(icake-j+1)*Q(i)/qsum)then
                           perco=percolate(icake-j+1)*(q(i)/qsum)
                       else
                           percosum=percosum+((percolate(icake-j+1)*
     +                             q(i)/qsum)-perco)
                       endif
                    endif
                    volperco=perco*(a**3.)
                    sumvolperco=sumvolperco+volperco
C
C                   REMEMBER R(I) IS THE PIPE RESISTANCE NOT PIPE RADIUS
```

```
C
                if (1/r(1) .le. volperco) then
                    percosum=percosum+(volperco-(1./r(i))+1.25e-4)
     +                    /(a**3)
                    r(i)=8000.
                else
                    R(I)=(1/r(i)-volperco)**(-1)
                endif
C
                  srvol(icake-j+1)=srvol(icake-j+1)+1/r(i)
C
             ELSE
                   srvol(1cake-j+1)=srvol(1cake-j+1)+1./r(i)
                   ime=ime+1
             ENDIF
C
970            CONTINUE
C
C
               VOLUME=0.0
               1f (icake-j .gt. 0)then
                  perconew(icake-j)=percosum
               endif
C
C              ISMAEND = # OF UNCLOGGED PIPES IN BOTTOM LAYER
               1f(1smaend .eq. 0)then
                  1s=el*6+1
                  1e=1s+2*el*6-1
               else
                  1s=1
                  ie=el*6
               endif
C
C
             IF(icake .ge. 2)THEN
                IF(j.eq.iend)THEN
                   qtot=0.0
                   do 996 1=is,ie
                     1f((q(1).ge.0.).and.(r(1).le.7999.9))then
                        qtot=qtot+q(i)
                     endif
996                  continue
C
                   depbot=percosum*(a**3.)
                   do 997 i=is,1e
                      1f(q(1) .ge. 0.)then
```

```
                        depsma=percosum*(a**3.)*q(i)/qtot
                     else
                        depsma=0.0
                     endif
                     if((depsma+smexc).le.((1/r(i))-1.25e-4))then
                         depbot=depbot-depsma-smexc
                         r(i)=1./((1./r(i))-depsma-smexc)
                         smexc=0.0
                     elseif((depsma+smexc).gt.((1/r(i))-1.25e-4))then
                         smexc=depsma-1./r(i) +1.25e-4+smexc
                         depbot=depbot-1./r(i)+1.25e-4
                         r(i)=8000.
                     endif
997                continue
C
                   srvol(iend)=0.0
                   do 1005 i=is,ie
                      srvol(iend)=srvol(iend)+1./r(i)
1005               continue
                 ENDIF
               ENDIF
C
C
1095             CONTINUE
C
C
               do 1097 jd=1,icake-1
                   percolate(jd)=perconew(jd)
                   particle(jd)=partnew(jd)
1097           continue
C
           ENDIF
C            ***********************************************
C
           ibalance = 2
          ENDIF
C     ************************************************************
C     ************************************************************
C
C
             if (irepeat .eq. 2) then
                 goto 540
              endif
              headloss=0.
              do 1100 M=1,el
                do 1000 i=M,tel,el
```

```
                headloss=headloss+ r(i)*q(i)
1000          continue
1100        continue
                lossave=headloss*el/(rows-1)/el
                permeab=1./(lossave)
                perm(icake)=permeab
                kold=permeab
          write (icount,*)'seed ',iidum,' layer ',icake,' k ',permeab
          write (*,*) 'seed ',iidum,' lossave ',lossave,' k ',permeab
              endif
           write(icount,*)'percolate(j)    j    srvol(j)    particle(j)
     +   brvol(j)  iclog ism ibig ineg'
           do 1300 j=1,icake
              ineg=0
              iclog=0
              ibsmend=0
              iiittle=0
              do 1200 i=(eL*6*(j-1)+1),(el*6)*j
                 if(r(i) .gt. 7999.9)then
                    iclog=iclog+1
                 endif
                 if((r(i).lt.7999.9).and.(r(i).ge.1./(fine**3.)))then
                      if(q(i).ge.0.)then
                         iiittle=ilittle+1
                      endif
                 endif
                 if(r(i).lt.1./(fine**3.))then
                  if(q(i).ge.0.)then
                     ibsmend=ibsmend+1
                  endif
                 endif
                 if(q(i).lt.0.)then
                       ineg=ineg+1
                  endif
1200          continue
              aclog(j)=iclog
              aiittle(j)=iiittle
              absmend(j)=ibsmend
              aneg(j)=ineg
          write(icount,1310)percolate(j),j,srvol(j),particle(j),brvol(j),
     +   aclog(j),alittle(j),absmend(j),aneg(j)
1300        continue
1310      format(e16.10,i4,F12.3,e12.4,F12.3,4f4.0)
C
C             ICLOG = # OF TUBES CLOGGED IN BOTTOM LAYER
              iclog=0
```

```
                ibigend=0
                ismaend=0
                ineg=0
                do 1400 i=1,el*6
                   if(r(i) .gt. 7999.9)then
                       iclog=iclog+1
                    endif
                    if(r(i).lt.7999.9)then
                        if(q(i).ge.0.)then
                            ibigend=ibigend+1
                        endif
                     endif
C
C    NOTE:  ibigend and ismaend are equal but before I had a condition
C           that allowed the fines to clog the pipes to r=0.005 and
C           the big particles to clog the pipes to r=0.05. I'm
C           leaving the setup this way so I can change the conditions
C           if I want to later on.
C
                     if(r(i).lt.7999.9)then
                          if(q(i).ge.0.)then
                              ismaend=ismaend+1
                           endif
                       endif
                if(q(i).lt.0.)then
                       ineg=ineg+1
                endif
1400            continue
C               write(icount,*)'iclog,ibig,ismall,ineg ',iclog,
C     +             ibigend,ismaend,ineg
                if(icake .lt. ilayer)then
                   rows=rows+6
                   tel=(rows-1)*el
                   n=loops*(rows-2)
                   do 2100 i=(tel-6*el +1),tel
                      ipipe(i)=0
                      r(i)=1.0/(r(i)**3)
2100               continue
                endif
2200            continue
C
                   write(icount,*)'icake   k        '
                   do 2250 i=1,ilayer
                      write(icount,2360)i,perm(i)
2250               continue
2300              continue
```

```
2350          continue
2360         format(i3,e15.5)
2400        continue
            end
C
C
C
C
C               log normal random number generator
                  function rlognor(idum)
C
                      real median
                      common icount
             if (icount .eq. 1) then
                std=0.6
                xo=1.0
                ao=0.5
                co=3.0
                median=1.0
             endif
             if (icount .eq. 2) then
                std=0.6
                xo=1.0
                ao=0.5
                co=3.0
                median=1.0
             endif
C
10           randx=ran1(idum)
             if((randx .ge. .494).and.(randx .le. .54))then
                  go to 10
             endif
             xx=ao*tan((3.141592654)*randx)+xo
             yy=ran1(idum)*(co)
             yy=yy/(1 +((xx-xo)**2)/(ao*ao))
             if (xx .lt. 0.0) then
                 go to 10
             endif
C
             px=(1.0/(sqrt(2*3.141592654)*std*xx))
             px=px*exp((-.5*(log(xx)-log(median))**2)/(std**2))
C
              if (px .ge. yy) then
                   rlognor = xx
              else
                 go to 10
```

```
      endif
      return
      end
C
C
      function ran1(idum)
        dimension s(97)
        integer ma,ia1,ic1,m2,ia2,ic2,m3,ia3,ic3
        m1=259200
        ia1=7141
        ic1=54773
        m2=134456
        ia2=8121
        ic2=28411
        m3=243000
        ia3=4561
        ic3=51349
        data iff /0/
        if (idum .lt. 0 .or. iff .eq. 0) then
            iff=1
            ix1=mod(ic1-idum,m1)
            ix1=mod(ia1*ix1 +ic1,m1)
            ix2=mod(ix1,m2)
            ix1=mod(Ia1*ix1+ic1,m1)
            ix3=mod(ix1,m3)
            do 11 j=1,97
              ix1=mod(ia1*ix1+ic1,m1)
              ix2=mod(ia2*ix2+ic2,m2)
              s(j)=(float(ix1)+float(ix2)/m2)/m1
11          continue
            idum = 1
        endif
        ix1=mod(ia1*ix1+ic1,m1)
        ix2=mod(ia2*ix2+ic2,m2)
        ix3=mod(ia3*ix3+ic3,m3)
        j=1+(97*ix3)/m3
        if (j .gt. 97 .or. j .lt. 1) then
            write(*,*) 'error'
        endif
        ran1=s(j)
        s(j)=(float(ix1)+float(ix2)/m2)/m1
        return
        end
```